Author:
Moreau, Nicolette

Title:
Manipulation of Macromolecular Uptake In Coacervate Systems

Towards the Functional Design of Hybrid Protocells

Manipulation of Macromolecular Uptake in Coacervate Systems

Towards the Functional Design of Hybrid Protocells

By

NICOLETTE GALATEA MOREAU

Bristol Centre for Functional Nanomaterials
UNIVERSITY OF BRISTOL

A dissertation submitted to the University of Bristol in accordance with the requirements of the degree of DOCTOR OF PHILOSOPHY in the Faculty of Science.

SCHOOL OF CHEMISTRY

MARCH 2018

WORD COUNT: 51163 WORDS

Abstract

Coacervates, often recognised as a protocellular containment system, are droplets comprised of a membrane-free, highly-charged matrix formed frequently by electrostatic matching and entropic drive between oppositely charged macromolecules and polymers. Selective molecular sequestration occurs depending on the constituent coacervates components, which induces enriched compartmentalised systems. Enhanced enzymatic rates are observed due to increased local concentrations and reduced diffusion distances. Here, both synthetic and biological components have been added to coacervates to explore the potential of creating functional hybrid protocells with higher order properties. In this manuscript, such systems are explored with adenosine triphosphate and poly(diallyldimethylammonium) chloride coacervate droplets.

The main objective of this thesis is to demonstrate the ability to create internal compartments within a coacervate droplet, allowing for the localisation of substrates and reaction cascades in imitation of biological sub-cellular organisation. A secondary objective shows the capability to add further functionalisation to the system with the addition of artificial membranes that can be further functionalised with components allowing for signal transduction, in this case a light-responsive protein.

A first study is concerned with characterising the dynamics and stability of the system. The effects of sequestering solutes individually are investigated with both small molecules, such as DNA and tetraethylene glycol (TEG), and larger molecules, including proteins and dextran carbohydrates. Here, it is shown that even small uncharged molecules are capable of perturbing the system to create internal compartmentation. The exchange in a binary population of coacervates is then examined using Förster Resonance Energy Transfer (FRET), where each population contains a single type of fluorescently tagged DNA oligomer, showing that transfer does not occur between two mixed populations.

In a second study, these observations are then exploited to create functional systems with multiple components in single coacervate populations. Here, a comparison between co-uptake and sequential uptake properties of macromolecules is shown. Aqueous two-phase systems within coacervates are also explored with TEG and dextran. This results in a synergistic system with altered uptake properties that yields internal compartments which can then be enzymatically manipulated to act as storage-release systems.

The final study explores macromolecular surface localisation on coacervates. The utility of the exclusion properties of the coacervate to generate membranes at the interface between the coacervate bulk matrix and the surrounding supernatant is analysed. A nanotectonic approach is used to add block copolymers to the surface and this is then further functionalised by the addition of a layer of purple membrane flakes, stabilised by the block copolymer interface. The

behaviour of the TEG-dextran system is also briefly investigated with block copolymer coacervates to show early investigations into a three-component system.

Dedication and acknowledgements

There are many people who have contributed to my experience as a PhD student and aided in my research. Primarily, I would like to thank my supervisors, Professor Steve Mann and Dr Ross Anderson, for giving me the opportunity to research under their guidance for the last four years. Additionally, I would also like to acknowledge Dr Dora Tang, my associated academic on this project, for her support and supervision. Thank you to my doctoral centre, the Bristol Centre for Functional Nanomaterials (BCFN) for selecting me to be a part of the cohort, and for providing me with the interdisciplinary training that has given me so many opportunities. Further acknowledgement also goes to my funding body, the EPSRC.

A special thank you goes to out to all the other members of both my lab groups in Chemistry and Biochemistry. There are too many to thank individually but I have enjoyed being a part of the groups and appreciate your kindness, and constant openness and helpfulness. I really appreciate all the time you have taken for conversations, collaboration and helping out, and couldnt have wished for a better group of scientists to spend my time with. To Dr Nicolas Martin there is an extra-large thank you, for the invaluable time and support you have given me throughout. You have been an inspiration to work and collaborate with.

Additionally, I would like to thank the numerous other colleagues outside my lab who have provided support. Thank you to Dr Joanna Komar and Dr William Allen from the Collinson group for your assistance with the purple membrane flake experiments, and to Professor Hampp (University of Marburg) for kindly donating the purple membrane for me to work with. Thank you also to Alan Leard in the Wolfson Bioimaging Suite for his assistance and training in the confocal fluorescence microscopy, and to Dr Andy Collins for his tutorship and help organising my international placement.

Finally, I have some important personal acknowledgements. Thank you to my partner Mihai, for your support and understanding throughout the writing-up process. Thank you also to my family for their encouragement and assistance. Your consideration throughout this process has been amazing and made a huge difference to me. I dedicate this thesis to my mother, Marie Moreau, for inspiring me and teaching me the value of logic and perseverance. Thank you for the support and opportunities you have given me throughout my life that have enabled me to undertake this PhD, and for conveying a passion for science that has only grown with time.

AUTHOR'S DECLARATION

I declare that the work in this dissertation was carried out in accordance with the requirements of the University's Regulations and Code of Practice for Research Degree Programmes and that it has not been submitted for any other academic award. Except where indicated by specific reference in the text, the work is the candidate's own work. Work done in collaboration with, or with the assistance of, others, is indicated as such. Any views expressed in the dissertation are those of the author.

SIGNED: ..... DATE: .....

TABLE OF CONTENTS

List of Figures

CHAPTER 1

INTRODUCTION & LITERATURE REVIEW

1.1 The Origins of Life

Living cells are perceived as the universal organisational biological unit [1]. Protocells, the simplest examples of autonomous cell-like structures, have been studied for decades [2].

There is much interest in the development of these primitive cells, resulting from Oparins now widely accepted proposal that life developed from simple non-living molecules into living cells by a gradual, spontaneous, and some may say inevitable, increase in molecular complexity [3]. After all, the molecules of complex life obey the simple rules of chemistry and physics. Therefore, it is commonly understood that small non-living components, so called prebiotic building blocks, are likely to have assembled spontaneously to create the more complicated living cells that are commonplace today.

It is widely accepted that there was once the existence of the last universal common ancestor (LUCA), of which subsequent generations were able to diverge genetically from [4, 5]. LUCA is thought to be one of the earliest examples of a living organism, providing enough basic capability for survival that all of the diverse populations that exist today were able to evolve from this one genetic point. If the genetic make-up or functional components, of LUCA could be derived, this would provide great insight into the origins of life on Earth, and the knowledge as to how living systems developed from prebiotic environments [6–11]. The specificity of interactions between the prebiotic components are the driving force in the assembly of cell precursors [12] and are discussed in more detail later in the introduction.

1.2 Protocells

Investigations into protocellular systems have three main goals; the construction of artificial cell-like systems, the production of biotechnological solutions [13] and the ability to better understand the origins of life. It is hoped that research in this sector will elucidate solutions in areas as diverse as fuel production, vaccines, pharmaceuticals, water purification, food production and computation [14]. In order for creative and directed design to be possible, an understanding of the components and processes involved is essential [15], alongside a need to recognise the requirements for cell viability.

1.2.1 Protocellular Requirements

To define the requirements for protocell construction, it is essential to determine which aspects of cellular processes are fundamental to life. However, it should be considered that not all parameters for life would be essential in a protocell - for example an ability to move, perhaps to escape from a dangerous or toxic environment. The requirements for a minimal protocell can therefore only include those processes which allow for survival and autonomy, compared to an inclusion of all the requirements for a true living cell. Commonly, it is thought that the ideal protocell should be capable of autonomy and evolution [1], which would be provided by the organisation of cellular components and, in very simple cells, the physiochemical conditions of the environment [3]. The cell must have a capacity to store information so that any newly developed characteristics, such as progression in the complexity of the entity, are passed on to future generations [16]. Five main essential processes have therefore been identified replication, metabolism, membrane uptake, growth and division [3, 17].

Replication allows for chemical systems to reproduce themselves. The process involves energy, so it follows that at least a basic form of metabolism is required. This metabolism also requires active chemical molecules which must be contained in a store until required, or freely available from the environment [16]. Whilst the ability to produce a new generation of cells may not be immediately obvious as essential if the cell is long-living, it becomes clear that it is a requirement if any evolvability is to be incorporated. In complicated biological systems, replication is the process where genetic material encoding the structure and function of a cell is copied. In a protocellular context, it can be defined as the action of reproducing an entity that is the same or (if evolved) enhanced, compared to the original. Due to the need for associated metabolism and any other essential properties of the parent cell, these reproduced protocells must also contain the same machinery and functional molecules in order to allow further cycles of replication. Replication must occur by growth and division of the existing cell for this reason. Simply assembling the same components again would not convey any evolved ability. Growth can also be useful for system adaptability. Division is particularly of importance in the replication and subsequent separation of any coded information. Metabolism may also refer to the movement

of active molecules and substrates between compartments and even other cells, which is useful when evolving protocell populations. A metabolism is the driving force in a cell which forces it into a non-equilibrium system allowing cellular components to be built and maintained. It also provides the energy source that is required for cell growth and division [18]. Enzyme catalysed reactions also play a part in all these processes, alongside their function in environmental signalling and response. The uptake of membrane in a cell controls the movement of substrates into and out of a compartment. Often the membranes of cells allow passive diffusion of some small ions but prevent large macromolecular entry unless specifically desired. The membrane can provide a method of actively controlling the contents of a cell by allowing selective sequestration based on molecular properties such as size and charge, and assisting in the removal of waste products [19].

These processes comprises only a small subset of the processes that occur in a canonical cell however, a high level of nanoscale co-ordination is required to achieve even these [17]. Specifically, a minimal cell would require the machinery for replication, transcription and translation and a genome encoding for these [20]. Additionally, all components would need to be able to interact through spontaneous self-organisation [3] forming a cell capable of sensing, signalling and environmental recognition [17]. Most protocells aim to encapsulate components within biologically-relevant water filled lumen, in order to act as simple synthetic cell models [21]. Additionally, further complexity to form hybrid protocells allows for chemical enrichment and spatial organisation [21].

Other schools of thought suggest that whilst membrane replication and metabolism are universal for living cells, they may not be essential in the construction of protocells. Metabolism, for example, is not necessary if permeable building blocks are used instead. This removes the need for membrane replication, as without metabolism there is not necessarily a need for a physical membrane barrier. Compartmentalisation may instead be described as the boundary created by a chemical barrier or component difference between two regions difference. Systems such as the coacervates, discussed later, therefore have an important role to play. They demonstrate that the act of compartmentalisation is essential, rather than the physical presence of a membrane [3]. A cell must be able to separate its internal contents from its environment, in order to achieve molecular crowding and therefore essential substrate interactions [22], through the confinement of pre-existing architectures in the system [23]. It is also necessary for spatiotemporal control, the required concentration gradients and the separation of components that are incompatible with one another [14]. The selective accumulation of molecules, whilst still allowing for the transfer of material, is a requirement that has to be met [17]. Without compartmentalisation and selective accumulation, the protocell would be unable to evolve [24].

Biological systems commonly display compartmentalisation in a huge variety of processes, demonstrating the importance of this factor in cell integrity [25]. For example, the cell membrane is responsible for containing all of the interior machinery whilst still allowing for interaction with

the environment outside the cell. Within the cell, there are further membrane-bound components, such as the nucleus, mitochondria and chloroplasts in plants. Each of these houses a separate function of the cell, maintaining output individually whilst interacting with the cell as a whole. These structures separate their contents from the environment, protecting the stability of the pathways involved without inhibiting their function or ability to adapt to the external environment inside the cell. Even within the nucleus further compartmentation is seen. The nucleolus resides inside as a membrane-free region responsible for the production of ribosomes. This interior is rich in nucleic acids and proteins, and is similar in properties to the phase separated coacervates mentioned as an alternative to membrane bound compartmentalisation. In fact, the nucleolar structure has been described as liquid-like with a porous framework capable of up-taking macromolecular species from the nucleoplasm [26, 27]. However, even in this well-studied example, the method by which this compartment is produced is still poorly understood [28, 29]. It is clear however, that compartments are essential for the transport and storage of biochemical molecules.

As mentioned, accumulated regions of molecules and concentration gradients are required. These are possible only with a compartmentalised system. Biological systems generally display internal cellular regions containing large volume fractions of macromolecules, in a phenomenon known as molecular crowding [30]. One such example is that of granules, which are locally concentrated protein-rich bodies that spontaneously assemble into liquid-liquid structures [31, 32]. These further highlight the importance of systems like the coacervates.

Although not discussed in detail here, there are also secondary processes that could be useful in a protocellular system, although not essential. These may involve the machinery required to adapt to environmental changes via a series of reactions involving molecular recognition, sensing and signalling. Homeostasis may also be considered to be important in some examples [3]. This allows for a mechanism where waste can be removed from the cell and desired molecules are absorbed in their place. Active molecules could also be recycled through this methodology. [33–35]

When considering the desired properties of a new protocellular system it is important to distinguish between the successful outcomes of a protocellular solution. It is clear that protocells may be developed to be self-maintaining, self-propagating or evolvable, depending on the desired outcome. It is also clear that it is not the inclusion of a single process that is important, but the interplay between related processes. The joining of some complicated processes, such as the replication of an internal component with the reproduction of a membrane, would represent huge advances in protocellular engineering [3].

1.3 Top-Down and Bottom-Up Approaches

Research to date in this area has generally been divided into two classes [36]: top down methods which aim to define the minimal requirements for cellular vitality, and bottom up methods which aim to chemically create cellular machinery from smaller components [37]. The latter is based on the knowledge that biology may be very complex but, as discussed previously, is comprised of much more simple molecules. These are governed by their physical properties which lead to self-assembly and the ability to participate in metabolism or to carry genetic information. Both methods have successfully validated protocell construction but have their own associated advantages and disadvantages.

Top-down methods have been utilised to produce minimal genomes and complete protocellular computation [38]. These include studies, such as those by Hutchinson *et al*., into the minimal genome of *Mycoplasma genetalium*; the smallest of any independently replicating cell [39], and those by Mushegian and Koonin to compare the genomes of a range of pre-sequenced gram positive and gram negative bacteria [40]. Additionally, Francois and Hakim modelled an evolutionary procedure to create small gene networks including switches and oscillators [41] and You *et al*. demonstrated programmed population dynamics in *Escherichia coli* controlled by the manipulation of cell-cell communication by coupling gene expression with cell survival [42]. The top-down method was also later employed by Venter and his team to produce the worlds first self-replicating synthetic cell from a manufactured DNA copy of the *Mycoplasma mycoides* genome transplanted into a *Mycoplasma capricolum* cell [43]. This recently culminated in the production of JCVI-Syn3.0, a minimal synthetic genome to demonstrate what is thought to be the essential genes required for life (although progress may still be made to reduce this genome further) [44].

Bottom up approaches have been utilised more widely than their top down counterparts, as they hold diverse potential to produce different structures and outcomes from a multitude of combinations of simple toolkit chemicals [45]. The methodology relies on the self=assembly of simple molecules that when combined have a higher order of structural complexity. Their combination may also give rise to new properties and influence their uptake and use in a protocellular system. Additionally, the outcomes of these experiments are generally easy to predict, as top down methods require an in-depth biochemical understanding of the large numbers of processes and components involved within a system and this is not always readily accessible [34]. Bottom up methods are also advantageous in terms of cost, efficiency of scale and low toxicity and avoid many safety and ethical concerns that would otherwise be encountered [15].

1.4 Lipid-Based Systems

Traditionally, lipid-based systems using phospholipid or fatty acid vesicles have been used as protocellular models due to their similarity to the evolved systems found in nature, and therefore

their biological relevance. Lipid vesicles are commonly thought to be an important intermediate from pre-biotic molecules to life due to the presence of their encapsulating membrane [46–49]. Predominately, bottom up approaches have made use of fatty acids, which avoid the problems associated with the complexity of phospholipids; their low nutrient permeability and their low aqueous solubility [3, 14]. These are produced via polyketide synthesis and are formed from an extended carbon chain, which can be partially unsaturated, and a carboxylic head group. These are found within phospholipids and triglycerides, which are common in biological systems.

Whilst phospholipids are widely used naturally, they have been suggested to be too complicated, and not dynamic enough for protocell construction [50]. Fatty acids have been shown to mediate exclusion and uptake of molecules, allow for fusion and growth via induction by salts, and allow small molecule division and macromolecule encapsulation. They also fulfil protocellular requirements by being integral in membrane mediated pH gradients and cell growth and division [51]. Their ability to uptake small molecules including nucelotides and amino acids has been widely studied [52–55]. This uptake is mediated by the simple processes of concentration gradients and passive diffusion. This results in a system which does not uptake unwanted species and inhibits uptake of functional components such as DNA, RNA or proteins, due to their size, structure and ionic nature [56, 57].

Hanczyc *et al.* converted fatty acid micelles to vesicles using montmorillonite clay minerals with adsorbed RNA [58]. Mavelli and Luisi furthered the production of minimal replicating cells [59] by modelling the outcomes of self-assembling vesicles to determine their method of evolution. Photochemical reactions have also been used to spontaneously convert surfactant molecules into vesicles [60] and to convert anchored decanoic acid bilayers into vesicles using ruthenium catalysis [61]. To a similar purpose, Chen and Szostak have conducted kinetic studies into the growth of fatty acid vesicles, showing that fatty acids spontaneously form predictable structures according to the pH of the surrounding aqueous medium [62], and that encapsulated dipeptide catalysis can be used to grow vesicles by amphiphile recruitment [14]. Other researchers have shown the de-novo generation of synthetic lipid membranes [63] and functional genetic expressions within liposomes: for example producing T7 RNA polymerase and GFP in a controlled sequence [64]. Ribosomal synthesis of polypeptides within lipid vesicles has also been demonstrated [65]. The latter can be compared with the similar research done in phospholipid vesicles encapsulating cell free expression systems [66]. Large unilamellar vesicles [15] have also been shown to be extremely important. In a totally synthetic manner, metabolism has also been initiated within lipid bound systems using feedstock complex carbohydrates and utilising the formase reaction to initiate a bioluminescent quorum sensing response in marine bacteria [67]. Once again, this demonstrates the potential of pursuing non-canonical paths.

Higher order complexity has also been demonstrated. Aqueous two-phase systems have been used to generate internal compartments which show selective protein localisation and phase transfer between compartments [68, 69]. Vesicle budding and the division of the protocells into

daughter cells with different phase compositions, and thereby evolved daughter populations has also been shown [70, 71]. Self-assembling nanostructured hydrogels within a phospholipid vesicle have demonstrated a mimic of a cell cytoskeleton [72] and Krishna Kumar *et al*. additionally showed the attachment of external nanoparticle motors to allow these vesicles to transport themselves [73]. Multi-compartment vesicles with enzymatic pathways linked by α-haemolysin pores have also been shown. These utilise a signal cascade, comprising several stages, beginning with a lactose substrate and culminating in the fluorescence of resorufin. Each enzyme stage was compartmentalised by spatial containment of the catalyst [13].

However, lipid-based systems have many associated problems and therefore other methods are also of importance. The fatty acids inhibit the function of some key enzymes and additionally are unstable when excess free cations are available [14]. The membrane is highly impermeable to small molecules, which restricts the entry of new reactants preventing continuously developing systems [21]. There are also restrictions due to the osmotic pressure of the system [21], for example increases in component concentration causes disruption of the lipid membrane [74]. Furthermore, the inner compartment does not resemble cytoplasm, but instead is the same composition as that of the surrounding environment [74]. Whilst there is an instinctive desire to mimic cells as we know them today, it is important to note that there may be other, more successful or useful pathways that can be followed instead [20]. Furthermore, fatty acid vesicles are sensitive to changes in pH, ionic strength, multivalent cation concentration and temperature [21]. The development of the non lipid-based systems discussed in the next section has therefore been a useful complementary tool in the exploration of protocellular systems [21].

1.5 Non Lipid-Based Systems

A widely used method for the construction of non-lipid based systems is using emulsion based protocols where liquid-liquid interfaces, normally water-oil interfaces, are stabilised with the spontaneous addition of other macromolecules, both natural and synthetic. Here, the difference between the hydrophobicity of the two components is exploited [75].

These alternative approaches have included self-assembling peptide cages (SAGES), balls composed of heterodimeric and homotrimeric coiled coils that can be used as constructs for protocell assembly [76] and hydrogel capsules [77]. DNA microchips are another option [78], where individual two dimensional compartments have been set up to carry out metabolism, protein synthesis and communication through the use of adhered double stranded DNA brushes which interacted with mobile cell extract, showing that oscillations and pulses of gene expression could be achieved [78]. The icosahedral structures formed by bacterial encapsulins can act as confinement systems for internal reactions [14] and biochemical oscillators have been incorporated into microemulsion droplets [79].

Water-in-oil droplets have been stabilised by the addition of a templated polyelectrolyte shell

[75]. Negatively charged agarose located in the water phase solidifies when the temperature is reduced, providing a solid sphere on which to adhere the positively charged polyelectrolyte. The authors referred to this system as gel-shell beads. DNA responsible for the production of phosphotriesterase, an enzyme that hydrolyses pesticides and nerve gas to safe components, was encapsulated and evolved within each bead . Successful outcomes were identified through the production of a fluorescent hydrolysed product, which were then screened by fluorescence assisted cell sorting (FACS). Mutants that operated at twenty times the original turnover speed were elucidated after just one hour, proving that protocell systems could be used for ultrahigh throughput directed evolution. However, any genotypic change must have an easily identifiable phenotypic change, in this case fluorescence. To further the utility of this system, the polyelectrolyte complex could be removed by deprotonation of the positively charged groups, by increasing the pH to 12, leading to disassembly from a reduction in electrostatic interactions [75].

The most commonly used alternatives, colloidosomes, polymersomes, proteinosomes and coacervates, are discussed in more depth in the next sections due to their relevance in this project. With the exception of coacervates and the other liquid-liquid phase separated systems, these structures are all often constructed with complicated or multi-step syntheses. They also often require the use of specialist equipment such as microfluidics [80]. This is a drawback when compared to facile systems, despite their advantages and importance in protocellular engineering. Furthermore, complicated synthetic approaches mean that the degree of flexibility of the final protocell is limited.

1.5.1 Colloidosomes

Colloidosomes are constructed with a water-oil interface, with droplets of one phase suspended within the other phase and stabilised by partially hydrophobic inorganic nanoparticles at the interface [21]. Colloidosomes are typically in the range of tens of micrometres in diameter and are also known as Pickering emulsions [21, 81]. The system is driven by a drive to reduce total free energy of the system, by localising the solid particles at the interface [21]. A variety of solid particles can be used as the stabilising agent, with inorganic particles such as silica [82, 83], clays [84] and calcium carbonate [85] all previously demonstrated [86]. Oxides [87–90], gold particles [91], and polyoxometalate organic hybrid particles have also been shown to be effective. The solid particles form a monolayer and, due to their geometry, pores are formed at the junctions between particles [21]. Pore size is controllable to some degree, as the size and shape of the solid particle can be adjusted [92] and the solid particles can be cross-linked together, which also allows transfer to a water environment. However, it is difficult to design a system that completely excludes small molecules as these can easily diffuse through the interface boundary particles [93].

More complicated colloidosomes have been developed to counter some of the difficulties of using

these systems as protocells. Environmental dependent cross-linkers can be used to create pores that allow selective gating of macromolecules [21], for example those dependent on pH [81, 94]. Other colloidosomes have been created that can swell and de-swell as a result of changes in the temperature of the system [95, 96]. One major limitation of most protocell systems is the lack of growth and division that natural cells undergo frequently, which allows them to evolve. However, a few colloidosomes systems have demonstrated the possibility of this. One such system is that by Li *et al*. [97]. Here, organosilane initiated methanol formation within the droplets caused swelling and subsequent rupture at a single weaker location, which then developed into a bud. This underwent growth and separation to form second generation colloidosomes. Both protocells were stabilised at the interface by further adsorption of excess silica nanoparticles in the oil phase [97].

1.5.2 Proteinosomes

Proteinosomes are similar to colloidosomes but instead of nanoparticles, protein-polymer globular nanoconjugates are used [21]. Generally, the globular protein is used in place of the nanoparticle, and this has three or more polymer molecules attached to enable crosslinking [21]. As with the colloidosomes, this allows transfer to produce water droplets in a water environment. The resulting droplets are on the micrometre scale, have a close-packed monolayer membrane and have controllable structure and function, according to the building blocks selected. The membrane of proteinosomes has been shown to be elastic and able to withstand shrinkage and rehydration, as well as remaining intact at temperatures as high as 70 °C for as long as 90 minutes [21]. Similar to colloidosomes, the membrane is semipermeable and stimuli responsive, but has the added advantage that the protein component can be enzymes, and these maintain their enzymatic activity even after cross-linking [98]. More complicated systems have also been demonstrated, such as the proteinosome by Huang *et al*. [99]. This produces internal hydrogel filaments that penetrate the membrane, leading to an additional membrane akin to a bacterial cell wall/ cell membrane mimic [99]. Controlled disassembly of the system can also occur with protease degradation, producing a release mechanism for encapsulated contents.

1.5.3 Polymersomes

Polymersomes are another form of protocells which use amphiphilic block copolymer alignment at the interface to make a membrane [21, 71]. These systems are the most similar to lipid-based systems in that they have a hydrophobic region, attached to a hydrophilic region, and can spontaneously self-arrange to point outwards of a phase separated droplet to form a boundary [100–102]. Tri-block copolymers can also be used for more complicated architectures. The block copolymer stabilised droplets are more stable than their lipid counterparts and can be composed of a large number of modular building blocks, making their chemistry appropriate to function [103–107].

The depth of the membrane can be controlled, and pores can also be introduced to make them semi-permeable. Channel proteins can be reconstituted into the synthetic membranes without loss of function, allowing pore size and selectivity to be controllable [104]. Stimuli responsive block copolymers can also be used as a method of introducing pores, to dissemble the protocell, or to modulate the internal environment to initiate or terminate reactions within the protocell [105]. Due to the variety of possible building blocks available, polymersomes are also good model systems for studying the behaviour of membrane proteins. The variety of options for each block region allows the properties of the final block co-polymer to mimic that of a biological double-layered membrane and infer the correct spacing between layers.

Polymersomes have been used to address several of the limitations in the other types of protocell, such as a lack of deviation from spherical shapes and internal compartmentalisation. Block copolymer blocks undergo temperature dependent transitions, which can be useful to address these restrictions. These were exploited by Wilson *et al*. in a poly(ethylene glycol) - polystyrene block copolymer membrane whereby the polystyrene block transitioned from a rubbery state to glassy state and this transition constrained the previously spherical droplet to a bowl shape [108, 109]. Changes in the cross-linking of the block copolymers can also have an effect on membrane, and therefore droplet, shape [110]. Internal compartments have been generated with polymersome-in-polymersome architectures, formed using emulsion and centrifugation [111] In this case, a three-component enzyme cascade was shown to be effective across compartments [111]. Liposomes have also been encapsulated inside polymersomes using a layer-by-layer formation technique [107].

1.5.4 Coacervates and Other Aqueous Phase Separated Systems

Whilst all the protocells mentioned have their advantages, aqueous liquid-liquid phase separations become particularly interesting when dealing with biological systems, as they are compatible with the storage and handling of biomacromolecules such as lipids and proteins. In other systems, these are easily oxidised or denatured causing loss of function. Additionally, as these phase separations occur spontaneously, the use of harmful or difficult chemicals, such as organic solvents, is avoided in the preparation, making them particularly advantageous over other synthetic protocellular systems . [63]

In nature, water-water liquid phase separations exist as a method of concentrating internal components and spatially organising different reactions. Membrane-less organelles have been shown in the cytoplasm of germ granules [31], inside nucleoli [112], and the ribonucleoprotein granules [113]. The ribonucleolar protein TDP43, for example, has been shown to cause the formation of vacuoles within the nucleolus through a very precise conserved sequence in the intrinsically disordered region of the protein. These vacuoles are micron sized, show coalescence behaviour, and contain components from the nucleoplasm [114]. Similar results have also been

observed previously with "fused in sarcoma" proteins [114].

Research suggests that compartments formed by liquid-liquid phase separation may also have been important in early cell evolution. These organelles are distinct in composition from the surrounding cytoplasm [115]. Synthetically, water-water phase separations can be utilised to form protocells or protocellular compartments. These can be in the form of complex coacervates, discussed here, or the aqueous two-phase systems discussed in more detail later in chapter 4.

Coacervates are growing in interest for their ability to act as protocells without possessing a membrane. Selective sequestration of other molecules, leading to enhanced enzymatic rates [116], makes them ideal candidates to fulfil many of the requirements of protocells, such as compartmentalisation and metabolic reactions, regardless of the lack of a membrane. They present an interesting solution to the problem of over- complicated protocellular models and are therefore a main focus of this research.

Coacervates were first mentioned by Tiebackx in his German paper [117] and then named by Bungenberg *et al*. after studies on flocculation with gelatin particles in 1929 [118]. In this paper it was determined that coacervation and flocculation are related phenomena with both requiring removal of stabilisation factors, charges and hydration [118]. However, in flocculation the dispersed particles form solid aggregates whereas in coacervation they present as a liquid droplet containing both solutes and also water. This water is not miscible with the large mass of surrounding water [118]. Put simply ,the coacervate phase is liquid as opposed to solid, and is formed through de-solvation that results in some retention of solvent as opposed to complete de-solvation. Coacervates are different to ionic liquids, which are continuous liquid phases of ionic organic molecules in ambient conditions and then absence of solvent [119].

The molecular interactions involved in the formation of coacervates are covered in more detail in Chapter 2,but rely on the relationship between the solubility of the free molecular species and the solubility of and bound molecules. This can seem trivial but in a system such as this, which contains water and therefore solvation interactions, it is actually quite complicated. Interactions between water and organic molecules and hydrophobic interactions all play a part [120, 121]. Molecular weight of the components is also a consideration.

A coacervate can be formed form a single species in solution by an alteration of the environmental conditions, such as pH, temperature or salt concentration. Alternatively, the solubility of the species can be manipulated by addition of another miscible component to induce phase separation. Coacervates have been produced in this way using gelatin, which can be induced to coacervate with the addition of sodium sulphate or through the addition of ethanol [122, 123]. Synthetic polyzwitterionic and polyampholytic molecules also show temperature and salt=induced coacervation [124]. All of these factors can force changes in the structure of the macromolecule, reducing its solubility and thereby reducing the entropic state of the system as a whole. When solvent is not added, coacervation occurs by polymer de-mixing. This is a phenomenon whereby

the poorly solvated macromolecule transfers into a condensed phase so non-solvent/solute interactions are reduced [124].

Due to their simplicity and properties, Oparin first suggested the potential of the coacervates as a protocellular containment system in the 1960s [125]. However, aqueous phase separations do have some limitations. With other protocells, it is possible to adhere nanoparticles and macromolecules at the interface, which decreases the free energy of the interface leading to increased stability [63]. This was illustrated with the proteinosomes and colloidosomes discussed in the last section. The boundary between the phases in water-water separations has very low interfacial tension, from 10^{-7} to 10^{-4} Nm^{-1} [126]. If one phase is suspended as droplets within the other phase, such is the case with coacervate droplets, this low tension limits the ability to stabilise the droplets to coalescence by the addition of particles at the interface. Macromolecules are able to adhere in some circumstances but tend to dynamically adsorb and detach, preventing a complete boundary from forming [63].

1.5.5 Complex Coacervates

Complex coacervates, referred to from this point only as coacervates, are most often formed when stoichiometric combinations of oppositely charged components are mixed [21, 50, 125]. This aggregation causes the formation of a meta-stable colloidal cluster with low solubility [118]. A membrane free, highly charged matrices in the form of droplets is produced. With coacervates, the droplet phase is rich in components, with the droplets suspended in a component deficient phase [127, 128]. These droplets can readily coalesce to form two continuous phases, but can be stabilised to some extent by altering the ratio of components leading to excess repulsive surface charge at the interface of the droplets [129]. The chemical structure of the components and the environmental conditions also play a part in particular pH as the charges must be ionised correctly in order to interact. As explained with simple coacervation, phase separation is driven entropically, although the electrostatic matching and hydrogen-bonding interactions also play a part [130]. Formation is dependent on the mixing ratios of the components, the total polymer concentrations, pH and temperature. Salt concentration is also highly important as the critical salt concentration required to form the coacervate is related to the number of possible ion pairs between the components and the charge density and screening of ionic groups [131].

Previously, the constituent components have included proteins, nucleic acids, polysaccharides, polyelectrolytes and mixtures of peptides and ribonucleotides with low molecular masses [116]. Frequently, polyvalent macromolecular species are used they possess strong non-covalent interactions. Their high molecular weight also assists with de-solvation and therefore phase separation [132–134, 134]. This observation can be exemplified with the case of high molecular weight PDDA (200 kDa) and BSA (67 kDa). This is especially relevant here as the experiments in this thesis use PDDA in coacervate construction. At the start, a small soluble aggregate is formed

which then grows through the formation of interchain charge interactions. Eventually complete de-solvation occurs and a coacervate solution is formed [135]. The internal structure of coacervate droplets has also been widely studied, although much is still as yet unknown. This is mainly due to the limitations of experimental equipment capable of determining the structure. For the PDDA: BSA system, a few models have been proposed [136]. One is that the coacervate phase consists of regions of high density with greater viscosity, accompanied by fluid-like, less viscous regions. Another is that the coacervate matrix is a network of polymer chains, with BSA concentrated in some regions and acting as a bridge conveying interchain connectivity. Experiments so far have indicated that structure may be a combination of both of these models, or as yet undescribed phenomenon. However, rheology has demonstrated that the coacervate is dynamic with some degree of internal polymer chain motion, mostly due to the transient behaviour of non-covalent interactions [137]. The high viscosity of the bulk coacervate phase has also been attributed to the strength of electrostatic interactions between polymer chains, with rheological properties indicating some nanoscopic internal structure. These hypotheses will have greater relevance when discussing internal compartmentation within a coacervate droplet, later in Chapters 3 and 4.

Advantages of a coacervate system include the fact that molecules are selectively sequestered into the droplet interior [116], due to its low dielectric constant [51], without compromising their thermodynamic stability or structural integrity. This induces enriched compartmentalised systems where enzymatic rates are consequently enhanced due to their increased concentrations and reduced diffusion distances [116]. Coacervates are prepared by a facile procedure involving simple mixing of components and these components can be selected from a huge range in order to control the properties of the droplet [51]. Varieties of coacervates have also been shown to be stable between a wide range of pHs (pH 2 to pH 10) and also temperatures up to 85 °C [50]. The fact that coacervates, despite their simplicity, can still spatially organise macromolecules also has interesting implications in origin of life studies, when constructed with biologically relevant components. As mentioned before, it is also interesting that they are found in biological organisation and have successfully been retained even in current cell structures. Furthermore, in contrast to the lipid based systems, coacervates can form from early, biologically relevant, simple components [138].

Coacervates have previously been constructed with biological macromoelcules including polysaccharides and proteins. Specific examples include anionic gum arabic which forms coacervates when combined with cationic chitosan [139]. Gum arabic, along with xanthan gum and agar have also been combined with whey protein, pea protein isolate and gelatin to produce coacervates [137, 140, 141]. Work has also been carried out to explore the potential of creating coacervates with functional molecules as part of the structure of the matrix. This has involved the use of enzymes such as alcohol dehydrogenase and trypsin, showing that activity can be maintained even after coacervation [142]. Di-block copolymers with at least one charged block section have been

combined with oppositely charge species and in one case, the resulting coacervate was used as the inner compartment of a polymer stabilised micellar particle [143, 144]. This latter research exemplifies the move to design more hybrid, higher-order coacervate structures.

Finally, a few examples of PDDA coacervate systems are shown, for their relevance in the work in this thesis. PDDA is a polyelectrolyte formed from quaternary amine groups that therefore has a single positive charge per monomer unit. With PDDA, the charge spacing allows for counter-ion binding which in turn screens the electrostatic repulsions that otherwise exist between monomer units [145]. PDDA has been used in conjunction with proteins such as bovine serum albumin and ribonuclease. It can also be combined with small molecules like ATP [123, 136, 146–150], as used in this manuscript.

1.5.6 Higher-Order Hybrid Coacervates

Some researchers have found ways to circumvent the difficulties of membrane formation on coacervates, allowing the phase separated droplets to be used as a template by which an interface is formed. The emulsions have been used to generate biomimetic templates for hydrogel synthesis [63] and to generate cell matrix mimics [151]. Protein nanofibrils have been used to develop cross-linked networks at the transition between bulk coacervate and surrounding supernatant, producing fibrillosomes, which continue to exist stably even in the absence of the interface [63]. This was demonstrated with the growth of amyloid nanofibrils in PEG dextran emulsions, initiated by heating at 60 °C. The process took several days but generated fibrils with average thicknesses of 15 nm and lengths of 600 nm. The tunability of these fibril properties also allowed the capsule produced to have controllable properties [63]. Where macromolecular adherence has been possible, it has been shown that the diameter must be more than 130 to 170 nm in order to generate absorption energies large enough to overcome the Brownian motion displacing the particles [152]. β-lactoglobulin protein and PEGylated phospholipids have been shown to adhere in this way [153]. In addition to particle size, the shape is also important for membrane coverage. Near spherical shapes only allow 20-40 % coverage at the interface, even if there are enough molecules present to sit in a close packed arrangement [63].

Partitioning 8-anilionapthalene sulphonate (ANS) at high concentrations into ATP oligolysine coacervates showed that an ANS-rich membrane could be formed at the interface [154]. Inorganic membranes can also be formed by the addition of poly-anionic phosphotungstate to the poly-cationic polymer of the coacervate. In this case, the coacervate also underwent internal rearrangement, resulting in a three-tier structure. This comprised the phosphotungstate-polyelectrolyte membrane, beneath which occurred a coacervate layer made of the original components of polyelectrolyte and ATP. In the centre was a water-filled lumen. Proteins in these protocells were protected from proteases and were shown to be capable of involvement in two enzyme cascade reactions [155].

Finally, fatty acid membranes have also been assembled at the interface of RNA oligolysine coacervate droplets, creating a system with some similarities to the traditional fatty-acid based protocells [155]. The coacervates were stabilised and no longer coalesced, and selective uptake of macromolecules was demonstrated in [156]. The internal coacervate could be disassembled, leaving a hollow interior, showing a potentially useful method of generating fatty acid membranes that could be preferable to that used to generate vesicles conventionally.

Internal compartments in coacervates have also been formed by electrostatically overcharging a polylysine RNA coacervate system with excess RNA [113]. The internal disassembly of the coacervate complex caused the formation of vacuoles inside the droplets. This was done via a two-step process whereby the polymer component condensed, followed by a subsequent decondensation. Droplet shrinkage occurred as a first step, followed by the formation of vacuoles which then coalesced until they came into contact with the interface, at which point they were ejected. The vacuoles could be stabilised to a small extent by using intermediate concentrations of RNA. The coacervate was subsequently used to contain a transcription reaction which produced the excess RNA in-situ.

Similarly, electrostatic interference has been demonstrated by localising polylysine DNA coacervates in the presence of an electric field [157]. At low electric field strength, no vacuoles were seen to form but as the field strength was increased to 30 to 40 $V.cm^{-1}$, vacuoles appeared and disappeared in a cyclical manner, as the electric field caused dissociation of ions. Due to osmotic pressure differences as a result of the local ion concentration increases, external phase components were driven into the vacuoles. The vacuoles were mainly observed in the polylysine domains as this is the larger molecule, is comprised of un-neutralised loops and has a higher ionic concentration. The water internalised in the vacuoles did not mix with the coacervate phase.

1.6 A Comparison of Protocells

It is clear that there are a large variety of protocellular options and, considering the environment and purpose of the desired system, that some may be better suited than others. Within the lipid based systems, those with phospholipids were shown to have low nutrient solubility and low aqueous solubility. Fatty acid based systems could be used to circumvent some of the associated issues and showed good fusion and growth capability. They were also good at excluding molecules that should not be involved in processes in the interior. However, these systems also have limitations. They inhibit the functional of useful enzymes in the interior and the impermeability may not always be an advantage if there is a requirement to introduce new molecules to the interior. Furthermore, these systems are very sensitive to pH, the ionic strength of the environment (i.e. the presence of excess free cations), and temperature can also be an issue. With the non lipid based systems there were four main protocells discussed; colloidosomes, proteinosomes, polymersomes and coacervates. The colloidosome systems also displayed growth and division

potential, and the pore size of the membrane could be adjusted or responsive to environmental stimuli. However, a drawback is that they are impossible to design to that small easily diffusible molecules are excluded. Proteinosomes function similarly but have the advantages of an elastic membrane and can be stimuli responsive as well. They also have been shown to be stable, even at higher temperatures. On the other hand, they retain the problem of easy diffusion of small molecules which could be quite inhibitive. Polymersomes represented an advantage compared to lipid systems, for use with similar construction ideas. They are more stable than their lipid counterparts, and provide the option for a large number of modular building blocks. Pores can be introduced as desired and, excitingly, droplet shape changes can also be induced. Finally, the coacervate systems were discussed. These have the advantage of no membrane so are very simple in comparison to the other systems and can be prepared in a one step spontaneous process. However, the main disadvantages of this system is that without a membrane it is very sensitive to pH, salt and temperature disruption. On the other hand, it does not involve the use of harmful or difficult chemicals, and exhibits selective sequestration properties. It has also been shown that coacervates may have played a role int he origins of life so for this reason they are very interesting, if constructed with biologically-relevant components.

1.7 Overview of the Thesis

It has been shown that whilst there are a large number of options for the construction of protocells, these have many associated limitations. The rules governing complex structure formation in bottom-up research are still poorly understood when multiple components are combined. Additionally, many of the systems do not allow for even the basic selection of processes that have been deemed essential for autonomy. Of particular interest in this research is the design of higher-order hybrid coacervates to overcome some of these issues. The coacervate system has been selected as the protocell model for its simplicity and ease of construction. Here, an ATP: PDDA system is used as this is well-characterised in comparison to other systems and was previously demonstrated to be stable and allows for biologically-based interior reactions to take place.

Chapter 2 first presents all of the materials and experimental methodologies used to produce the research described here. It also contains an explanation of the interactions that govern coacervate formation and behaviour, allowing for a better concept of the experiment design that is explored. A brief introduction to each piece of equipment is also included, so that experimentation is aided by an understanding of equipment parameters and optimisation of samples.

Chapters 3, 4 and 5 form the experimental section of this thesis, focusing on the construction of hybrid protocells with higher order properties. Chapters 4 and 5 concentrate on the development of internal sub-structure within the cocaervate droplets and Chapter 5 begins to investigate the possibilities of adding membranes that are additionally functional and capable of signal

transduction. Specifically, Chapter 3 contains the characterisation of the ATP:PDDA coacervate system to investigate the dynamics and stability of the system as a base protocell from which to add further functionality. It then goes on to observe the effects of small molecules on the system, specifically experimenting with negatively charged DNA and the neutral molecule tetraethylene glycol (TEG). Larger molecules such as dextran, of a variety of molecular weights, and proteins are also considered. Finally the chapter concludes by investigating the movement of molecules between mixed populations of coacervates (containing differently tagged single stranded DNA), to determine if they are suitable storage compartments.

Chapter 4 explores a new system of complementation in the coacervate interior, based on the findings of Chapter 3. It utilises functional systems with multiple components in a move to enhance the complexity of the system developed here. Specifically, the compartment produced inside coacervates with the addition of TEG is further enhanced by the creation of an aqueous two-phase system inside the droplets with the addition of dextran alongside the TEG. This allows for the creation of a storage system which can be utilised with the addition of enzymes to break down the confined dextran. The novel system is fully characterised and compared to the TEG-only system of compartmentation.

Chapter 5 begins to investigate another topic of protocellular requirements; that of a membrane. Although coacervates do not require a membrane for some simple processes, this addition allows for higher-order functionality. The macromolecular interaction observations previously discussed in the earlier chapters aid the addition of macromolecules to the coacervate bulk/supernatant interface. This is shown to be successful with some block copolymers. The block copolymers are then used to template the addition of purple membrane flakes and some early research is conducted into the light-driven proton pumping behaviour of this new membrane. Finally, the TEG and dextran systems described in Chapters 3 and 4 are introduced to this membrane coated coacervate system, demonstrating the options for further research.

CHAPTER 2

GENERAL METHODS

This chapter presents all of the materials and experimental methodologies used to produce the research described here. It also contains an explanation of the interactions that govern coacervate formation and behaviour, allowing for a better concept of the experiment design that is explored. A brief introduction to each piece of equipment is also included, so that experimentation is aided by an understanding of equipment parameters and optimisation of samples.

2.1 The Molecular Interactions Involved In Coacervate Formation

As stated in the introduction (Chapter 1), an understanding of the intermolecular interactions at play are fundamental for the formation of coacervates. This elucidates information such as why simple molecules can spontaneously assemble to form biologically relevant components under equilibrium conditions [158]. With macromolecules, these interactions are based on their physical properties, such as molecular weight, polymerisation degree, structure and monomer distribution, all of which contribute to the strength of their chemical interaction potential.

In coacervation, polyelectrolytes are often employed as constituent components. These are polymers that have a permanent charge, irrespective of pH. For these molecules, the charge separation along the polymer is defined in terms of the Bjerrum length, which is the distance at which the electrostatic repulsion contribution between two points is equal to kT (the Boltzmann constant multiplied by the temperature). If the distance between point charges is less than kT, repulsions between the charges will be dominant which favours interactions between the polymers and any counterions. [159] It is also important to consider the behaviour of these polymers in solution. The Flory-Huggins theory states that for a polymer in solution, the magnitude of the

mixing entropy decreases as the degree of polymerisation increases. The overall polymer/solvent interactions relative to the solvent/solvent interactions and the interpolymer interactions can be described using the Flory interaction parameter. Solubility is dictated by the relationship between mixing entropy and the enthalpic barrier that must be overcome. Ultimately phase separation will occur if there are strong polymer-polymer interactions or weak polymer-solvent interactions. Covalent bonds can be formed in short-range interactions and are extremely strong. However long-range electrostatic interactions can be as strong as covalent interactions. Electrostatic interactions between point charges is commonly used as a method by which to assemble materials, often in an irreversible manner due to the strength of interaction [160]. Charged species will also interact with polar molecules such as water, which is important in biological systems. Another type of interaction is that of Van der Waals forces. These are present between all molecules, including those without charge, but the strength of interactions decreases rapidly with distance. The interactions can be divided into three categories, Keesom forces, Debye forces and London forces. The first encompasses those between permanent diploes, the second between dipoles and induced dipoles and the last between non-polar molecules with temporary dipoles.

In the case of coacervation, hydrogen bonding and hydrophobic interactions are very important contributions. In hydrogen bonding, an acceptor hydrogen atom that is connected to an electronegative atom, for example oxygen, interacts with an electronegative atom with a lone pair. The bond that is formed is highly directional. Hydrogen bonds are responsible for many biological features including protein structure and polysaccharide cohesive forces [161, 162]. Hydrophobic interactions are related and form due to the extensive hydrogen bonding between water molecules in solution [120, 121, 163]. It is believed to arise entropically, due to the dynamic rearrangement of the hydrogen bonds in solutions of hydrophobic moieties leading to the rearrangement of hydrophobic groups so that they are shielded together.

2.2 General Experimental Information

2.2.1 Experimental Conditions

All experiments were performed at room temperature and pressure unless otherwise stated. Distilled water was obtained from a Merck Millipore water MilliQ Elix Integral 3 water purification system, with a resistivity of 18.2 MΩ.

2.2.2 Materials

Unless specified otherwise, all chemicals were purchased from Sigma Aldrich. Coacervate components of ATP disodium salt hydrate and PDDA (from Polysciences, in liquid form) were prepared as stock solutions at 50 mM and pH adjusted to pH 8 with aliquots of 0.1 M sodium hydroxide or 0.1 M hydrochloric acid. Both these stock solutions were stored in the freezer and defrosted

immediately before use. The sodium hydroxide and sodium chloride for pH adjustment were also purchased from Sigma Aldrich as a liquid and solid solution respectively. Stock solutions were made as 1 M solutions in water. For salt disruption experiments, sodium hydroxide was used at a concentration of 10 mM unless a higher concentration is specified.

Dextran-FITC of a range of molecular weights were used throughout. These were 20 mg/mL stocks of 4 kDa, 4.4 kDa, 10 kDa, 20 kDa, 40 kDa, 70 kDa, 150 kDa, 200 kDa and 2000 kDa. Dextran-RITC of molecular weight 70 kDa was also used at a stock concentration of 20 mg/mL. CmDextran of 70 kDa was also used at this stock concentration. These were all made up with water and then stored at 4 °C in the fridge.

A wide range of other sequestered molecules were used in these experiments and the excitation and emission data for the fluorescent molecules are given in Section 2.1.3. The DNA oligomers were purchased from Eurofins Genomics as a custom order, with and without the attachment of fluorescent cy5 and fluorescein. Tetra(ethylene) glycol (TEG) was used as purchased, as a 100 % (w/v) solution, as was PEG 600. PEG 300 was obtained as a solid and dissolved to a 100 % (w/v) solution in water. RITC and FITC were acquired as a solid and made up as stock solutions in water which were stored in the fridge. Alkaline phosphatase, horseradish perioxidase, cytochrome C, lysozyme, myoglobin, carbonic anhydrase and BSA were also used in sequestration studies. Purple membrane flakes were kindly donated by Dr Hampp at the University of Marburg and stored in solid form in the dark at room temperature, according to the supplier instructions. To determine the location of coacervate components, ATP was doped with 2,3-O-(2,4,6-trinitrophenyl) ATP at a doping level of 1:2 and PDDA was doped with PDDA-RITC, at a doping level of 1:10. PDDA-RITC was kindly synthesised and donated by Sam Briggs at the University of Bristol.

For the enzyme cascade experiments, dextranase, maltase, o-phenylenediamine (OPD), glucose oxidase, Amplex red and glucose were purchased from Sigma Aldrich. Isomaltase was obtained from Megazyme and purified according to the manufacturers advice. For the membrane studies, stock solutions of sodium oleate were made up at pH 9, with sodium hydroxide and hydrochloric acid adjustment, to ensure the oleate was not forming micelles. BODIPY-FL was dissolved in chloroform. These were stored in the -20 °C freezer.

For the block copolymer experiments, Poloxamer-188 and Pluronic F-127 solutions were used as provided by the manufacturer. The same was true for Pluronic 31R1 and Pluronic L121 although these were obtained from BASF. The Nile Red used for imaging the locations of these was obtained as a solid and dissolved in acetone. Pyranine was made up in ethanol and used at the concentrations specified in individual experiments.

When buffers were required, sodium bicarbonate buffer was produced from 0.5 M sodium bicarbonate and 0.5 M sodium carbonate. Alternatively, phosphate buffer was used in some cases and this was made up to 50 mL in water after the combination of 2.68 g of disodium phosphate

and 1.38 g monosodium phosphate. Both buffers were pH adjusted with sodium hydroxide and hydrochloric acid solutions to the correct pH.

2.2.3 Dye Properties

Figure 2.1 shows the excitation and emission properties of fluorescent molecules used in this research.

	Acridine Orange	BODIPY-FL	Calcein	FITC	Fluorescein	GFP	Hoechst	Kiton Red	mCherry	Methylene Blue	Nile Red	Rhodamine 6G
Peak Excitation (nm)	502	503	496	490	494	498	352	565	587	609	535	530
Peak Emission (nm)	525	512	515	525	512	509	461	586	610	688	575	566

Figure 2.1: Peak excitation and emission wavelengths of fluorescent molecules used throughout this research

2.3 Techniques

2.3.1 Spectrofluorimetry

A Horiba FluroMax 4 spectrofluorimeter was used to investigate the emission spectra of molecules sequestered in the coacervates. The spectrofluorimeter passes incident light through a sample and detects fluorescence produced by any molecules within the sample. This fluorescence is a result of electrons in a molecules being excited at specific wavelengths to a higher energy state and then dropping back down to their ground state by emitting a photon. Commonly, spectrofluorimeters have two beams of incident light; one to pass through the sample and one which passes through an attenuator in order to adjust the intensity signal to an appropriate level for the detector. These signals are then combined and analysed by a computer (Figure 2.2).

Note that the set up involves the detectors being placed at right angles to the incident light. This is to prevent the incident light from interfering with the data collection for emission. Excitation and emission ranges are selected using monochromators with diffraction gratings to ensure only wavelengths of interest are included.

In the FRET studies, the concentration of cy5 and fluorescein used on the fluorimeter was 0.1 mM. Spectrofluorimetry measurements on gels were taken using a Typhoon FLA 9500.

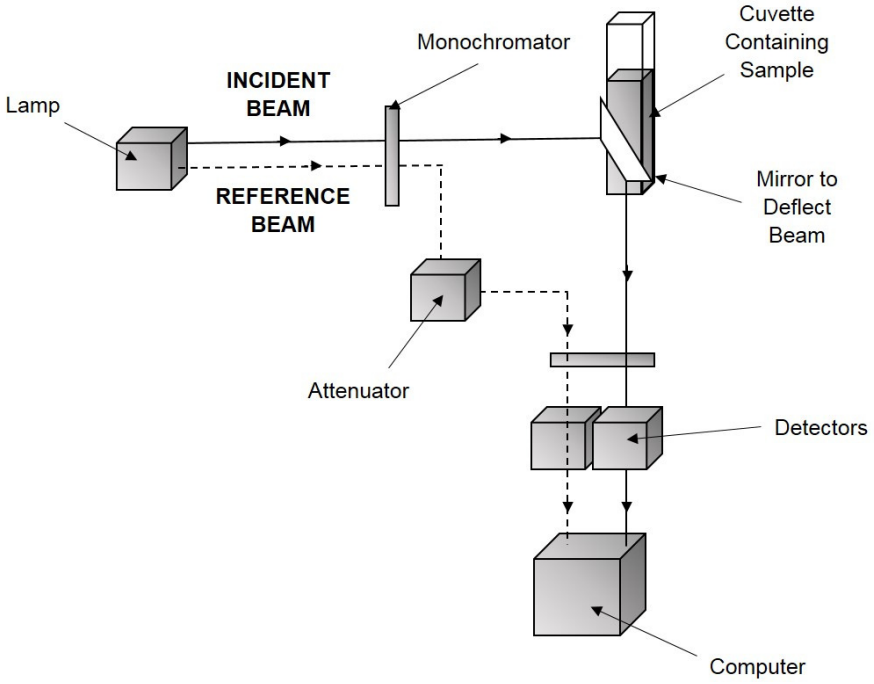

Figure 2.2: Schematic showing the set-up of a spectrofluorimeter

2.3.2 Microscopy

Fluorescence and Brightfield optical microscopy were carried out on a Leica DMI 6000 inverted epifluorescence microscope and a Leica PMI3000B Fluorescence Optical Microscope. Confocal microscopy used a Leica SP5-AOBS or Leica SP5-II confocal laser scanning microscope attached to a Leica DMI 6000 inverted epifluorescence microscope.

Optical light microscopy uses a white light source to provide illumination and optical filters to select the desired wavelength of excitation light. Light is passed through a bandpass filter and then a dichroic mirror before being focused on the sample. The emitted light from the sample is then passed back through the dichroic mirror and reflected from a prism to produce an image at an eyepiece or camera with multiple focal planes. Often the filters and dichroic mirror are combined as one piece in a filter cube [164, 165].

Widefield microscopy is very similar, however the samples are often filtered through another bandpass filter between the sample and the camera or eyepiece. Lasers with various wavelength ranges may also be used as the light source instead of white light. This allows wavelength ranges of a few nanometres rather than tens of nanometres to be selected if desired. Due to the fact that lasers produce a narrow beam, the image is produced from a scan of multiple points rather than an instant view of the entire image. This is done by collecting the photons emitted from the sample using a detector with a photomultiplier tube (PMT). The view from multiple focal planes

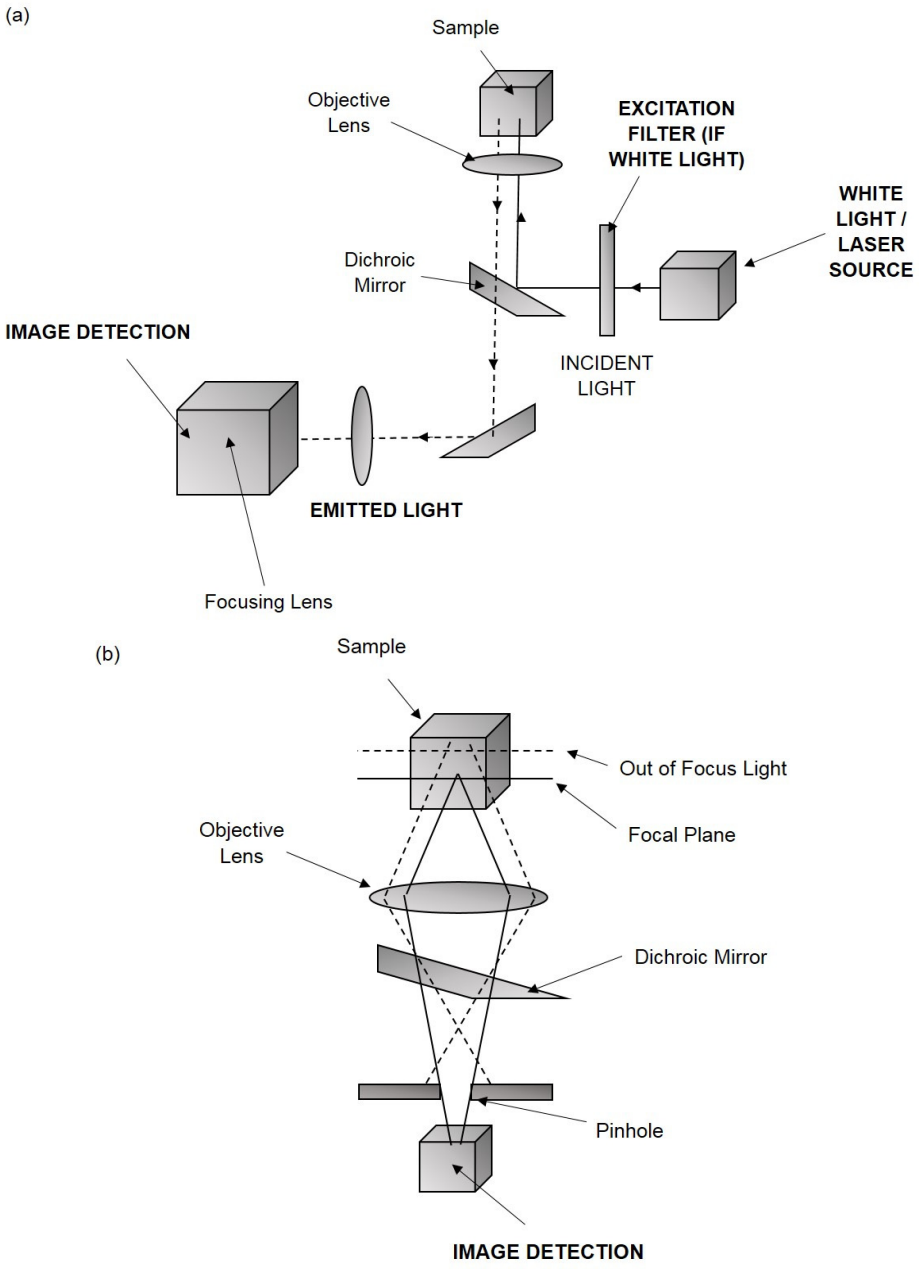

Figure 2.3: Arrangement of a Microscope. (a) Schematic of a general light microscope, (b) the pinhole arrangement of a confocal microscope. Adapted from the John Innes Centre website [166]

is collected so some objects appear in focus and others appear out of focus [164, 165].

In a confocal microscope, the main difference to a widefield microscope is that the light is focused to make a narrow beam at the appropriate z-stack position using a pinhole before the PMT (2.3). This allows imaging of a single thickness of samples rather than an amalgamation of all the focal planes. Consequently, only objects in focus are seen [164, 165].

Fluorescence microscopy was used to image the fluorescent molecules added to the coacervate systems used in this research. Specific concentrations for each experiment are given in the relevant sections. Where size analysis has been conducted, images were post-processed in ImageJ software and the sizes determined manually using the imaging software ruler. Automatic software was available. However, after investigation this was not used as it was deemed inaccurate at measuring the diameter of droplets in the coacervate populations. Sample frames showed random fields of view of the population, taken by sequentially moving across and then down the sample in the imaging dish, taking care that no fields of view overlapped or were duplicated. A droplet was selected for measurement if it was in focus in the plane that the confocal microscope had captured. Where appropriate, the mean and standard deviations of a representative population were calculated. In these cases, the population contained in excess of 800 measured droplets. Line profiles were produced and the intensities calculated with ImageJ software during post processing.

For TEG, and TEG dextran experiments time points were photographed every 1.29 seconds, the fastest possible on the equipment at the resolution required. 72 μL of coacervate was added to an imaging dish and then 5 μL of dextran added. After a minute, to give the dextran time to diffuse to the imaging location, 5 μL of TEG was added. Dextran was always added before TEG as the experiment does not work the other way around. Both additions occurred at a site distant to the location being imaged in order to avoid disruption to the droplets being observed. Individual frames of interest were then analysed and inserted into the manuscript with a time stamp attached.

For fluorescence imaging of untagged PM, an excitation 561 nm was used as this is close to the observed maximal absorption of bacteriorhodopsin. The observed emission wavelengths were set to between 600 nm and 800 nm. For the sodium oleate partitioning on the coacervates, BODIPY-FL was used to see the location of the oleic acid. This was dissolved in chloroform which may have contributed to destabilisation of the coacervates so was not ideal. All the successful samples shown in these experiments were produced by the addition of 40 μL of coacervate combined with 20 μL sodium oleate and 2 μL BODIPY-FL. Stock solutions of sodium oleate were made up at pH 9, with sodium hydroxide and hydrochloric acid adjustment, to ensure the oleate was not forming micelles. Sodium oleate was made up fresh for each experiment to avoid degradation.

Nile Red was used to visualise the location of all block copolymers via its intercalation into the hydrophobic domains. In all experiments 10 μL coacervate was added to 5 μL of Nile Red dis-

solved in acetone combined with 5 μL of block copolymer. When purple membrane flakes were also added, 10 μL of these were combined with the block copolymer before addition to the coacervates. Ratios of these components are given in figures as coacervate (mM) : block copolymer (%) : purple membrane (mg/mL). ζ-potential experiments with block copolymers were done with samples diluted to coacervate concentrations of 10 mM. When localisation of the Poloxamer-188 was examined, Poloxamer-188-Rhodamine B was both used in place of the untagged Poloxamer-188 and doped in at a 1:10 ratio.

2.3.3 Digital Holographic Microscopy

This technique works in a similar manner to traditional microscopy except that information about the light wave front is recorded as well as the intensity of the light. It can therefore be applied to any microscopy technique, but for biological systems it is most commonly used in conjunction with light microscopy. the information from the wave front is recorded as a hologram, and will also contain information about the amplitude and phase of the signal. A computer then takes this signal and converts it to an image using a pre-determined algorithm. This processing usually involves a CCD camera or similar device. Digital holographic microscopy can be used to obtain information from a sample on its three dimensional surface structure, optical thickness, amplitude, phase and polarisation. It is a particularly useful technique for the probing of biological samples as it does not involve sample staining or induce damage, allowing the sample to be imaged repeatedly over a long time frame.

2.3.4 Ultraviolet-Visible (UV-Vis) Spectroscopy

A Perkin-Elmer Lambda 25 or Perkin-Elmer Lambda 35 UV-Vis spectrophotometer was used to monitor concentrations of molecules with a distinctive absorption in the coacervates samples. Fundamentally, absorbance of molecules in a UV-Vis machine is a result of electrons absorbing energy from the incident light, between wavelengths of 190 nm to 1100 nm, so that these wavelengths are no longer emitted once it passes through the sample (Figure 2.4).

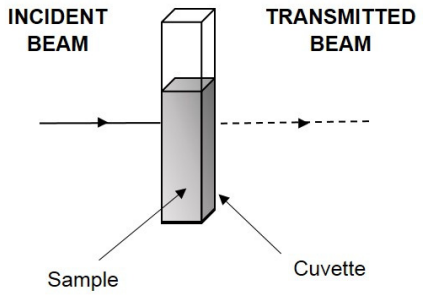

Figure 2.4: Light absorbance from a sample in a cuvette

The concentration of a molecule within a sample can then be calculated by the Beer Lambert Law,

$$A = \varepsilon c l, \tag{2.1}$$

where A is the absorbance, ε is the extinction coefficient of the molecule, c denotes the concentration of the molecule, and l is pathlength of the cuvette.

The transmittance of the incident beam through the sample is given according to

$$T = \frac{I}{I_0}, \tag{2.2}$$

where T is the transmittance, I is amount of light transmitted through the sample, and I_0 = amplitude of the incident light beam.

The absorbance (the input of the Beer-Lambert equation 2.1) is inversely proportional to the transmittance and can therefore be calculated from Equation 2.2, such that

$$A = \log_{10} \frac{I}{I_0}. \tag{2.3}$$

UV-Vis spectroscopy was also used here to monitor turbidity of samples over time by recording the absorbance of the solution at a wavelength where coacervate components had no specific absorption. For all turbidity investigations, absorption was monitored at 500 nm unless otherwise stated. It should be noted that turbidity cannot be measured directly from UV-Vis absorbance as it is measured from the scattering of light by particles and not simply by the amount of light that passes through the sample. However, the UV-Vis is a standard method of estimating turbidity in the literature so this was used to provide an appropriate approximation. Pathlengths were 1 cm in all UV-Vis spectroscopy experiments, unless otherwise specified.

UV-Vis data was collected with 1 mL samples in low volume disposable cuvettes unless specified otherwise. For partitioning experiments, DNA oligomers were added to a final concentration of 4 μm unless otherwise specified. 5 μL of sequestered molecules was added to 72 μL coacervate solution in all cases. Where the partitioning coefficient, k, is calculated, the concentration of sequestered molecule in the bulk phase is divided by the concentration in the supernatant phase. The location of coacervate components was measured by the absorbance of ATP at 260 nm. PDDA did not absorb at any region in the UV-Vis spectra.

Droplet turbidity was calculated as a function of absorbance at 500 nm where no coacervate component absorbance would occur. It was deemed that the droplets would sink faster after coalescence due to their increased size. This could therefore be used as a measure of stability

of the droplets, although it is an estimation and a means to compare samples rather than a true measure of turbidity, as it assumes all change in absorption are due to an alteration in scattering of the beam. To determine the effect of temperature on the stability of re-suspended droplets, the samples in cuvettes were first placed in the cuvette heating block of the UV-Vis spectrometer for 20 minutes in order to equilibrate to the desired temperature. Stability was then detected by loss in turbidity as previously described.

To calculate the ATP content in the supernatant before and after re-suspension, the ATP was measured by UV-Vis spectroscopy as described previously. From these values, the number of moles of ATP in each phase could be estimated using the Beer-Lambert law and the percentage of ATP in each phase could be calculated as a function of the total ATP left in the system after preparation. It was assumed that the amount of ATP removed in the re-suspension process was equal to that seen in the supernatant of the non re-suspended sample.

2.3.5 Dynamic Light Scattering (DLS) & Zeta Potential Experiments

A Malvern Zetasizer Nano ZS machine was used to measure the stability of coacervate samples via measurement of ζ-potential, the electrokinetic potential of a dispersed colloid. The ζ-potential gives a measurement of the stability of the surface because of the behaviour of ions surrounding each droplet. For each droplet, two additional layers form; a Stern layer, where ions of the opposite charge are strongly bound, and a diffuse layer, where ions are free to exchange with the rest of the medium but are attracted to the droplet [167]. This is shown in Figure 2.5 for a positively charged particle.

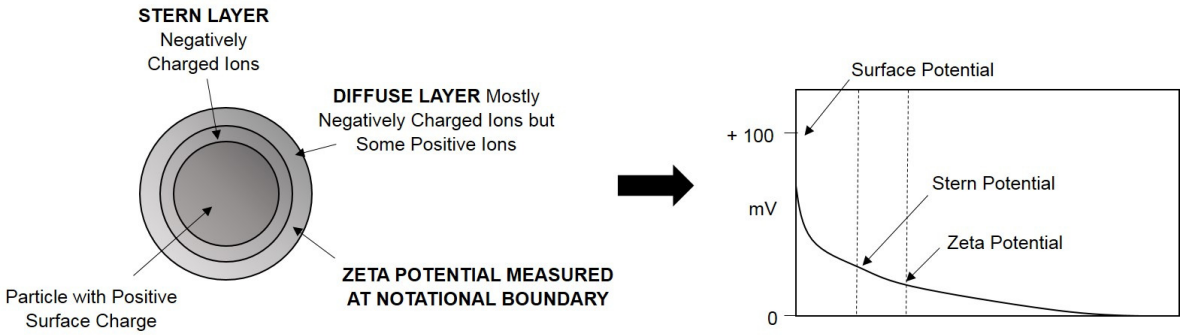

Figure 2.5: Explanation of ζ-potential. Adapted from Malvern Instruments [168]

The Stern potential is described as the potential between the particle and the stern layer, and the ζ-potential is described as the potential at a notational boundary within the diffuse layer. This boundary is defined as the surface of the particle or slipping pane, due to the fact the one side of it ions are moving relatively freely whilst on the other they are interacting strongly with the droplet surface. Due to this, the ζ-potential is dependent on both the sample and medium [167, 169].

The DVLO theory (named after Boris Derjaguin, Evert Verwey, Lev Landau, and Theodoor Overbeek) states that for colloidal stability, repulsive contributions of a droplet must outweigh attractive contributions, otherwise coalescence will occur between droplets during movement induced by Brownian motion [169]. In a coacervate droplet, the attractive contributions come from Van Der Waals interactions whereas the stronger, repulsive forces are a result of the electrically charged double layer. This is the phenomenon whereby the net charge at the particle surface causes oppositely charged ions in the surrounding solution to gather at the surface, causing an increased concentration of ions in a local area. Repulsive forces arise from a combination of factors including particle radius, solvent permeability, ionic composition and ζ-potential. Therefore ζ-potential can be used as a measurement of repulsion and consequently stability [169].

In a zetasizer, zeta potential is calculated from electrophoretic movement velocity, as charged particles are attracted to electrodes of the opposite charge. When viscous forces oppose this, an equilibrium is reached and constant velocity is obtained. It is this that gives a proportional value for the ζ-potential [169]. A schematic of the equipment for this is shown in Figure 2.6.

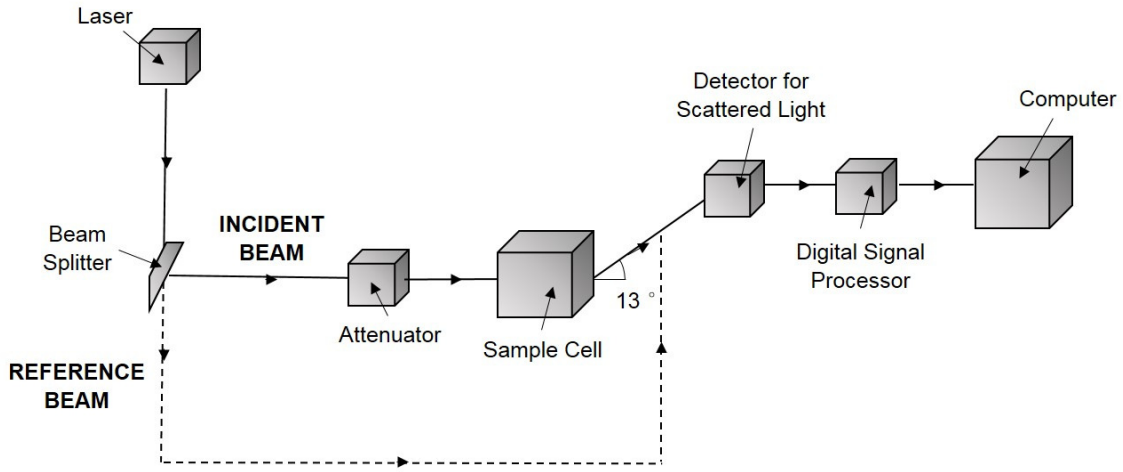

Figure 2.6: Schematic of a Zetasiser. Adapted from Malvern Instruments [169]

A laser is split into an incident beam and reference beam, and the incident beam is passed through an attenuator so that the intensity is appropriate for the device. The light then passes through a sample cell and scattered light is detected at an angle of 13 °C. An electric field is applied and any particle movement towards electrodes results in fluctuation of this signal, the frequency of which is proportional to velocity. This is then converted to electrophoretic mobility and then a ζ-potential signal via a digital signal processor and computer [169].

Resulting calculated ζ-potentials give a good impression of stability, and it is generally taken as standard that ζ-potentials around $\pm$ 30 mV indicate a stable suspension [169]. However, it is important to note for the experiments here that because ζ-potential is calculated as an overview of a population, and the coacervates produced in these experiments are a polydisperse population

which may vary between samples, higher ζ-potentials do not necessarily indicate more charged particle surfaces.

It should also be noted that ζ-potential measurements on this machine are accurate for particles larger than 0.2 μm, which made it appropriate for the samples measured here. For all ζ-potential measurements shown in this text, the samples were diluted to approximately 1 mM unless otherwise specified. Dilution was done with the appropriate coacervate supernatant to avoid affecting the ionic balance between droplet and supernatant. A disposable capillary cell was used for all measurements, and this has the advantage of taking the measurement point at a location away from the electrodes to avoid anomalies from electrolysis and air bubbles [170]. All zeta potential measurements shown in this work were conducted with 10 runs and then averaged from at least three repeats. Samples were allowed to equilibrate for 2 mins after any environmental adjustments before measurements were taken. The attenuation and beam positioning were done automatically by the pre-installed Malvern software.

2.3.6 Nuclear Magnetic Resonance (NMR) Spectroscopy

1H and 13C NMR spectroscopy measurements were performed on a 500 MHz Bruker Advance III HD 500 Cryo spectrometer. 1H NMR spectra are reported as δ in units of parts per million (ppm) relative to methanol (δ 3.30, s). Multiplicities are reported as follows: s (singlet), d (doublet), t (triplet), q (quartet), quin (quintuplet), dd (doublet of doublets), m (multiplet), and bs (broad signal). Coupling constants are reported as a J value in Hertz (Hz). The number of protons (n) for a given resonance is indicated as nH, and is based on spectral integration values. 13C NMR spectra are reported as δ in units of parts per million (ppm) relative to CD3OD (δ 49.15, septet).

2.3.7 Mass Spectrometry

High resolution mass spectrometry was carried out on a Brucker Daltonics microTOF II.

2.3.8 Refractometry

An Abbe refractometer was used to measure the refractive index of a variety of coacervate samples at 25 °C. The equipment was set up so that the samples were compressed between two highly refracting glass prisms (Figure 2.7).

The underlying prism is roughened so that the incident ray of light is dispersed and hits the interface between the prism and sample at many different angles. When the incident angle is above a certain value, total reflection occurs and no light is passed through the specimen. A dark area is seen through the eyepiece. When the incident is below the value for total reflection, light is passed through to the eyepiece, via the measuring prism and a focusing lens. Adjustment of the angle of the light allows the angle at which dark and light regions meet to be observed [171].

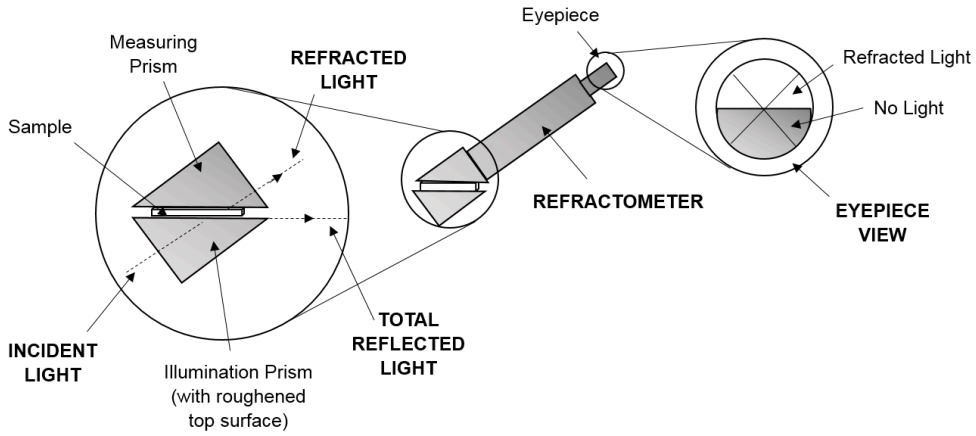

Figure 2.7: Set-up of a refractometer

This angle, known as the critical angle, allows the refractive index to be calculated from Snell's law, such as

$$\frac{sin(\alpha)}{sin(\beta)} = \frac{A}{B}, \tag{2.4}$$

where α is the incident angle, β is the refracted index, A is the refractive index of glass prism, and B is the refractive index of solution. When total reflection occurs (i.e. β = 90°), this equation can be simplified to

$$sin(\alpha) = \frac{A}{B}. \tag{2.5}$$

Therefore, the refractive index of the solution can be calculated from the refractive index of the prism divided by the incident angle, which is measured through the eyepiece. On a refractometer, the critical angle is converted into a refractive index scale on the eyepiece as well [171]. Refractive index measurements taken in this way are highly dependent on temperature changes, particularly for liquids, so this may remain constant or have a correction factor applied later. As stated previously, all samples were measured at 25 °C for this reason [171].

In experiments, 10 μL samples of known concentrations were used and the refractive index measured directly. Refractometry was also carried out in the same way on samples with different amounts of water used in the resuspension process.

2.3.9 Forster Resonance Energy Transfer (FRET)

If the excitation peaks and emission peaks of two fluorophores overlap, a phenomenon known as Förster resonance energy transfer (FRET) occurs. In this region, the energy that would be emitted as a photon from the molecule with the lower wavelength emission (the donor molecule) will instead be donated to a ground-state acceptor fluorophore - the molecule with the higher excitation wavelength (known as the acceptor molecules). Consequently the energy is converted to a higher wavelength emission. This process is non-radiative and is driven by long range dipole-dipole interactions between two molecules [172] and quantum mechanical coupling between the electronic transitions [173, 174].

The efficiency of FRET is dependent on the Förster distance which is affected by a variety of factors including orientation and the donor quantum yield. In this study, the fluorophores fluorescein and Cy5 were used for FRET investigations; their regions of overlap are shown in Figure 2.8. Fluorescein has a maximum emission of 515 nm, and overlaps with the excitation range of Cy5. Although this area of overlap is small and does not encompass the peak of Cy5 excitation, the quantum yield of fluorescein is high, enabling this to be an efficient FRET pair.

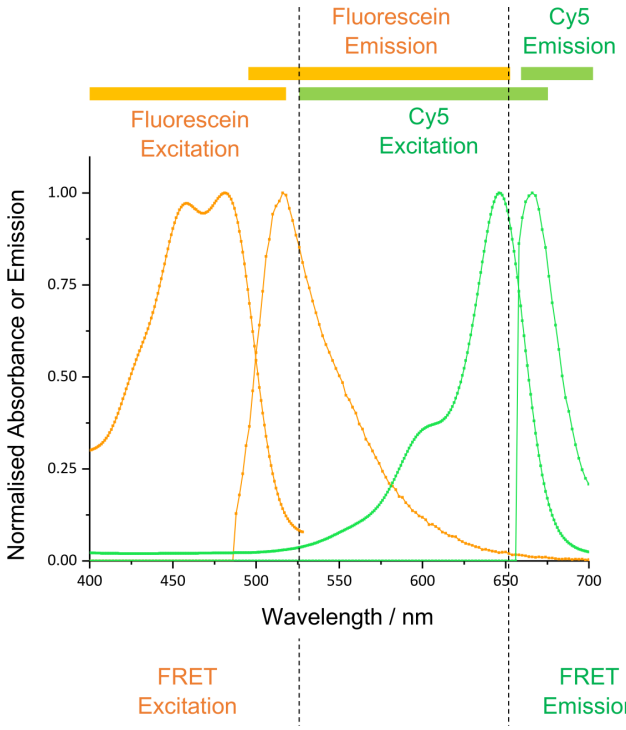

Figure 2.8: Absorption and emission spectra of fluorescein-ssDNA and cy5-ssDNA showing the spectral overlap that leads to FRET. The regions of excitation and emission for each fluorophore are represented by the appropriate colour bar at the top of the spectra. The regions of excitation and emission when FRET occurs are shown underneath the graph. The black dotted lines bound the region of spectral overlap between fluorescein emission and cy5 excitation.

In this case, the base pairing of the DNA oligomers constrains the orientation of the fluorophores with relation to one other, although there is some flexibility and other pairings can also occur. Typical Forster distances for viable FRET pairing molecules are normally in the region of twenty to sixty angstroms and the fluorescein and Cy5 pair is in the mid region of this with a Forster distance of forty-four angstroms. Forster distance is related to FRET efficiency by

$$E = \frac{R_0^6}{r^6 + R_0^6}, \tag{2.6}$$

where R_0 is distance where efficiency of FRET transfer is 50%, and r is the distance between the donor and the acceptor [164, 165]. This shows that even a small angstrom sized increase in r, the distance between two fluorophores such as fluorescein and Cy5, causes a large decrease in the efficiency of FRET and the amount of energy transfer that occurs. Here, a co-localisation of the fluorescein and Cy5 fluorophores causes a decrease in the fluorescein peak at 525 nm compared to that when in the absence of Cy5. The concentration of Cy5 and fluorescein was 0.1 mM for all measurements.

For measurement of the FRET occurance in individual coacervates, a method known as FRET-acceptor photobleaching (FRET-AP) was employed. The FRET is disrupted if the acceptor is photobleached and therefore unable to accept any transferred energy. Control experiments showed that fluorescein droplets did not display a confocal intensity signal in the Cy5 channel output and vice versa so any resulting signal could be attributed solely to the relevant fluorophore. It was also important to use a laser intensity that resulted in the smallest amount of photobleaching possible, as this limited the amount of FRET that could be observed. All gains and imaging parameters were kept consistent between experiments. Gains were set to 542 V. FRET-AP was selected as direct measurement of the increase in intensity in the cy5 region would not yield useful results, as any increase in the opposing fluorophore could be disguised by photobleaching.

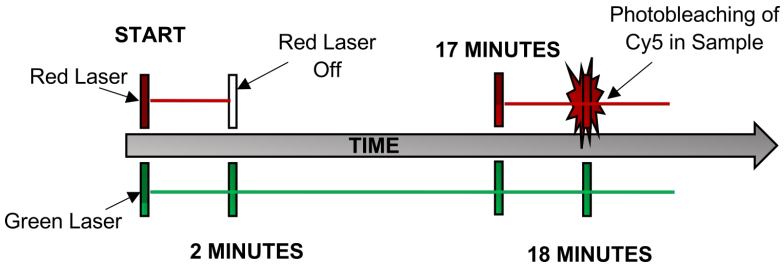

Figure 2.9: A schematic showing a summary of the methodology of FRET acceptor photobleaching (FRET-AP)

Mixed populations of droplets containing either cy5 tagged oligomers (red) or fluorescein tagged oligomers (green) were tracked and their intensity observed over time. The methodology is summarised in Figure 2.9. Laser excitations of 488 nm and 633 nm were used for fluorescein and

cy5 respectively. Emissions across wavelengths of 515 nm to 530 nm were monitored for cy5 and wavelengths of 665 nm to 690 nm for fluorescein. At time zero, both lasers were activated so a full view of droplets could be seen. At two minutes, the 633 nm laser was turned off and the droplets were imaged via only the fluorescein emission and brightfield view. This was due to an issue with the cy5 fluorophore photobleaching rapidly, making intensity measurement difficult even after short time periods if this laser was left on continuously. At seventeen minutes, the 633 nm laser was switched back on, allowing the Cy5 oligomer droplets to be seen again, alongside the fluorescein oligomer droplets. One minute later, the 633 nm laser was switched to maximum intensity and the cy5 molecules deliberately photobleached, temporarily damaging them so that they could no longer accept energy from the fluorescein molecules. Any increase in fluorescein intensity was then monitored at this cy5 photobleaching time point.

2.3.10 Atomic Force Microscopy (AFM)

Atomic force microscopy (AFM) [175] allows for horizontal and vertical picometer resolution three-dimensional surface structure imaging, by monitoring the interaction between a sharp probe and a surface [175, 176]. Resolution limits are generally dictated by the contact radius of the tip with the substrate [177]. In contact mode AFM, measurements can be observed on a force-distance curve, determined from the cantilever deflection causing a piezoelectric feedback response as the tip approaches the sample and then retracts [178]. Attractive forces cause negative cantilever deflection, with repulsive forces initiating positive deflection [179]. In tapping mode AFM, the principle is similar but the cantilever does not have continuous contact with the substrate. Measurements conducted here were done with a Bruker Peakforce Multimode 8 AFM [180]. This utilised an advanced form of tapping mode AFM that operates in a non resonant mode with oscillations below the cantilever resonance [176]. The equipment is a vertical probe microscope, whereby the cantilever rests vertically above the sample, improving the resolution of the piezoelectric detection of the cantilever deflection.

2.3.11 Transmission Electron Microscopy (TEM)

TEM builds up an image of a sample by analysing the transmitted electrons that have passed through it. These electrons are deflected or reduced in energy according to their interactions with the sample in their path, which provides information on a samples internal structure. Initially electrons are accelerated to between 60 and 120 KeV. The general set-up of a TEM can be seen in Figure 2.10. The objective lens forms an initial image or diffraction pattern which is then magnified sequentially by the intermediate and projector lenses.

TEM can be used to investigate size, shape, dispersion and aggregation properties of a substrate by utilising the high resolution and magnification available. Experiments are done under vacuum and low pressure to maximise the distance of electron travel and samples kept as thin as

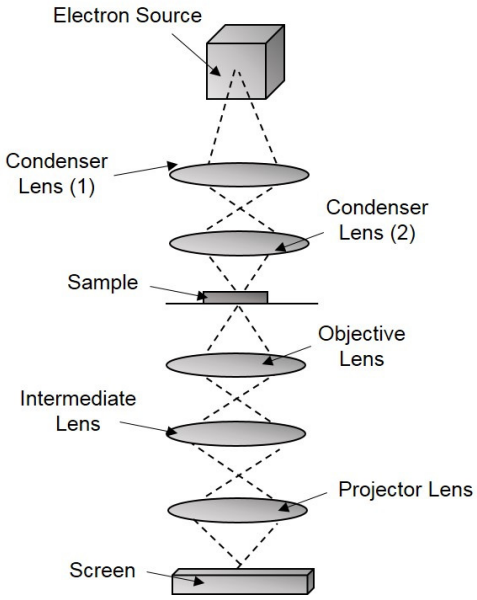

Figure 2.10: Equipment arrangement within a transmission electron microscope

possible to maximise the resolution pattern produced and minimise image blurriness.

The technique can be used to visualise biological samples, although these require preparation with staining by a heavy metal solution, as electrons interact better with elements of high atomic weight which can be viewed directly on a TEM. All samples here have therefore been stained with uranyl acetate. Samples were then drop cast onto carbon coated copper grids with filter paper used to remove excess liquid before being left to dry. Analysis was performed using a JEOL 1200 EX TEM in Brightfield mode.

2.3.12 Circular Dichroism (CD)

Circular dichroism (CD) allows for determination of protein secondary structure by utilising the fact that different chiral molecules absorb circularly polarised light differently. Anticlockwise and clockwise circularly polarised light is passed through a sample in a cuvette in turn and the difference in their absorption, resulting from the asymmetry of chiral molecules, calculated and outputted as ellipticity. To account for protein size and conformation, ellipticity is then converted to standard units to allow for comparisons between different samples. When plotted against the wavelength of light used, characteristic spectra are produced for alpha helices, beta sheets and randomly coiled proteins (Figure 2.11). Alpha helices show negative peaks at 208 nm and 222 nm and a positive peak at 193 nm, whereas beta pleated sheets show a negative peak at 218 nm and a positive peak at 193 nm. Measurements were taken on a Jasco J-1500 CD Spectrometer with a cuvette pathlength of 1 mm.

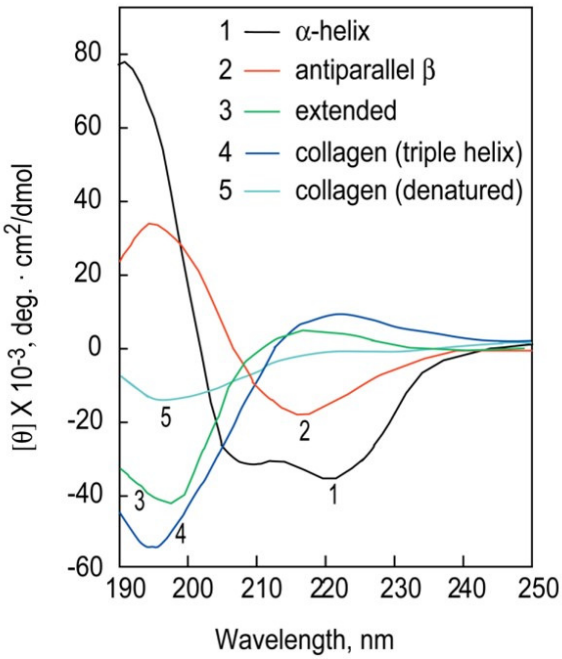

Figure 2.11: Example circular dichroism spectra, showing different representative tertiary structures. Source: N. Greenfield doi:10.1038/nprot.2006.204 [181]

2.3.13 Sodium Dodecyl Sulphate Polyacrylamide Gel Electrophoresis (SDS-PAGE)

SDS is a negatively charged detergent that is capable of denaturing proteins by forming complexes with the protein backbone. This means that regardless of secondary or tertiary structures, and of the amino acid sequence, all proteins of the same length will have a uniform charge to mass ratio when bound to SDS [182]. The proteins are then loaded into an acrylamide gel, which intrinsically contains gaps between the polymers, and connected to an electric current. Repulsion from the negative electrode causes the proteins to move along the gel proportionally to their size. Larger proteins have more difficultly passing through the mesh of the gel and travel slower than small proteins which migrate faster. The resulting bands are compared to a ladder, comprising of a mix of known and easily identifiable protein sizes.

It should be noted that proteins with a large hydrophobic content, such as membrane proteins like bacteriorhodopsin, are harder to accurately determine the weight of as the ratio of SDS to each amino acid can vary due to incomplete denaturation and retention of structure [183].

To carry out the SDS-PAGE experiments detailed here, 15 μL of sample was added to 5 μL of loading buffer and denaturised at 90 °C for five minutes. These 20 μL samples were then added to the wells in the gel and ran for forty minutes at two hundred volts. 6 μL of PageRuler was ran at either end as a molecular weight ladder comparison.

2.4 Preparatory Methodologies

2.4.1 Coacervate Preparation

2.4.1.1 Non Re-suspended

Polydiallyldimethylammonium chloride (PDDA) was purchased from Polysciences, Inc as a solution and adenosine triphosphate (ATP) disodium salt hydrate was purchased from sigma in solid form and then dissolved in milliQ water. For the coacervate preparation, stock solutions of PDDA and ATP were prepared to 50 mM. The solutions were pH adjusted to approximately pH 8.0 (± 0.1) with 1M sodium hydroxide or hydrochloric acid (purchased from BDH and Sigma respectively) as required. ATP and PDDA were then combined 1:1 molar ratio (PDDA: ATP) unless specified otherwise. They were then inverted several times to form a turbid solution. In all cases, the PDDA was added to the ATP solution. To obtain supernatant from coacervate samples, the mixture was centrifuged to induce phase separation and the supernatant phase removed by pipette. Note that with a PDDA molecule of 8500 kDa molecular weight, it is calculated that this contains 53 monomers on average.

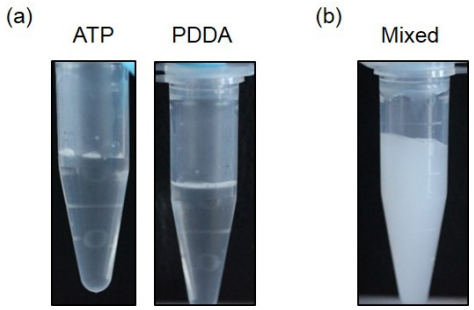

Figure 2.12: Coacervate preparation. Components shown (a) before and (b) after mixing

PDDA and ATP coacervates were chosen as the model system as these components have previously been shown to readily undergo easily identifiable coacervation via a facile procedure [116]. 100 mM concentrations of components were initially tried, in order to obtain a higher concentration of droplets, however this was unsuccessful as no coacervation occurred. This is believed to be due to the increased concentration of ATP and PDDA solutions inhibiting the molecular orientations of PDDA and ATP required for electrostatic interactions between the two to occur. Therefore, 50 mM was used for the continuation of the investigations here, as this produced a sufficient concentration of droplets for analysis.

2.4.1.2 Re-suspended

The procedure here was as described for non re-suspended coacervates with some additional steps at the end as shown in Figure 2.13. After mixing the components the coacervate solutions

were centrifuged to induce phase separation into the bulk phase, a component rich phase, and the supernatant, a component poor phase. The supernatant was then removed and replaced with milliQ water. The two phases were then integrated by re-dispersing the bulk phase for approximately ten seconds to reform droplets.

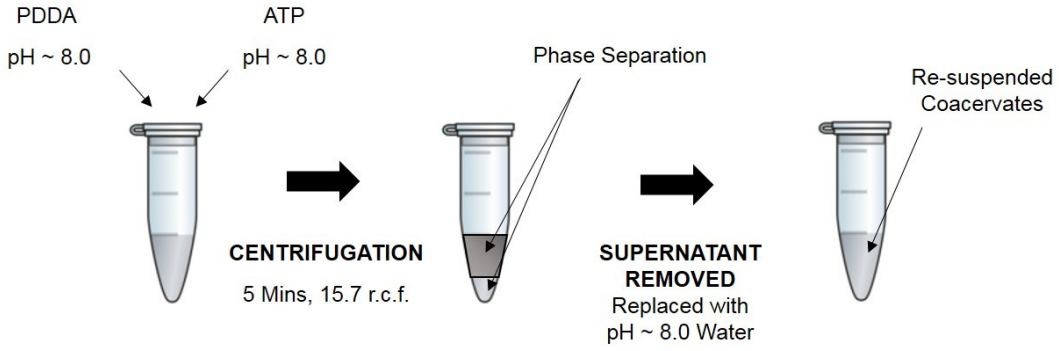

Figure 2.13: Coacervate re-suspension method. Shown schematically

2.4.2 Preparation and Imaging of TEG-induced Vacuolization in Coacervate Micro-droplets

A 72 μL aliquot of a freshly-made coacervate droplets suspension was deposited on a PEG-functionalized imaging dish (see Supplementary Methods), the coacervates droplets were allowed to settle on the slide for 1-2 min and a region was selected for imaging. Pure TEG, TEG-CH3 or H3C-TEG-CH3 (5-100 μL) was then pipetted into the supernatant solution at approximately 0.5 cm from the imaging region to minimize disruption to the droplets. Additions occurred from the same site in all experiments. Coacervate microdroplets were imaged by bright-field and confocal fluorescence microscopy on a Leica SP5-AOBS or Leica SP5-II confocal laser scanning microscope attached to a Leica DMI 6000 inverted epifluorescence microscope equipped with an oil immersion 100Œ objective lens, 1.4 NA. To observe the localization of the coacervate components, TNP-ATP was doped into ATP to a final concentration of 10 ţM and RITC-PDDA was doped into PDDA to a final concentration of 2 mg/mL. Alternatively, the localization of TEG within the coacervate micro-droplets was determined by doping TEG with FITC-TEG at a FITC-TEG:TEG volume ratio of 1:1000. Images were acquired before and after TEG addition, and fluorescence line profiles extracted using ImageJ and normalized to the highest fluorescence value. Real-time imaging of the TEG-induced coacervate restructuration was also performed after TEG injection. Analyses of the structures obtained were undertaken on images acquired 5 min after TEG addition. More precisely, the number of droplets that contained a single vacuole rather than no vacuole were counted as a percentage of the total number of droplets in the imaging region. Droplets that contained a couple of small vacuoles were counted as not having a vacuole to avoid overestimating the percentage of vacuole formation. This was

repeated on three separate samples and the results averaged. Standard deviations were used to plot the error bars. Similar experiments were repeated with tetraethylene glycol monomethyl ether (TEG-CH3) or tetraethylene glycol dimethyl ether (H3C-TEG-CH3) in place of TEG. To determine the number of vacuoles, droplets that had produced only a single vacuole once the system had reached the quasi-equilibrium were counted. These measurements are given as a percentage of the total number of droplets in the population sample. Vacuole size analysis was carried out by measuring the diameter of the vacuole, as a percentage of the diameter of the whole droplet.

2.4.3 TEG/dextran phase separation in coacervate micro-droplets

A 72 μL aliquot of freshly made coacervate droplets suspension was deposited on a PEG-functionalized imaging dish, then the droplets were allowed to settle on the slide for 1-2 min and a region was selected for imaging. 5 μL of 20 mg mL-1 dextran (70 kDa) were added to the coacervates approximately 0.5 cm away from the imaging site, followed by an aliquot of pure TEG. FITC-TEG (doped as 1:1000 (v/v) with untagged TEG) was used to identify the TEG location, and RITC-dextran (70 kDa) was used in place of non-labelled dextran to identify the location of the dextran chains. Images were acquired before and after TEG addition by bright-field and confocal fluorescence microscopy, and fluorescence line profiles extracted using ImageJ. Droplets that formed a single vacuole were calculated in the same way as previously described for TEG-only samples. Analyses were performed on three different samples, the results averaged, and the standard deviation reported.

2.4.4 The Partitioning of Coacervate Components Within the System

Unless otherwise stated, all partition co-efficients were calculated as the quantity of a component in the bulk phase of the coacervate divided by the quantity of the same component in the supernatant phase. These values are therefore unit-less.

2.4.4.1 Measurement of the Partitioning of ATP

1 mL of freshly made coacervate droplet suspensions were supplied with aliquots of pure TEG, then centrifuged (15 min, 1000 Œ g). The resulting supernatant and coacervate phases were diluted by 2 or 200, respectively, in sodium carbonate buffer (200 mM, pH 9) to reduce the amount of scattering from the coacervate microdroplets. The absorption at 280 nm of both fractions was measured on a UV-vis spectrophotometer (PerkinElmer). The absorption values were corrected by taking into account the absorption of TEG at 280 nm. For this purpose, a calibration curve of TEG absorption at 280 nm against TEG concentration was made, and the concentration of TEG in both phases (coacervate and supernatant) was determined from measurements of TEG partition coefficients at each TEG concentration by using volumes of supernatant and coacer-

vate phases of 993 μL and 7 μL, respectively. The corrected absorptions at 280 nm were used to calculate the concentration of ATP in both phases, using an extinction coefficient of 15,400 mol/L/cm. Results are reported as the percentage of the mass of ATP in the bulk phase divided by the total mass of ATP (in the bulk and supernatant phases).

2.4.4.2 Measurement of the Coacervate Water Content

1 mL of freshly made coacervate droplet suspensions were supplied with aliquots of pure TEG (equivalent to the microscopy samples), then centrifuged (15 min, 1000 Œ g) and the supernatant discarded. The remaining coacervate bulk phase was dried in an oven at 100 °C until the dry weight remained constant. The water content of the coacervate phase was calculated using the weight difference before and after drying. Measurements were repeated on three different samples, and the average value and standard deviation reported.

2.4.4.3 Measurement of the Partitioning of TEG

10 mL of freshly made coacervate droplet suspensions were supplied with aliquots of pure TEG, then centrifuged (15 min, 1000 Œ g). The resulting supernatant and coacervate phases were diluted by 2 or 200, respectively, in sodium carbonate buffer (200 mM, pH 9) to reduce the amount of scattering from the coacervate microdroplets. The absorption at 280 nm of both fractions was measured on a UV-vis spectrophotometer (PerkinElmer). Partitioning was determined as the concentration of TEG in the bulk phase divided by that in the supernatant phase.

2.4.4.4 Partitioning of Different Molecular Weight Dextran

Stock solutions of FITC-dextran of varying molecular weight (4,000-2,000,000 g/mol) were prepared in water at 20 mg/mL. A 65 μL aliquot of these solutions was added to 935 μL of freshly-made coacervate droplets suspension (final FITC-dextran concentration of 1.3 mg/mL), followed by centrifugation (15 min, 1000 Œg). The supernatant and bulk coacervate phases were separated and diluted by 2 or 200, respectively, in sodium carbonate buffer (200 mM, pH 9). UV-vis absorbance was measured in each phase at 492 nm to determine the concentration of FITC-dextran, and the partition coefficient calculated as the bulk coacervate concentration divided by the supernatant concentration.

2.4.5 Tagging Molecules As Probes

2.4.5.1 Synthesis of TEG-FITC

TEG-amine (6.6 mg, 34 μmol, 1 eq.) was added to a solution of FITC (13.4 mg, 34.3 μmol) in deuterated methanol (500 μL). The reaction was left to proceed for 48 hours and the resulting product dried under high vacuum and used without further purification.

2.4.5.2 Fluorescent Labelling of Dextranase

Dextranase was dissolved in 200 mM sodium bicarbonate buffer (pH 9) at a concentration of 6.2 mg/mL. 140 μL of a freshly-prepared 10 mg/mL solution of fluorescein isothiocyanate (FITC) in DMSO was added dropwise to 900 μL of the protein solution to reach a FITC:protein molar ratio of ca. 40:1. The reaction mixture was stirred at room temperature in the dark for 4 hours, then purified by size exclusion chromatography using a Sephadex G-25 resin (Sigma-Aldrich) eluted with Milli-Q water. Fractions were collected and freeze-dried to obtain FITC-labelled dextranase.

2.4.5.3 TEG-FITC Partitioning Compared to Untagged TEG

Although scaled up, the same ratios of coacervate:dextran:TEG were used as those in the experiments whereby 5 μL of dextran and 5 μL of TEG are added to 72 μL coacervate solution. This meant that 65 μL of dextran was added to 936 μL of coacervate, followed by 65 μL of TEG or TEG-FITC (doped 1:1000 into TEG). In samples that did not contain one or more of these components, the component was replaced by the same volume of water to maintain the overall concentration of the components included. Six vials were pre-weighed and then samples prepared as follows: (i) coacervate + untagged TEG, (ii) untagged TEG, (iii) coacervate + TEG-FITC, (iv) TEG-FITC, (v) coacervate + dextran-RITC (70 kDa) + TEG-FITC and (vi) dextran-RITC (70 kDa) + TEG-FITC. The samples were then centrifuged at 1000 rpm for 10 minutes to gently separate them into bulk coacervate and supernatant. The supernatant was carefully removed by pipetting and lyophilised to remove the water. The resulting powder was redissolved in chloroform, in which TEG is soluble but ATP and PDDA are not. The insoluble component was filtered and then chloroform evaporated from the TEG using a rotary evaporator. The vials were then re-weighed and the mass of TEG calculated.

2.4.5.4 Tagging Dextran to Proteins

The procedure to tag dextran onto BSA and myoglobin was carried out in multiple parts. The dextran monomer weight was assumed to be 161.5 Da on average. The first stage was to oxidise the dextran to dextran-aldehyde. Literature states that theoretically two moles of aldehyde dextran is produced per mole of periodate used but experimental statistics in the literature seem to suggest that this is nearer 1.5 moles produced per mole of periodate. Most protocols seem to stick to 1:2 dextran:periodate ratio but this heavily oxidises the dextran, and it was important for the experiments here that the dextran maintained its large molecular weight so that it would be excluded from the coacervate interior. Both dextran-FITC 70 kDa and 150 kDa were used.

Stage 1: Dextran Oxidation 1.24 mmoles of dextran in water (at a concentration of 33 mg/mL) is combined with a 0.05 molar equivalence of solid sodium periodate. The reaction is stirred at room temperature for 2 hours, maintaining the temperature lower than 30 °C with external cooling if necessary. Then the oxidized dextran is dialysed against water at 4 °C with 100 equiv-

alent volumes of water to remove the by-product formaldehyde. The dextran is then lyophilized to allow accurate concentration calculations for Stage 2.

Stage 2: Addition of aldehyde dextran to BSA/ myoglobin The protein is made to a concentration of 3 mg/mL (BSA) or 12 mg/mL (myoglobin) in phosphate buffer at pH 7.5. 500 μL of this is added to 22 mg of dextran aldehyde (which is a 15 times excess). 2.2 mg of solid trimethyl amino borane is then added, before the reaction is left to precede at room temperature for 26 hours. The solution is then reduced by the addition of 1 mL of sodium bicarbonate buffer at pH 8.5 containing 3 mg/mL sodium borohydride. This is done at 4 °C and is left to proceed for 30 minutes. The latter step stabilizes Schiffs bases produced in the reaction, and also reacts with any remaining aldehyde. Finally, the pH is lowered to pH 7 using hydrochloric acid in order to destroy the remaining. Dialysis is then conducted with 10 volumes of water over 48 hours.

2.4.6 Dextranase-mediated Dextran Displacement

Freshly made coacervate droplets were doped with dextranase by adding 5 μL of a 2 mg/mL stock solution of dextranase to 72 μL of coacervate droplets suspension (final concentration of dextranase 0.13 mg/mL). This aliquot was deposited on a PEG-functionalized imaging dish, then the droplets allowed to settle on the slide for 1-2 min and a region was selected for imaging. 5 μL of 20 mg/mL FITC-dextran (70 kDa) were added to the coacervates approximately 0.5 cm away from the imaging site, followed by 5 μL of pure TEG (final concentrations of dextran and TEG of 1.2 mg/mL and 6 wt%, respectively). Alternatively, to identify the localisation of dextranase, non-labelled dextran and FITC-dextranase (at 0.13 mg/mL) were used. Images were acquired by bright-field and confocal fluorescence microscopy as a function of time. Radial fluorescence profiles on an individual droplet were extracted as a function of time using ImageJ across the whole droplet. Vacuole and droplet boundaries in the fluorescent images were identified from the corresponding brightfield images.

2.4.7 Imaging

2.4.7.1 Coverslip Functionalisation

Glass is composed of silica oxide which carries a negative charge. As a result, the positive coacervate droplets wetted out when directly applied to the channel slide or imaging dish coverslips. To prevent this from occurring, the coverslips were functionalised by the addition of 2-[Methoxy (polyethyleneoxy) propyl] trimethoxysilane (PEG) side groups (from ABCR GmbH). This makes the glass slide more neutrally charged and therefore repellent, preventing wetting-out of the droplets.

The process was carried out by applying 70 % ethanol and vigorously rubbing the surface of the coverslips which exposed hydroxyl groups on the glass and removed excess grease and dirt. The coverslips were then rinsed with water and dried using a steady stream of nitrogen. The

side groups were converted to PEG groups by the addition of a mixture of 2 % PEG in toluene (v/v) so that the coverslips were completely suspended in the solution and incubated at room temperature for one hour. The coverslips were then washed with water and dried with nitrogen. Functionalised coverslips were glued onto either channel slides or petri dishes as described previously. Note that when using channel slides with functionalised coverslips, the slide is held upside-down for imaging to ensure that wetting out of the droplets does not occur on the non-functionalised glass slide.

2.4.7.2 Channel Slides

Channel slides were constructed according to Figure 2.12. A glass slide was placed horizontally then three 18 mm by 18 mm glass coverslips were glued side by side on top using number 81 UV-curing optical glue (purchased from Norland). Once the glue had reached the edge of the coverslips this was cured for a minimum of twenty minutes under a UV lamp at a wavelength 365 nm. Number 63 optical adhesive (purchased from Norland) was then added in a line either side of each gap and another two cover slips glued over the gap to create a channel. This was then cured under the UV lamp, again at 365 nm for at least twenty minutes.

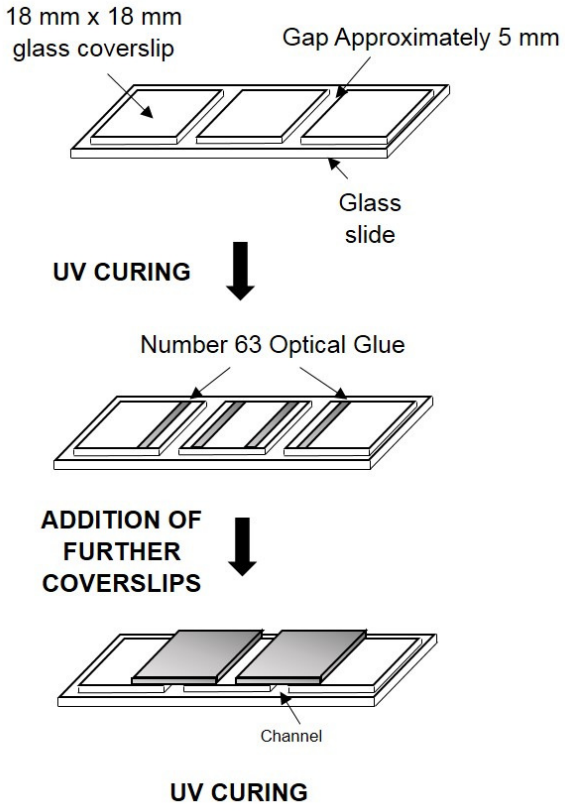

Figure 2.14: Preparation of channel slides

2.4.7.3 Dishes

Imaging dishes were prepared by using a Dremel to file a hole through the centre of small petri dish. Number 63 optical glue was then applied in a circle around the hole and an 18 mm by 18 mm coverslip affixed. The glue was then set under a UV lamp for at least twenty minutes (Figure 2.15)

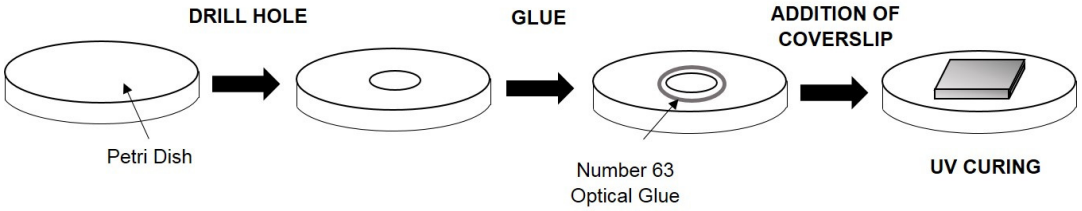

Figure 2.15: Preparation of imaging dishes

2.4.8 Phase Diagrams

In order to construct the phase diagrams, 1 mL samples of varying concentrations of TEG and dextran were produced using a TECAN Biorobot Liquid Assay robot. The stock solutions of 89% TEG and 50 mg/mL dextran-FITC were pre-adjusted to the appropriate pH with sodium hydroxide and hydrochloric acid as appropriate. They were then stored at the temperature being investigated overnight before and after preparation by the robot. Centrifugation of the resulting samples was done 24 hours later, with the system deemed to have phase separated if a fluorescent residue of dextran-FITC was seen after centrifugation.

For the partial phase diagram, 5 μL of dextran (70 kDa) were added to an imaging dish under the microscope, followed by the addition of 5 μL of TEG to reach final concentrations for dextran and TEG, respectively, of 2.9 mg/mL and 86 wt%, 0.5 mg/mL and 50 wt%, 2 mg/mL and 50 wt%, 10 mg/mL and 50 wt%, 1.2 mg/mL and 6 wt%, and 10 mg/mL and 25 wt%. A partial phase diagram was created by observing on the microscope if the samples appeared to phase separate or not after addition of TEG.

CHAPTER 3

COACERVATE CHARACTERISATION & MACROMOLECULAR UPTAKE PROPERTIES

This chapter contains the characterisation of the ATP:PDDA coacervate system to investigate the dynamics and stability of the system as a base protocell from which to add further functionality. It then goes on to observe the effects of small molecules on the system, specifically experimenting with negatively charged DNA and the neutral molecule tetraethylene glycol (TEG). Larger molecules such as dextran, of a variety of molecular weights, and proteins are also considered. Finally the chapter concludes by investigating the movement of molecules between mixed populations of coacervates (containing differently tagged single stranded DNA), to determine if they are suitable storage compartments.

3.1 Introduction

A variety of molecules have previously been shown to be sequestered into coacervates and understanding the partitioning of these molecules is crucial for the construction of protocellular systems. Particularly, with the case of the coacervates in this research, the droplets are used as containment systems in cimple mimics of biological cells, so knowledge of the partitioning and exclusion of molecules is key to the rational design of synthetic self-assembling constructs capable of higher order functionality. Additionally, the PDDA:ATP system is fully characterised so that novel systems can be developed with an advanced understanding if the behaviour of the initial coacervates.

Molecular partitioning of molecules has been particularly well studied with protein sequestration in liquid-liquid phase separated systems with observations applicable both to coacervates and systems such as the aqueous two phase separation (ATPS) discussed later in Chapter 4.

Albertson's pioneering work in this area demonstrated that the partitioning behaviour depends of hydrophobicity, molecular weight, molecular conformation and environmental factors. These may include pH, buffer components and concentrations, ionic strength, temperature and protein concentration [184], many of which are also relevant when considering synthetic molecular sequestration. Other researchers have since extensively examined the effects of salt [185], protein hydrophobicity [186, 187], and molecular weight [188] on partitioning.

3.2 Results & Discussion

3.2.0.1 Increasing Coacervate Stability

Previous experiments have shown that non re-suspended coacervate droplets will readily coalesce due to the low surface tensions at their interfaces. However, it has been previously demonstrated that coacervates can become more stable to coalescence if re-suspended (see methodology in Chapter 2). Figure 3.1 illustrates the effects of re-suspension on the PDDA:ATP system. ζ-potential measurements were used to compare non re-suspended droplets with droplets that had been re-suspended once or twice, in order to determine the optimum coacervate system for future experiments.

Non re-suspended droplets have a mean zeta potential of +20 mV, which is similar to the droplets that are re-suspended twice (Figure 3.1a). However, when the droplets are re-suspended once, this mean potential increases to +43 mV, indicating a more stable system. Whilst these coacervates are theoretically charge matched, in practice, due to the differences in size of the molecules involved, it is possible that they exist as a tangled matrix of PDDA polymer which is charge neutralized by ATP encapsulated inside that is able to interact with multiple polymers simultaneously. This could lead to a system whereby the spherical droplets are charge neutralized with slightly less ATP than calculated. It is hypothesized that increased stability of re-suspended systems occurs as a result of removal of free charged ions in the supernatant, likely ATP. Therefore, it is also possible that an excess of positively charged PDDA remains in this system leading to more positively charged droplets, as well as more stable droplets. It could be that after one re-suspension, ATP from the supernatant is removed but the droplets are mostly unchanged but that after two re-suspensions, ATP begins to be stripped from the coacervate droplets as well, leading to decreased stability. All the coacervates have a positive surface charge, although the relativity in charge between these samples cannot be determined by this method alone in a system with high polydispersity in size such as this.

Turbidity measurements were taken for coacervates that were not re-suspended and compared to coacervates that had been re-suspended once (Figure 3.1b) . As the droplets get larger and heavier, due to coalescence, they will sediment over time, falling below the beam line, and leading to a reduction in the measured absorbance and a decrease in solution turbidity. Absorbance

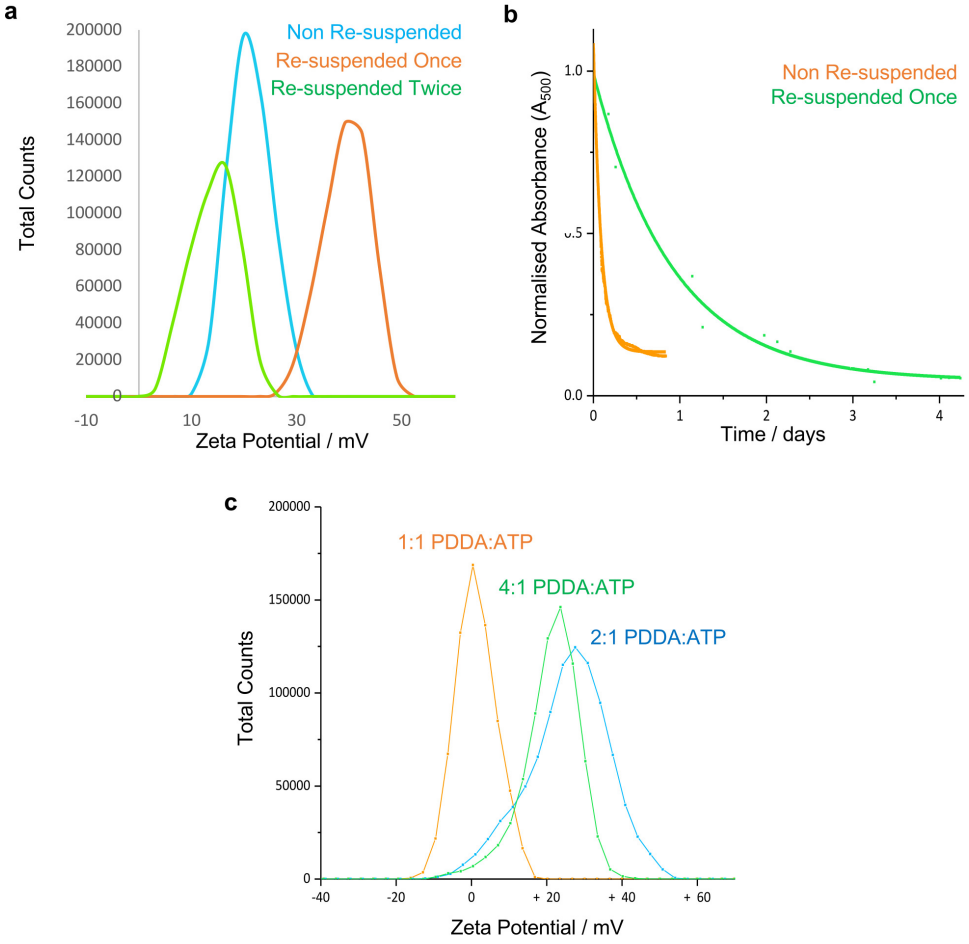

Figure 3.1: The effect of re-suspending PDDA:ATP coacervate droplets. ζ-potential measurements determining the stability and charge of a: 1:1 PDDA:ATP non re-suspended droplets compared to 1:1 PDDA:ATP coacervates that have been re-suspended one or two times. b: Turbidity measured by UV-visible absorbance at 500 nm where neither coacervate component absorbs. A loss of absorbance indicates removal of coacervates by coalescence (which leads to a larger size and therefore sinking of these droplets below the beam line). c: ζ-potential measurements of coacervates composed of different molar ratios of PDDA to ATP.

was observed at 500 nm where neither coacervate component absorbs by itself, and measurements were taken until a plateau was reached. The plateau is assumed to be the absorbance of the supernatant alone, containing components that have not formed coacervates or are not prone to sedimentation.

It is clear that the re-suspended droplets are more resistant to coalescence as they do not reach a plateau for over four days. This is compared to just under one day for the non re-suspended droplets. Additionally, the gradient of decay in absorbance is much steeper for the non-suspended droplets. These results agree with the zeta potential measurements, showing a clear difference in stability between the two methodologies. Turbidity decline in droplets that were re-suspended twice was not observed.

The effect of altering the ratio of components in coacervates that had been re-suspended once was then examined (Figure 3.1c). The ratios of PDDA to ATP were altered to produce solutions with 1:1, 2:1 and 4:1 ratios and the stability examined. The 1:1 droplets did not appear to be stable, with a mean peak value of 0 mV, whereas the the 2:1 and 4:1 droplets had mean peak values of 28 mV and 25 mV respectively. However, microscopy had shown that 1:1 re-suspended droplets were stable so these measurements were deemed to be a result of neutral charge of these droplets rather than stability.

Due to the fact that each PDDA monomeric unit carries a charge of +1 and each ATP a charge of -4, it was expected that the 1:1 and 2:1 (PDDA: ATP) ratio droplets would have a negative surface charge and the 4:1 droplets would have a neutral surface charge because the initial components had the same molar concentrations as each other. However, 2:1 and 4:1 droplets all actually had a positive surface charge and the 1:1 droplets were neutrally charged. This suggests that either the PDDA: ATP ratio within the droplets is not the same as that of the added components. Alternatively, the more negative component, the ATP, may be being shielded by the longer positive polymer, the PDDA, so that the orientation of molecules at the surface causes a surface positive charge. This demonstrates that a knowledge of the characteristics of each system can allow for tunability when other components are added. The surface charge becomes particularly important in the research encompassed in this thesis.

As previously stated, one hypothesis is that the removal of components from the supernatant and their replacement with water during the re-suspension process is responsible for the increased stability of re-suspended droplets. This is due to the decrease in free ions that would be available in the supernatant to interact with the droplets, encouraging coalescence. However another possibility could be that free ions are removed but the equilibrium of component concentrations between the bulk phase of the droplets and the supernatant then re-adjusts. This would mean that some components would be removed from the coacervates to rebalance the equilibrium between the bulk and supernatant phase (which then becomes a water phase depleted in components when replaced).

To determine whether structural changes occurred due to the change in content of the components, ATP content in the supernatant was measured using UV-Vis spectroscopy (Figure 3.2). Concentration was then calculated using the Beer Lambert law with an extinction coefficient of 15.4 x 10^3 M^{-1} for ATP at a wavelength of 260 nm. These results indicate that there is less ATP in the supernatant of re-suspended coacervates compared to non re-suspended coacervates.

Sample	A_{260}	Concentration of ATP / mM	No. of Moles ATP	Total No. of Moles Remaining	ATP In Phase / %
Non Re-suspended Supernatant	0.753	5	5 x 10^{-6}	5 x 10^{-5}	10
Non Re-suspended Bulk	-	-	4.5 x 10^{-5}		90
Re-suspended Supernatant	0.169	1	1 x 10^{-6}	4.5 x 10^{-5}	2
Re-suspended Bulk	-	-	4.4 x 10^{-5}		98

Figure 3.2: Measurement of ATP content in the bulk and supernatant phases of non re-suspended and re-suspended coacervate samples. a: UV-vis measurements of the concentration of ATP in the supernatant phases of each sample are used to calculate the approximate percentage of ATP in each phase.

Knowing that the initial concentration of ATP was 50 mM, and assuming that the amount of ATP removed from the re-suspended coacervate is similar to that remaining in the supernatant of the non re-suspended coacervate, it is possible to make an estimation of the number of moles of ATP in each system and therefore the percentage in each phase at equilibrium. Direct measurements of the bulk phase content could also be done, using salt to dissemble the coacervates so an accurate measurement can be taken. The other assumption made in this calculation was that the bulk phase is the same volume in both samples, which may not be true but is difficult to measure accurately.

The percentage of ATP that exists in the bulk phase is considerably higher for the re-suspended droplets, indicating that the re-suspension process changes the position of equilibrium between the supernatant and bulk phase, which leads to increased stability. UV-vis spectroscopy with a synthetic fluorescent PDDA could be used to determine whether the molar ratio of PDDA: ATP is still the same in the supernatant compared to within the droplets, even though the total equilibrium has shifted. This was not attempted but determination of the concentration of both molecules within the supernatant will provide an insight into the relative distribution of macromolecules within the coacervate.

Refractometry offers another method by which to determine the changes in coacervate concentration that occur during re-suspension (Figure 3.3). The refractive indices of increasing concentrations of ATP and PDDA were plotted to obtain a standard, and the green line on the plot demonstrates an estimate for a standard coacervate refractive index plot, which would lie between these. The line's exact position cannot be determined without further information

i

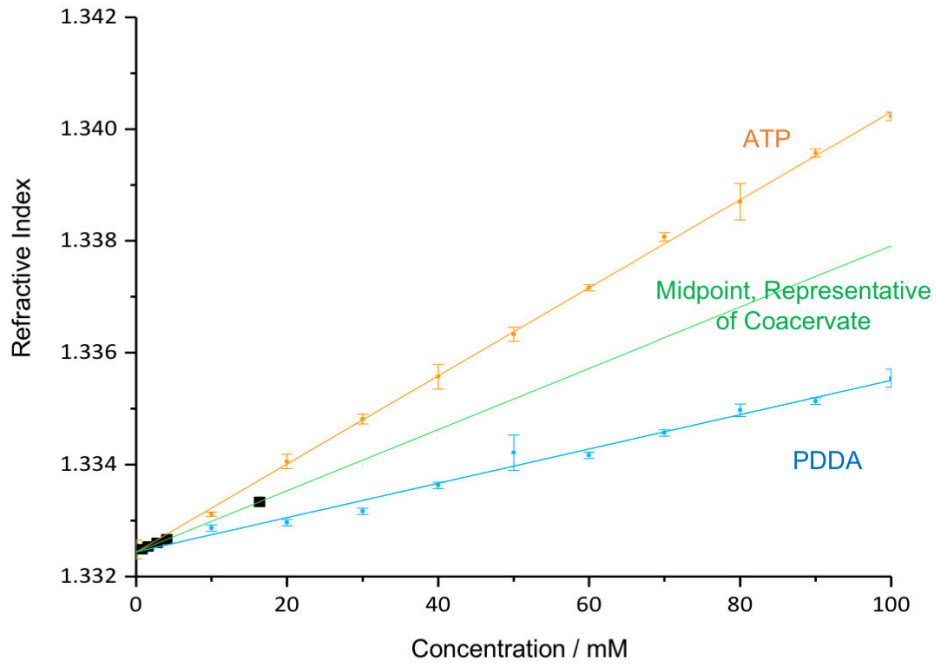

ii

Sample	Average Refractive Index	Concentration of Coacervate / mM
Re-suspended with 50% Water	1.3323	0.8
Re-suspended with 25% Water	1.3325	1.6
Re-suspended with 40% Water	1.3326	2.8
Re-suspended with 75% Water	1.3327	4.1
Non Re-suspended	1.3333	16.4

Figure 3.3: Estimation of coacervate bulk content based on the refractive index measurements of PDDA and ATP. i: Calibration plot for coacervate refractive index measurements showing the refractive indices for increasing ATP and PDDA concentrations. The black measurement points show refractive measurements for supernatant from non re-suspended and re-suspended coacervate samples. The green line shows a midpoint between the ATP and PDDA standard, representative of the coacervate refractive index estimation ii: refractive indices for the coacervate samples, alongside their estimated concentrations of coacervate.

about the ratio of ATP to PDDA within the droplet. It does however allow direct comparison between the samples, assuming that the different samples contain similar ratios of ATP to PDDA. The estimated refractive indices of several supernatant samples are shown in Figure 3.3(ii). All the supernatant was removed in all samples but the amount of water that was used in the re-suspension was varied. Percentages were determined as a fraction of the normal amount of water that would be used (the same volume as that of the removed supernatant). The refractive indices of these samples were then used to calculate the concentration of coacervate, based on their location along the green midpoint line.

It is clear that non re-suspended droplets have much higher coacervate content in the supernatant than re-suspended coacervates, as suggested with previous experiments. However, the results for re-suspending in various amounts of water are less clear as these do not follow a distinctive pattern. This suggests that the amount of water used makes little difference but the act of centrifuging the bulk and re-suspending this into droplets is what makes these re-suspended coacervates more stable. If the ratio of components in these samples could be obtained, the representative coacervate line location could be updated to provide a more conclusive set of results. However, the data so far indicates that there is not an equilibrium between the bulk and supernatant fractions that is maintained after resuspension.

3.2.0.2 Size Distribution Monodispersity From Different Re-suspension Methodologies

As demonstrated previously, one re-suspension improved the stability of the coacervates but two re-suspensions reduced the stability back to the level of non-re-suspended droplets. Therefore altering the parameters of the re-suspension process is likely to alter the properties of the droplets. It also became apparent that a more uniform size distribution of droplets would be useful, in order to make the population easier to analyze, for example with ζ-potential analysis. This would also make the concentration of any encapsulated components more consistent and the results therefore more reproducible. The re-suspension parameters were investigated with this in mind and the resulting populations were analyzed by optical microscopy to obtain mean diameters and standard deviations for the coacervates droplets (Figure 3.4).

The parameters investigated are summarised in (Figure 3.4a). These included altering the method of re-suspension, with vortexing, hand shaking and ultrasonic bath re-suspension all considered. However, the ultrasonic bath method of re-suspension was unsuccessful as bulk phase was still seen after re-suspension should have occurred. These results were therefore not investigated further or included. The amount of water in which the coacervates was re-dispersed, as a percentage of that removed, and the time taken for agitation were also explored, as was the number of times re-suspension occurred but the latter were also inconclusive.

The length of time the sample was vortexed did not appear to have an effect on the mean size

a

	Amount of Water Added / %	Agitation Method	Agitation Time / sec	Mean Diameter / µm	Standard Deviation
i	100	Vortex	10	3.0	1.9
ii	100	Vortex	30	3.1	1.9
iii	100	Shake By Hand	10	3.2	1.6
iv	100	Shake By Hand	30	3.1	1.7
v	50	Vortex	30	2.8	1.3
vi	50	Shake By Hand	30	2.7	1.3

b

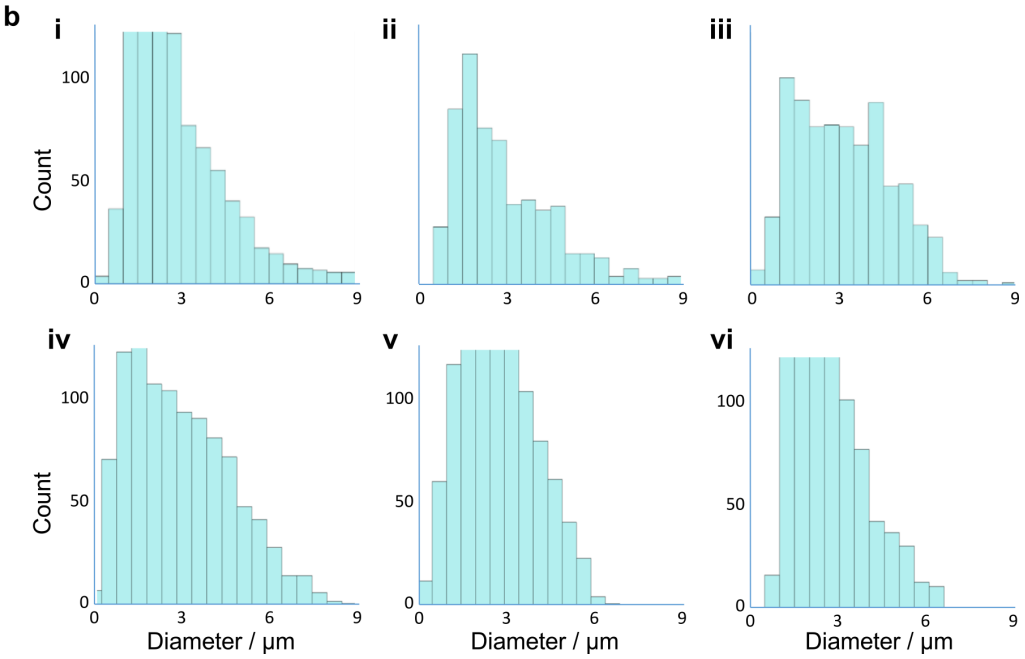

Figure 3.4: The effects on coacervate size distribution from the variance of re-suspension technique. a: A summary of the sample parameters investigated. The amount of water, the agitation method and then length of time of the agitation were all investigated. The mean diameters alongside their standard deviations have also been measured from optical micrographs and a statistically relevant number of droplets measured. b: The resulting histograms of coacervate diameter. The variations in the samples are as follows: i: 100% water replacing supernatant and vortexing for 10 seconds, ii: 100% water replacing supernatant and vortexing for 30 seconds, iii: 100% water replacing supernatant and hand-shaking for 10 seconds, iv: 100% water replacing supernatant and hand-shaking for 30 seconds, v: 50% water replacing supernatant and vortexing for 30 seconds, vi: 50% water replacing supernatant and hand-shaking for 30 seconds. Count represents the number of coacervate droplets in each diameter range.

or the distribution of sizes in the population of droplets as shown by a comparison of samples (i-ii). This is most likely due to the vigorous vortexing procedure quickly succeeding in fully re-dispersing the sample. The same was true for the agitation method of shaking by hand; a comparison between samples (iii-iv). In the samples with only 50% water added to re-disperse the bulk phase (compared to the original supernatant volume), the mean size and standard deviation of the population is decreased compared to the same procedure with 100% water ((v) and (vi) compared to (ii) and (iv), respectively). This may be due to a shift in the equilibrium between the bulk phase and the supernatant phase contents. It may be that there are less components now in the supernatant so that the equilibrium constants are similar between the 50% water addition compared to the 100% water addition. This leads to more components in the bulk comparatively, allowing smaller droplets to form and stabilise faster as more components are readily available.

ζ-potential measurements of coacervates made with the different re-suspension methods were also undertaken (Figure 3.5). This determined whether the change in methodology altered the surface properties of the coacervate droplets. The ζ-potential distribution shows that each sample where 50% water was used, has a similar mean peak position to it's equivalent sample with 100% water, indicating that the variance in amount of water doesn't affect the surface potential of the droplet. This agrees with the data obtained previously. The number of total counts is also lower in each case, likely due to the increased concentration of coacervate components in these samples. Additionally, all the peaks have similar mean peak positions illustrating once again that the method of re-suspension does not have a huge potential on the droplet properties, so long as the bulk components are effectively re-dispersed. As a point of future experimentation, it would be interesting to see the effect of using solutions other than water in the re-suspension.

Preliminary experiments were also undertaken to investigate the effect of temperature on the stability of the coacervates. The turbidity of a solution of 4:1 PDDA: ATP re-suspended coacervates was monitored at increasing temperatures from 18° C and 28° C, at wavelengths above those where the coacervate components absorbed (Figure 3.6).

At 18° C and 24° C the absorbance of the droplet, which as explained in the materials and methods section could be used as a guide to coacervate turbidity, does not change very much. However, at 28°C the absorbance of the sample is greatly reduced suggesting the coacervates are less stable at this higher temperature. This may be due to the increased energy provided to the system causing increased movement between component molecules, and breaking down the weaker electrostatic interactions holding the droplets together. Turbidity reduction could also be due to a shrinkage in coacervate droplets, as these would scatter light less. It would be interesting to compare these results with non re-suspended droplets but this was not done here. However, these results should not be taken as definitive as the same sample was used for all three measurements. Although the experiment was conducted within a time frame that would not normally show significant coacervate coalescence, it could be that the last sample measured

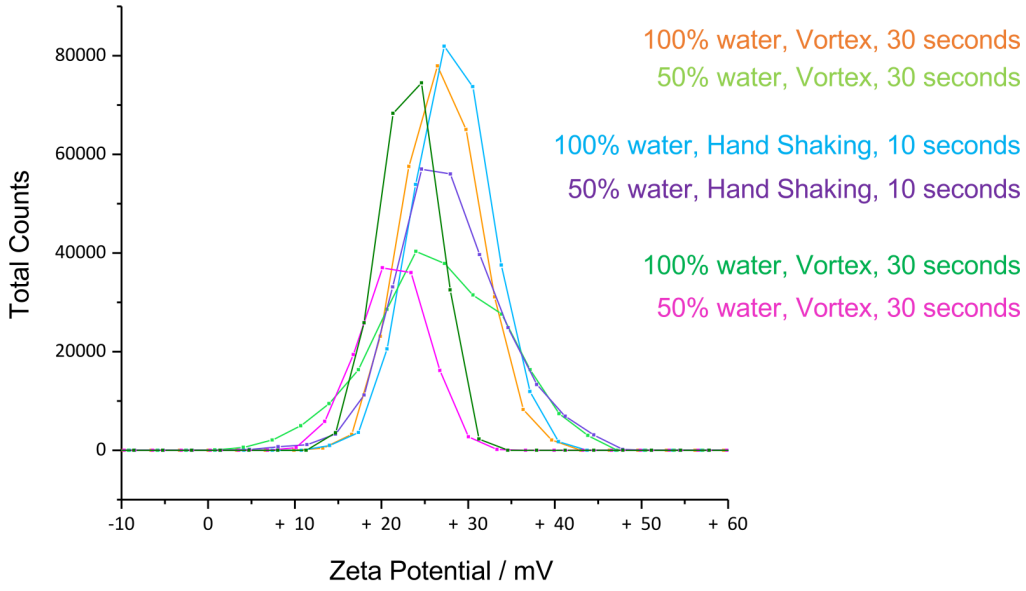

Figure 3.5: ζ-potential measurements of coacervates with varying re-suspension protocols. The amount of water used to replace the supernatant and the method of agitation were varied. Sample parameters are as follows: 100% water replacing supernatant with vortexing for 30 seconds, 100% water replacing supernatant with hand-shaking for 10 seconds, 50% water replacing supernatant with vortexing for 30 seconds, 50% water replacing supernatant with hand-shaking for 10 seconds. Note that these parameters are different from the previous figure. The percentages represent the volume of water that replaced the starting volume of supernatant; e,g. for 1 mL of supernatant, a 50% water replacement is adding 500 μL water.

(at 28° C) suffered greater coalescence and associated drop in turbidity simply due to the length of time taken for the experiment.

3.2.1 Macromolecular Uptake In Non-Re-suspended & Re-suspended Coacervates

3.2.1.1 Sequestration of a Single Solute in a Single Population - Small Molecules

A range of molecules were added to the coacervates in order to determine their sequestration properties (Figure 3.7). These molecules encompassed a range of sizes, from small molecules to large proteins. Regardless, all the molecules were sequestered into the droplets with no obvious differences seen between the molecules. To further this experiment, a larger range of molecules should be tested, as GFP and mCherry are quite similar and acridine orange and methylene blue have similar structures also, so this set of molecules is not a true representation of sequestration properties. It may be that the sequestration properties of the coacervate droplets is more dependent on a molecule's hydrophobicity rather than charge and this should also be

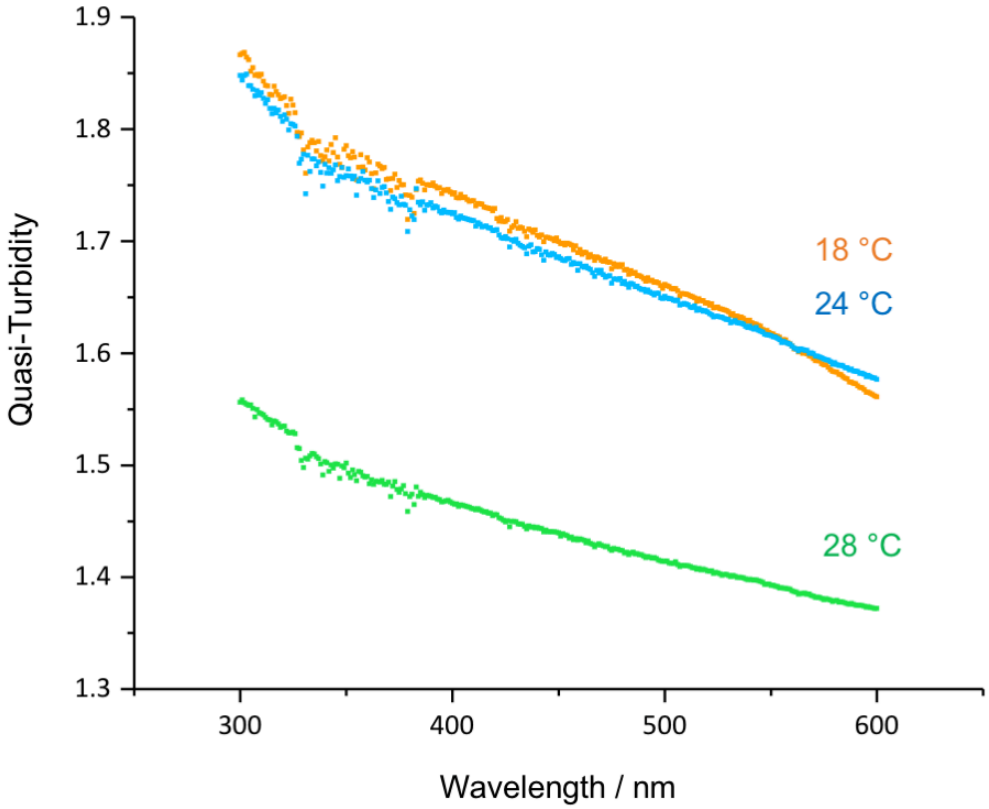

Figure 3.6: The effect of temperature on the stability of re-suspended coacervate droplets. Turbidity is measured via absorbance at wavelengths where the coacervate components do not absorb.

investigated. Furthermore, partition coefficients of each probe should be measured qualitatively to determine whether the partitioning is indeed similar for each molecule. With a larger variety of probes, more information could be determined about the sequestration properties of the ATP: PDDA coacervates, in relation to the impact of a molecule's charge, hydrophobicity and structure on sequestration. However, this experiment does provide some information about the system. Proteins must be folded correctly in the droplet interior as GFP maintains it's fluorescence inside the coacervate, which would not be the case if unfolding had occurred. This means that it is also likely that enzymes would retain their function in the interior of the droplet as well, which has previously been suggested by the literature.

To investigate the sequestration of small single solutes, single-stranded DNA tagged with either fluorescein or cy5 was added to the coacervates (Figure 3.8). These were both readily sequestered into the coacervate matrix. Note that the two single-stranded DNA strands are capable of annealing to form double-stranded DNA oligomers. This is exploited later in the research when single populations of coacervates with multiple solutes are examined (Chapter 4).

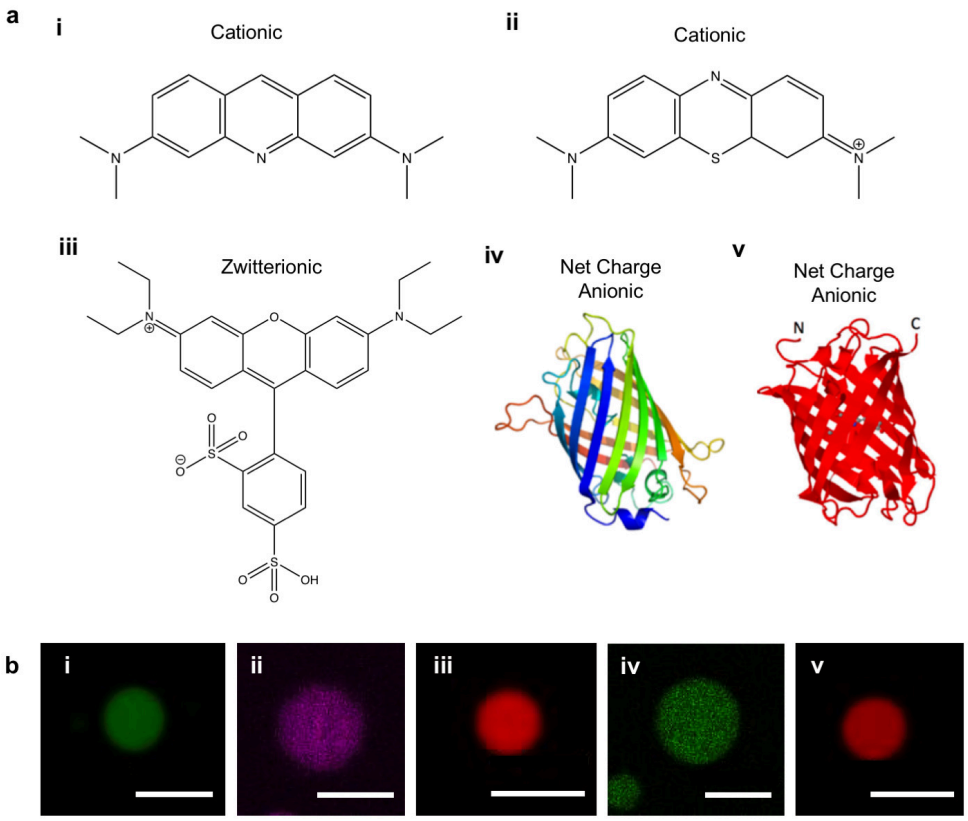

Figure 3.7: The sequestration of fluorescent macromolecules inside coacervates. a: molecule properties alongside b: confocal fluorescence microscopy showing their sequestration into coacervates. Dyes are as follows: i: acridine orange, ii: methylene blue, iii: Kiton red, iv: eGFP, v: mCherry. Scale bars 5 μm.

The sequestration properties of single-stranded DNA were observed by measuring the partition coefficient for the cy5-tagged DNA oligomer. This is shown in Figure 3.9. The maximum partitioning occurs at a final concentration of 8 mM of single-stranded DNA. The partitioning value is high, suggesting this molecule is easily sequestered. It is also possible that the ATP is being replaced by the DNA and the coacervate is becoming a DNA:PDDA structure instead, resulting in a loss of ATP. In fact, the ATP molecule exhibits four negative charges at pH 8 whereas the DNA exhibits 23 negative charges per strand. It is interesting that the DNA strand has 5.75 times as many negative charges and that the partitioning of DNA is highest at a concentration approximately 6 times lower than that of ATP. More experiments would need to be conducted to determine if this partitioning effect is caused by displacement of ATP. The partition coefficient value for this system is given by the gradient of the initial straight line portion of the graph, which is approximately 50.

The mean diameter of coacervates with sequestered oligomers was analysed and these results

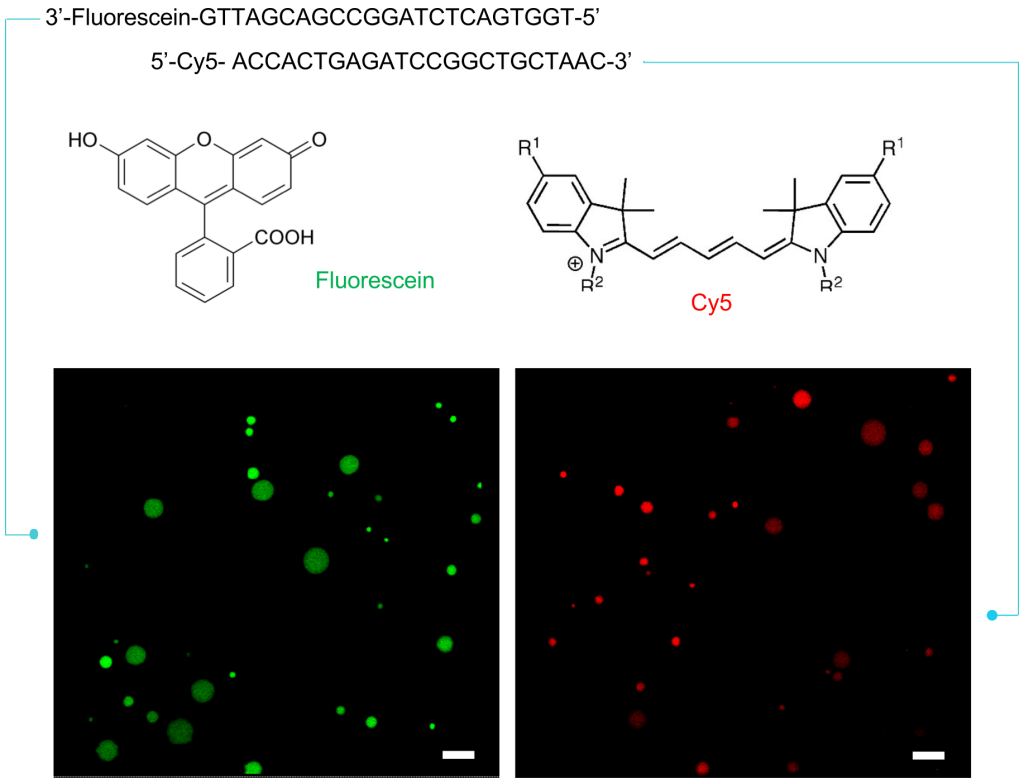

Figure 3.8: The sequestration of single-stranded DNA in coacervates. The sequences of fluorescein and cy5 tagged single stranded DNA oligomers along with the structures of fluorescein and Cy5 and confocal fluorescence micrographs showing sequestration of i: ss-DNA-fluorescein and ii:ss-DNA-cy5. Scale bars 10 μm

are displayed in Figure 3.10. Coacervates with either cy5 or fluorescein oligomers inside were assessed, in comparison with coacervates without oligomer addition. The mean sizes for all samples are very similar, although it could be said that the coacervates containing the oligomers are consistently slightly smaller. There does not seem to be any difference between cy5 oligomers and fluorescein oligomers but these measurements do not take into account any changes on the nanoscale.

Internal rearrangements of the coacervate matrix upon the addition of the cy5 oligomer were then investigated using digital holographic microscopy (DHM which maps refractive indices across a microscopy field, in this case the refractive index across a single coacervate droplet. The interfacial effects on the droplet were then observed by ζ-potential measurements (Figure 3.11).

The digital holographic microscopy did not show any difference in internal structure between those with single stranded DNA and those without. They did interestingly show changes in refractive index across a single droplet, indicating that coacervates may not be homogenous throughout, although this was not investigated further. The ζ-potential experiments demon-

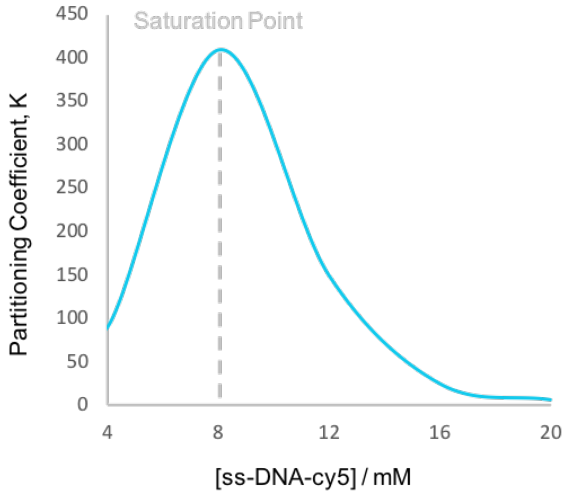

Figure 3.9: The partitioning of single-stranded DNA into the coacervates. The partitioning coefficient of ss-DNA-cy5 into PDDA: ATP coacervates at increasing concentrations, calculated as the concentration of ss-DNA-cy5 in the bulk divided by that in the supernatant. The saturation point shown on the graph indicates where no more ss-DNA-cy5 is entering the coacervate and the supernatant concentration therefore increases in comparison to the bulk concentration. The partition coefficient value for this system is given by the gradient of the initial straight line portion of the graph, which is approximately 50.

strated there may be a small increase in stability with increasing concentrations, but high concentrations may start to destabilise the droplets. This suggests that the DNA is fully sequestered and contributing to the properties of the internal matrix. DNA is negatively charged so it stands to reason that it would be able to interact with the positively charged PDDA inside the coacervates.

3.2.1.2 Sequestration of a Single Solute in a Single Population - Small Molecules: TEG

Although the sequestered molecules investigated up to this point had no effect on coacervate morphology on a macroscopic scale, it has previously been demonstrated that sequestered molecules could be used to disrupt the coacervate matrix, leading to vacuole formation with the coacervate. Commonly, these studies use charged molecules to interfere electrostatically with the matrix. Banerjee et al. showed this with RNA introduction into a coacervate system, demonstrating that overcharging a coacervate matrix leads to repetitive nucleation and growth of subcellular structures [113]. It has also been shown that restructuration can be driven by osmotic pressure effects [155]. Finally, in a different manner, compartmentation within coacervate droplets has also been shown to occur under electric field induced excitation in a cyclic manner by Yin et al. [157]. To date, no investigation of the sequestration effects of an uncharged small molecule,

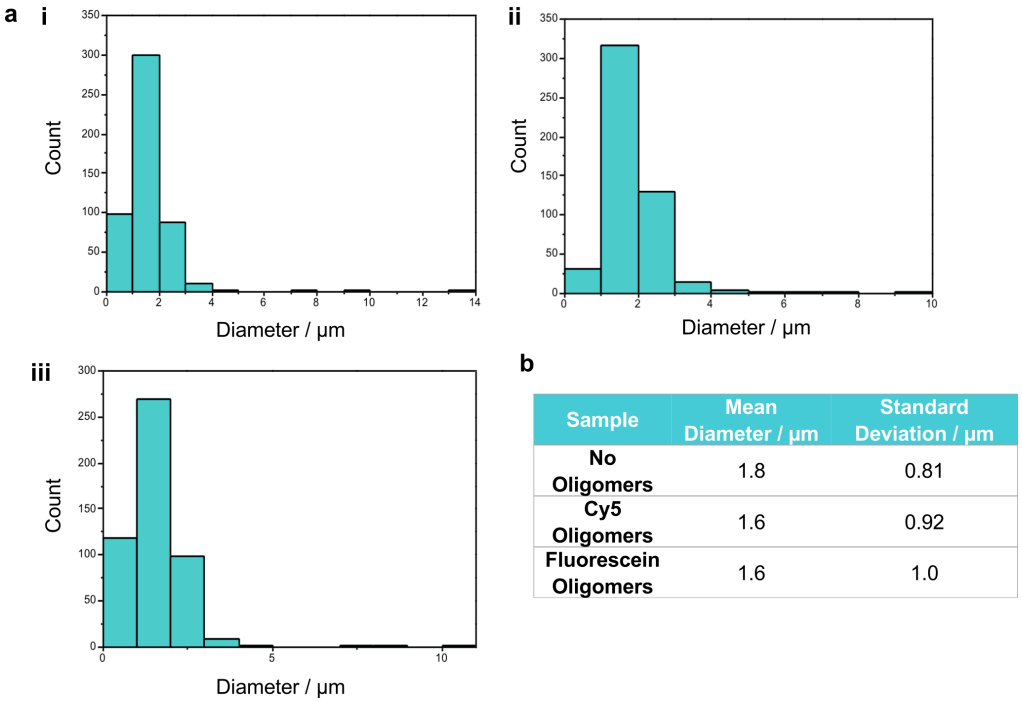

Sample	Mean Diameter / µm	Standard Deviation / µm
No Oligomers	1.8	0.81
Cy5 Oligomers	1.6	0.92
Fluorescein Oligomers	1.6	1.0

Figure 3.10: The effect of adding single-stranded DNA oligomers on coacervate size. a: Distributions of diameters in a population of droplets for coacervates containing i: no ss-DNA, ii: ss-DNA-cy5 and iii: ss-DNA-fluorescein. b: Statistical analysis showing mean diameter and the standard deviation of the populations.

which was unlikely to interfere electrostatically with internal coacervate interactions but had the potential to affect other forms of bonding within the coacervate matrix, had been explored. A decision was made to investigate this with the addition of tetraethyene glycol (TEG), which had the potential to affect bonding such as the hydrogen bonding resulting from hydroxyl groups on the ATP, interacting with the double bond oxygen groups on nearby ATP molecules as a single example.

Initially, a 30 μL aliquot of TEG was added to a sample of 72 μL of re-suspended coacervate droplets, as described in the materials and methods (Figure 3.12). The coacervates appeared to go through a phase whereby blebbing, i.e. expulsion of material from the coacevate, was seen at the surface, followed by retraction of these surface structures and vacuole emergence.

Upon further examination, it was observed that there were three different processes within which the coacervates could participate (Figure 3.12b). i/ Some coacervates were seen to develop internal aggregates, followed by development of a very small amount of surface blebbing. Aggregates were then seen in a ring at the surface of the droplet before clearance by gradual expulsion. ii/ In other cases, the coacervates initially blebbed at the surface and vacuoles were subsequently produced. The coacervates appeared to remain extant during the process but the identity of the blebs at this stage was unknown. In one of these cases, the ring-like arrangement

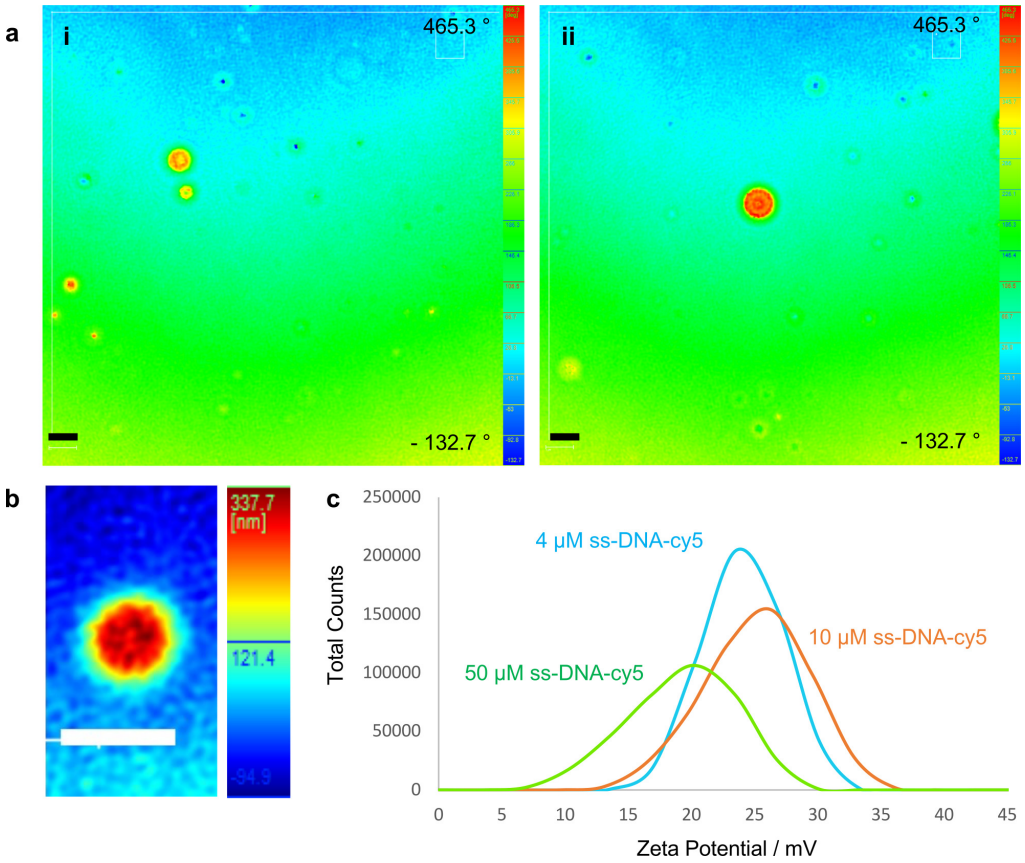

Figure 3.11: Characterisation of coacervates containing cy5-tagged single stranded DNA. a: Digital holographic microscopy large fields of view displaying changes in the refractive index within single coacervate droplets i: without and ii: with cy5 DNA, b: DHM of a single coacervate droplet without DNA showing possible internal structure, c: ζ-potentials of coacervates with increasing concentrations of ss-DNA-cy5. Image scale bars: 10 μm.

of aggregates also formed at the surface. Due to the coalescence of these into the vacuole, it is assumed that these are initial small vacuoles which then merge to make a larger single droplet. iii/ Alternatively, after surface blebbing the coacervate shifts on the slide creating a vacuole at the surface, within the blebbed material, which is then consumed by the coacervate as a pre-formed vacuole. The reason for this droplet shift to occur is unknown but hypothetically could be due to convection currents as a result of the heat from the laser or flow caused by the pipetting of the TEG into the solution. Another explanation could be that unbalanced bleb expulsion causes droplet movement in the opposite direction to that where most blebbing occurs. However, this seems unlikely as the image at 12 seconds seems to show an even thickness of bleb around the coacervate. In all cases, the coacervates appeared to reduce in size immediately after TEG addition and then remain at this smaller size for the remainder of the process. For example, for the addition of 20 μL of TEG, the diameter of the droplets shrink to 83 % of their original diameter, on average. For the addition of 40 μL of TEG, the diameter of the droplets shrink to 66 % of

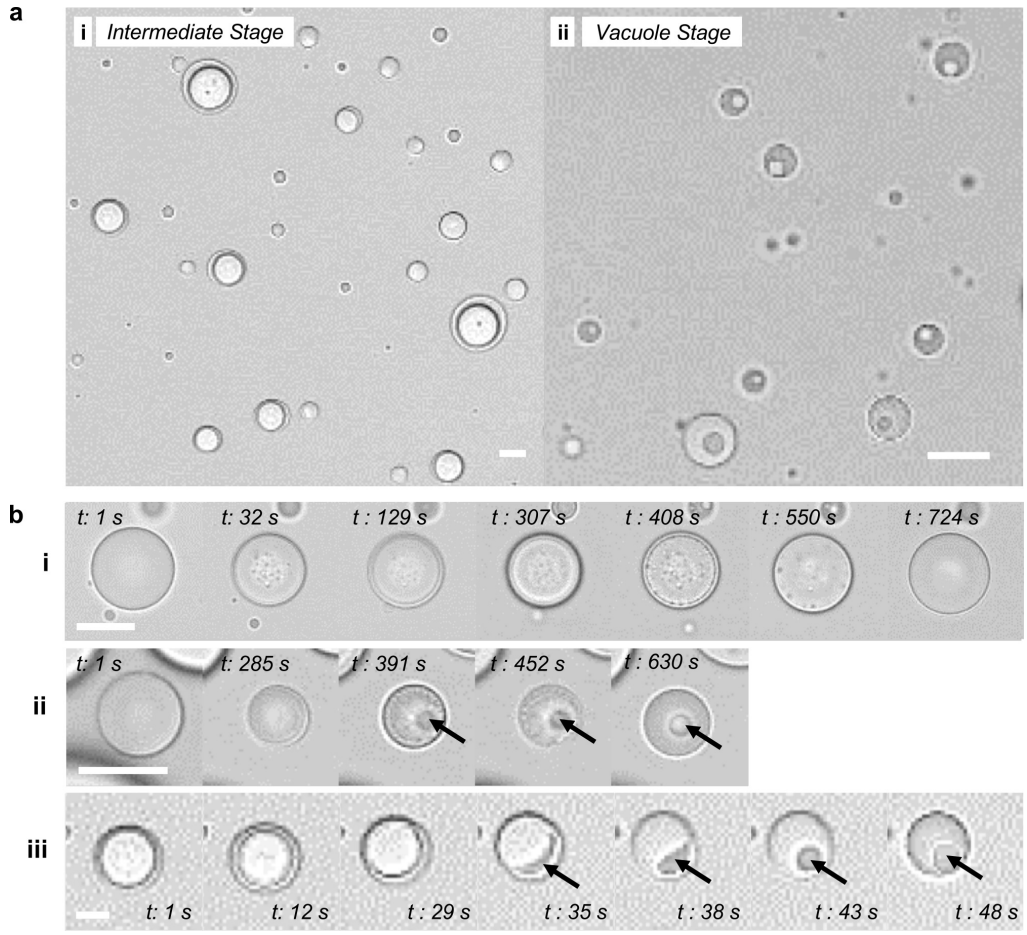

Figure 3.12: Coacervate vacuole formation induced by the addition of 30 μL TEG. (a) large scale brightfield images showing the coacervate structural changes at (i) an intermediate stage of vacuole formation & (ii) after the vacuoles have formed. (b) Structural changes in individual droplets representative of the population, imaged in the brightfield. The coacervates appear to go through one of three types of alteration: (i) the development of internal aggregates followed by subsequent clearance, (ii) the development of vacuole precursors at the droplet surface with subsequent coalescence into a single vacuole and (iii) blebbing at the surface and shifting of the droplet, followed by an uptake of a vacuole formed within the blebs. Time points shown in seconds; scale bars: 5 μm

their diameter before TEG and for an addition of 100 μL of TEG, the diameter of the droplets shrink to 72 % of their original diameter. This indicates that there is component removal from the coacervates on TEG addition or, more likely, that there is a loss of water from the coacervates when TEG is added. This is explored in more detail in further experiments As there is no apparent size change of the coacervates during vacuole formation, some questions were raised here about the implications of this with respect to the contents of the coacervate matrix during and after vacuole formation. This is also discussed later. The reason for the appearance of blebs is unknown but could be related to the affinity of TEG for a water phase. Usually, TEG is very

miscible with water so it could be assumed at this point that the TEG is re=equilibrating to be in a water phase. Further investigations in this chapter therefore investigate the location of TEG in the coacervate after compartmentation more closely.

The mechanism selection does not seem to be dependant on droplet size and is likely to be more affected by the concentration of TEG. This may be uneven due to the addition of TEG, at a distant site, into one side of a dish containing the coacervate population. The TEG then diffuses to droplets within the imaging region. The mechanism may also be affected by inhomogeneity in the coating on the glass slides. The time scale for coacervate rearrangement also varies, probably for the same reasons.

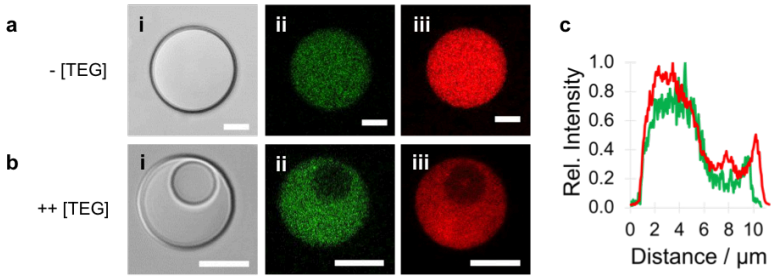

Figure 3.13: The location of coacervate components, ATP and PDDA, with and without vacuole formation. (i) Brightfield & (ii-iii) confocal fluorescent microscopy images showing coacervate droplets without (a) and with (b) the addition of 30 μL TEG to induce vacuoles, showing the location of (ii) ATP, doped with ATP-TNP (green) and (iii) PDDA, doped with PDDA-RITC (red). Neither coacervate component is seen in large quantity in the vacuole. (c) Line profile across the droplet containing a single vacuole (as shown in (b)) showing the relative fluorescent intensity of ATP (green) and PDDA (red) across the diameter of the droplet. Scale bars: 5 μm

To determine whether the vacuole was indeed a true vacuole without any components, or if it contained either coacervate components, fluorescently tagged molecules were doped into this system, at concentrations believed to not affect the overall behaviour of the system. This is shown in Figures 3.13 and 3.17. The system was compared to coacervates without any TEG addition. Here, the distribution of ATP and PDDA components of the coacervate matrix appeared homogeneous on the length scale investigated, and no background fluorescence of ATP or PDDA could be observed at this resolution. With the addition of 30 μL TEG, the resulting vacuole did not seem to contain ATP or PDDA in large quantity but did seem to indicate that there was fluorescently-tagged ATP and PDDA at approximately 20 % the intensity of that seen in the region of the coacervate exterior to the inner compartment. This may be due to smaller regions of coacervate within this compartment, or some coacervate components free in the inner vacuole. The coacervate remaining around the vacuole still had a homogeneous distribution of components. This indicated that the coacervate matrix mostly made space to accommodate the vacuole, either by increasing the concentration of components in the matrix or by ejecting some components

rather than the ATP and PDDA components also moving to reside in the compartment in large quantities. This detail is discussed later in this chapter.

TEG was then produced with the addition of a fluorescent tag, FITC. An NMR spectra was taken to determine that the product was indeed TEG-FITC, and only TEG-FITC (Figure 3.14). High resolution mass spectrometry (HRMS) also confirmed that the product was TEG-FITC. (Figure 3.15)

As the molecular weight of FITC (389.382 g/mol) is larger than that of TEG (194.227 g/mol), it was deemed appropriate to dope the TEG-FITC 1:100 (by volume) into a solution of untagged TEG for all experiments using fluorescent TEG. To check that this had no effect on the partitioning of TEG into the coacervate droplets, an experiment was conducted whereby the supernatant of samples containing TEG or TEG-FITC were extracted and the TEG purified. The six resulting vials contained samples as follows: (i) coacervate + untagged TEG, (ii) untagged TEG, (iii) coacervate + TEG-FITC, (iv) TEG-FITC, (v) coacervate + dextran-RITC (70 kDa) + TEG-FITC and (vi) dextran-RITC (70 kDa) + TEG-FITC. NMR spectra were taken to determine that the product was indeed TEG and only TEG. The preparation and results are summarised in Figure 3.16 (a)).

Figure 3.16 b is a photograph of the six vials after the TEG has been purified. It can be seen that there is no fluorescence in vials (i)-(ii), as expected because these vials contain only TEG and not TEG-FITC. Vials (iv)-(vi) show the yellow fluorescence characteristic of the emission of FITC. Considering that the density of TEG is 1.125 g/cm^3, the mass of TEG added initially should be 73 mg. Accounting for some errors in the accuracy of the weighing, the resulting masses in the three samples that did not have coacervate added ((ii), (iv) & (vi)) are very similar to this. This indicates, as anticipated, that all the TEG is retained in the supernatant because there is no bulk in these samples. It also indicates that this is an appropriate methodology for determining the TEG content in the other samples, because it does not appear that there has been TEG loss at any stage of purification. When coacervate was included in the sample, it is clear that some TEG is partitioning into the bulk phase. There appears to be slightly more TEG-FITC partitioned into the bulk phase compared to TEG. This is likely explained by the fact that FITC is readily sequestered into the coacervates. However, this increase is also within the boundaries of weighing inaccuracies so it does not appear that the addition of the FITC tag is having a drastic effect. For all further experiments a doping level of 1:1000 was used to minimise any effect of the FITC tag further, unless stated otherwise.

It also appears that the addition of dextran to the system has no effect on the partitioning of TEG-FITC, and therefore presumably TEG. It is interesting to note that in the samples with dextran added the intensity of TEG-FITC is lower than that in the samples without dextran. FITC emission is very dependent on local environment so it could be hypothesised that the dextran is altering the pH or local concentration of the FITC.

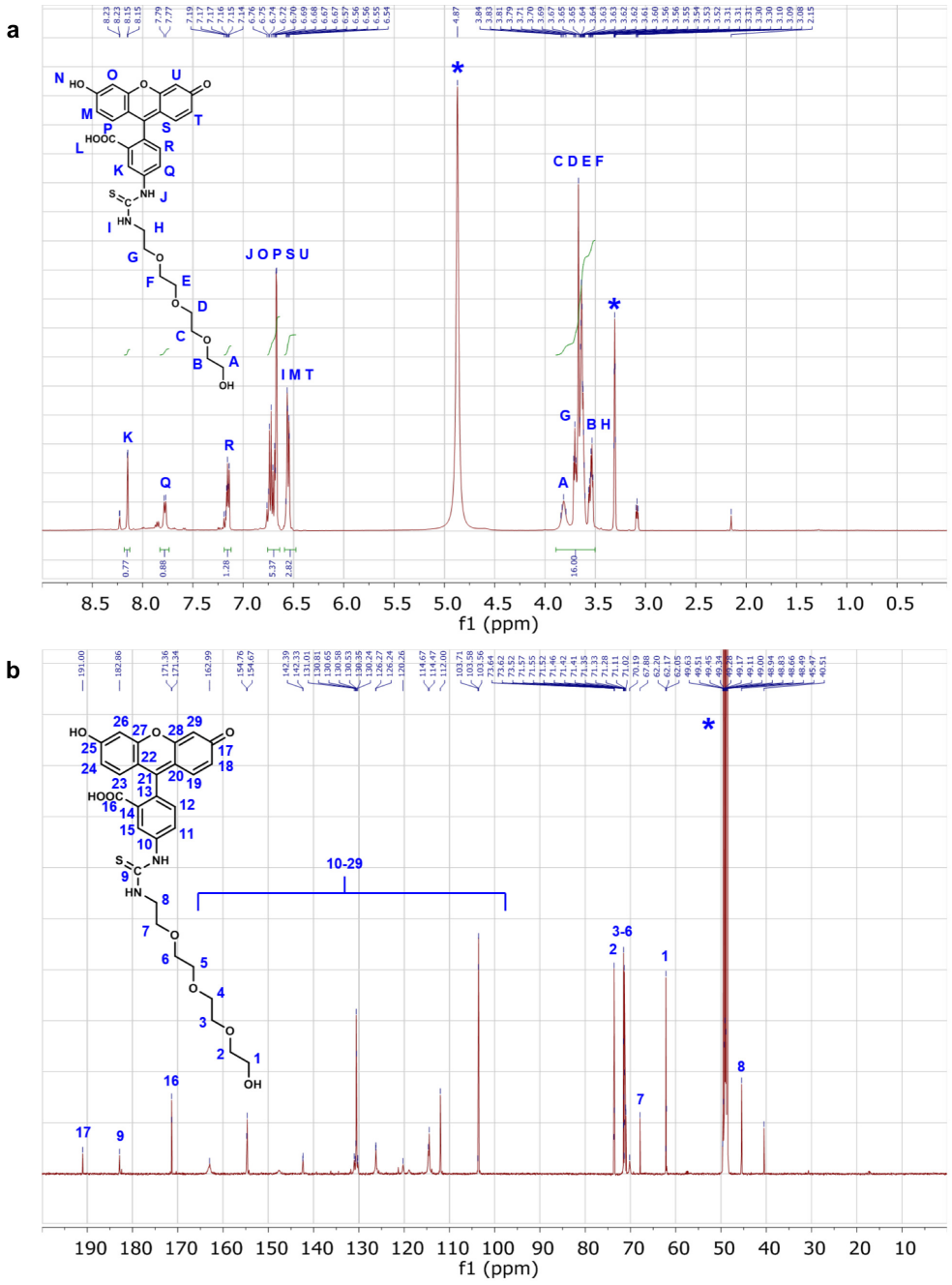

Figure 3.14: NMR spectra showing correct attachment of FITC to TEG. (a) ^{1}H NMR spectra (500 MHz, methanol-d4) δ 8.15 (s, 1H, K), 7.77 (d, J = 10, 1H, Q), 7.16 (d, J = 10, 1H, R), 6.76 - 6.67 (m, 5H, J, O, P, S, U), 6.56 (d, J = 5, 3H, I, M, T), 3.84 3.30 (m, 16H, A-H). (b) ^{13}C NMR spectra 150 MHz, methanol-d4) δ 191.0 (17), 182.9 (9), 171.4 (16), 163.0, 154.7, 142.4, 142.3, 131.0, 130.8, 130.7, 130.6, 130.5, 130.4, 130.2, 126.3, 126.2, 120.3, 118.9, 114.7, 114.5, 112.0, 103.6, 103.6 (10-29), 73.6 (2), 71.5, 71.4, 71.1, 71.0 (3-6), 67.9 (7), 62.2 (1), 45.5 (8).

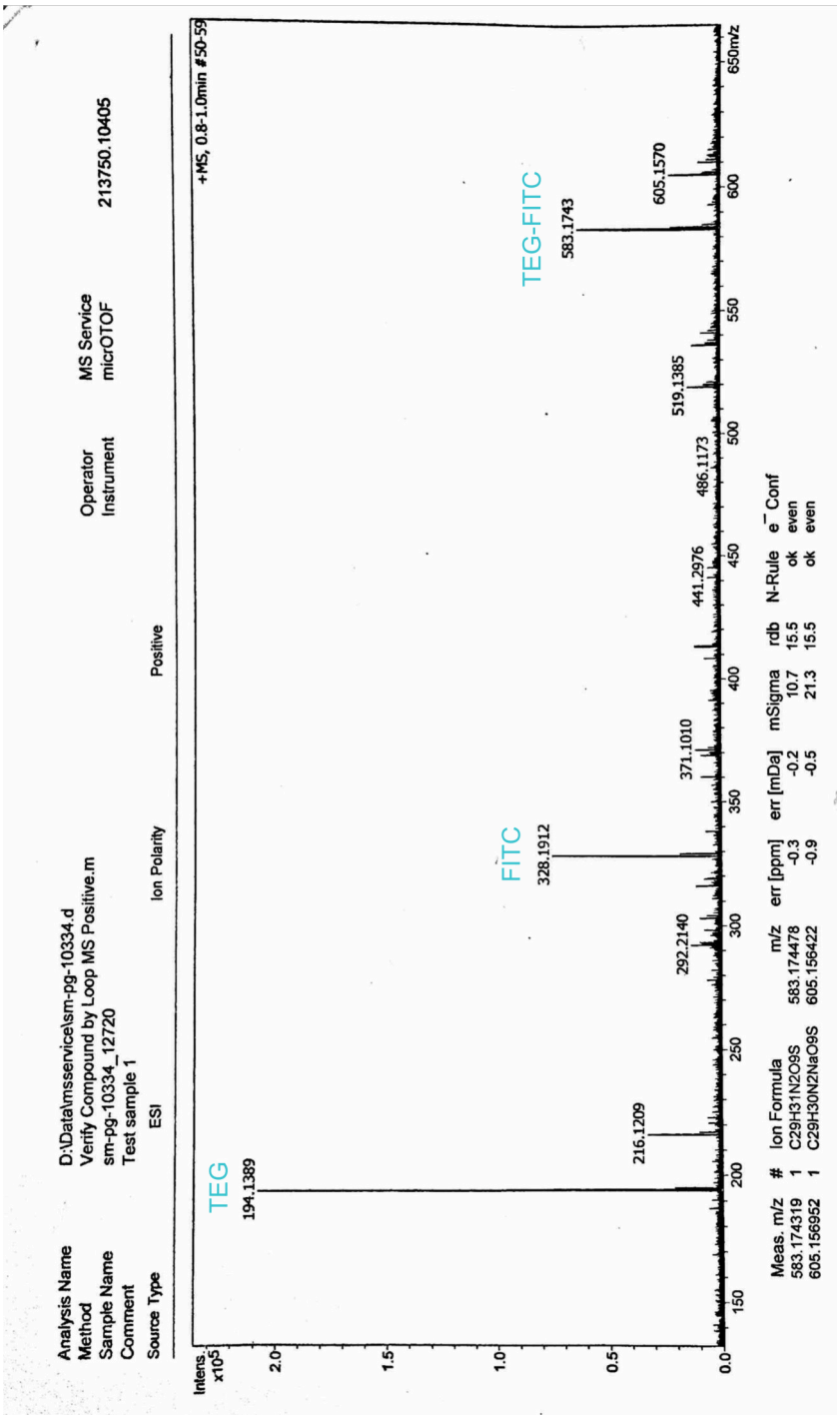

Figure 3.15: Printout of a high resolution mass spectrometry (HRMS) (ESI) spectra confirming that the product of the synthesis is TEG-FITC. The theoretical calculation for C29H31N2O9S [M+1] is 583.1745, here it was found to be 583.1743. The theoretical calculation for for C29H30N2NaO9S [M + Na] is 605.1564, here it was found to be 605.1570

a

	i	ii	iii	iv	v	vi
Coacervates Added	Yes		Yes		Yes	
Dextran Added					Yes	Yes
TEG Added	Untagged	Untagged	Tagged	Tagged	Tagged	Tagged
TEG Mass (mg)	70.8	77.6	64.3	74.9	63.8	71.8

b

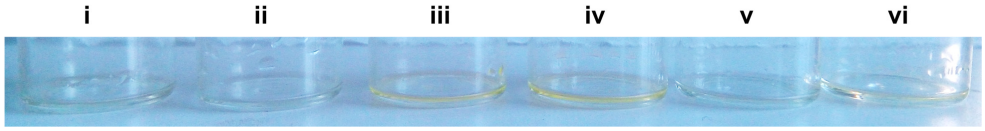

Figure 3.16: Determination of the difference between TEG and TEG-FITC partitioning into the coacervates. (a) A summary of the components added to each vial alongside (b) the TEG product purified from the coacervate supernatant solution. Vials (i)-(ii) are colourless with vials (iii)-(vi) showing the characteristic yellow colour of FITC.

The location of TEG in the compartment forming system was then investigated using a solution doped with TEG-FITC (Figure 3.17). This allowed some elucidation of the mechanism of TEG-induced vacuole formation and allowed the interaction between TEG and the coacervate to be monitored. Although previous experiments indicated that the attachment of FITC to TEG did not make a difference to the partitioning properties of doped TEG, the large size of FITC, almost two times as large as the TEG, indicates that this could still be a possibility. However, the method of doping in a small amount of a fluorescently tagged molecule is a standard procedure and there was no sensible alternative here to find the location of TEG in the system.

The TEG did indeed enter the coacervate as predicted but, interestingly, was not immediately distributed homogeneously throughout the coacervate droplet, as evidenced by the absence of green fluorescence at the centre of the droplet until t = 70 s. Instead the TEG appears to be slowed by the coacervate matrix and therefore temporarily exists in a band just outside the interface of the droplet. The coacervate matrix is a densely entangled network but, due to the small size of the TEG, is unlikely to impede entry by size exclusion alone. As more TEG is attracted to the coacervate, presumably by the same principles that govern sequestration of other molecules, it is unable to enter at a rate as fast as it is collecting at the surface so this ring region becomes brighter. Over approximately 30 seconds, the TEG gradually disperses to a more uniform concentration within the coacervate however, a non-uniform pattern can still be seen in the brightfield microscopy which indicates a difference in light refraction presumably due to a difference in density. This is likely to be caused by a difference in TEG concentration throughout the droplet. After this time point structural changes continue to occur, indicating that the system is still in a transitory non-equilibrium state. The TEG appears to separate into two distinct regions, one at the centre of the coacervate and one at the interface, leaving a region with less TEG in-between (t = 85 s). This TEG-minimal region could contain water or

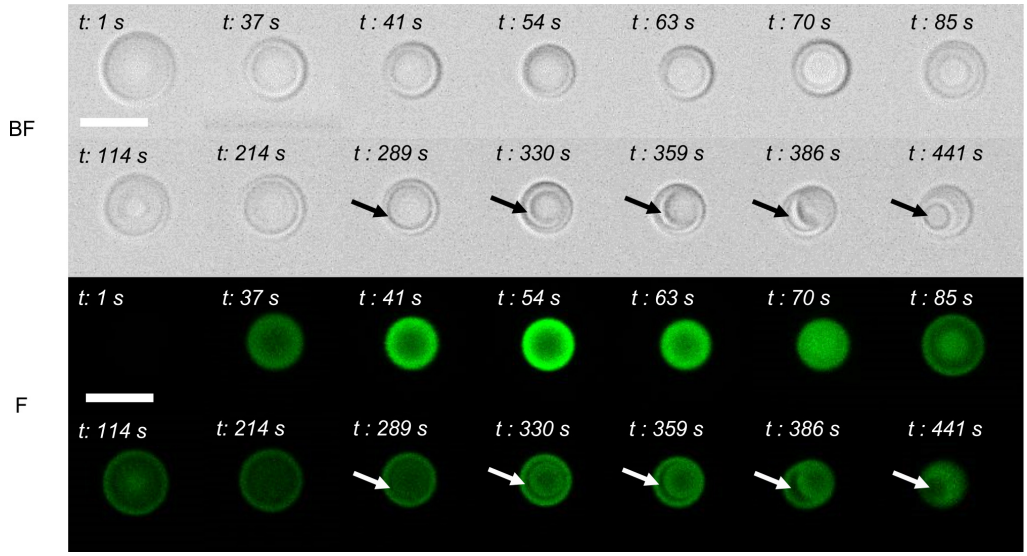

Figure 3.17: Observation of the mechanism of vacuole formation induced by 30 μL of TEG, using TEG tagged with FITC. Brightfield (BF) and confocal fluorescence (F) time point sequences of a single representative droplet during vacuole formation. The arrows identify the vacuole as it is formed. Time points shown in seconds; scale bars 5 μm.

either coacervate component as these are untagged, and therefore cannot be directly observed in this timepoint sequence. The separate exterior ring may result because TEG molecules near the interface of the coacervate would experience slightly different interactions, influenced in part by the surface tension of the droplet. It is also known that TEG can be surface active so this may explain the coating of the coacervate at the interface. Either of these factors could contribute to changes in the behaviour and diffusional properties of TEG whilst at the interface.

The fluorescence of the central region then seems to dissipate, or become quenched, whilst the ring remains at a similar level of fluorescence (t = 114 s). If the TEG is indeed hydrogen bonding to the ATP and therefore displacing water molecules, as hypothesised earlier, it is possible that the region free of TEG is caused by mass expulsion of water from the coacervate matrix, causing internal rearrangement whereby water molecules surround a central region of coacervate components and TEG. These water molecules, which would be expected to enter the supernatant, may be inhibited by the outer region of TEG and, at least partially, are trapped inside the coacervate boundary. This structure is not stable and further rearrangements occur so that the TEG, and probably the ATP and PDDA, in the central region becomes more evenly distributed across the whole coacervate. This would lead to a reduction in TEG concentration in the central region, explaining the apparent reduction in the fluorescence. The outer TEG region still remains during these stages for the reasons stated in the previous paragraph. Once the TEG had equilibrated, a line profile analysis (not shown) was undertaken which indicated that again the inner compartment contained TEG at a concentration approximately five times lower than that in the

surrounding coacervate region. This suggests that some TEG may indeed reside in the central compartment but that most of the TEG is retained in the surrounding coacervate.

The water molecules are still trapped and the coacervate must reach an energetically stable state. A proposed mechanism for this is that the water molecules amalgamate into a single droplet separate from the coacervate matrix, which consequently becomes stabilised by surface tension effects. This breaks the continuous barrier separating the two regions of TEG, enabling the TEG to rearrange to form a single more stable region. The coacervate becomes a single homogeneous TEG-containing droplet, with an internal TEG-minimal compartment.

Referring back to Figure 3.13, it was shown that the final vacuole contains little ATP or PDDA. As it appears that the TEG-minimal region goes on to form the vacuole, an assumption can be made here that this TEG-minimal region also has minimal coacervate components, indicating that mostly only water molecules are present there. This suggests that the compartment formed can be described as a vacuole as it is mostly free from all components aside from water. It is therefore also possible that at the points where inner and outer separated regions of TEG exist there is actually an unstable transitory structure whereby the coacervate components actually exist as one coacervate inside another with a boundary of water in between. Indeed at 289 seconds (3.17), when the water droplet starts to form (identified by arrows) and TEG is pushed back into the coacervate matrix, a boundary region can temporarily be seen in the inner droplet similar to that seen on the outside of the original coacervate structure.

To elucidate further information on the mechanism, the concentration of TEG added to the coacervate population was varied. Microscopy images were analysed to provide statistical information about the vacuoles formed, as shown in Figure 3.18. Concentrations of TEG in each case are equated as the volume of TEG added, as it seems likely that considering the single localised addition of TEG, diffusion, and TEG interactions with other coacervate droplets that the true concentration in a given region is hard to quantify accurately.

The percentage of the population of coacervates that produced a single coalesced vacuole was determined and this identified an interesting two-peak distribution (Figure 3.18(i)). For an addition of 10 μL TEG or lower no vacuoles were formed. As TEG concentrations were increased, the percentage of droplets containing a single vacuole also increased, up to a maximum of around 80% with a 15 μL addition. Unexpectedly, after this point increasing the volume of TEG, and therefore the final concentration of TEG, reduced the percentage of coacervate droplets that had a vacuole until an addition of 30 μL when the percentage started to increase once more. With TEG additions of 45 μL, all the population were transformed to have a vacuole. With only slightly higher volumes, 50 μL or above, no coacervates showed vacuole transitions. These observations could indicate that there is actually more than one mechanism of TEG-induced vacuole formation, depending on concentration.

The vacuole size, as a function of the total coacervate diameter, and the vacuole lifetime were

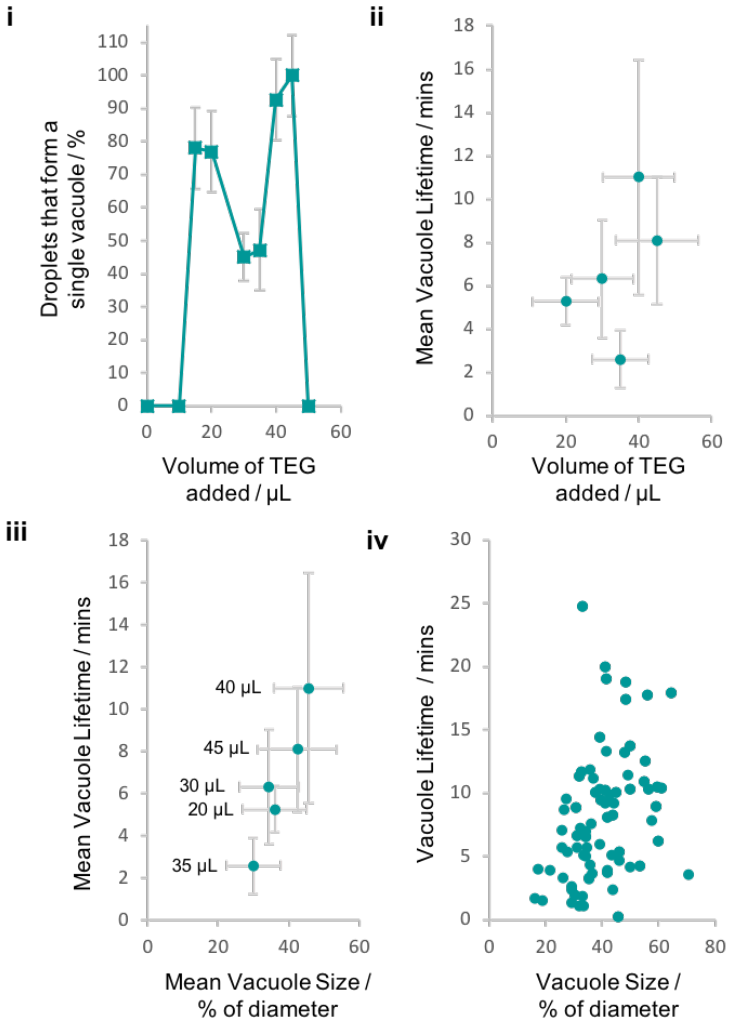

Figure 3.18: Statistical analysis of vacuole properties with varying concentrations of TEG. Analysis taken from microscopy images showing (i) the percentage of droplets that form a single vacuole within a population as a result of the concentration of TEG, (ii) the mean vacuole lifetime of the compartments formed inside the droplets relative to the volume of TEG added & (iii-iv) the correlation between the lifetime of the single vacuoles that are formed and the size of the vacuoles as (iii) groupings by the mean average of a population for each concentration of TEG and (iv) all droplets individually, regardless of TEG concentration.

also investigated to determine whether the amount of TEG altered the size of the vacuole. In contrary, the size of the vacuole and it's lifetime appeared to be unrelated to the concentration of TEG. This could be explained by the large range in coacervate size distribution and the method of TEG addition causing variation in TEG concentration across the sample, thereby preventing accurate analysis of the concentration of TEG on a single droplet scale. Further investigations in this area could be enhanced using microfluidics to narrow the size distribution of the coacervates, removing this variable from the analysis.

Interestingly, the lifetime of the vacuole did seem to correlate with its size (Figure 3.18(ii-iii)). Vacuole clearance was seen to occur by rapid 'popping' of the vacuole into the supernatant or gradual vacuole shrinkage until no vacuole remained but there was no predictable pattern as to which mechanism would occur. It is possible that this is also affected by inhomogeneity in the the slide coating which would affect coacervate surface interactions and therefore stability of compartments within the droplet. Vacuole location within the coacervate, i.e. whether the vacuole resided at the edge of the coacervate or centre, also appeared not to affect lifetime. Average vacuole lifetime was around 10 minutes, although a few outliers were seen to last more than 20 minutes. Furthermore, no vacuoles were measured that were more than 70%, or less than 17%, of the final diameter of the coacervate droplets. No conclusions have yet been drawn from this however, this observation may prove helpful in elucidating more information about the mechanism of the vacuole formation with further experiments.

It can be hypothesised that there is a relationship between vacuole size and lifetime because the proportion of coacervate compared to vacuole in the droplet affects vacuole stability, due to changes in electrostatic and hydrogen bonding in the matrix and with sequestered components such as TEG. However further evidence is required to determine the causal property, as it could also simply be an effect of differences in the localised TEG concentration affecting both the lifetime and size of the vacuole. It has previously been shown in Figure 3.17 that there are multiple methods of vacuole formation and this could also influence the stability of the vacuole, despite no visible differences in the final vacuole composition at the resolution obtainable. Further investigations into the mechanisms determining stability and size would be worth investigating as an understanding here may provide a means to control stability and lifetime of internal compartments, allowing a more predictable system as more components are introduced.

With this in mind, the confocal microscopy images used in the statistical analysis were examined alongside further time point sequences of vacuole formation with varying concentrations of TEG. It was hoped that this would also provide information to determine whether the mechanism was consistent with all concentrations, in order to explain the double peak distribution seen in Figure 3.18(i), and to determine why vacuoles did not form above or below threshold concentrations of TEG.

The investigation was started with concentrations of TEG lower than the 30 μL previously stud-

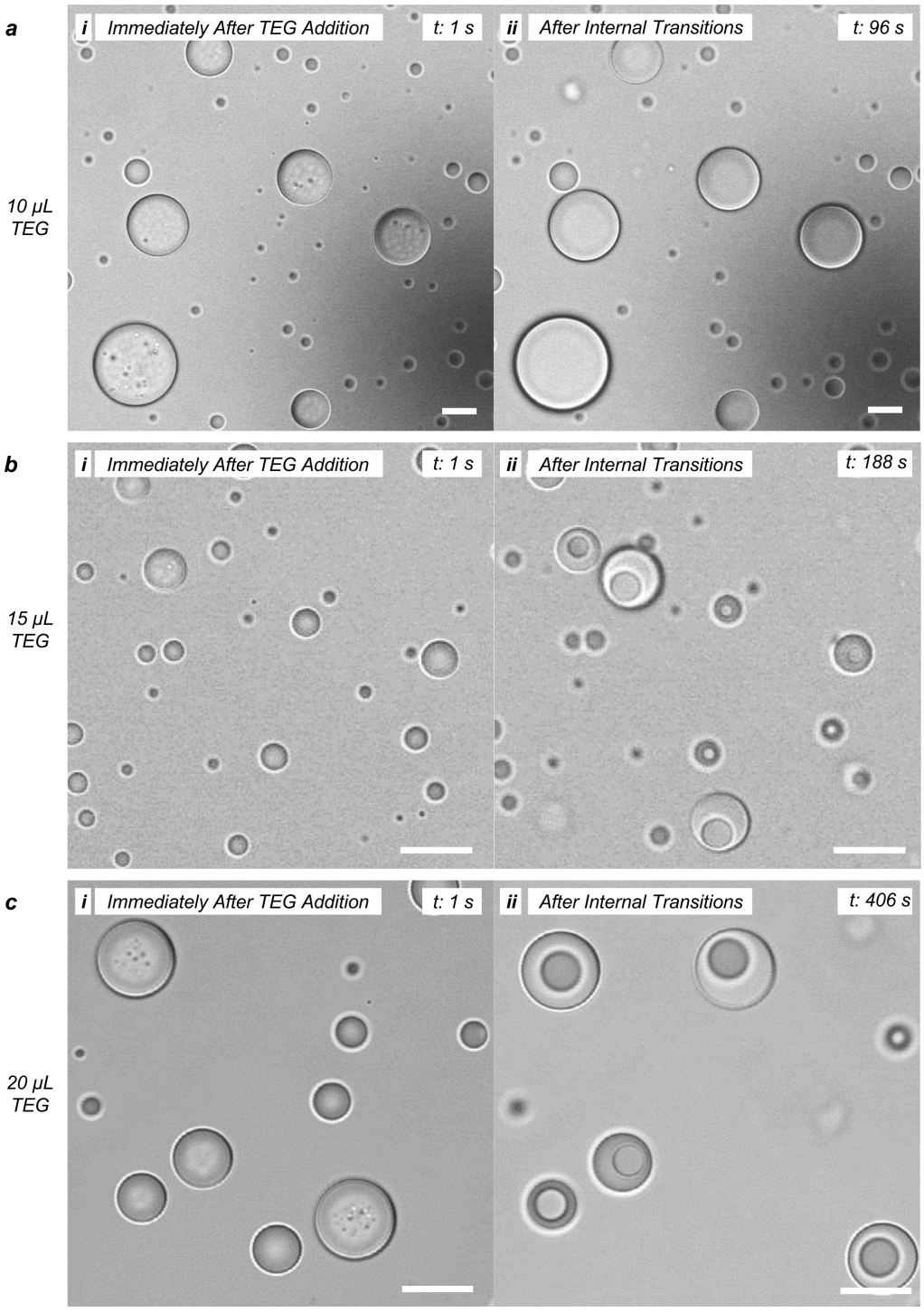

Figure 3.19: The effect of decreasing the concentration of TEG on vacuole formation. Large scale brightfield microscopy images showing (i) the immediate effects of adding 10, 15 and 20 μL of TEG and (ii) the morphology of the coacervate droplets after any internal transtitions caused by the TEG addition. Time points shown in seconds; scale bars 10 μm.

ied. Additions of TEG of 10, 15 and 20 μL are shown in Figure 3.19. The 10 μL addition is in the region where internal vacuoles do not form, whereas the 15 and 20 μL additions are in the first peak region of vacuole formation. Small aggregates, or possibly very tiny vacuoles, were seen to appear immediately after TEG addition with all three concentrations. After any internal transitions were completed, the coacervate populations with 15 and 20 μL additions of TEG looked morphologically very similar. Time point sequences of individual droplets were then investigated to observe any concentration dependant differences in the transitory states (Figure 3.20).

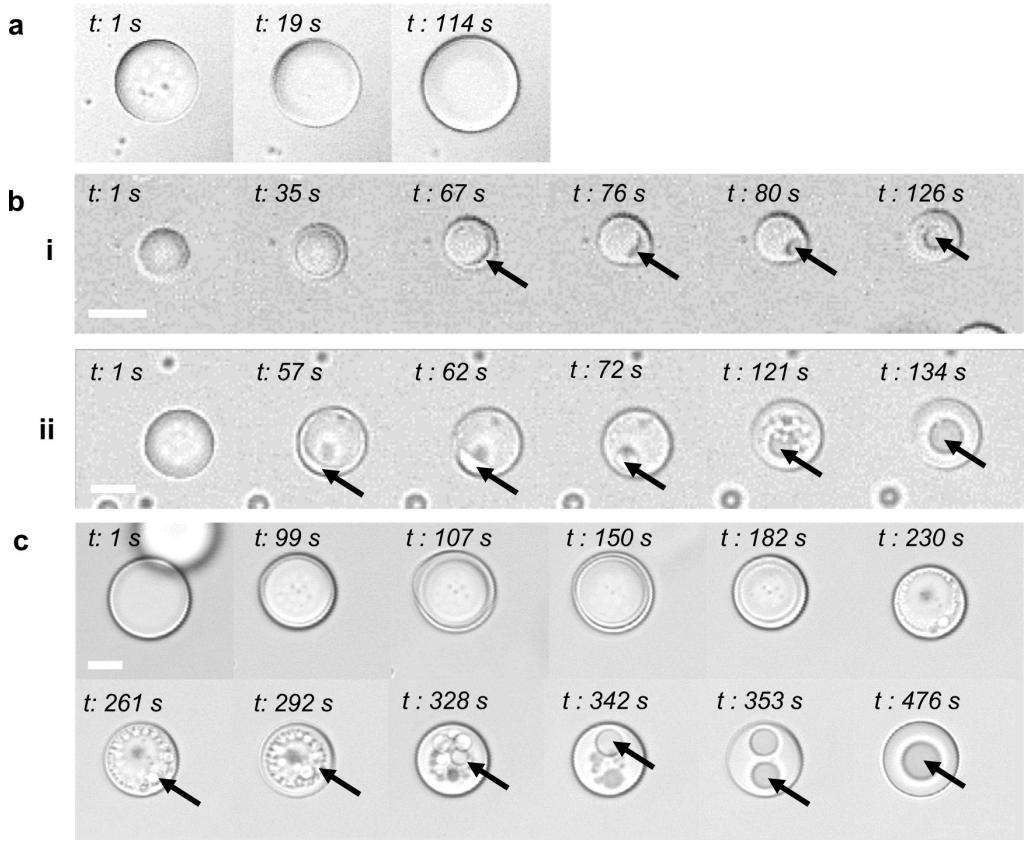

Figure 3.20: The effect of decreasing the concentration of TEG on vacuole formation. Individual droplet time point sequences shown as brightfield images for TEG additions of (a) 10 μL , (b) 15 μL & (c) 20 μL. (b) (i-ii) indicate two examples of vacuole formation in different droplets. The arrows identify the vacuole as it is formed. Time points shown in seconds; scale bars 5 μm.

Very few observations could be made from the addition of 10 μL of TEG (Figure 3.20a). An initial shrinkage of all droplets in the field of view was observed (not shown), followed by development of small aggregates that then rapidly disappeared. With a 15 μL TEG addition (Figure 3.20b), two examples of the mechanism observed are shown, whereby the droplet undergoes surface blebbing followed by re-internalisation of the blebbed material. In Figure 3.20(b)(i), the coacervate droplet appears to shift after blebbing, either causing the blebbed material to accumulate

in one position or as a result of this action. The resulting vacuole is engulfed into the coacervate matrix from the edge of the droplet and then moves to the centre of the droplet. In Figure 3.20b(ii), a similar mechanism occurs but the blebbing and uptake does not appear to shift the coacervate. Smaller vacuoles are also created which coalesce with each other, and the larger vacuole, to form a single vacuole. The noticeable difference between these two cases is that the droplet in (ii) is larger than that in (i) which indicates that it is probably the action of coalescence of trapped water molecules, forming a vacuole, that shifts the droplet if it is small enough to react to this fluctuation, rather than a shift from the droplet causing vacuole formation. Due to the similarities seen here compared to the images obtained in Figure 3.17, it was presumed that the same mechanism was occurring. When the 20 μL TEG addition was investigated as single time point images, a slightly different mechanism was seen. Blebbing occurred as previously, but this appeared more pronounced in several locations around the droplet rather than at one site alone (seen in Figure 3.20(c) at 107 seconds). After bleb retraction, a multitude of small vacuoles were seen to form just inside the droplet interface rather than a single vacuole on one side. These vacuoles then moved towards the centre of the matrix as they coalesced, eventually producing two similar size vacuoles that merged to form a single vacuole.

It was previously noted that an addition of 30 μL TEG experienced impeded entry to the coacervate, consequently forming an interfacial coating, thought to be as a result of both self-hydrogen bonding causing it to behave as larger, more viscous molecules and also it's surface coating properties. Based on the time point sequences of lower concentrations of TEG, it is thought that additions of TEG of 10 μL are too low to be particularly hydrogen bonded, and therefore impeded, and this prevents a coating from being formed. This means that any water molecules that are displaced can easily exit the coacervate matrix and are cleared from the coacervate soon after formation. This is investigated later in this chapter with fluorescently-tagged TEG. Additionally, due to the lower concentrations of TEG it is likely that the number of molecules of TEG are insufficient to displace a significant amount of water molecules from their hydrogen bonded position within the matrix and therefore there is less water to contribute to a vacuole and a larger volume of matrix between any small water-rich patches that do form, making coalescence of water to form a vacuole the less likely option compared to small vacuole clearance. Hypothetically, with an addition of 15 μL the lower threshold of TEG required to form a vacuole is overcome because there are now enough TEG molecules to displace a significant amount of water molecules. Additionally, there could now be a coating at the interface of the droplets. With further increases to 20 μL additions, an even larger amount of TEG could mean that a less penetrable surface coating formed and more water was displaced which explains the increase in the number of small vacuoles near the surface around the whole droplet. The increase in concentration of TEG inside the coacervate matrix may also now be affecting the movement of water molecules through the matrix, making the formation of multiple small vacuoles more likely than the formation of a single vacuole at the surface. However, more data is required to determine if

this is the case and this concept is revisited later in this chapter.

Concentrations of TEG above 30 μL were then investigated in the same manner to determine the mechanism that resulted in a second peak distribution for single vacuole formation. Figure 3.21 shows the effect of adding TEG in volumes of 35, 40 and 45 μL. Internal aggregates were seen in the addition of 35 μL TEG but these rapidly disappeared and vacuoles were still formed. Unfortunately, for the 40 μL TEG addition, only an intermediate stage seemed to have been formed during the time frame investigated but it is thought that this would have eventually gone on to form vacuoles based on the results of the other concentrations in this figure.

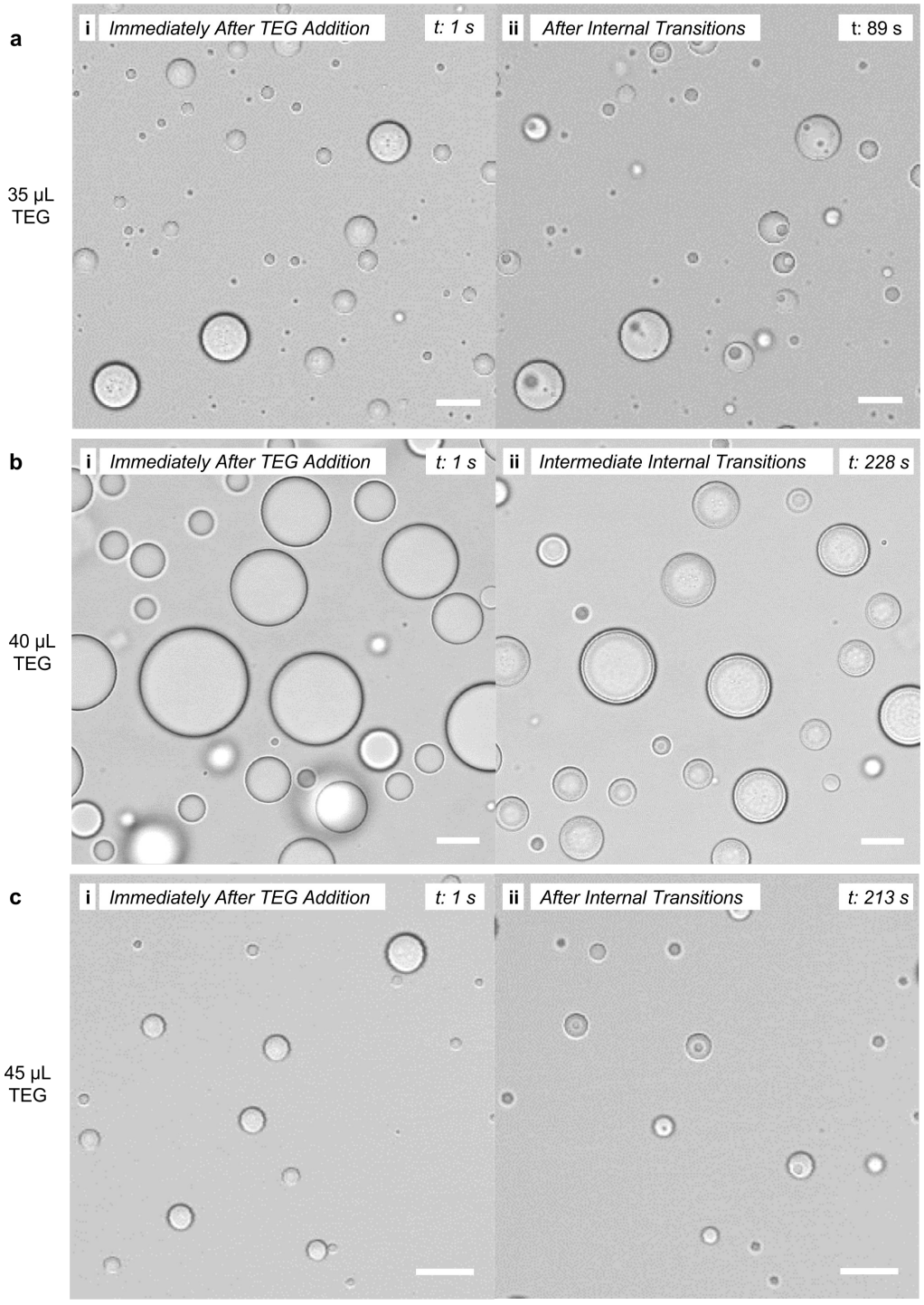

Figure 3.21: The effect of increasing the concentration of TEG on vacuole formation, within the vacuole forming region of the graph. Large scale brightfield microscopy images showing (i) the immediate effects of adding 35, 40 and 45 μL of TEG and (ii) the morphology of the coacervate droplets after any internal transitions caused by the TEG addition, with the exception of 40 μL TEG whereby the intermediate internal transitions are shown instead. Time points shown in seconds; scale bars 10 μm

The individual droplet time points were then examined for these concentrations (Figure 3.22). With the 35 μL addition of TEG, vacuole formation occurred almost entirely by the formation of small vacuoles beneath the whole interface and subsequent coalescence of these vacuoles. A 40 μL addition seemed to follow the same pattern but took considerably longer to progress beyond the blebbing stage and begin to produce tiny vacuoles at the interface.

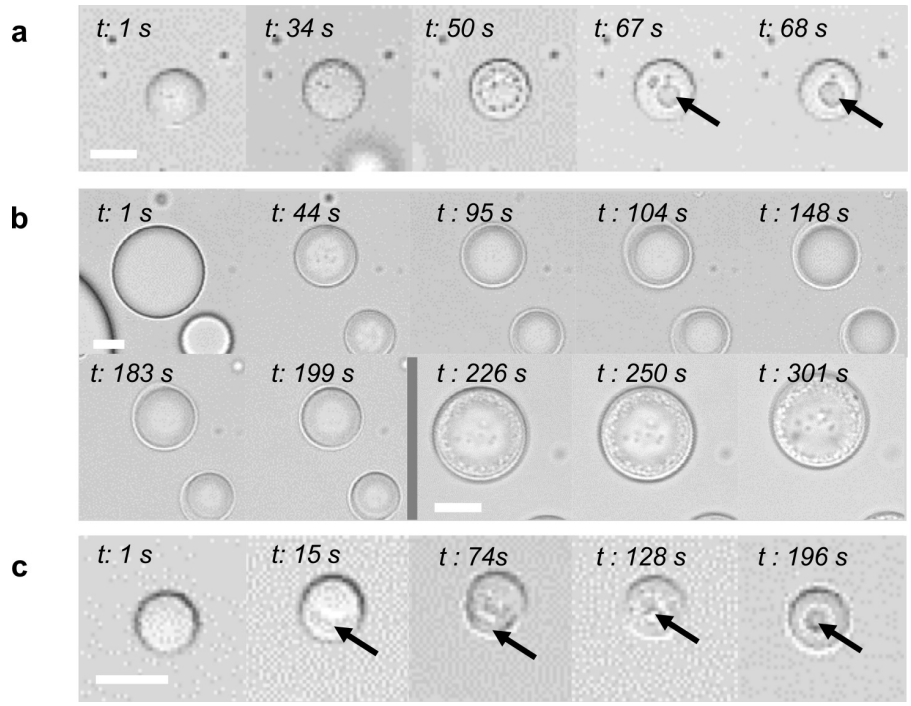

Figure 3.22: The effect of increasing the concentration of TEG on vacuole formation, within the vacuole forming region of the graph. Individual droplet time point sequences shown as bright-field images for TEG additions of (a) 35 μL , (b) 40 μL & (c) 45 μL. The arrows identify the vacuole as it is formed. Time points shown in seconds; scale bars 5 μm. A change of scale in (b) is indicated by the vertical grey line.

Indeed, during the time frame monitored, vacuole coalescence did not occur, indicating that there was some factor significantly delaying the progression of the normal mechanism. One possibility determined from this data is that the increased concentration of TEG within the coacervate droplet is able to form hydrogen bonds to itself, the ATP and any free water molecules. Potentially, the amount of TEG inside the coacervates reaches a point where it also inhibits the movement of water through the coacervate matrix, causing the tiny vacuoles to take longer to coalesce and preventing rapid progression of water molecules towards the interface of the droplet. Interestingly, the 45 μL addition was seen to progress more rapidly and by the alternative mechanism seen previously, whereby a single vacuole forms near the interface on one side and is then taken up into the matrix. This is contrary to what had already been seen, as the data up to this point suggested that increases in TEG concentration made the formation of multiple small vac-

uoles more likely compared to the formation of a single vacuole. Therefore a decision was made to investigate concentrations of TEG higher than 45 μL.

Figures 3.23 shows the large scale effect of TEG additions of 50 μL and 100 μL. Although difficult to see in this figure, with 50 μL TEG, almost all the coacervates bleb as anticipated. However, these coacervates do not go on to form vacuoles. With 100 μL TEG no blebbing nor vacuoles are seen. Despite this, significant shrinkage of the droplets does occur.

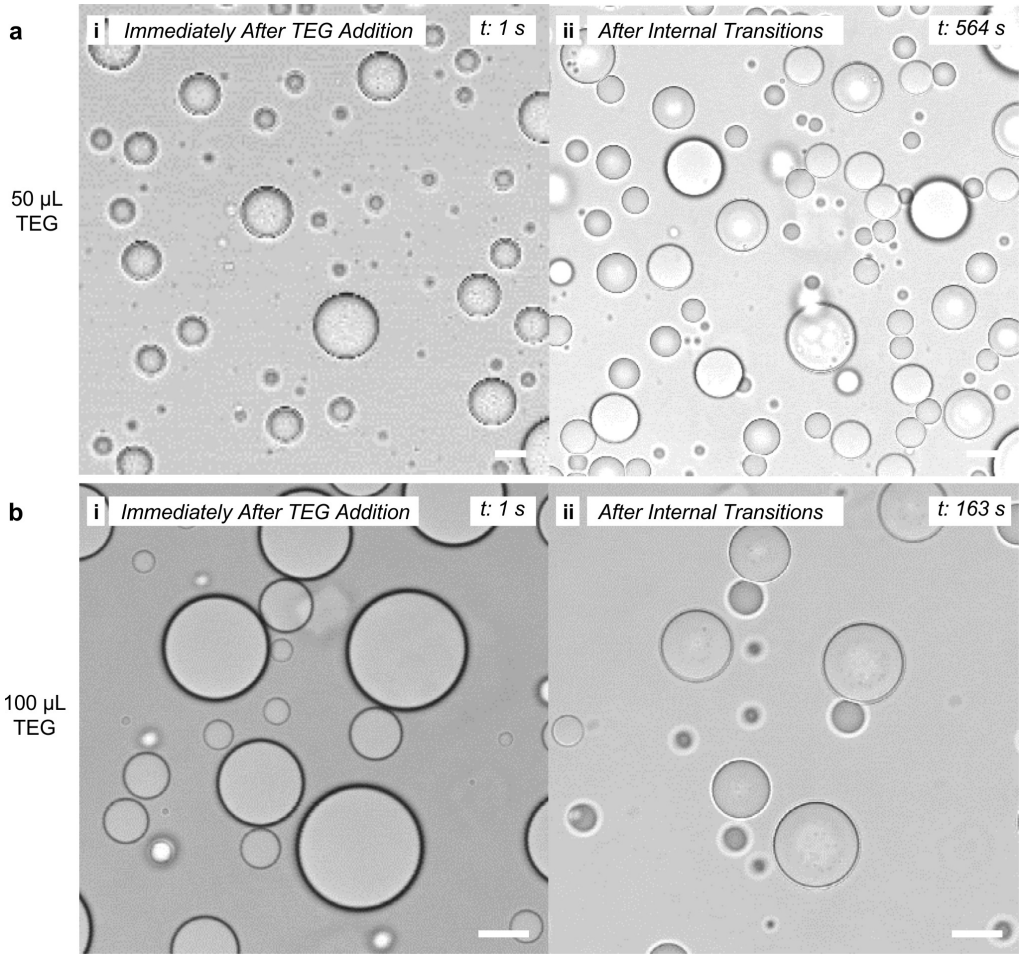

Figure 3.23: The effect of increasing the concentration of TEG on vacuole formation, above the vacuole forming region of the graph. Large scale brightfield microscopy images showing (i) the immediate effects of adding 50 and 100 μL of TEG and (ii) the morphology of the coacervate droplets after any internal transitions caused by the TEG addition. Time points shown in seconds; scale bars 10 μm

Individual droplets were then viewed over time (Figure 3.24). With the 100 μL TEG addition, some droplet wetting can be seen where the coacervate interacts with the coated glass slide (Figure 3.24b, at 22 seconds). However, this interaction is transient and the droplet recovers its normal non-wetted state before developing some aggregates at the centre of the droplet. Note

that these are different in appearance to the small vacuoles seen forming just below the interface in the other concentrations studied and, in contrast, form from the centre of the droplet not the surface. These aggregates are then cleared, and no indication of any mechanism of vacuole formation is observed. With the 50 μL addition of TEG, pronounced blebbing is seen at the interface of the droplet but upon retraction of these blebs small-scale structure formation can be seen, reminiscent of the aggregates that are also seen in the 100 μL addition system. These aggregates then coalesce to a ring of small vacuoles below the interface as seen previously, but before coalescence to a single large vacuole, are cleared from the coacervate. This presumably occurs by diffusion out of the matrix or re-equilibration of the matrix to accommodate the released water. When taking into account the results seen for an addition of 45 μL of TEG, this is surprising, as it was thought that this result may represent an inflection point whereby the system was moving back to a regime where the single vacuole mechanism was more likely.

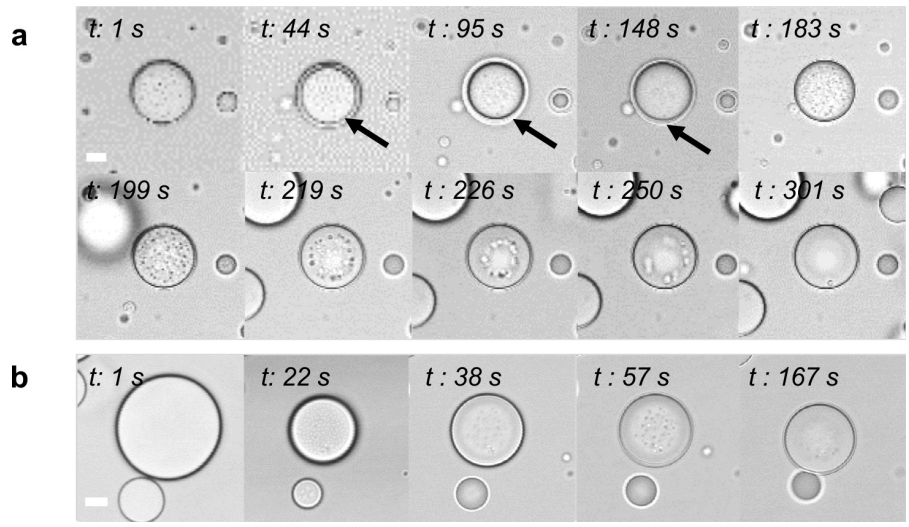

Figure 3.24: The effect of increasing the concentration of TEG on vacuole formation, above the vacuole forming region of the graph. Individual droplet time point sequences shown as bright-field images for TEG additions of (a) 50 μL & (b) 100 μL. The arrows identify the vacuole as it is formed. Time points shown in seconds; scale bars 5 μm.

If the suggested hypothesis is considered, there is clearly still a significant amount of water displaced in the system as small vacuoles are seen to form. However, it should be taken into consideration that the prior aggregates were not seen at any of the lower concentration additions. Also, the small vacuoles are cleared in a outwardly fashion, rather than coalescing in an inwardly fashion, despite initial inwardly coalescence.

To capture more information about the changes in mechanism between high and low concentrations of TEG, doped fluorescent ATP and PDDA were once again used to identify the location of coacervate components, with the 5 μL and 100 μL additions (Figure 3.25). The 5 μL addition did not appear to have any effect on the distribution of either coacervate component, and

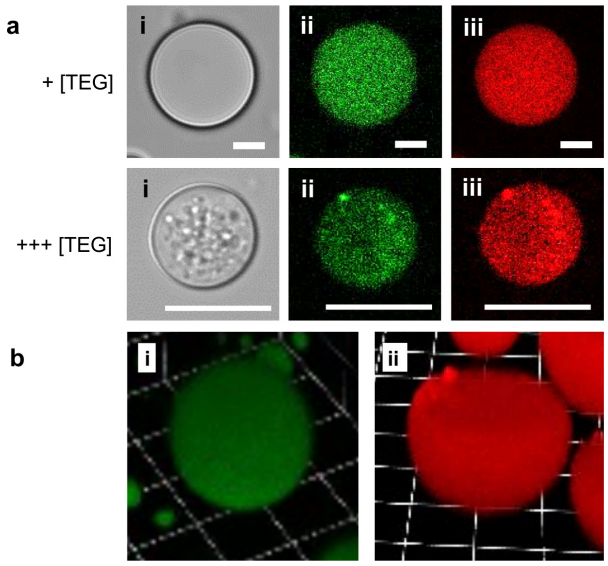

Figure 3.25: The location of coacervate components, ATP and PDDA, with lower and higher concentrations of TEG. (a)(i) Brightfield & (ii-iii) confocal fluorescent microscopy images showing coacervate droplets with a TEG addition of 5 μL (top row) and 100 μL (bottom row), showing the location of (ii) ATP, doped with ATP-TNP (green) and (iii) PDDA, doped with PDDA-RITC (red). Vacuoles are not apparent in either case although aggregates are seen with the 100 μL addition. (b) Re-constructed z-stacks from confocal microscopy slices after a 5 μL addition of TEG, showing (i) ATP, doped with ATP-TNP (green) and (ii) PDDA, doped with PDDA-RITC (red).(i) Scale bars: (a) 5 μm, (b) grid segment length (i) 12 μm & (ii) 10 μm.

both remained homogeneous throughout the droplet. This was also visible in the reconstructed 3D microscopy of the droplets after TEG addition, as no changes were seen over time (before images not shown as identical). With the 100 μL addition of TEG, aggregates were once again seen to form in the brightfield. In the ATP and PDDA fluorescence channels, the fluorescence no longer showed homogeneity. Whilst the resolution of the microscopy makes it hard to clearly determine the reasons for this, it appears that the aggregates are less fluorescent than the rest of the coacervate. This suggests that they could in fact be very small vacuoles, empty of coacervate components. It cannot be determined here whether these vacuoles contain TEG or not, however it could be implied that these vacuoles are of the same character as the larger vacuoles, which have already been shown not to contain TEG, as the components in the system are the same.

To elucidate more information about the mechanism of the system, fluorescently tagged TEG was used to obtain images of vacuole formation over time for some of the concentrations previously investigated in the brightfield view. The level of doping of fluorescently tagged TEG into untagged TEG was kept at a low level so that it would not interfere with the system. First, an addition of 20 μL of TEG was chosen, as this produced a large number of coacervates containing vacuoles, and all the vacuoles were seen to form by the mechanism whereby multiple small vacuoles formed under the interface of the droplet. This is shown in Figure 3.26.

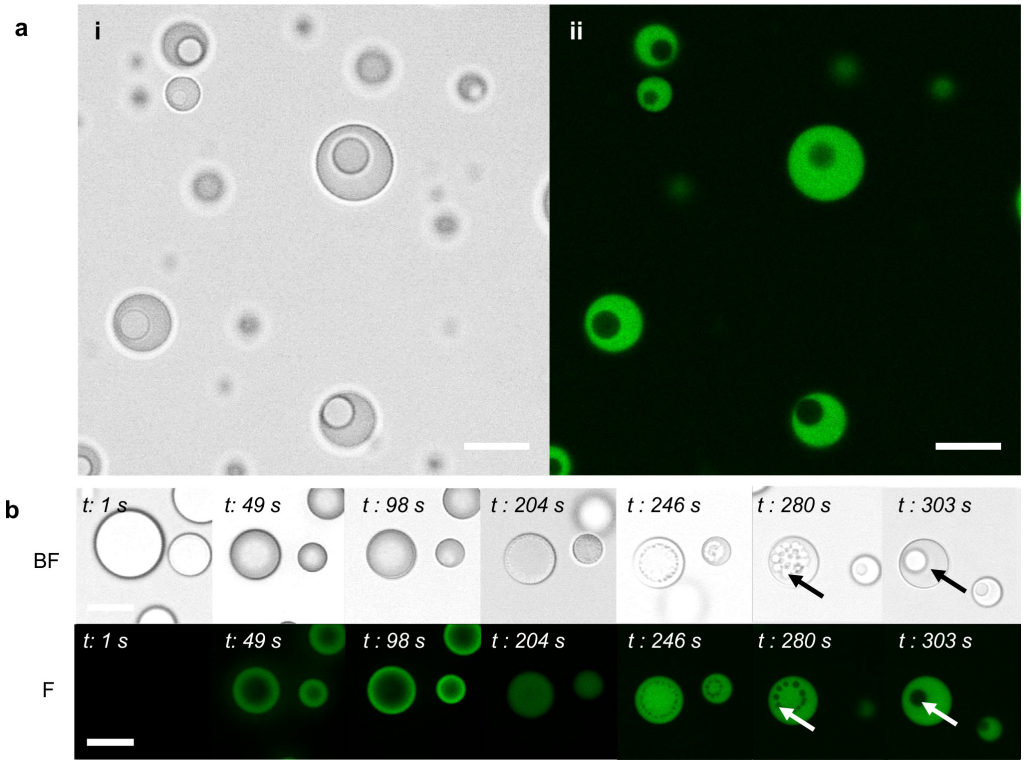

Figure 3.26: Observation of the mechanism of vacuole formation induced by 20 μL of TEG, using TEG tagged with FITC. (a) Large scale (i) brightfield and (ii) confocal fluorescence images after vacuole formation. (b) Brightfield (BF) and confocal fluorescence (F) time point sequences focused on a single representative droplet during vacuole formation. The arrows identify the vacuole as it is formed. Time points shown in seconds; scale bars 10 μm.

When comparing this to the 30 μL addition (Figure 3.17), it is clear that, although the fluorescent TEG coating looks similar initially, as time progresses the fluorescent coating here remains as a sharp band as though more TEG is collecting at the surface but less is immediately penetrating the matrix. Over time, the droplet becomes fluorescent homogeneously and no blebbing is seen at any time point (although this may be occurring at a unobservable scale). The small vacuoles that form below the interface, and the single large resulting vacuole, are clearly free of TEG.

The two extreme concentrations that did not seem to form vacuoles were also examined with the fluorescently doped TEG (Figure 3.27). These confocal fluorescence images showed that with low concentration additions, demonstrated here with 5 μL TEG, the TEG immediately enters the coacervate and no interfacial layer is formed. In contrast, with high concentration additions, demonstrated with 100 μL TEG, the TEG is inhibited at the interface in the first instance. It then takes a lengthy period of time to enter the coacervate and when this does eventually occur, the coacervate has lost integrity and appears wetted out on the slide.

These results may indicate that at low concentrations the TEG is not as hydrogen bonded to it-

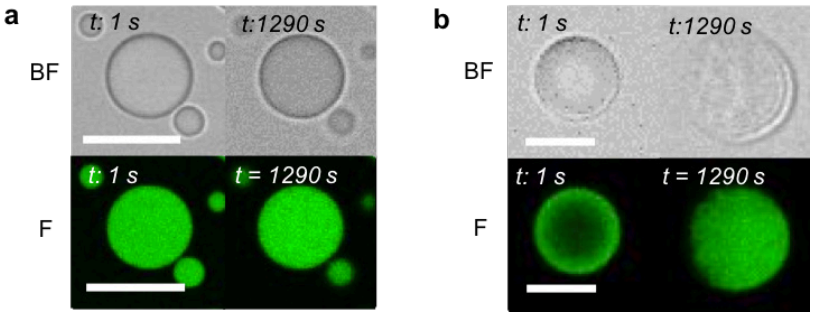

Figure 3.27: The progression of TEG into the coacervate at the two extremes of TEG concentration. Brightfield (BF) and confocal fluorescence (F) images focused on a single representative droplet before and after addition of (a) 5 μL and (b) 100 μL TEG doped with TEG-FITC (green) Time points shown in seconds; scale bars 5 μm.

self and displays properties based more on individual molecule interactions. The TEG molecules are able to penetrate the matrix quickly and hydrogen bond within this matrix. There is insufficient TEG to cause a massive expulsion of water molecules so the coacervate equilibrates quickly without any vacuole formation. With the high concentrations of TEG, the TEG is more hydrogen bonded to itself and the TEG addition behaves more like an interconnected mass of TEG. This collective behaviour, inducing an effective size increase, may be enough to severely inhibit the entry of the TEG into the coacervate matrix. Additionally, the wetting out of the coacervate, over a time period where this would not normally occur, indicates that the TEG may be displacing so many water molecules within the coacervate matrix that the coacervate loses integrity. At this point it is unclear whether it is just water that is lost, or any of the coacervates components as well, but it is clear that the structural integrity is severely affected by high concentrations of TEG.

The 100 μL addition was then investigated further, and time point images analysed to gain a better understanding of the destabilisation of the coacervate (Figure 3.28). Here the coacervates also wetted out as a result of the TEG addition but another morphology was observed in addition. Unusually, as further time points were monitored, the coacervates shrunk as seen previously but also became compressed on one side. An aura around each coacervate was also seen and this seemed to occur in a similar position to the perimeter of the initial droplet before further shrinkage occurred. This is therefore thought to be be TEG intercalated with coacervate matrix that has been dissembled and, as a result, wetted out on the slide. Towards the end of the experiment, one droplet can be seen with the remains of a very small coacervate whilst the others seem to have no coacervate left. In the brightfield microscopy view, all that can be seen are wetted out outlines of where the coacervates once existed. This implies that the coacervate is dissembled from the outside towards the centre, further adding evidence that as the TEG moves into the droplet matrix at high concentrations, it destabilises the structure of the coacervate

droplet.

The one sided compression of the droplets can also be seen in 3D reconstructions of z-stack confocal fluorescence slices (Figure 3.28b), both in the top-down view and the side view. This phenomenon was only seen in the largest droplets in the field of view and may well be coacervate size dependent. Examining an individual droplet time point sequence (Figure 3.28c) shows that a very distinct interfacial surface coating is first formed, which then stars to blur as fluorescence spreads outwards from the droplet. This is seen in the brightfield as well, and appears to be TEG leaching back into the supernatant perhaps as a result of some breakdown of the coacervate matrix near the interface. The way that this protrudes from the droplet appears to be similar to the way in which the blebbing seen previously occurred, however it can be seen by the difference in appearance of the brightfield images that this is wetted out material as opposed to blebbed material that still holds some structure. The flattened surface of the coacervate forms at the side where most wetted out material has been expelled, however the reason for a loss of shape in the coacervate is unclear. Thermodynamically, a spherical structure is most stable and perturbations to this are rarely observed, especially those that are more than momentary. It can be therefore be presumed here that the external TEG material that is contained within the wetted out material, is stabilising this abnormal structure.

The distinct interfacial coating appears to indicate the the TEG barely penetrates the coacervate matrix in this case, potentially because individual TEG molecules are very strongly hydrogen bonded to one another. If this is the case, the TEG coating may be providing a compressive force around the droplet as the forces involved in sequestration of the molecules into the coacervate are outweighed by the size exclusion properties of the TEG moving as a large mass of interconnected molecules. The TEG then begins to interact with the matrix only at the interface and coacervate disassembly begins at these points. TEG interaction and coacervate disassembly may both be affected by differences in the functionalisation across the glass slide, so it stands to reason that the some areas of the droplet will end up surrounded by a higher proportion of TEG and/or wetted out material. These regions would then induce a higher compressive force than regions with less TEG, leading to a difference in coacervate morphology around the droplet perimeter. To better understand this process, and to understand if this hypothesis is reasonable, further information is required about the potential loss of coacervate components during the addition of higher concentrations of TEG. This is explored later in the chapter.

All the evidence to date appeared to show that low volume TEG additions, such as 5 μL, had little effect on the coacervate internal structure and were below the threshold of TEG concentration required to induce vacuole formation. Therefore a decision was made to further investigate the effect of these low concentration additions by measuring other coacervate properties using sequestered GFP. This is shown in Figure 3.29.

By encapsulating the GFP, it was possible to obtain fluorescent confocal z-stacks which were

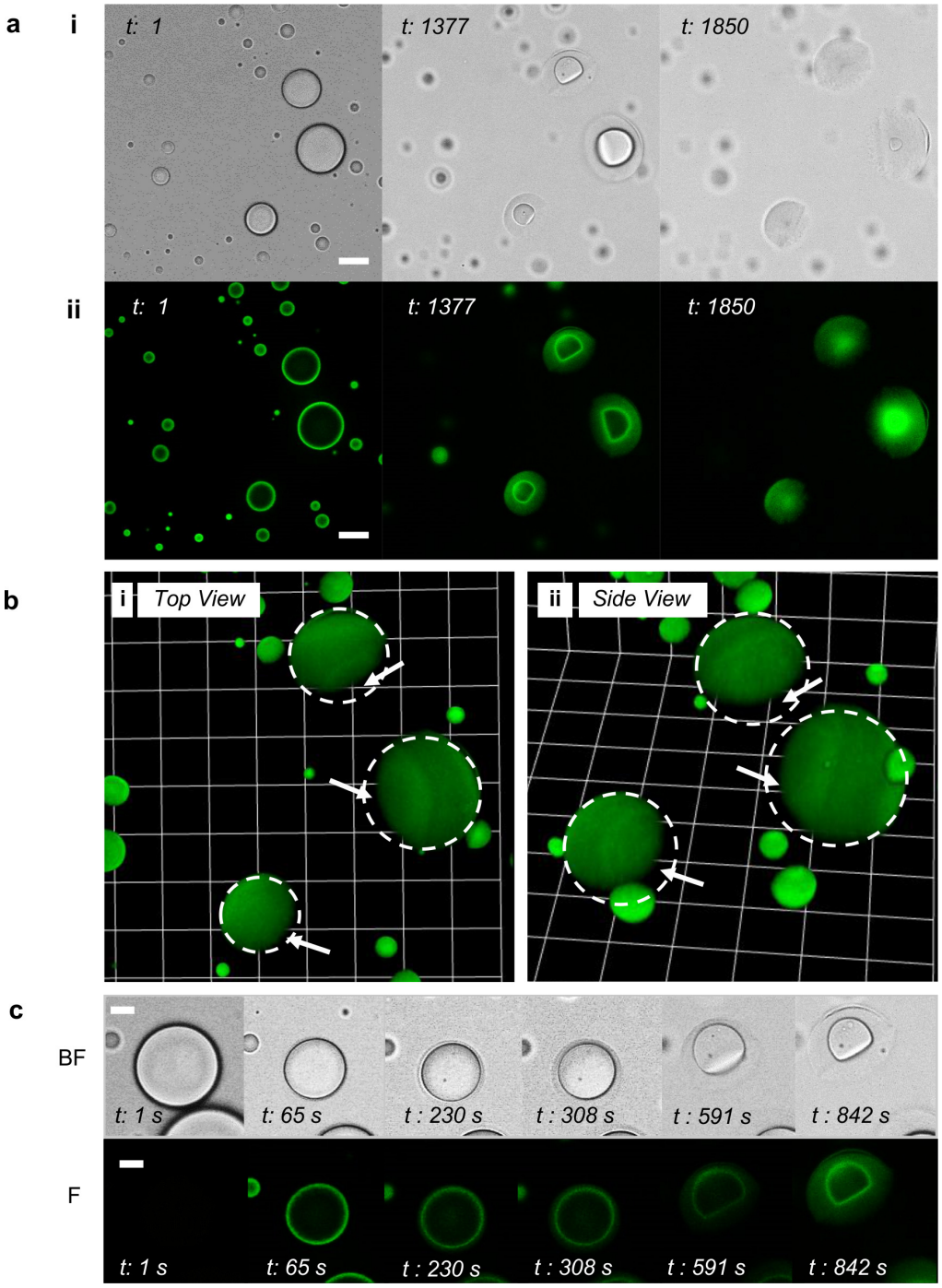

Figure 3.28: Alterations to coacervate morphology as a result of additions of high concentrations of TEG. (a) Large scale (i) brightfield and (ii) confocal fluorescence images after addition of 100 μL TEG. (b) Reconstructed images produced from 3D confocal fluorescence z stacks showing the perturbed morphology of coacervate droplets from a (i) top view and (ii) side view. Dotted circles identify the expected spherical coacervate boundary and the arrows show the space that would normally be occupied by coacervate. (c) Brightfield (BF) and confocal fluorescence (F) time point sequences focused on a single representative droplet. Time points shown in seconds; scale bars: (a) 10 μm, (b) grid segment length 9.5 μm, (c) 5 μm.

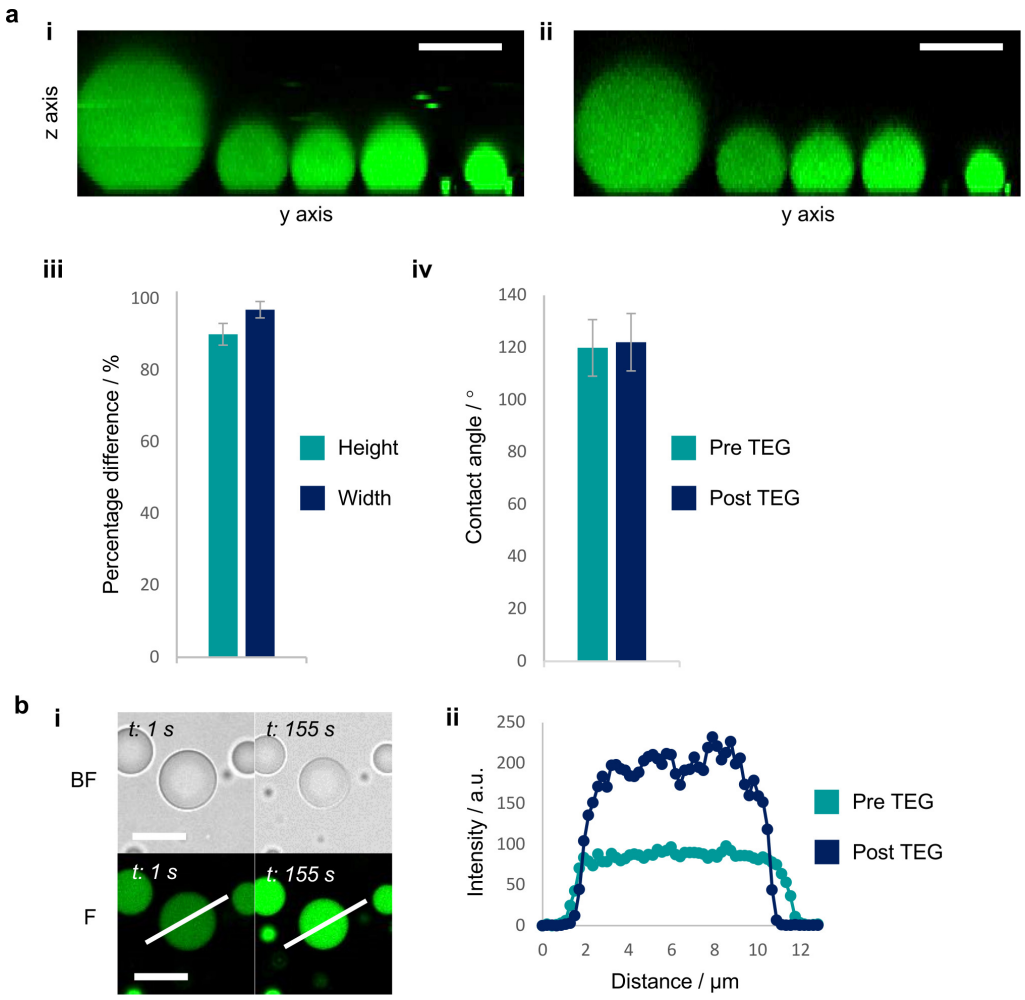

Figure 3.29: Observing the effect of low concentration TEG additions with sequestered GFP. (a) yz axis reconstructed z stack confocal fluorescence images showing coacervates containing GFP (green)(i) before and (ii) after the addition of 5 μL TEG, alongside statistical analysis of (iii) droplet height and width and (iv) contact angle changes after TEG addition. An example of the methodology for contact angle measurements is shown on the images in (a)(i). (b) Brightfield (BF) and confocal fluorescence (F) images showing GFP fluorescence change as a result of a 5 μL addition of TEG. Line profiles are shown in (i) and the corresponding plots show in (ii). Scale bars: 10 μm

then reconstructed to allow 3D visualisation of the droplets before and after low volume TEG addition (Figure 3.29a). Statistical analysis determined that the height and width of the droplets decreased, in line with the confocal results seen previously, but that this was not a proportional shrinkage and the height decreased more than the width (Figure 3.29a(iii)). This indicates that the droplet matrix becomes less rigid and compacts in the y axis due to gravity. It would be anticipated that this would have an effect on the contact angle of interaction between the droplet and glass slide but this was difficult to corroborate. Contact angle analysis (Figure 3.29a(iv)) did show an increase after TEG addition, but this could be considered irrelevant when the error is taken into account. However, these results demonstrate that the addition of TEG could be increasing the wetting of the coacervates on the glass slide, by impacting the internal properties of the coacervate matrix.

Figure 3.29(b) shows fluorescence confocal microscopy images of the intensity of the GFP prior and post TEG addition in an individual representative droplet, alongside the statistical analysis from a line profile across the droplet. A small shrinkage of the coacervate is observed, along with a significant increase in GFP fluorescence. This increase could be an indication that sequestered components within the coacervate are retained during droplet shrinkage and therefore become more concentrated. However, this increase could also be due to changes in the optical behaviour of the coacervate due to increased refraction as a result of the TEG now sequestered inside the coacervates. For reference, the refractive index of ethylene glycol (of which there are four units in the TEG) is 1.43 compared to a refractive index of 1.33 for water. The fluorescent output of the GFP may also change with environment. Unfortunately, due to these factors, it is impossible to de-convolute whether the GFP is concentrated or partially released as a result of TEG sequestration using these images.

Statistical analysis was done to elucidate the ATP, TEG and water content of the coacervates (Figure 3.30). This remained consistent until the 50 μL TEG addition, which is also the point vacuoles are seen to stop being made on the microscopy. As only the ATP is measured here, it is unknown whether the ATP is being displaced or PDDA as well as it could be the case that the coacervate is disassembling or that one component is leaving the matrix. With the TEG partitioning graph, the partitioning decreases even though the coacervates are equilibrated over 24 hours, i.e. long after the effect of TEG just diffusing in slowly should have disappeared. This is confusing however confocal images showed that sequestration of the TEG did occur but that sometimes the coacervates wet out so perhaps TEG is being released from coacervates in this way. Finally, the bulk water content decreases as TEG is added. The vacuoles would be displaced during centrifugation but this shows that water is also displaced from the coacervate matrix as TEG is added. This complements the theory that TEG could be replacing water in the hydrogen bonds with ATP.

If the hypothesis stands that TEG is interfering with the hydrogen bonding within the coacervate matrix, it stands to reason that replacing the TEG with a similar molecule, less capable of

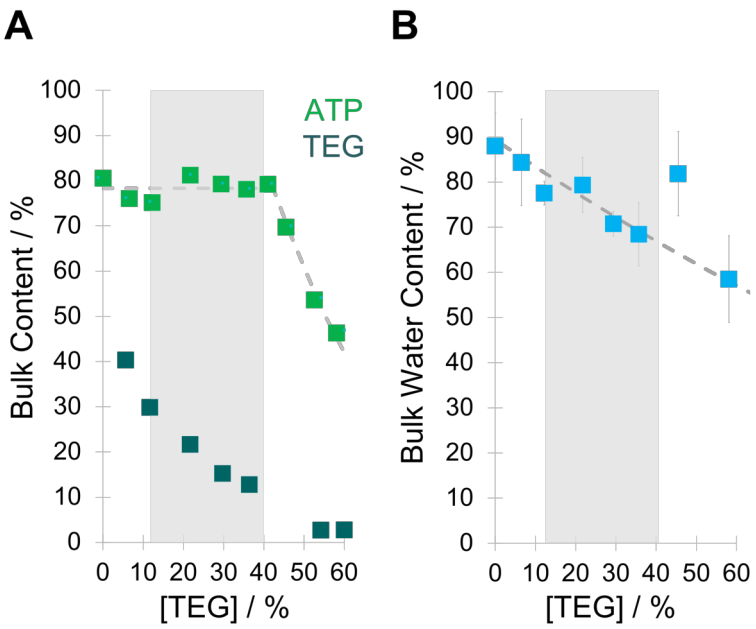

Figure 3.30: Effect of increasing concentrations of TEG on ATP, TEG and water content within the bulk coacervate phase. (a) ATP and TEG content in the bulk coacervate phase compared to the total ATP/ TEG added (in wt %) as a function of TEG concentration . (b) Water content in the bulk coacervate phase (in wt %) as a function of TEG concentration . The dotted lines in (a) and (b) indicate a line of best fit and the grey region identifies the TEG concentrations at which compartments are seen to form in the droplets from microscopy analysis. Error bars represents the standard deviation measured on three different samples.

hydrogen bonding, would alter the behaviour of the system drastically. With this in mind, either tetraethylene glycol monomethyl or tetraethylene glycol dimethyl ether, which have the terminal hydrogen at one, or both, ends of the TEG replaced with a methyl group, were substituted in place of the TEG. This would be expected to reduce the hydrogen bonding capability of the TEG with itself and the coacervate matrix.

The effect of using tetraethylene glycol monomethyl is shown in Figure 3.31. Additions of TEG between 5 μL and 100 μL were examined but no vacuoles were seen to form in any case. However, aggregates were observed in all examples, with the exception of the 10 μL addition although this is thought to be an anomaly. These aggregates were cleared outwardly from the coacervates without any coalescence into vacuoles. As this molecule was not fluorescently tagged, it is unknown whether these are aggregates or tiny vacuoles but it seems appropriate to consider that these may be small vacuoles based on the mechanism of vacuole formation seen with TEG.

However, it was observed that this molecule had an effect of the interaction of the coacervate with the glass slide (Figure 3.31b), despite not inducing the formation of vacuoles. When the microscope was focused onto the bottom of the droplet, where it rested on the slide, small patches

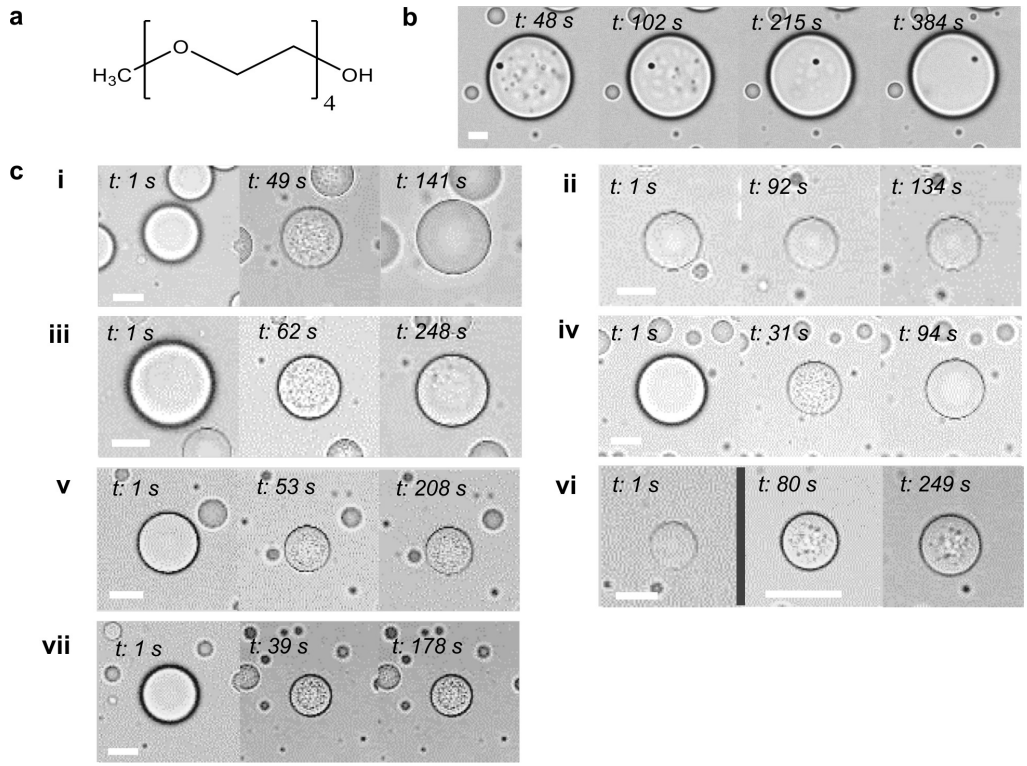

Figure 3.31: Substituting TEG with similar molecules - the effect of adding tetraethylene glycol monomethyl ether in place of TEG. (a) Chemical structure of tetraethylene glycol monomethyl ether, (b) brightfield microscopy focused on an individual droplet in the plane of the glass slide, showing the changes in interaction with the surface over time with a 30 μL addition. (c) time point sequences focused on a single representative droplet with varying concentrations of tetraethylene glycol monomethyl ether: (i) 5 μL, (ii) 10 μL, (iii) 20 μL, (iv) 30 μL, (v) 40 μL, (vi) 50 μL & (vii) 100 μL. Time points shown in seconds; scale bars: 10 μm. A change of scale in (b) is indicated by the vertical grey line.

that looked like wetted out material were seen to appear, as though the coacervate was interacting more with the slide. Over time, these wetted out patches disappeared and the coacervate returned to normal. It seemed here that the tetraethylene glycol monomethyl ether did cause some changes in the properties of the droplet, perhaps due to some hydrogen bonding, but that this was not significant to the overall structure and the coacervate was able to re-equilibrate quickly. This equilibration may include some loss of water resulting from displacement from the matrix, but to an extent far less than the TEG, which has the ability to hydrogen bond at both ends of the molecule. It should also be noted that the addition of tetraethylene glycol monomethyl ether causes a shrinkage of the coacervate droplets, as seen previously, indicating some loss of coacervate material as a result of the addition.

When this was then compared to tetraethylene glycol dimethyl ether (Figure 3.32), no initial shrinkage was seen at any concentration and no vacuoles or aggregates were observed. This

indicates that the this molecule either does not interact with the coacervate at all, or causes no disruption to the matrix when sequestered.

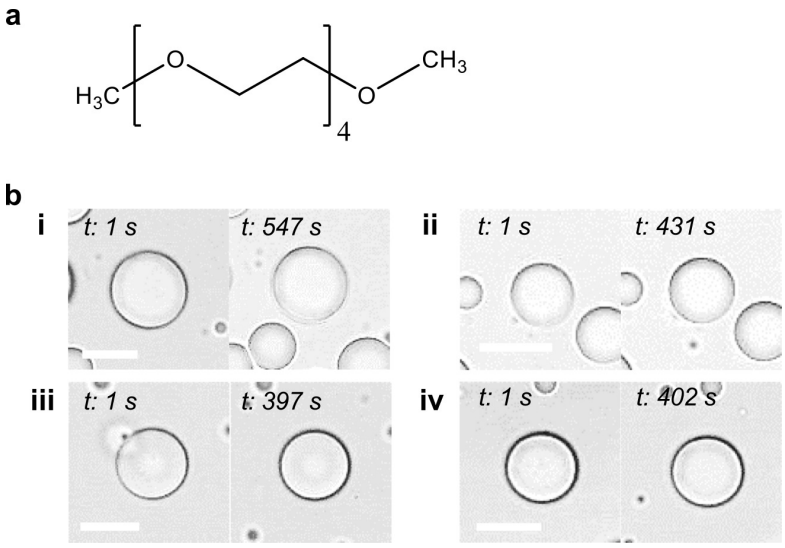

Figure 3.32: Substituting TEG with similar molecules - the effect of adding tetraethylene glycol dimethyl ether in place of TEG. (a) Chemical structure of tetraethylene glycol dimethyl ether, (b) time point sequences focused on a single representative droplet with varying concentrations of tetraethylene glycol dimethyl ether: (i) 5 μL, (ii) 20 μL, (iii) 50 μL & (iv) 100 μL. Time points shown in seconds; scale bars: 10 μm.

When comparing the three TEG-like molecules, their relative densities (taken from the literature) should also be taken into account. TEG has a density of 1.125 g/cm^3, whereas tetraethylene glycol monomethyl ether has a lower density of 1.045 g/cm^3. Tetraethylene glycol dimethyl ether has an even lower density of 1.009 g/cm^3. These values are all measured at 25 degrees C and indicate that there is less intramolecular bonding between TEG molecules as the number of hydroxyl groups at the ends is reduced. Methyl groups are also more hydrophobic than hydroxyl groups so this could also explain the reduction in effect seen when these alternative TEG molecules are added to the coacervates, although it may be expected that a higher hydrophobicity would result in more alternative TEG uptake into the coacervate droplet which is more hydrophobic than the surrounding supernatant. It should also be considered here that if small changes to the structure of the molecule replacing TE causes these large differences in uptake, the replacement of some TEG with TEG-FITC is likely to also have some effect despite the partitioning of TEG-FITC appearing to be similar to the of untagged TEG. The structure of TEG-FITC has a greater difference than these molecules and the effect of this molecule is discussed further with Figure 3.33.

Referring back to the statistical analysis of the coacervate populations with different concentrations of TEG (Figure 3.18), it is interesting to note that that in this first peak, lower concentrations of TEG (15 μL) actually cause more coacervates to posses a single vacuole than an increase

in the amount of TEG (to 20 μL and 30 μL), despite the hypothesis that more TEG would cause more water displacement. The author believes that this may be due to the hydrogen bonding between TEG molecules causing the TEG to penetrate the coacervate matrix at a slower rate the more TEG is added. This would mean that the concentration of TEG inside the droplet initially would be lower, displacing less water, but also that a slower rate would provide more time for the coacervate matrix to adjust to water loss by arrangement. At this point, it seems that the vacuole formation is, at least in part, caused by a rapid rearrangement of the matrix in response to a water loss which leads to the vacuole being retained.

It was also noted from the microscopy that the time taken to form the vacuoles varied hugely and was not seen to correlate with the amount of TEG added. This once again indicates that there is probably variation in the concentration of TEG interacting with each droplet in a given population, or an effect caused by an uneven slide coating. Additionally, the shrinkage in droplet size observed when TEG addition of all concentrations occurred was attributed to water loss prior to the formation of any interfacial TEG coating to inhibit water loss.

If the proportion of charged TEG (TEG-FITC) to uncharged TEG is increased, another effect is seen (Figure 3.33). Other literature has already shown that increasing charge can disrupt the coacervate matrix, causing the formation of vacuoles. Here, vacuole formation still seems to occur across the whole droplet but then, once again, begins to look like a ring of vacuole droplets below the surface that coalesce to a single vacuole. Dark patches are seen in the PDDA field indicating that these are PDDA deviod, and probably coacervate component free. TEG is sequestered and fills up outside the droplet as well as entering, although the background slightly further from the droplets remains black. TEG appears pushed out of the regions just below the interface which may have something to do with TEG's ability to surface wet. This effect happens at the same time as as the vacuoles become visible, although these are seen across the whole droplet initially. The next frame shows droplets forming a ring of vacuoles only.

This explanation here could be a culmination of effects. Predominantly there may be hydrogen bonding effects at the edge driving vacuole formation but electrostatic interactions with the FITC in the centre may also play a part. There is still a lot of TEG outside the droplet at this point but no pronounced interfacial boundary as seen previously. This could however be obscured. This is interesting as the concentration of TEG is the same but has a higher FITC component so the presence of the tag seems to inhibit entry, despite the fact that FITC goes in very easily. This is unlikely to be a size inhibition effect of TEG-FITC as it is much smaller than other molecules, e.g. the 4 kDa dextran that has been seen to go in easily. It is possible that the presence of the FITC tag means that more intramolecular bonding occurs between TEG-FITC and/or TEG molecules. The vacuole is produced off centre, but inside at the side of the coacervate showing more TEG fluorescence. Vacuoles on this side of the circle seemed to coalesce quicker, possibly suggesting more disassembly. The vacuole has no TEG inside and by the end, the TEG outside of the droplet seems to have evenly distributed.

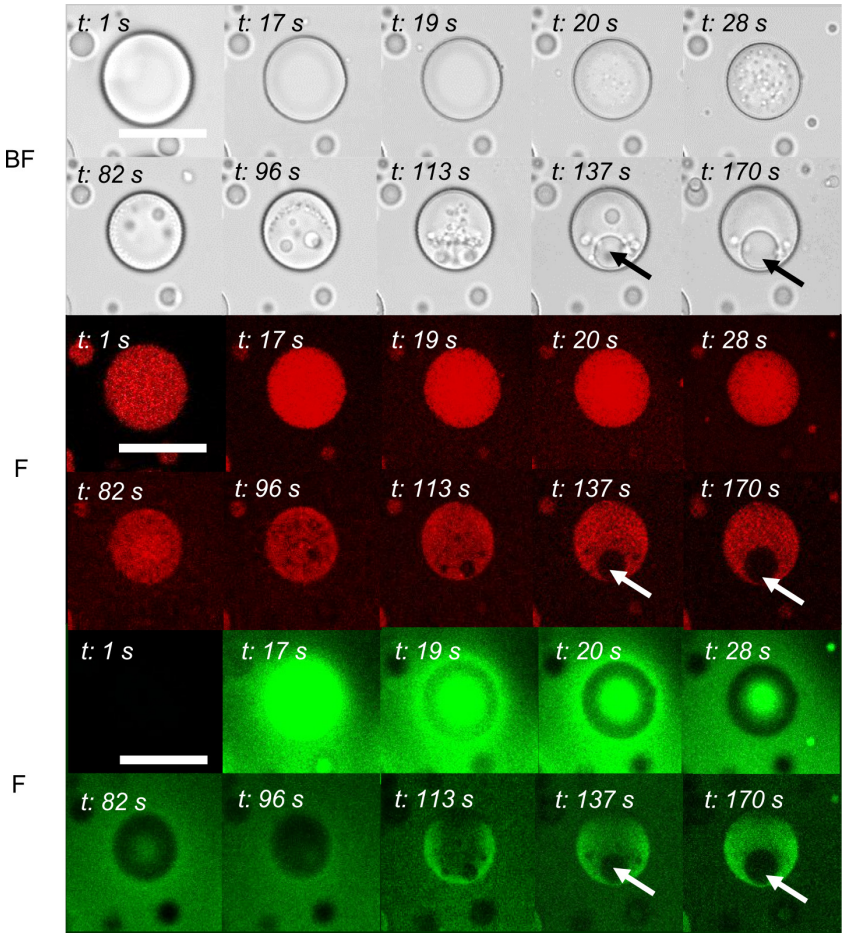

Figure 3.33: The effect of increasing the level of doping of TEG-FITC into untagged TEG. Doping was increased by a factor of ten-fold, to a 1:100 doping rather than a 1:1000 doping. The interaction of TEG with the coacervate is shown with Brightfield (BF) and confocal fluorescence (F) images focused on a single representative droplet after addition of 5 μL TEG doped with TEG-FITC (green). PDDA localisation is also monitored with PDDA-RITC (red). The vacuole is shown to contain no PDDA or TEG. Time points shown in seconds; scale bars 10 μm.

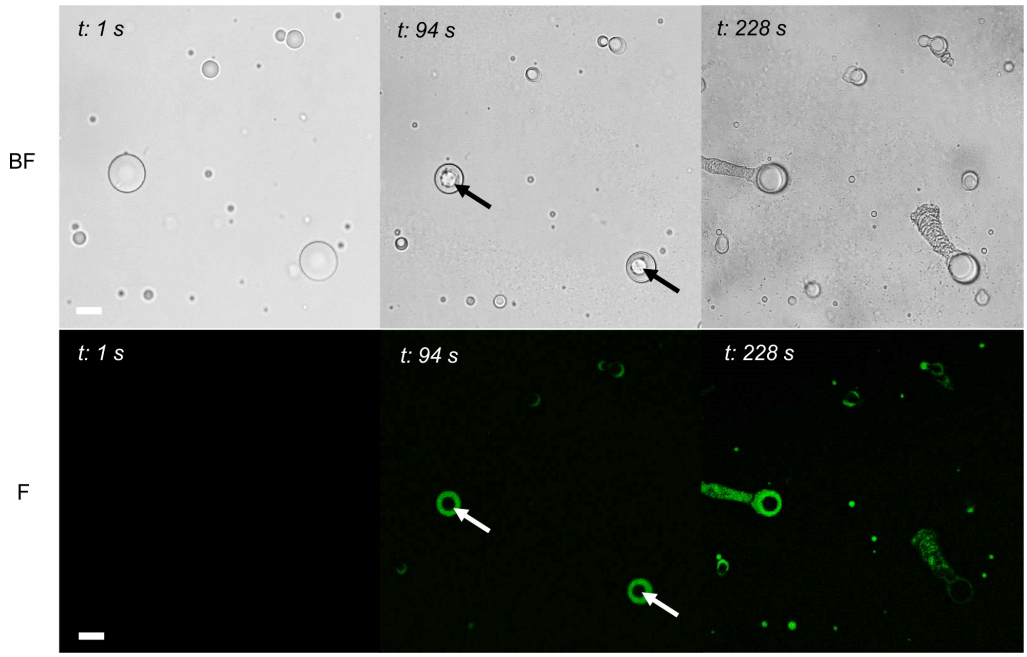

Figure 3.34: A ten-fold increase in the level of doping of TEG-FITC into TEG causes coacervate morphology changes, as a result of interactions with the glass slide. Large scale images of vacuole formation and subsequent directional blebbing of the TEG in the brightfield (BF) and confocal fluorescence (F) views. The arrows identify the vacuole as it is formed. Time points shown in seconds; scale bars 10 μm.

With the 100x doping, in some cases, other effects apart from simple vacuole formation are also seen (Figure 3.34). These include finger like projections and directional blebbing. It is suspected that the directionality seen with these blebs is due to inhomogeneity in the glass coverslip coating. This could potentially be investigated with coverslips that have been left to react with PEG silane for longer, to see if this reduces the effect seen. However, it is hypothesised that expulsion of material takes the path of least resistance. The blebs are fluorescent and therefore must contain TEG, and vacuoles are formed rapidly. This data indicates that the slide covering influences the speed of vacuole formation and blebbing, and also that some expulsion of TEG (and maybe coacervate) has to occur to stabilise these systems with higher proportions of TEG-FITC. It would be interesting to develop this system further to see if it could be used as a controlled mechanism for coacervate material transfer.

The effects are studied in more detail in Figure 3.35. Small vacuoles seem to form in a circle just inside the interface, as though the normal TEG interactions may still be dominating. The bleb from the vacuole seems to form out of focus of the microscope as though it is expelled from the bottom of the droplet. This agrees with the hypothesis that the phenomena are a result of interactions with the coated slide. Previous investigations with the other types of TEG suggested that even in the normal TEG system, interactions with the glass slide change the system slightly so

this may be a more extreme version of processes seen previously, due to the additional properties of the FITC. The TEG in the coacervate portion appears to get less fluorescent as time goes on as though the concentration is decreasing, suggesting that TEG-FITC, and probably TEG, is flowing out of the coacervate into the finger projections. The samples with 100x doping were shown to behave only slightly differently in partitioning experiments, indicating that the effects seen here are exacerbated by other effects that were not present in those experiments, such as interaction with the slide. It is possible that there is an induced osmotic drive to release the contents and collapse which may or may not be driven by the slide interaction.

Another example with 100x doping is seen in Figure 3.35b. The TEG still blebs and removes TEG from the coacervate but the vacuoles form at a later point. This suggests that the blebbing is not a result of the vacuole formation but a by-product of the interaction that causes vacuole formation. It may also be an effect of having too much destabilisation but instead of disassembling the coacervate as seen before, the system ejects some of the component and then a vacuole is able to form in the coacervate that remains once the concentration has reduced. However, again what is interesting is that the TEG inside the droplet does not seem to be homogenous even after the vacuole has formed. The blebs don't spread into finger projections and there is also a lot more TEG remaining in the background, compared to the previous sample. This decreases as TEG-FITC is sequestered into the bleb and the background also decreases. The bleb spreads around the coacervate possibly due to a surface tension effect. There is scope here to suggest that TEG interactions with the glass slide may have been playing a part all along at the base of the coacervate, which has helped to drive the interactions. However, the effects seen can't entirely be due to this. Statistical analysis of TEG, water and ATP content in the samples showed that changes occured even in solutions not interacting with glass slides.

3.2.1.3 Sequestration of a Single Solute in a Single Population - Larger Molecules

The sequestration properties of larger molecules were then analysed, to see how these behaved differently to the smaller macromolecules.

3.2.1.4 Sequestration of a Single Solute in a Single Population - Larger Molecules: Dextran

Dextran-FITC is readily available to purchase, so dextrans with a range of molecular weights were used to determine the behaviour of this class of molecules with the ATP: PDDA coacervate system. Microscopy and calculated partitioning values for these are shown in Figure 3.36.

Taken together, this set of data indicates that dextran with molecular weights of 70k and above are mostly excluded from the droplet interior. It is interesting that the relationship between molecular weight and partition coefficient is not linear. It has been shown that dextrans with lower molecular weights form very different structures to those with higher molecular weights in

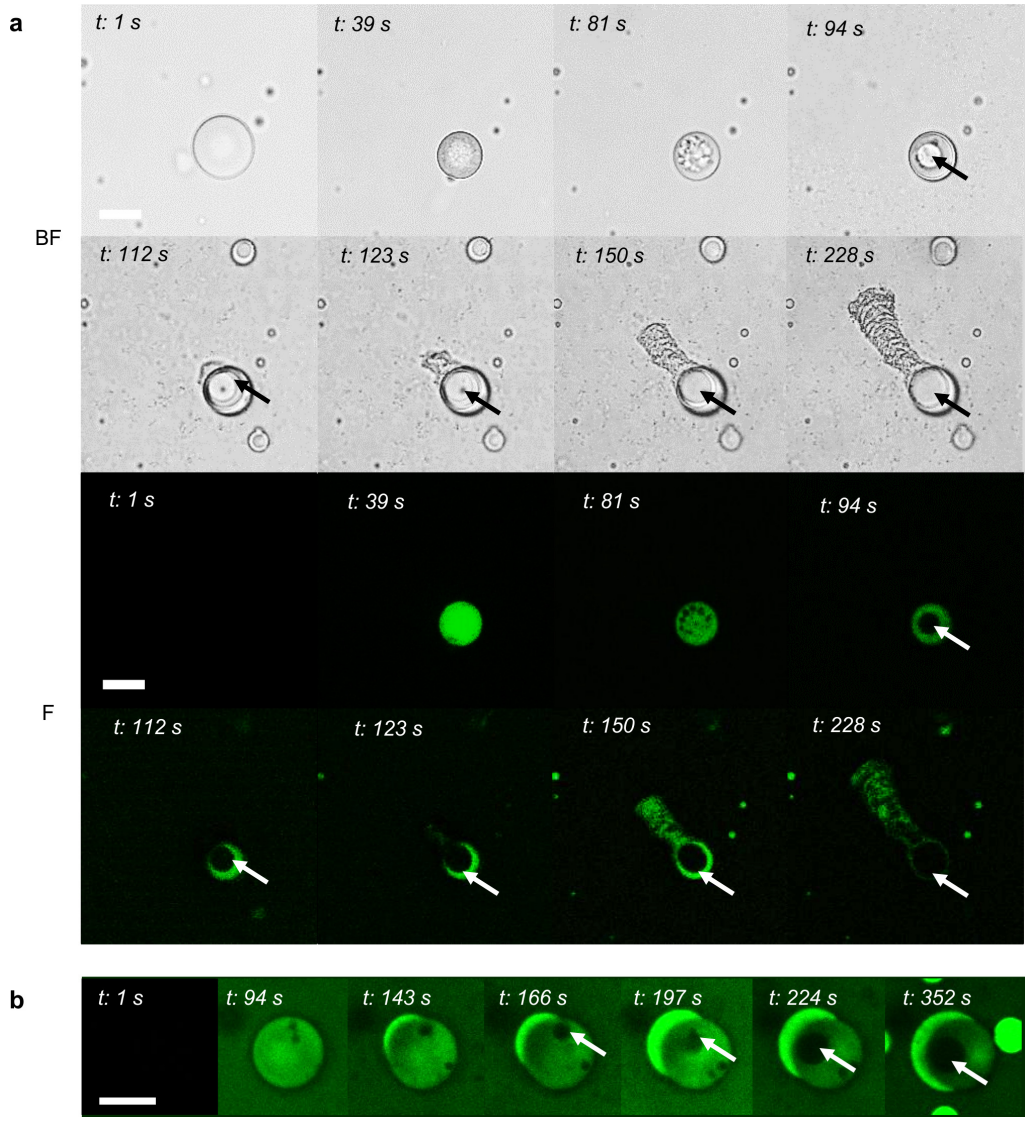

Figure 3.35: A ten-fold increase in the level of doping of TEG-FITC into TEG (to 1:100 doping rather than 1:1000) causes coacervate morphology changes, as a result of interactions with the glass slide. Two types of slide interaction are observed: (a) finger-like protrusions that spread away from the droplet and (b) blebbing that surrounds the droplet. Brightfield (BF) and confocal fluorescence (F) timepoint sequences show vacuole formation and subsequent blebbing of the TEG (b) Confocal The arrows identify the vacuole as it is formed. Time points shown in seconds; scale bars 10 μm.

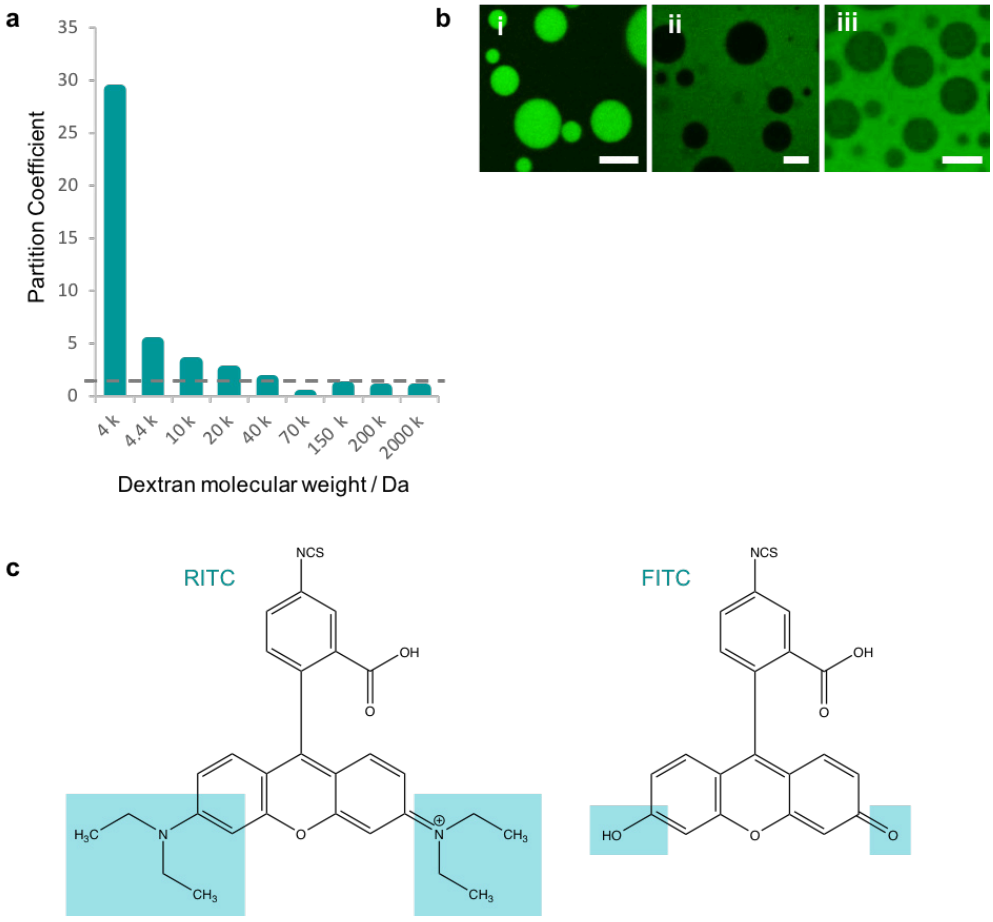

Figure 3.36: Entry of the dextran into the coacervate matrix is dependent on molecular weight. (a) Partition coefficients of dextran-FITC, calculated from UV-Vis spectroscopy data. The grey line illustrates the point where the partition coefficient falls below one, indicating that the concentration of dextran excluded from the coacervate is greater than that incorporated. (b) Confocal fluorescence microscopy images of coacervates with dextran-FITC of molecular weights (i) 4k, (ii) 70k and (iii) 150k. Scale bars: 10 μm. (c) The structures of RITC and FITC showing the differences in side groups highlighted in blue.

that 2000-1000 Da dextrans branch less and exhibit properties similar to an expandable coil but very low molecular weight dextrans behave like rods. This may explain the pattern seen, as even at higher molecular weights the dextrans may have ranges of structure. It may be that dextrans of shorter molecular weights are able to diffuse through the PDDA molecule network formed with the ATP in the coacervate, whereas longer chain polymers, i.e. the higher molecular weight dextrans, are unable to diffuse through so easily and remain trapped at the surface despite being attracted to the interior environment. This could be investigated further. It also suggests that the addition of dextran does not seem to interfere with the structure of the coacervate and, other than sequestration, no internal changes are seen at the resolution observed.

Dextran-FITC 70 kDa was then compared with dextran-RITC 70kDa (structures shown in Figure 3.36), to examine the effect of charge on dextran partitioning into the coacervate droplets (Figure 3.37). Dextran-FITC and dextran-RITC have nearly identical structures although their molecular charge is slightly different in the coacervate environment. FITC is neutral at pH 8 whereas RITC is slightly positively charged, as is the coacervate interior, and this difference may be the driving force of the effects seen here with a slightly greater repulsion between the dextran-RITC and the coacervate compared to the dextran-FITC and the coacervate. When the partitioning of the two molecules into the system was compared, FITC-dextran 70 kDa partitioned at a value of 0.014 and the RITC-dextran 70 kDa at a value of 0.017. This would indicate that the FITC-dextran partitions slightly better, although the values are close. However in both cases, the dextran does not contain huge numbers of these fluorescent side groups (0.002-0.015 mole RITC per mole glucose and 0.003-0.020 moles FITC per mole of glucose). Neither dextran enters the coacervates but at both concentrations examined the dextran-RITC coated droplets do not seem to form rings at the surface even though the dextran-FITC coated droplets do. The confocal fluorescence data also corroborates the fact that graduated rings of dextran-FITC were forming around the coacervates, with slices and subsequent 3D reconstructions showing that the addition of higher concentrations of dextran-FITC increased the background fluorescence but did not encourage the dextran to enter the droplet interior. These observations indicate that the behaviour of the tagged dextrans with the coacervates is dependent on both the chemical and physical properties of the tag. Dextran itself carries insignificant charge to contribute to the interaction but the size of the dextran is likely to dominate the interaction with coacervates.

The next stage was to see whether dextran addition to the surface of the coacervates was making the droplets more stable to coalescence. This was measured via the ζ-potential and UV-vis absorbance of the turbidity over time (Figure 3.38). Increasing the concentration of dextran-FITC (70 kDa) added to the coacervates did not have any effect on the value of the ζ-potential peak. This indicates that the droplets do not become more stable with increasing concentrations of dextran-FITC and are no more stable than those without any coating. Additionally, whilst it is impossible to draw conclusive conclusions about the changes in surface charge due to the droplet size distribution varying between samples, it appears that the surface charge of the droplet has

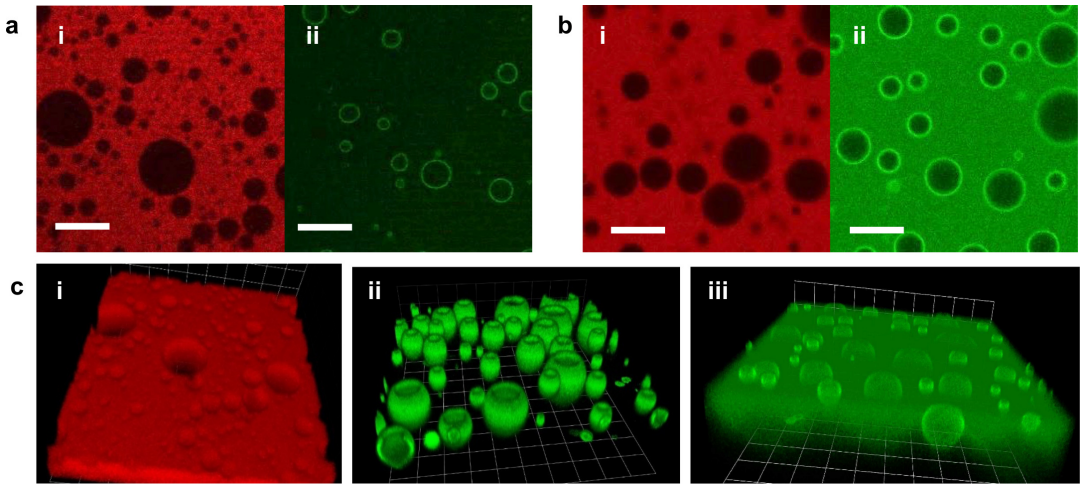

Figure 3.37: Differences in the partitioning of the same size dextrans when the charge of the tag differs. Confocal fluorescence images of a: 0.6 mg/mL dextran and b: 10 mg/mL dextran with either i: RITC or ii: FITC attached to the dextran. C: reconstructed confocal z stacks of i: 10 mg/mL dextran-RITC, ii: 5 mg/mL dextran-FITC, and iii: 10 mg/mL dextran-FITC. All dextran is 70 kDa. Scale bars: 10 μm.

not been altered even though the FITC carries a negative charge and therefore would be expected to increase the negativity of the surface if it was partitioned at the interface. This data suggests that the droplets have not undergone any significant surface change but it may be that the dextran coating is in fact forming within the coacervate as a separate phase just below the surface, in which case the ζ-potential data would not show an alteration.

However, the UV-Vis data seems to suggest that there is a difference in the speed at which coacervates coalesce over time with the different dextran coatings. It can be seen that 0.6 mg/ml additions of dextran-FITC, both 70 kDa and 150 kDa, and 10 mg/ml additions of Dextran-FITC 70 kDa show a decreased stability to coalescence compared to droplets with no dextran coating at all. This indicates that the droplets have been altered in a counter-productive manner for stability. Furthermore, both the Dextran-RITC concentrations show similar behavior to coacervates with no coating, corroborating the earlier microscopy images suggesting that dextran-RITC does not coat the droplet surface whereas Dextran-FITC does. However, the addition of 10 mg/ml dextran-FITC 150 kDa does show a repeatable increase in coacervate stability over time. It may therefore be that the increased length dextrans hold an advantage for coacervate stability and suggests that dextran-FITC partitioning does have an effect on coalescence, but perhaps only when it reaches a certain saturation on the droplet surface.

The localisation of the dextran-FITC coating was also monitored over time to understand whether the dextran remains on the surface of the droplet or diffuses away from the surface over time, either into the droplet or back into the surrounding supernatant. A video taken over four hours (shown in attached videos on disk) with dextran-FITC 70 kDa suggests that the dextran remains

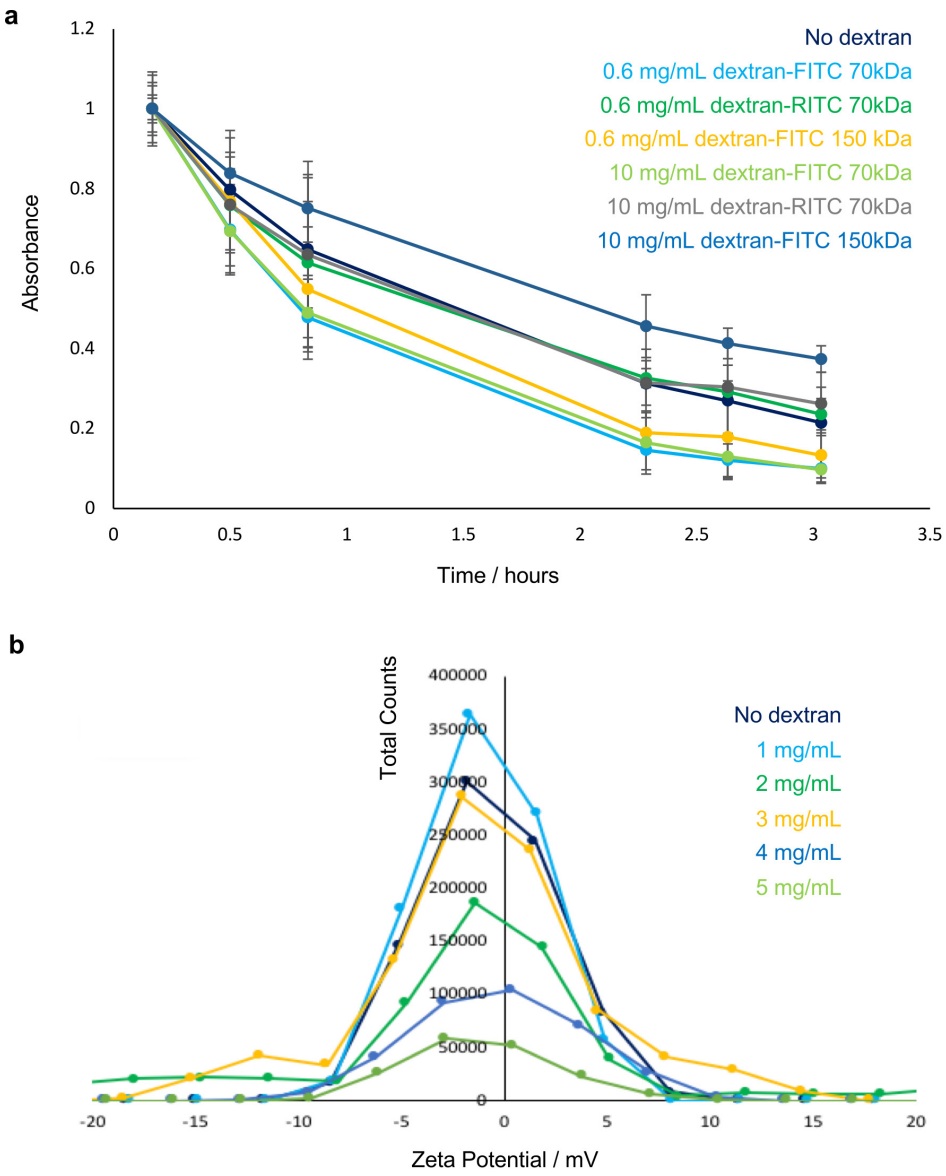

Figure 3.38: Effect of dextran addition on the stability of coacervates. Shown by a: reduction in turbidity over time when dextran size, concentration and fluorescent tag are altered. The data has been normalized to account for differences in coacervate concentrations between samples. concentration b: ζ-potential measurements showing the effect of increasing the concentration of dextran-FITC 70 kDa on the surface potential of the droplets.

on the surface of the droplet and that the droplets behave similarly to re-suspended coacervates without dextran, with respect to the coalescence of droplets.

In order to see if dextran contributed to a separate coacervate phase at the surface of the droplets, possibly an ATP: dextran phase, fluorescent PDDA-RITC and TNP-ATP were used to determine the location of coacervate components within the droplet. The coacervates were then observed with and without the addition of dextran (Figure 3.39).

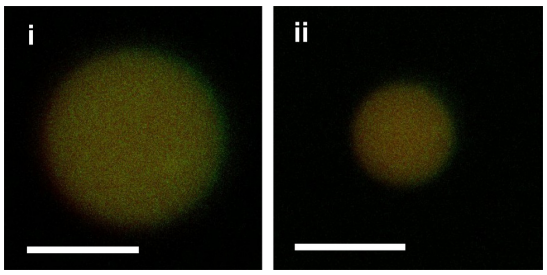

Figure 3.39: A dextran surface coating on coacervates does not alter the location of coacervate components. Coacervates are shown i: before and ii: after the addition of 200 kDa dextran. ATP is doped with 2',3'-O-(2,4,6-trinitrophenyl) ATP (TNP-ATP), shown in green, and PDDA doped with PDDA-RITC shown in red. Scale bars 5μm.

In these instances, labelled dextran could not be used as this would overlap the emission of the tagged ATP and PDDA. TNP-ATP and PDDA-RITC were doped in with normal ATP and PDDA so that any unusual interactions caused by the fluorescent molecules would be kept to a minimum and would not affect coacervation. 200 kDa dextran was chosen as it was clear from the UV-vis data that higher molecular weight dextran would have the largest effect on surface partitioning. Confocal microscopy slices of the droplets did not appear to show any difference in structuration between those droplets with and without dextran. Whilst there may be some difference on the nanoscale, which is not visible in these image, this suggests that dextran addition does not cause a large difference in coacervate component arrangement.

To see if the dextran coating was inhibiting molecular entry, a range of dye molecules were selected for sequestration into the coated coacervates (Figure 3.40). These had a variety of properties with positively charged molecules, such as rhodamine 6G and methylene blue, observed alongside negatively charged molecules, such as fluorescein and calcein, Large globular proteins such as mCherry and GFP, were also investigated. When the partitioning of these molecules within the dextran coated coacervates was observed by confocal microscopy, it became clear that the surface coating was not inhibiting any macromolecule entry. This suggests that the dextran boundary is entirely penetrable.

Dextran-FITC was exchanged for CmDextran-FITC to see the effect of this on partitioning (Figure 3.41). The carboxymethyl group carries a positive charge which could be used to encourage positively charged molecules to adhere to the surface, or to prevent entry of negatively charged

Sequestered Macromolecule	Macromolecule Class	Charge (at pH 8)	Successful Partitioning Into Coacervate
Rhodamine 6G	Small Molecule	Cationic	✓
Fluorescein	Small Molecule	Anionic	✓
Calcein	Small Molecule	Anionic	✓
Methylene Blue	Small Molecule	Cationic	✓
mCherry	Globular Protein	Anionic	✓
GFP	Globular Protein	Anionic	✓

Figure 3.40: Dextran coating on coacervates does not prevent the sequestration of macromolecules. The sequestration of macromolecules with different properties was determined by confocal fluorescence microscopy and the partitioning summarized in the table. Dextran is dextran-FITC 150k Da.

macromolecules. However, when CmDextran is added, in place of dextran-FITC with the same molecular weight, no surface partitioning occurred. It may be that the positively charged groups on the CmDextran alter the global structure of the molecule such that their repulsion causes the molecule to be more fluid, and can therefore more freely diffuse through another polymer, such as the PDDA.

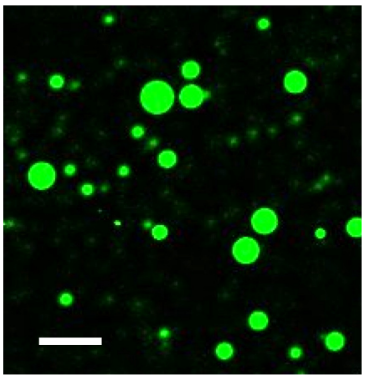

Figure 3.41: Carboxymethyl-dextran (CmDextran) addition to coacervates does not result in exterior partitioning. The CmDextran has a molecular weight of 70 kDa, similar to the dextran used in the other experiments.

3.2.2 Exchange Between Coacervates

As stated in the introduction, in a minimal protocell, it is essential that it is able to effectively sequester required components and stably separate its internal contents from the external environment, whilst allowing the controlled transfer of useful materials. Without this, the cell would be incapable of the means to evolve and would not have the capacity to emulate the confinement required for enzymatic reactions. It was also important to investigate the movement of oligomers between droplets.

3.2.2.1 Exchange in a Binary Population, Where Each Population Contains a Single Solute

For these experiments the ability of the two DNA oligomers, used previously, to base pair to form double-stranded DNA was exploited. The complimentary sequences initiate base pairing, which in turn brings the two fluorophores close enough together for Förster Resonance energy Transfer (FRET) pairing to occur (Figure 3.42).

The fluorimetry plots show the absorptions and emissions for the fluorophores, with maximum peaks at 480 nm excitation and 520 nm emission for the fluorescein and 650 nm excitation and 670 nm emission for the cy5. These are the values expected for such fluorophores. or all three measurements, however the total counts for fluorescein when combined with Cy5 are an order of magnitude higher than expected. This is probably due to the fact that cy5 begins to quench at higher concentrations (data not shown). The excitation emission efficiency plot for the combined DNAs does not show the emission of cy5 at 670 nm resulting from co-localisation of the fluorophores and an excitation of 480 nm. However, this is because the FRET emission here is at a much lower level than the direct emission and so is lost in the background of the contour maps. When the individual excitation line plot is interrogated at 480 nm, the FRET can be seen at 670 nm with a total count number of approximately 5000 counts, compared to the 200000 counts seen from the direct fluorescein emission. Once the fluorophore parameters had been characterised, the oligomers were loaded into coacervate droplets to observe the difference between two populations versus a co-localized population of DNA. Droplets can be seen clearly as either red if cy5 is present, green if fluorescein is present, or yellow if mixing has occurred.

The FRET occurring in individual coacervates was then measured (Figure 3.43). Low concentrations of salt were used as a control to begin to disassemble the coacervates in order to release the coacervate components. These components are then taken up by other droplets, inducing mixing of the single-stranded DNA. The fluorescein droplets within the mixed population are observed, as it is the reduction in fluorescein signal that is being analysed by FRET acceptor photobleaching (FRET-AP). The fluorescein and Cy5 intensities are shown over time, for the droplets shown in Figure 3.43a. Each coloured line represents one droplet. Across each pair of graphs, the same coloured line represents the same droplet in both channels. The signal is normalized to droplet volume in each case.

Collectively, these results indicate that with the addition of salt to dissemble the droplets, the movement of fluorophores produces a clear FRET signal, above the level of the noise and photobleaching of the sample. In contrast, when no salt is added, the signal is low and cannot be seen above the noise. It appears that the addition of salt allows transfer of oligomers but that without salt, movement of fluorophores does not occur over time. Therefore, the coacervate system appears to fulfil the potential of a protocell to stably contain its contents without transfer over time. The droplets do not appear to show mixing of contents except when salt is added to ini-

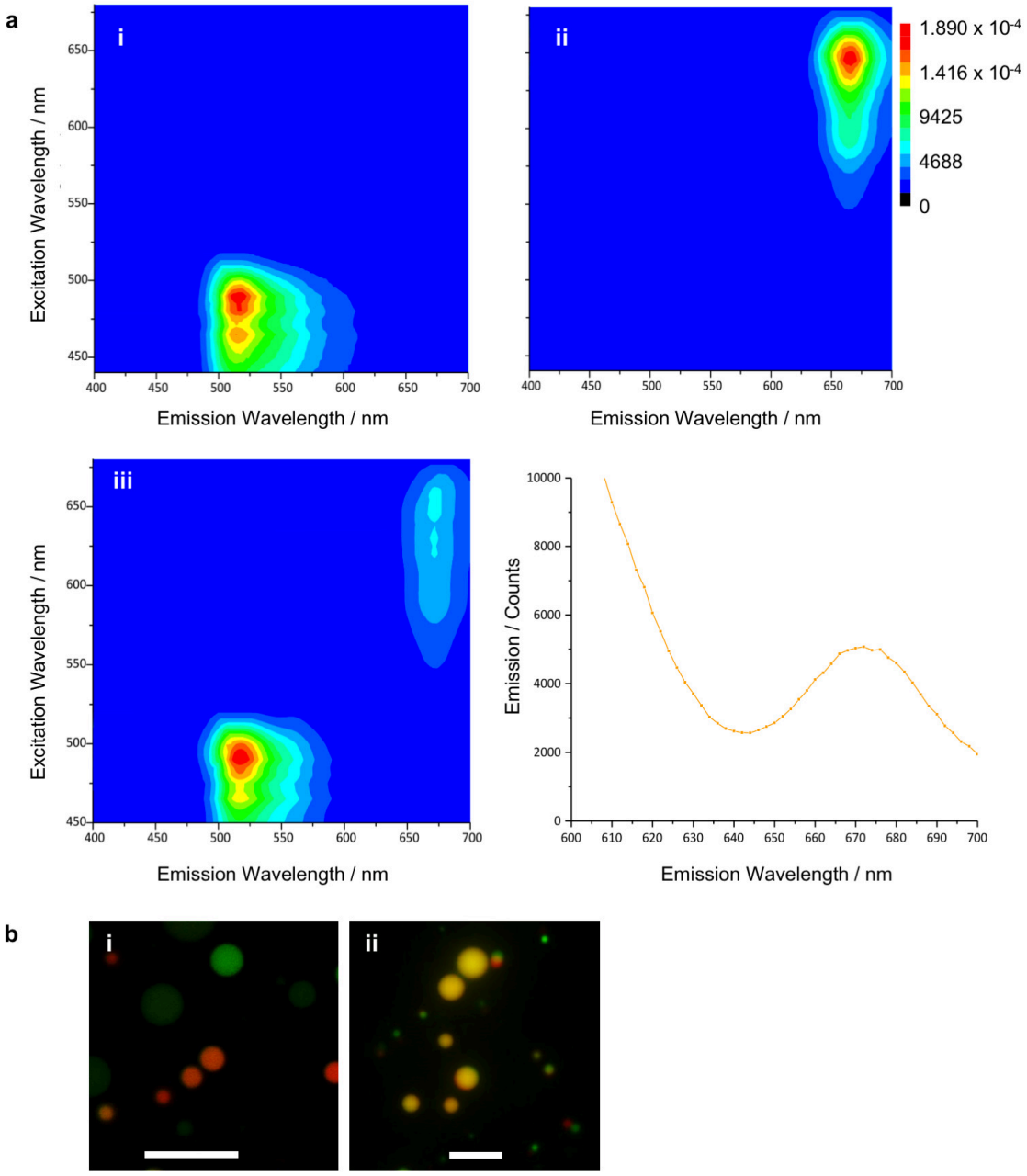

Figure 3.42: FRET pairing is seen between cy5 and fluorescein molecules co-localised by the base pairing of two complementary single-stranded DNA oligomers. a: Fluorimetry showing the excitation and emission efficiencies for i: ss-DNA-fluorescein, ii: ss-DNA-fluorescein and iii: ss-DNA-fluorescein base paired with ss-DNA-cy5. Scale: black indicates no emission, red indicates maximal emission. iv: The emission profile at an excitation of 480 nm, where fluorescein is excited, showing the emission produced from cy5 as a result of FRET. b: Confocal fluorescence images showing i: a mixture of populations of coacervates containing either ss-DNA-fluoroscein (green) or ss-DNA-cy5 (red) and ii: a population of coacervates where the ss-DNA-fluorescein (green) or ss-DNA-cy5 (red) have been combined before addition. Scale bars: 10 μm.

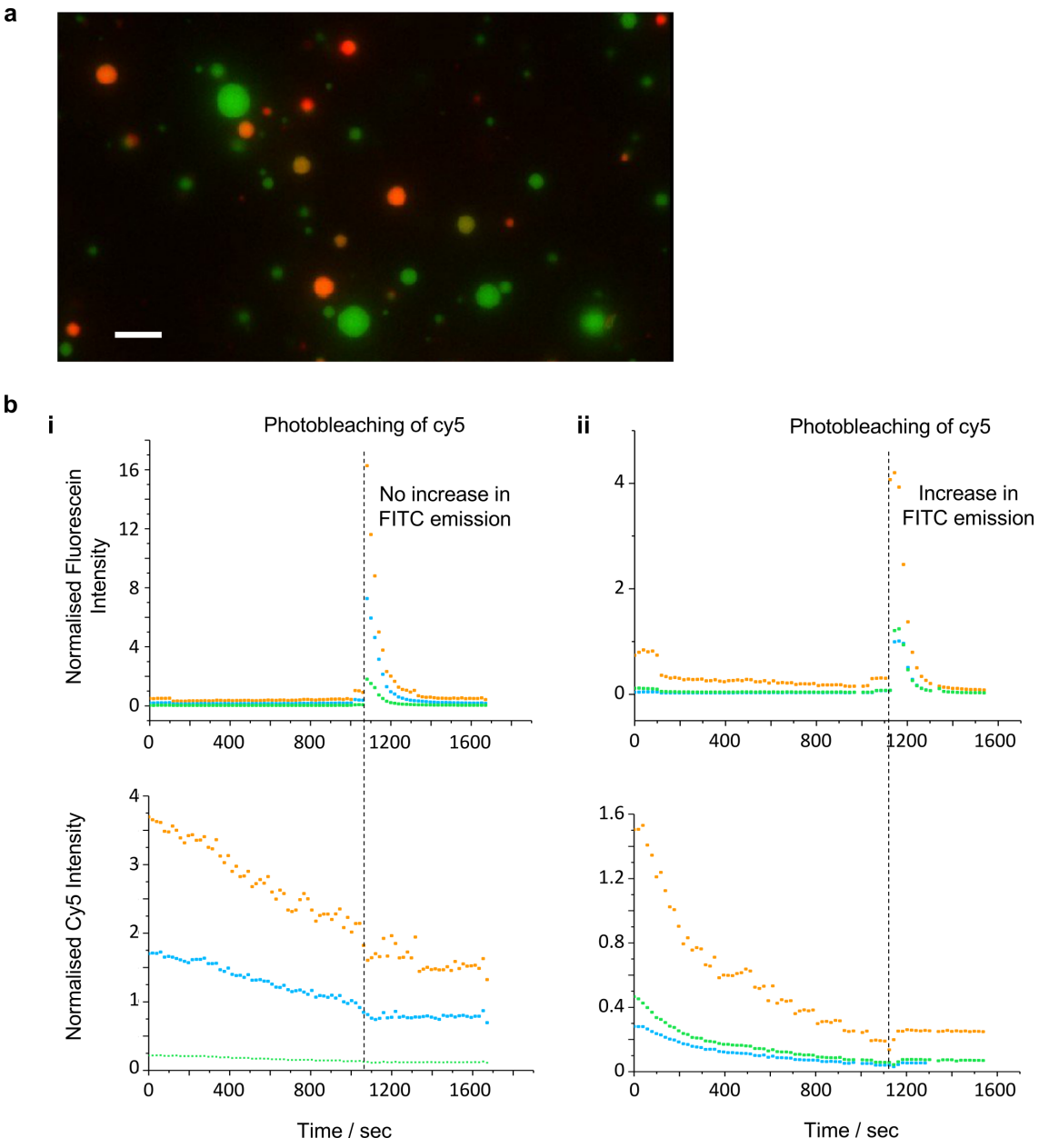

Figure 3.43: FRET analysis of the transfer of single-stranded DNA between coacervates. FRET-AP measured in ss-DNA-fluorescein droplets in a population containing a mixture of ss-DNA-cy5 containing droplets and ss-DNA-fluorescein droplets. a: Confocal fluorescence microscopy of the mixed population of droplets. Scale bar: 10 μm b: Intensity of fluorescein signal from ss-DNA-fluorescein containing coacervates over time i: without and ii: with low concentration sodium chloride addition. Signal in the fluorescein channel is observed at the top, with signal in the cy5 channel shown underneath for each experiment. The intensity has been normalised to droplet volume. The dotted line identifies the point in time where cy5 was photobleached so it could no longer accept energy from the fluorescein fluorophore. Each coloured set of points represents a single droplet.

tiate disassembly of the coacervate structure. However, note that a small amount of FRET can be shown in droplets without salt due to mixing forces at the start causing inherent rearrangement of the coacervates, allowing some of the opposing fluorophore to be taken up. This is due to the fact that coacervate droplets are not very stable to shear pressures caused by pipetting. Instead, they disassemble and spontaneously reassemble. IT is assumed that however carefully the experiment is conducted, some shear will be caused by manual pipetting when the two populations are introduced together, causing some minor disassembly and therefore a small amount of release of the contained single stranded DNA cargo. It is believed that this is responsible for the low levels of FRET seen when the two samples are combined.

3.2.3 The Effect of Salt on Re-suspended Coacervate Properties

To determine the concentration of salt that would dissemble coacervates, the sensitivity of the UV-Vis first had to be interrogated, to see whether low concentrations of coacervate still produce a noticeable UV-Vis absorbance. Non re-suspended coacervate sample concentrations of 0 to 10 mM were investigated and their absorbance recorded (Figure 3.44(a)). This demonstrated that even very low concentrations of coacervate produced a readable difference in absorption.

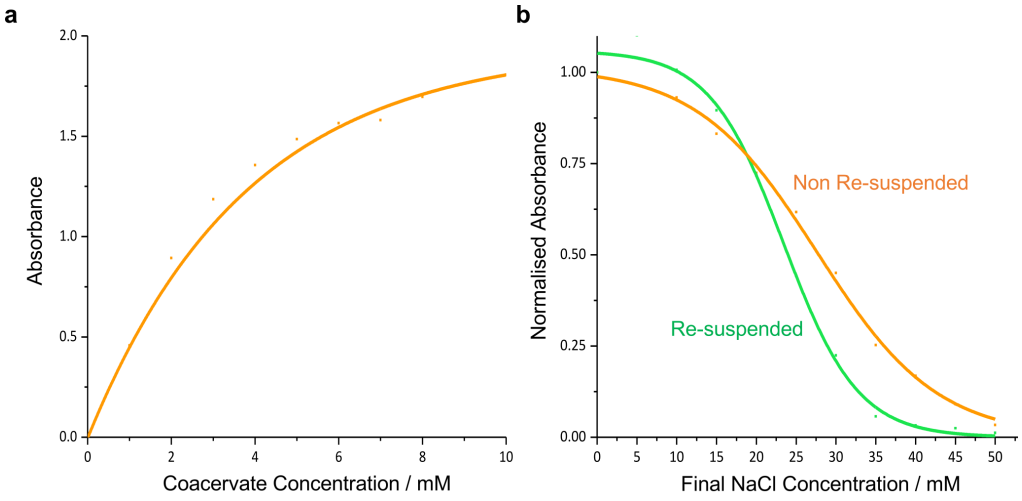

Figure 3.44: The effect of the addition of sodium chloride on coacervate disassembly. UV-visible spectroscopy measurements of the turbidity (A_{500}) of coacervates to a: determine the sensitivity of the equipment to detect the presence of coacervates at low concentrations and b: explore the differences in stability to salt with non re-suspended and re-suspended coacervates.

The effect of increasing concentrations of salt was then investigated by adding sodium chloride to the droplet samples and measuring their turbidity (Figure 3.44(b)). The sodium chloride interferes with the coacervate matrix as its positive and negative ions dissociate, causing interference in the electrostatic interactions between positive and negative groups, which here are positive PDDA groups and negative ATP molecules.

It can be seen that the re-suspended droplets were more susceptible to salt disruption by salt addition than the non re-suspended droplets. The non re-suspended droplets seem to be entirely disrupted at 50 mM sodium chloride but the re-suspended droplets are disrupted at 35 mM. This was unexpected as the ζ-potential data indicated that the re-suspension process made the droplets more stable. Therefore, the hypotheses for this observation is that the re-suspension produces a better arrangement of electrostatic interactions, leading to more stable droplets, but these are more easily disrupted by the positive sodium ions and negative chloride ions in sodium chloride than the non re-suspended droplets.

Optical microscopy of non re-suspended and re-suspended coacervates with sodium chloride was also carried out and the droplets here were also seen to be disrupted at the sodium chloride concentrations indicated by the UV-Vis data. 50 mM were sufficient to disrupt both types of coacervate completely.

The effects of sodium chloride addition on the coacervates was also observed with confocal fluroescence microscopy (Figure 3.45). Whilst the coacervates usually disappear instantly with salt addition, in this case the salt was added very slowly at a site distant from the droplets.

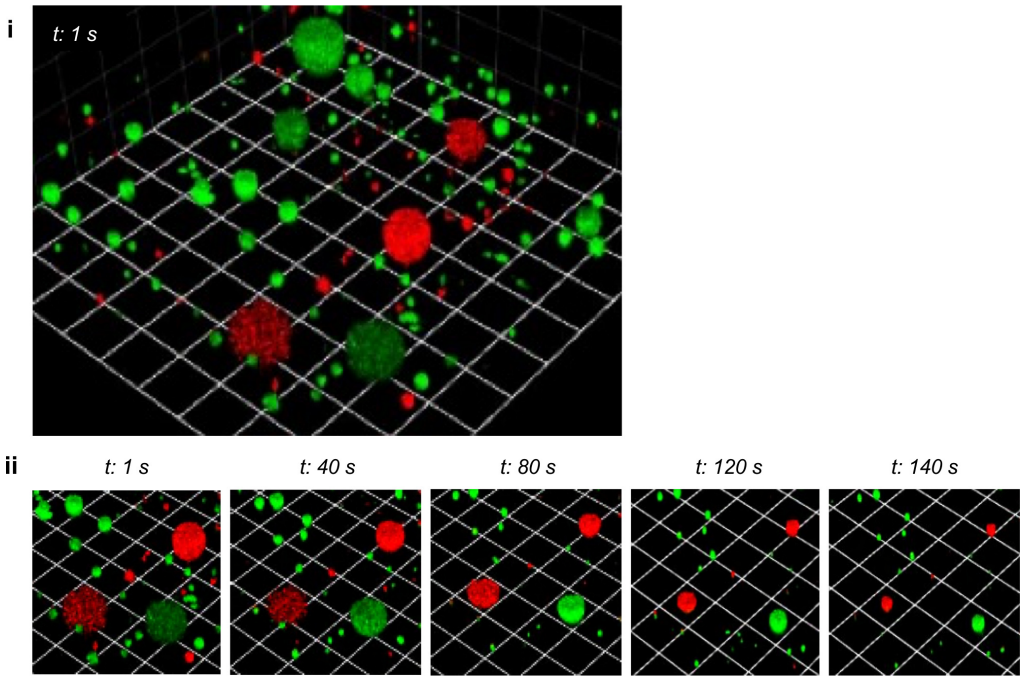

Figure 3.45: The effect of addition of salt on coacervate structure. PDDA: ATP coacervates containing fluorescein (green) and cy5 (red) tagged ss-DNA oligomers with sodium chloride addition, showing shrinkage over time. Confocal fluorescence microscopy of i: the droplets before and ii: after salt addition. Scale bars: 1 unit = 8 μm, time points shown in seconds.

At the start of the experiment, a mixed population of Cy5 (red) and fluorescein (green) droplets were observed and droplet shrinkage was seen. This illustrates that salt may dissemble the

coacervate from the outside as it interacts with the interface. It would be interesting to see if it is possible to re-grow the droplets by diluting the salt concentration again, or whether this simply causes formation of new droplets entirely. However, this was not done here. Note that these droplets appear slightly elongated in the z axis due to an artefact of the microscope which results in spherical aberration.

The salt investigations with sodium chloride were then repeated to determine if the addition of oligomers had had affected the coacervates ionic strength and ability to resist disassembly. Increasing concentrations of salt were added to solutions of non re-suspended and re-suspended droplets, that contained no oligomer or one of the two fluorophore tagged oligomers. The turbidity of the droplets was measured by UV-Visible spectroscopy and the presence of droplets was corroborated by optical microscopy. The concentration of sodium chloride at which disassembly occurred is recorded in Figure 3.46.

a

Sample	[NaCl] Required for Disassembly / mM		
	Without DNA	ss-DNA-fluorescein	ss-DNA-cy5
Non Re-suspended Coacervates	45	25	25
Re-suspended Coacervates	25	45	45

b

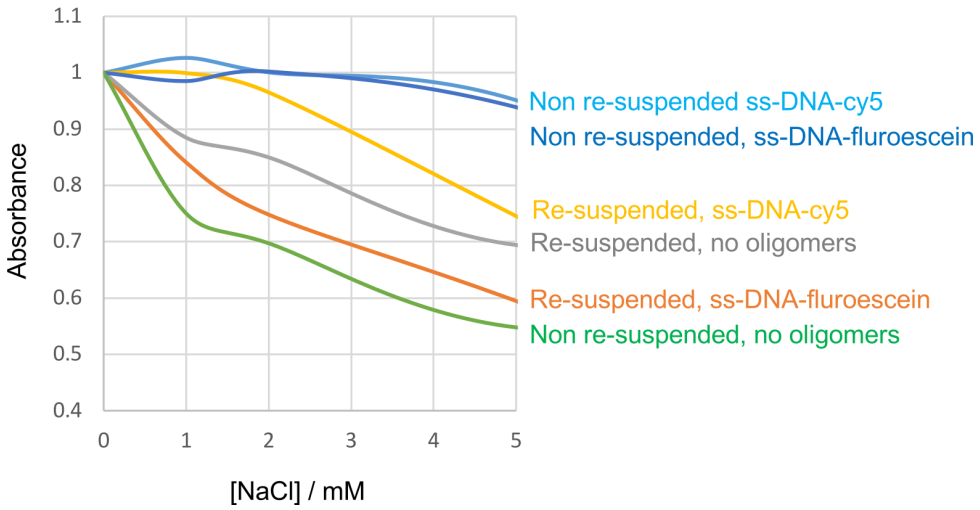

Figure 3.46: The effect of salt on coacervates containing a cargo of ss-DNA. a: The concentration of sodium chloride required to disassemble non re-suspended and resuspended coacervates containing ss-DNA oligomers, b: The effect of low concentrations of sodium chloride on coacervate solution turbidity.

As seen previously, at higher concentrations of sodium chloride, 25 mM concentrations of salt were sufficient to disrupt re-suspended coacervates, whereas salt concentrations of 45 mM were required for non re-suspended droplets. However, when the coacervates containing oligomers

were examined, the re-suspended coacervates were in fact more stable to salt dissolution than the non re-suspended droplets. The cy5 and fluorescein tagged oligomers behaved similarly to one another in all cases. On the other hand, at low concentrations of salt, the non re-suspended coacervates containing ss-DNA are the most stable, despite the fact that these are the least stable at higher salt concentrations. The non re-suspended coacervates without oligomers are the most susceptible to low salt additions. This data shows that when tuning the properties of a system, a variety of conditions must be considered. It is not simply the case that an effect seen by the addition of a component can be extrapolated.

It was previously hypothesised that re-suspended coacervates contain more ATP, making them more stable to coalescence but also increasing that number of electrostatic bonds that can be disrupted by sodium chloride. Single-stranded DNA is more negatively charged than ATP, so the DNA may not be so easily displaced by sodium chloride, retaining the droplet structure at higher concentrations of salt. However, this doesn't explain why non re-suspended droplets become less stable.

3.3 Conclusions & Further Work

The aim of this chapter was to develop an understanding of the partitioning and exclusion of molecules in the ATP:PDDA coacervate system and to characterize the coacervate properties including the effects and mechanism of re-suspending coacervate to increase stability. First it was shown that re-suspending the coacervates clearly improved stability, except in some cases with the addition of salt where stability was actually decreased. The mechanism of re-suspension induced stability increases was thought to be related to a redistribution of coacervate components when the supernatant is replaced with water. However, the method of re-suspension had little effect on the stability or size distribution of populations of coacervates. This is likely to be because the system is re-suspended quickly and completely in all cases. It was also shown that temperature affected the stability of the re-suspended coacervates, with increases to 28° C heavily reducing their stability. This agrees with information given in the introduction and also the theory section in Chapter 2, explaining that the molecular interactions that result in a coacervate are energy dependent and temperature increases provide enough energy to overcome these temporary bonds.

Macromolecular sequestration was demonstrated, with the coacervates partitioning a wide range of molecules into the interior at high concentrations. An in-depth investigation was then shown with TEG which, at intermediate concentrations, altered the structure of the coacervates and induced vacuole formation. The resulting vacuoles were free of coacervate components. The mechanism of this was explored and it was hypothesized that the vacuole formation may be as a result of TEG interfering with hydrogen bonding in the coacervates, disrupting intramolecular bonds within the coacervate, leading to destabilisation. Another hypothesis is that the hydrophobicity

of the TEG induces the changes in the system, by drawing water molecules away from the coacervate matrix. Both hypotheses were explored and compared in this Chapter. Manipulation of the TEG solution added was used to cause structural changes in the droplets, causing finger-like projections from the coacervates and variations in the blebbing properties observed.

Larger molecule sequestration was then examined with dextrans of varying size and charge used as examples. Stability and partitioning was characterised extensively and the experiments demonstrated that dextran partitioning could be manipulated to induce surface partitioning of dextran on the coacervates. Finally, the mixing of components between coacervate components was studied, with results showing that coacervates do not exchange small DNA oligomers. This further demonstrates that the coacervates are appropriate systems in which to contain components, such as enzyme cascades, with the ability to act as protocellular compartments.

On the whole, this chapter has demonstrated the creation of a compartment within the coacervate droplets, induced in a novel manner by the addition of an uncharged molecule, TEG. A few papers have demonstrated internal structuration in recent years but none have successfully shown this with an uncharged molecule. Yin et al. showed that the introductioin of an elcetric field to coacervates in a microfluidic system produced vauoles that cycled in growth and destruction, according to the fluctuations of the field [157]. Williams et al. showed that you could introduce a re-structuration of the interior of the droplet by providing an osmotic strain on the system, via the addition of other components [155]. Simon et al. took another approach, rationally designing modular building blocks that would layer on top of each other to build a coacervate with a compartment from the inside out [189].

These systems all rely on rational design or a method of de-stabilising the coacervate matrix, to allow water ingress to a vacuole, which is also believed to be the underlying mechanism here. However, the difference between the work conducted here and these previous investigations in the literature is that the destabilisation has not occurred between ionic bonds but through the destabilisation of hydrogen bonds or by influencing the hydrophobicity of the coacervate system.

It is suggested that future work should include further development of the systems where only early characterisation has occurred here, in order to generate systems with more functionality. The salt shrinkage of coacervates should be investigated further to see if it is possible to re-grow coacervates by dilution of salt and, if so, to see if these droplets then contain a mixture of components. This could be used to generate systems whereby reactions could occur and then the products could be randomly mixed allowing evolution. Further studies on the coacervates with high levels of dextran-FITC doped into dextran should also be done as the ability of these droplets to expel their contents is very interesting. The utility of the vacuole created by the TEG addition is explored further in the next chapter.

CHAPTER 4

MACROMOLECULAR INTERACTIONS WITHIN COACERVATE DROPLETS - THE SYNERGISTIC EFFECT OF MULTIPLE SOLUTES IN A SINGLE POPULATION

This chapter explores a new system of complementation in the coacervate interior, based on the findings of Chapter 3. It utilises functional systems with multiple components in a move to enhance the complexity of the system developed here. Specifically, the compartment produced inside coacervates with the addition of TEG is further enhanced by the creation of an aqueous two-phase system inside the droplets with the addition of dextran alongside the TEG. This allows for the creation of a storage system which can be utilised with the addition of enzymes to break down the confined dextran. The novel system is fully characterised and compared to the TEG-only system of compartmentation.

4.1 Introduction

The research so far has demonstrated that a TEG coacervate system can induce the formation of water filled vacuoles within a protocell, and that molecules normally encapsulated by the PDDA ATP coacervates still reside in this matrix after TEG addition. The further development of this system, examining the effect of adding other macromolecules, is described herein. Firstly, the addition of molecules encapsulated by the coacervate is shown, followed by an exploration of the potential of adding molecules that are not encapsulated in an attempt to partition useful molecules into the new vacuole compartment. Large molecular weight dextrans are chosen to demonstrate this, based on their exclusion from the coacervates, which was shown in the previous chapter. Furthermore, the separation of aqueous two phase systems (ATPS) into two distinct regions, each rich in a single component, has been shown in the literature to be a useful method

by which to induce multiple coexisting environments inside protocell constructs. Dextran and PEG systems have been widely studied and it is hoped that the selection of dextran as the excluded component in this coacervate system will allow an ATPS between the dextran and TEG to encourage partitioning of dextran into the vacuole, where TEG does not reside.

Aqueous two-phase separation is another form of liquid-liquid phase separation, distinct in character from complex coacervation. These systems have been extensively studied since their discovery by Beijerinck in 1896. He demonstrated a two-phase system involving water, agar and gelatin [190]. In both complex coacervation and aqueous two-phase separation, the mixed solution appears turbid before separation. However, as previously discussed, the phases separate to form a component rich phase and a component poor phase in complex coacervation, with each phase containing a mixture of components. In contrast, the distinct thermodynamic phases in aqueous two-phase systems (ATPS) can be produced by the mixing of macromolecules at high concentrations [191] leading to phases with different compositions and sequestration properties. Most commonly, each phase is rich in components that are depleted in the other phase. The two components are combined in water such that they are in a solvated state [190]. The two forms of liquid-liquid phase separation (LLPS) are known as associative LLPS and segregative LLPS respectively.

The utility of ATPS was later propagated by Albertsson in 1955, with the use of a phase separated system containing PEG, potassium phosphate and water to partition plant cell components [192]. Soon after, he observed that biomolecules could be unevenly distributed within some systems composed of two components and that they could therefore be used for the purification of biomolecules [193].

One of the most extensively studied polymer-polymer systems is that involving PEG and dextran. After separation, the upper phase is PEG rich and the lower phase is dextran rich [190]. In this system, it has been established that most native proteins selectively partition into the dextran phase whereas denatured proteins prefer the PEG phase, as more hydrophobic interactions are exposed. Characterisation of this system has shown interfacial tensions of 0.0001 to 0.1 dyne/cm and have also demonstrated that the phases contain 88-99% water [190]. Biomolecular activity has also been demonstrated [190]. Formation and composition of the phases is dependent of temperature, concentration and ionic strength of the phase components [194]. As a consequence, the composition can be optimised by altering the molecular weight or ratios of the components [194]. ATPS can also occur with combinations of a polyelectrolyte and a non-ionic polymer, two polyelectrolytes or a polymer and a low molecular weight component such as salt, for example a combination of PEG and potassium phosphate [190].

Molecular interactions in ATPS have been characterised by a number of researchers. Early work by Diamond and Hsu in 1989 began to develop simply methodologies, based on Flory-Huggins thermodynamics, to predict the partitioning of dipeptides and low molecular weight proteins

according to the concentration difference between phases of PEG 8000 and dextran [190]. Later work produced a generalised expression to determine protein partitioning behaviour in PEG dextran systems, accounting for the partitioned protein properties, polymer molecular weight, interactions between the protein and water, the protein and polymer and also the polymer and water, and electrostatic potential difference between the phases [190]. Ultimately, this yielded a relationship between the concentration difference between phases and the natural logarithm of the protein partition coefficient [190]. However, it is important to recognise that whilst these systems provide a model to predict behaviour, many assumptions have been made to reduce complexity. For example, hydrogen bonding and ionic interactions in more complicated systems may play an important part [190]. Sequestration is also dependent on the properties of the protein, as discussed in the introductory section on coacervate sequestration. Solute size has a contributory effect, as the larger molecules have more surface area by which to interact with the phase [191].

These properties make the systems very interesting as reaction containment systems. Biomineralisation within ATPS has been shown to be possible with calcium carbonate formed as a result of urease catalysis [191]. Liposomes can also be constructed with dextran phase droplets surrounded by a continuous PEG phase, stabilised by the addition of a lipid bilayer. In this case, RNA and DNA can still diffuse to both phases and a ribozyme cleavage reaction can occur within the dextran liposomes [195]. Giant lipid vesicles have also been shown with both PEG and dextran phases in the interior of the droplet. These can be induced to bud with the addition of sucrose, either fully or partially at the phase boundary. By manipulating the ratios of components, some droplets that had undergone budding could be seen to contain both systems after splitting and undergo a second round of budding. Excitingly, this new generation contained a different set of lipids to the first so could be shown to have evolved [71]

4.2 Results & Discussion

4.2.1 Single Populations of Coacervates with Multiple Solutes

4.2.1.1 Co-uptake of DNA

Single-stranded DNA-cy5 and DNA-fluorescein were base paired to form double stranded oligomers, and then added to the coacervates. The mean diameter of coacervates was then re-assessed and compared to previous data (Figure 4.1). The distribution in coacervate diameters with sequestered double-stranded DNA oligomers is similar to that of the individually sequestered oligomers.

The ζ-potentials for droplets with either fluorescein or Cy5 single stranded DNA were investigated, along with droplets where the two oligomers had been pre-mixed to induce base pairing. Droplets consisting of a combination of the two populations were also tested. This is shown in

a

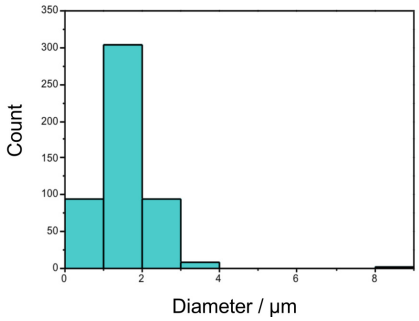

b

Sample	Mean Diameter / µm	Standard Deviation / µm
No Oligomers	1.8	0.81
Cy5 Oligomers	1.6	0.92
Fluorescein Oligomers	1.6	1.0
Base Paired Oligomers	1.6	0.67

Figure 4.1: The effect of adding double-stranded DNA oligomers on coacervate size. a: Distribution of diameters in a population of droplets for coacervates containing ss-DNA-fluorescein base paired with ss-DNA-cy5 before addition. b: Statistical analysis showing mean diameter and the standard deviation of the population, in comparison with previously seen data for the single-stranded DNA alone.

Figure 4.2. The distributions lie in a similar place for all samples, suggesting that the addition of oligomers has not influenced the surface potential. This leads to the conclusion that either the oligomers are sequestered internally in the droplets and are therefore having no effect on the external surface potentials. This agrees with the partition coefficient data which showed high partitioning of cy5-tagged single stranded DNA. Another possibility is that the oligomers have interacted with the PDDA, perhaps in place of ATP, and formed electrostatic interactions but have not altered the surface potential in doing so.

4.2.1.2 PEG Vacuole Formation with Molecules Encapsulated by Coacervates

4.2.2 PEG Dextran Phase Separated Systems

The one phase to two phase transition occurs when the components in the system reach a concentration at which the phase boundary is crossed. Figure 4.3 shows combinations of varying concentrations of TEG and dextran, highlighting the samples that undergo a two phase transition. When viewed with a confocal fluorescence microscope, the six samples look very similar when only dextran is present. However, with the addition of TEG, two samples, (i) & (iv), show aggregates of dextran-FITC, occurring as a result of their transition to a two phase system in which the TEG and dextran separate. The fluorescence of all the dextran samples is decreased when TEG is present. The reasons for this are unknown, however FITC fluorescence is highly dependent on its local environment so this may be because the charge or concentration of the FITC has changed.. Alternatively, it may be because there is some phase separation occurring which causes small aggregates to be formed, quenching the FITC fluorescence due to localised high concentration and elucidating areas that have no dextran-FITC in. However, this latter explanation seems unlikely as the fluorescence is still evenly dispersed in these samples, unlike those where it is clear phase separation has occurred.

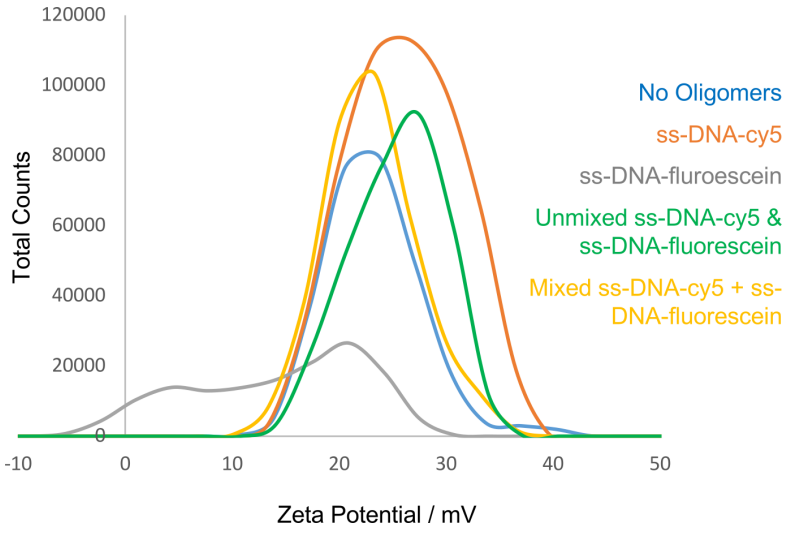

Figure 4.2: ζ-potentials of coacervates showing the effect of single-stranded and double-stranded DNA oligomer sequestration on surface stability. Samples are as follows: coacervates without DNA oligomers (No oligomers), coacervates with only single-stranded-cy5 DNA contained inside (ss-DNA-cy5), coacervates with only single-stranded-fluorescein DNA contained inside (ss-DNA-fluorescein), coacervates containing ss-DNA-cy5 combined with coacervates containing ss-DNA-fluorescein (Unmixed ss-DNA-cy5 & ss-DNA-fluorescein) and coacervates containing pre-mixed and base-paired ss-DNA-cy5 with ss-DNA-fluorescein (Mixed ss-DNA-cy5 + ss-DNA-fluorescein).

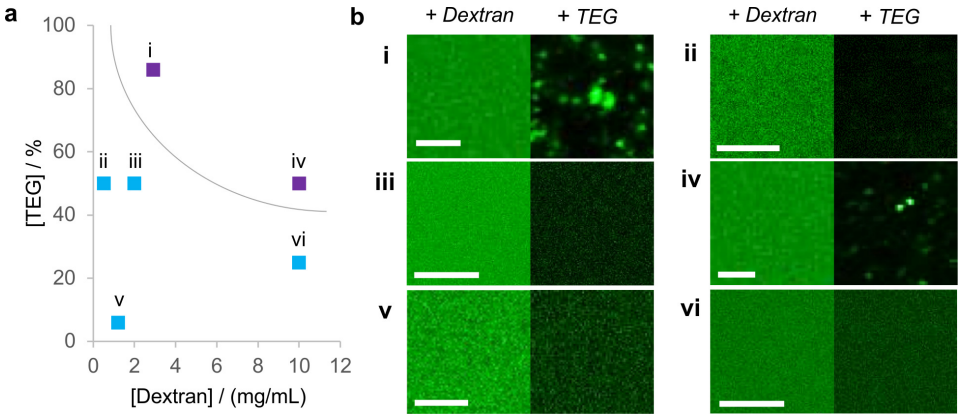

Figure 4.3: PEG and dextran phase separate in solution. a: Scatter graph showing a variety of combinations of different TEG and dextran concentrations (molecular weight 150 k) alongside b: the confocal fluorescence images of the same concentrations. The samples that demonstrate phase separation are shown in purple on the graph. The grey line in (a) is representative of a boundary between the one phase systems and two phase systems, based on the confocal fluorescence images in (b), although the exact concentrations at which this boundary occurs has not been determined. Concentrations of dextran (mg/ mL) and TEG(%) respectively are as follows: i: 2.9, 86, ii: 0.5, 50, iii: 2, 50, iv: 10, 50, v: 1.2, 6 and vi: 10, 25. Scale bars: 10 μm, except b:i: and iv: which are 2 μm so that the two phase aggregates can be seen more clearly.

4.2.2.1 Effects of Temperature & pH on the ATPS

The one to two phase transition boundary can also be affected by temperature and pH. Experiments to determine the boundary of phase separation in the TEG Dextran system used here is shown in Figure 4.4.

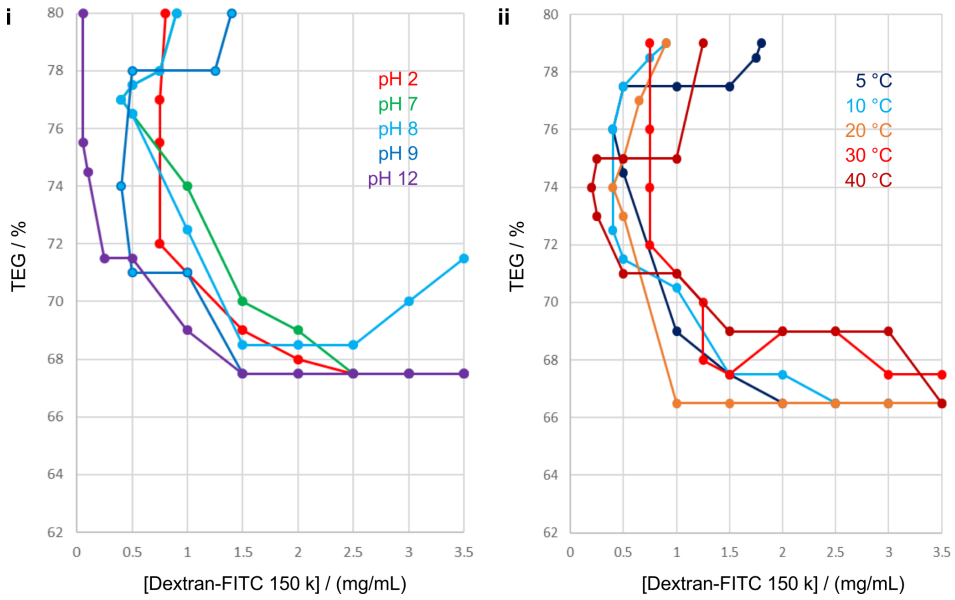

Figure 4.4: The effect of changing the environment on the one to two phase transitions of the system comprising of dextran-FITC 150 kDa and TEG. The effect of changing the i: pH at a fixed temperature of 20 $^{\circ}C$ and ii: temperature at a fixed pH of 8 are shown

From the data, it is possible that an increase in pH causes the transition to a two-phase system to occur at lower concentrations of TEG and dextran. An increase in pH increases the de-protonation of hydroxyl groups on the TEG which may make it more hydrophobic, causing greater separation from dextran. However, the data for pH 2 does not seen to follow the same trend. When temperature is altered the results are more inconclusive, suggesting that temperature change makes very little difference to the system partitioning. Although it would be expected that temperature and pH alterations would have a greater effect, these plots were repeatable indicating that data is likely to be accurate for this system. The lack of effect compared to other PEG dextran systems may be due to the fact that the TEG is very short compared to most of the PEG molecules used in other systems in the literature.

4.2.3 PEG Dextran ATPS In Coacervates, Leading To Membrane-Free Compartmentalisation

4.2.3.1 Characterisation of the System

Untagged dextran was added to the coacervates, followed by addition of TEG at a variety of concentrations. The percentage of droplets that formed a single vacuole in each sample was calculated and plotted in Figure 4.5(a). Internal compartments formed only with low concentrations of TEG, despite higher concentrations also investigated. These concentrations were too low for vacuoles to be formed without the dextran present. The range of concentrations at which compartments could be formed was also much narrower. This can be seen from the narrowed distribution on the graph. The graph shows a single distribution when dextran is present, compared to a bimodal distribution with TEG alone. These results suggest that perhaps the compartments are formed via a different mechanism than those with only TEG, rather than the same mechanism which is then stabilised by an ATPS.

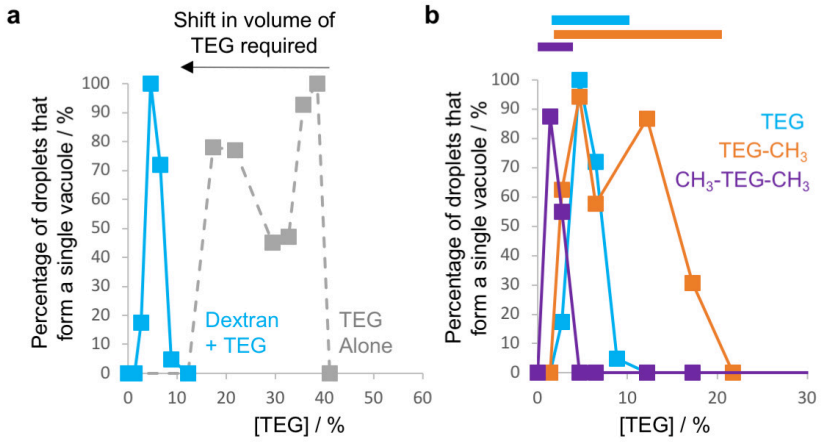

Figure 4.5: Addition of dextran to the system allows vacuole formation to occur with lower concentrations of TEG. Statistical analysis of the percentage of droplets that form a single vacuole shows a: a reduction in the amount of TEG required for vacuole formation in the presence of dextran, and b: the concentrations required for formation of vacuoles in the presence of dextran with TEG, tetraethylene glycol monomethyl ether and tetraethylene glycol dimethyl ether. Coloured bars show the range of TEG concentrations at which vacuoles form for each type of TEG.

The same experiment was then repeated with the TEG variants described in the previous chapter (tetraethylene glycol monomethyl ether and tetraethylene glycol dimethyl ether) in order to elucidate more information about the mechanism of this new TEG dextran coacervate system (Figure 4.5(b)). With the TEG only system, these analogues did not produce vacuoles at any concentration. However, with the dextran present, internal compartments were seen to form. When TEG was substituted for the analogue with two methyl groups, it indicated that an increase in

hydrophobicity of the terminal groups (from a hydroxyl group to a methyl group) decreased the amount of TEG required. Again, the single distribution here was very narrow.

It was anticipated that the tetraethylene glycol monomethyl ether would show similar behaviour, with a distribution between that of the tetraethylene glycol dimethyl ether and the TEG. However, this displayed a bimodal distribution, not dissimilar to that displayed by TEG without dextran. The peak at lower concentrations of this molecule did fall between the TEG and tetraethylene glycol dimethyl ether peaks, suggesting that whilst the system with dextran may be different to that with only TEG, the second peak may additionally point to yet another mechanism.

As discussed in the last chapter, the effect of altering the end group moieties may have an effect on hydrophobicity or a reduction in the ability of the molecules to hydrogen bond intermolecularly with similar molecules or intermolecularly with ATP in the coacervate matrix. If the change in mechanism when dextran is present is related to an effect of ATPS, it would make sense that less TEG was required to induce internal compartment formation because there would also be repulsive forces associated with the formation of an ATPS contributing to separating the TEG (contained within the coacervate) and the dextran (excluded from the coacervate). Lowering the hydrophilicity of the TEG would also be expected to lower the amount of TEG required as dextran is hydrophilic and this would be expected to increase the repulsive effects between TEG and dextran molecules. However, neither of these observations explain the second peak in the tetraethylene glycol monomethyl ether distribution. More information is required to speculate as to a mechanism and this will therefore be revisited later in this chapter.

To determine whether the system was akin to the TEG only system, the location of the coacervate matrix components was again determined by confocal fluorescence microscopy (Figure 4.6). After internal compartment formation, it was clear that ATP and PDDA both surrounded the compartment and, at the resolution here, indicated that no coacervate components were present inside. The coacervate droplets with internal structuration look very similar to those achieved with TEG alone. When individual coacervates are examined, the ATP and PDDA appear homogenous within the coacervate.

However, these experiments did not identify the location of the dextran and the TEG. Dextran-FITC of the same molecular weight, 150 kDa, was used in place of the untagged dextran to determine where the dextran ended up at the end of the restructuration. This dextran has an FITC tag only every 1:160 units so was deemed to be a reasonable substitute for the untagged dextran without perturbing the system too greatly. Indeed, Figure 4.7 shows that the resulting compartments look similar in the brightfield view to those in Figure 4.6, indicating that the system overall is likely to be behaving in the same way.

With the TEG alone system, it was postulated that the internal vacuole could be created with one of two mecahnisms, or a combination of them both. Either water is released from the coacervate as a result of being displaced by the hydrogen bonding of TEG, or another TEG effect,

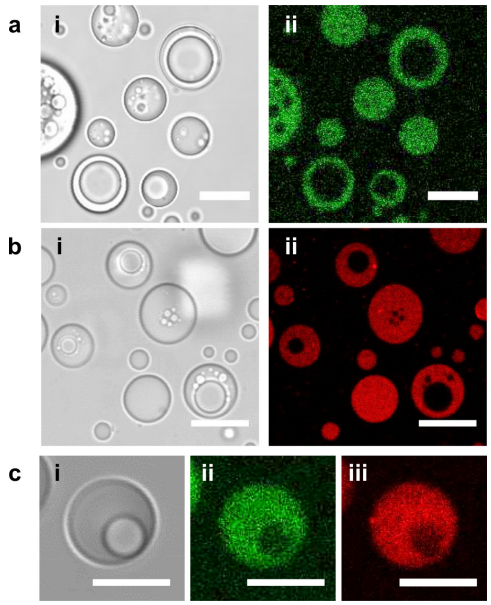

Figure 4.6: Microscopy images showing that the vacuoles formed in the presence of dextran also do not contain coacervate components. a & b: Large scale images of coacervate populations with a single coloured coacervate component, i: brightfield images and ii: ATP-TNP (green) or PDDA-RITC (red). c: Single droplet microgprahs in the i: brightfield and showing the coacervate component, ii: ATP-TNP (green) and iii: PDDA-RITC (red). Scale bars: 10 μm.

or water is pulled in from the supernatant outside the coacervate and sequestered into the interior as the process causes the coacervate to require further hydration to combat the effect of the TEG sequestration. It was hoped that the addition of fluorescent dextran would help to provide a more definitive answer, if the systems were behaving similarly. Either a result would be anticipated where the internal compartment contained no dextran or a lower concentration of dextran compared to the supernatant, or a result where the concentration of dextran was similar supernatant. However, this is not what is seen from the confocal microscopy data. Instead, it appears that the concentration of dextran in the internal compartment is far higher than that in the supernatant, which does not appear to fluoresce at all.

A 3D reconstruction was completed from individual z-stack micrographs (Figure 4.7(b)). The fluorescence was enhanced in post processing to also visualise the inherent autofluorescence of the coacervate droplets so that the coacervate boundary could be seen. Even at this level, no fluorescence can be seen from the supernatant, indicating that nearly all of the dextran is likely to be inside the internal compartment.

Since all the data so far suggested a difference from when higher concentrations of TEG were used alone, the dextran-FITC was then used to examine the process by which the compartments are formed (Figure 4.8). As expected, after the addition of dextran, the fluorescence can be seen surrounding the droplets. This agrees with previous data showing that dextran of this molecular

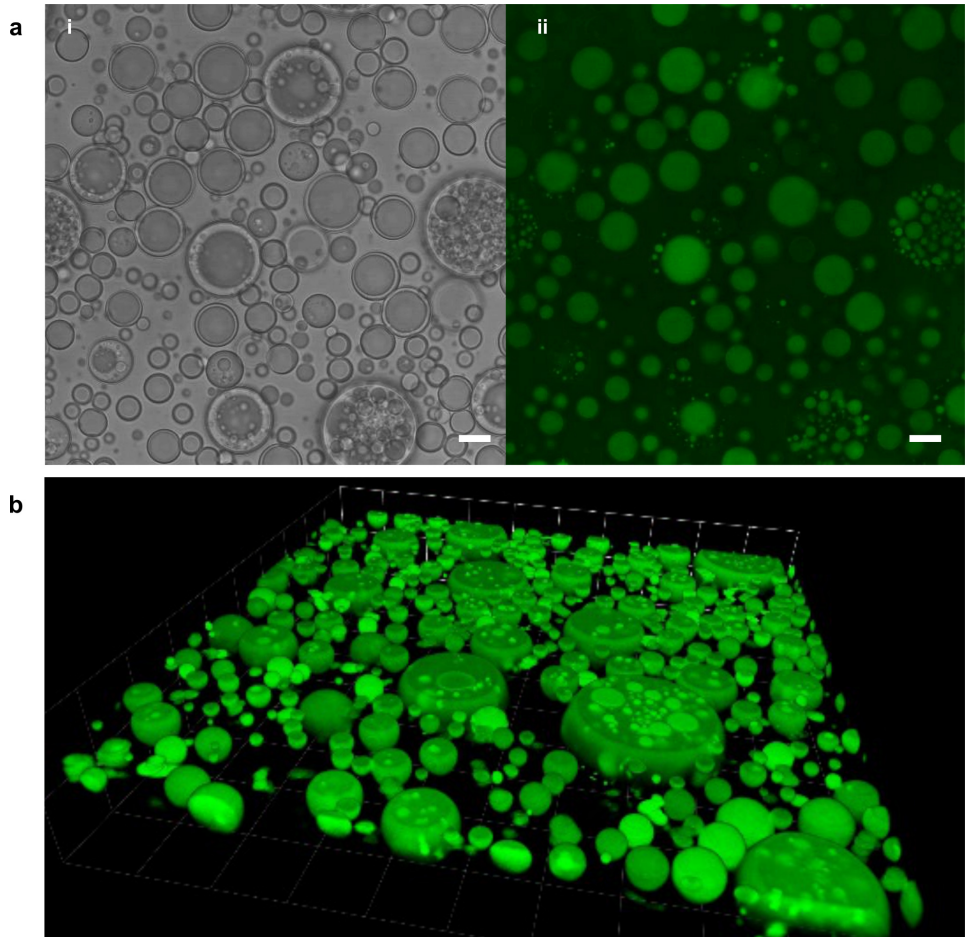

Figure 4.7: Dextran is ultimately partitioned into the internal compartment. Large scale images with dextran-FITC at the end of the compartmentation process. The dextran is at a concentration of 20 mg/ mL and has a molecular weight is 150 k. The same population shown in a: 2D in the i: brightfield and ii: confocal fluorescent channels, alongside a slice through a 3D reconstruction built from multiple 2D slices. Scale bars: 10 μm.

weight is excluded from the coacervate. However, when TEG is added (at the 84 s timepoint), the exclusion properties of the matrix demonstrates change, as dextran is then able to enter the coacervates, but the dextran is not homogenous across the droplets at this timepoint.

Figure 4.9 shows the same process at a scale where a small selection of droplets are visible, from the point of TEG addition. The dextran appears to enter the larger droplets from a single location at the coacervate interface. With the smallest droplets, it is harder to tell whether it enters from a single location and then rapidly fills the coacervate or from all sides of the droplet. The dextran exhibits significantly higher fluorescence when the TEG is present, and the fluorescence then reduces once the compartment is formed. This could be due to a change in FITC envirnment or simply that the TEG is quite viscous at high concentration and therefore increases the refractive index of the coacervate changing the detection of the fluorescent signal. If TEG is still residing

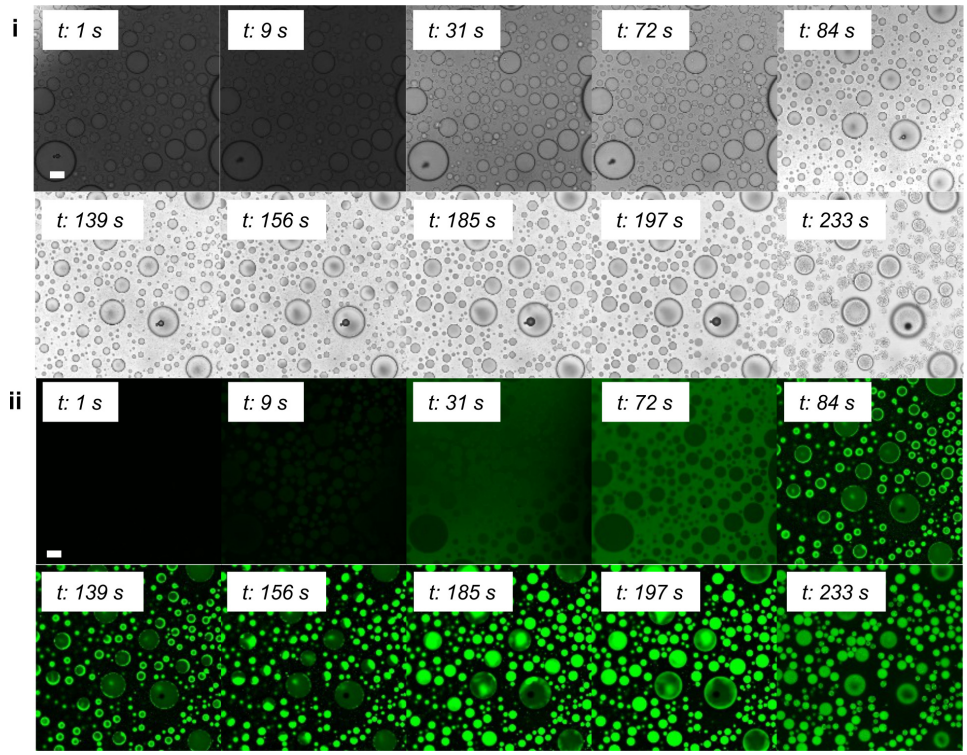

Figure 4.8: Large scale timepoint sequences showing the formation of dextran compartments inside coacervates, upon addition of TEG. The dextran is at a final concentration of 1.3 mg/ mL, has a molecular weight is 150 k and is labelled with FITC (green). i: brightfield and ii: confocal fluorescence microscopy is used to observe the compartment formation. Timepoint sequences are shown in seconds, scale bars: 10 μm.

in the coacervate matrix, this indicates that the FITC becomes less fluorescent as it is separated from the TEG. Although not completely clear at this scale, it does appear that the internal compartments are visible in the brightfield view as well.

Single droplet timepoint sequences were then examined. Figure 4.10 shows the creation of internal compartments within the coacervate in two different coacervates. With both droplets, the timepoint sequence starts with the addition of dextran-FITC to the coacervate solution. The dextran is excluded from the coacervate matrix and the background supernatant is seen to fluoresce green. With the addition of TEG (the second frame in both sequences), the dextran starts to move into the coacervate. This collects at the interface as though entry is still restricted to some extent and a highly fluorescent ring is seen.

This ring is then fragmented and it appears that the dextran at the interface coalesces so that a portion at one section of the interface becomes brighter as the dextran is concentrated here. At this point, the dextran is still excluded from the coacervate droplet. The dextran then moves into the droplet from this section and begins to fill the interior of the matrix. A darker patch is seen in the brightfield view, where the dextran is located, demonstrating that the dextran is changing

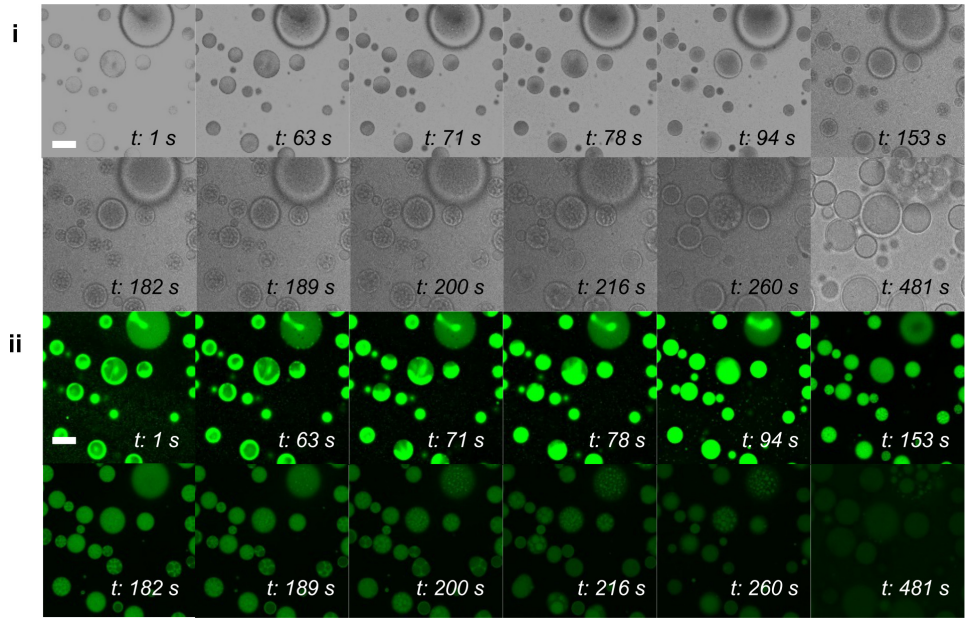

Figure 4.9: Medium scale timepoint sequences showing the formation of dextran compartments inside coacervates, upon addition of TEG. The dextran is at a final concentration of 1.3 mg/ mL, has a molecular weight is 150 k and is labelled with FITC (green). i: brightfield and ii: confocal fluorescence microscopy is used to observe the compartment formation. Timepoint sequences are shown in seconds, scale bars: 10 μm.

the refraction of the light or causing another component to alter the refraction from a knock-on effect. The dextran then fills the whole coacervate and appears to be homogeneous, based on both the brightfield and fluorescence confocal views. A bright halo inside the interface then starts to appear in the brightfield, despite the fluorescent view remaining homogeneous, and soon after the central darker region beings to separate into multiple tiny compartments. In the fluorescent view, this is seen as an overall decrease in fluorescence, alongside the appearance of brighter regions inside the compartments. This may indicate that TEG is moving apart from the dextran and therefore the FITC fluorescence is decreasing but this cannot be verified without knowledge as to the location of the TEG. These internal compartments then coalesce to eventually form a single large dextran compartment. This then breaks through the droplet and the internal compartment pops out of the droplet, releasing the dextran-FITC into the supernatant.

From the first to second timeframe, it can also be observed in the brightfield view that the droplet has shrunk in size, to approximately 3/4 of its original diameter. This indicates that either coacervate material is being lost or that the matrix becomes more dense at this point, and there is some expulsion of water. However, it is important to remember that this system is induced by very low concentrations of TEG in comparison to those that created vacuoles before. The droplets then remain a consistent size until internal compartments begin to form, at which point the droplet grows to accommodate this. During coalescence of the smaller internal com-

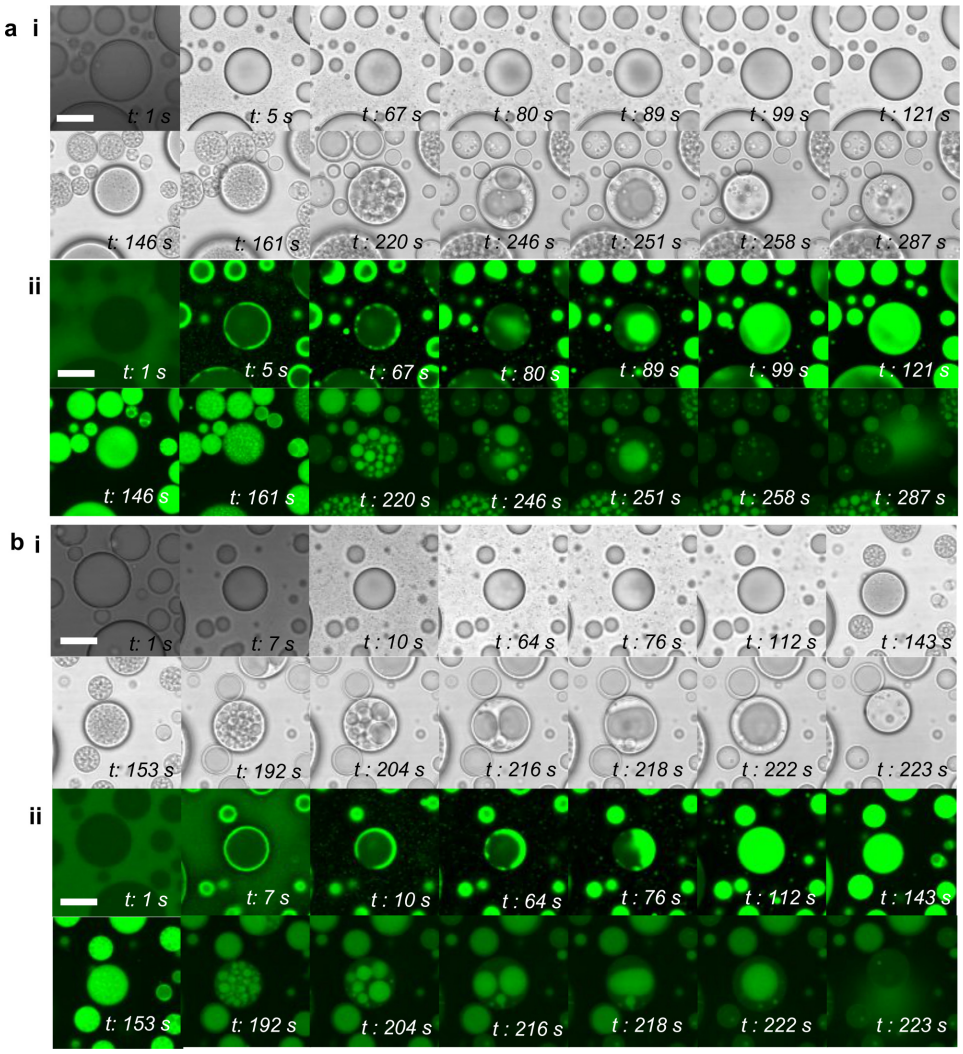

Figure 4.10: Timepoint sequences of individual coacervate droplets with dextran compartment formation. (a and b) The formation of dextran compartments inside the droplets, upon addition of TEG. The dextran is at a final concentration of 1.3 mg/ mL, has a molecular weight is 150 k and is labelled with FITC (green). i: brightfield and ii: confocal fluorescence microscopy is used to observe the compartment formation. Timepoint sequences are shown in seconds, scale bars: 10 μm.

partments, the coacervate remains a constant size, before returning to its original size at the start of the timeframe sequence at the point the dextran compartment is released.

Progression of this process to the point of a single dextran compartment is likely to be dependent on droplet circumference as the two droplets shown here are comparative in size and take a similar amount of time to move through each stage, although a much larger study would be needed to confirm this.

One interesting observation of droplets undergoing this process is shown in Frigure 4.11. For transient periods of time the coacervates are not spherical, indicating that the creation of a dextran vacuole occurs fast enough to cause re-arrangement of the coacervate matrix more rapidly than it can re-equilibrate to a more stable spherical shape.

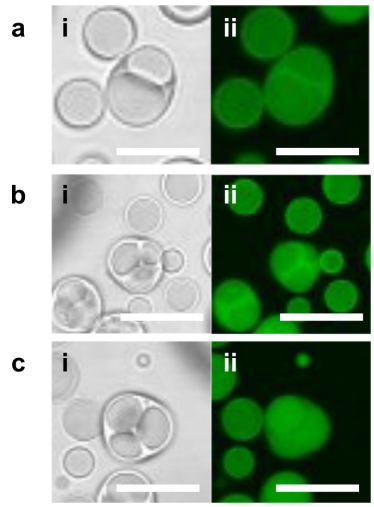

Figure 4.11: Internal compartment formation causes transient perturbation of the coacervate matrix. Intermediate state of the compartment formation are shown in three different coacervate droplets (a-c), by both i: brightfield and ii: confocal fluorescent microscopy. Scale bars: 10 μm.

In the fluorescent confocal views, it can also be seen that in two of the droplets (a and b) the intermediate stage dextran compartments have lower fluorescence whilst the boundary between them has higher fluorescence. However, with the other droplet, the higher fluorescence is contained inside the dextran compartments as expected. In all cases, the dextran ultimately ends up located mostly in the central coalesced dextran compartment. This provides insight into the mechanism, as it suggests that the period where the dextran still exists in the coacervate phase may not end as the internal compartment is formed. In the cases where lower fluorescence is seen in the dextran compartments during perturbation indicate that the point at which the compartment is formed is not always the same point that the majority of dextran is separated from the matrix. The three droplets here are of comparable size, which means that this difference in the speed of dextran sequestration into the compartments that ultimately form the central

region is not dependent of the size of the droplets. It may be related to the location of droplets in relation to the point of addition of dextran, and therefore local dextran concentration, but this has not been studied fully.

To obtain more information about the mechanism, and its dependence on droplet size, sequential images were obtained for droplets of a range of sizes (Figure 4.12). The droplets have diameters of approximately 10 μm, 7 μm and 3 μm and are shown at the same time frames, across the sequence. The two larger droplets behave similarly to one another, as do the two smaller droplets. By the end of the sequences, all the droplets look the same.

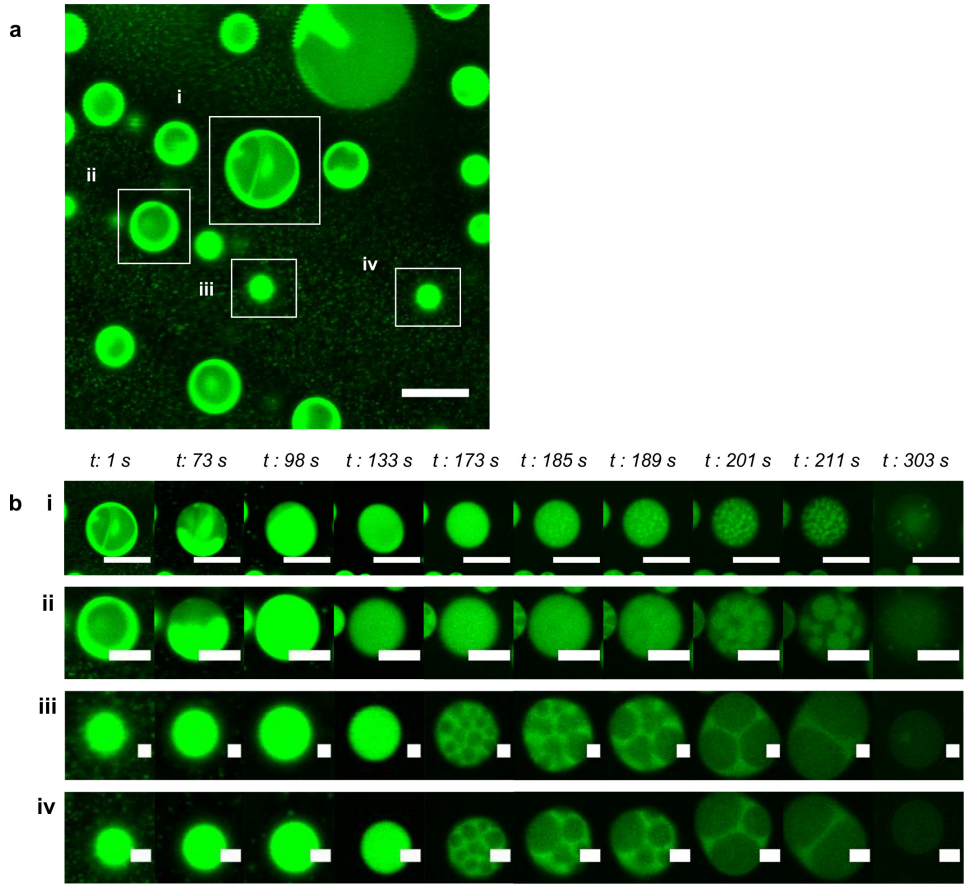

Figure 4.12: The coacervates undergo a series of transient shape changes in the process of forming a quasi-stable intermediate internal dextran compartment. Confocal fluorescent microscopy showing a: the location of the four droplets investigated over time at small scale, shown in b (i-iv). The dextran has a molecular weight of 150 k and is labelled with FITC (green). Scale bars: a: 10 μm, b: i: 10 μm, ii: 5 μm, iii: 1 μm and iv: 2 μm. Time point sequences are given in seconds.

At the start, the dextran fills the small droplets and appears homogeneous throughout. Little change is visible until 173 seconds, when small regions depleted in dextran start to appear. At this stage, it is unknown whether these are vacuoles which then fill with dextran or dextran free coacervate starting to separate from the dextran. These compartments coalesce at similar

rates in both droplets before reaching a stage at 201 seconds where three internal compartments are seen in each droplet, the dextran is concentrated around these compartments, and the coacervate spherical shape is perturbed. With one droplet (Figure 4.12 (iii)), the three compartments are similarly sized, whereas in the other (Figure 4.12 (iv)), two are similarly sized and one is smaller. By 211 seconds, these have merged into two compartments, with the smaller compartment from the droplet in Figure 4.12 (iv) clearly subsumed. In appearance, the whole process could be considered a synthetic analogue of reverse cell division in appearance. Logically, it would be assumed that the whole of one compartment is subsumed into one other by removal of the intermediate boundary. In Figure 4.12 (iii), it is hard to tell why the bottom right compartment would be subsumed rather than one of the others, or which compartment it has been incorporated into. Both compartments in the two compartment stage still appear to be similar in size. One hypothesis is that local flow within the droplet dictates which compartments are the least stable. Another is that it is affected by inhomogeneous slide coating which has a stabilising effect on some areas of the droplet. At the last stage, the two compartments form one central compartment and all the dextran is located here. There appears to be no higher concentrations of dextran at the compartment boundary. Furthermore, the fluorescence of the dextran is significantly lower, suggesting a lower concentration now it is more homogeneous.

With the larger droplets, the dextran is heterogeneous at the start. Although it appears to be located around the whole droplet it seems to enter the coacervate from a single point as seen previously. One droplet, Figure 4.12 (i), is momentarily oval shaped rather than spherical at 133 seconds but then reverts back to spherical. No changes in the dextran localisation are seen until 185 seconds, at which point many spherical compartments of higher fluorescence are seen to appear. These gradually get larger whilst the surrounding coacervate region becomes less fluorescent, presumably as dextran is depleted, and eventually forms a single central compartment through coalescence at 303 seconds. Interestingly, this is the same period of time that it takes the smaller coacervates to form a single compartment but the mechanism appears to be different. Once again, the fluorescence of this central compartment is significantly lower than the individual compartments, suggesting that the same amount of dextran is now occupying a larger volume.

The differences may be size related but an explanation for the mechanism in both cases is unclear at this stage. More information is required about the location of the components, particularly the TEG, in the transitory states. Although not explored in the scope of this research, it may be interesting in future to see if there is a method by which the non-spherical coacervates could be stabilised and maintained, perhaps by a gelation method.

Interestingly, the sequestration of dextran also occurs in a similar manner with partially wetted-out coacervate droplets, as shown in Figure 4.13, with slides that have less PEG coating. Apart from the fact that the droplets are no longer spherical, the mechanism appears to be the same at the start. This indicates that the entry of dextran into the coacervates is not dependent on

the slide coating and is driven by interactions with the coacervate only. After the dextran has filled the droplet it can be seen that the dextran remains in the coacervate matrix as well as in the internal compartments, as the contrast between these two regions is much less clear in the fluorescent channel. In contrast, the internal compartment formation can still be seen in the brightfield view. At the end of the compartment formation, a large amount of dextran is seen in the background supernatant and this can be attributed to release from internal compartments in other coacervates that have completed wetted out due to the low levels of PEG coating on the slides. However, little dextran is seen inside the coacervates that remain, except in the internal compartments, indicating that the process has completed in the same manner as usual, unaffected by the lower PEG coating on the slide. As the dextran appears to be completely sequestered up to this time point, it is unlikely that this excess in the supernatant is due to any change in sequestration behaviours due to the slide coating. It is unclear why the middle-stage sequestration of dextran into the coacervate would differ when the start and end appear similar but perhaps may be due to differences in the TEG sequestration with these droplets that cannot be seen at this scale.

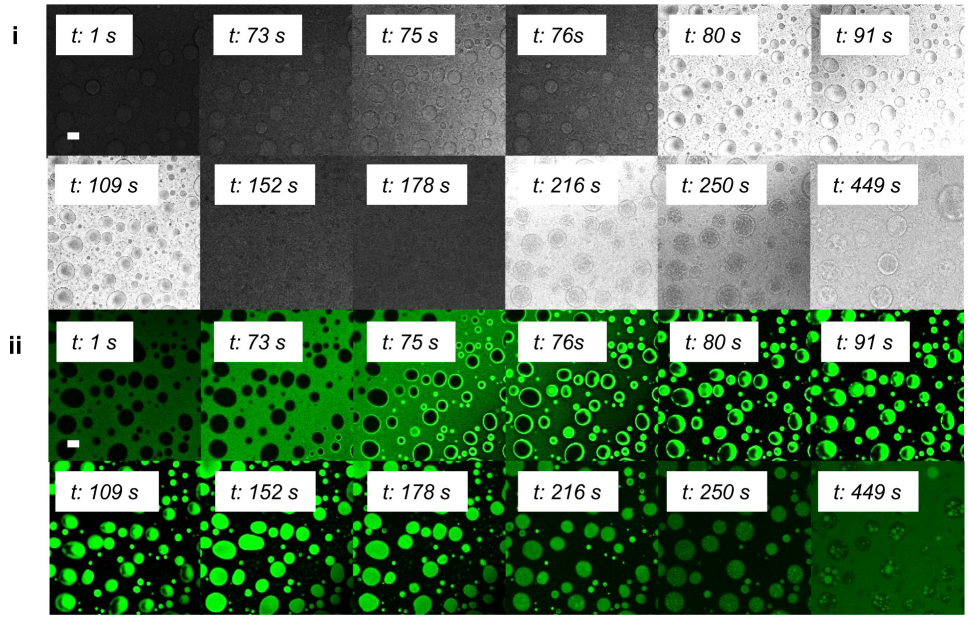

Figure 4.13: The TEG dextran separation is also observed with partially wetted out droplets. Time point sequences shown by i: brightfield and ii: confocal fluorescence microscopy. The dextran has a molecular weight of 150 k and is labelled with FITC (green). TEG is added at 74 seconds. Scale bars: 10 μm, time point sequences are given in seconds.

This figure also demonstrates the characteristic sequestration pattern caused by diffusion of TEG as it enters the field of droplets. This is seen in all experiments to date. The TEG enters from the bottom right corner of the images and the sequestration of dextran from the supernatant into the droplets can be seen to also begin at this location (Figure 4.13, 75 seconds).

However, the dextran, whilst diffusing into the coacervates from a single location at the interface, does not always diffuse from the point closest to this TEG entry. These results suggest that the TEG alters the coacervate matrix or dextran in the supernatant so that the dextran can enter the droplet, at the point in reaches it and this is logically dependent on diffusion distance. In contrast, each individual droplet is too small for the entry side to be drastically different to the far side , in terms of TEG concentration, and therefore this entry point is either random or dependent on another factor that succeeds this time point. It should also be noted that droplets far from the location of the TEG addition do not undergo any visible change, presumably because the concentration of the TEG is too low by the point of interaction with these droplets.

Based on the results of the experiment so far, it became obvious that it was necessary to simultaneously view the location of the TEG and dextran. As the TEG had previously been tagged with FITC (as described in Chapter 3), the dextran-FITC with a molecular weight of 150 k was swapped for dextran-RITC with a molecular weight of 70 k, and this is shown in red in the remaining figures. Unfortunately, dextran-RITC of 150 k was unavailable to purchase but the two weights of dextran were thought to behave similarly at the same concentration.

Figure 4.14 demonstrates a sequential time point sequence where both TEG and dextran can be seen. The dextran appears to behave as previously, corroborating the view that dextran-RITC 70 k behaves similarly to dextran-FITC 150 k. Based on the dextran sequestration information in the previous chapter, this would be expected. The dextran starts outside of the coacervate droplets and then TEG is added. The TEG enters the droplets immediately, preceding the dextran which then starts to enter a few seconds later. The dextran and TEG appear to initially stay separate, and this is confirmed by observing the fluorescence from each of these channel individually (not shown). The pattern seen inside the coacervates is visually similar to, and perceived to be, Marangoni flow [196]. This is the effect that creates a flow field around around an emulsion droplet initiated by a non=uniform surface tension at the droplet interface [197]. This can be caused by concentration gradient, and it would be anticipated that the dextran and TEG would have different surface tensions as the TEG is viscous at high concentrations. The two components then mix, although a corona of TEG without dextran appears to be maintained at the interface (seen in Figure 4.14, at 62 seconds). At this time point, the TEG is dispersed evenly across the droplet. The dextran then simultaneously splits into lots of small compartments which then coalesce to form a single large inner compartment containing dextran.

This behaviour is then examined at a smaller scale with a time point sequence of a single droplet (Figure 4.15). At the point of TEG addition, the background supernatant fluorescence gets noticeably brighter, once again showing that TEG has an influence on the intensity of dextran fluorescence visualised from the microscopy, possibly resulting from the difference in TEG refractive index compared to that of water as discussed earlier. Critical here is that this effect is seen despite the TEG being contained in the coacervates, demonstrating that the TEG has either altered the dextran as it has passed through the supernatant or that there is sufficient

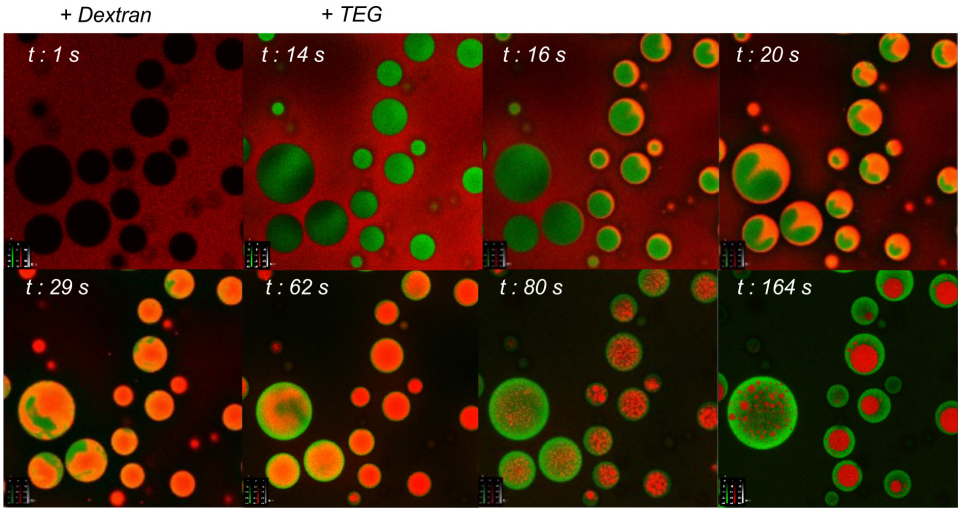

Figure 4.14: The location of the TEG within the system is observed by confocal fluorescence microscopy with a doped solution of TEG-FITC in TEG. To simultaneously observe the dextran location, dextran-RITC is used instead of dextran-FITC. The molecular weight of this is 70 k. Time point sequence shown in seconds.

TEG remaining in the supernatant to cause this effect despite the concentration of TEG being below the threshold able to be viewed on the confocal microscope.

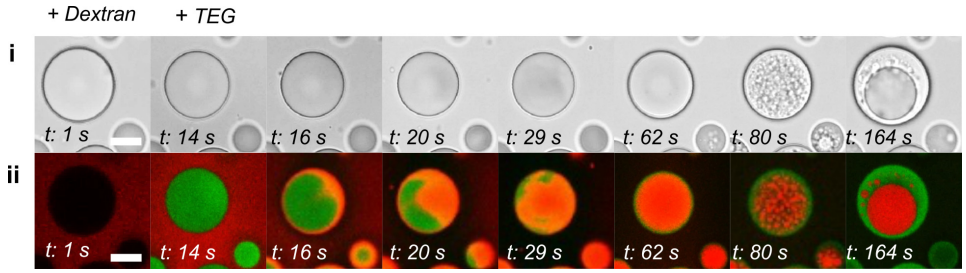

Figure 4.15: Small scale observation of the location of TEG and dextran in the phase separated system inside a single coacervate droplet. The molecular weight of the dextran-RITC (red) used is 70 k and the TEG-FITC is shown in green. i: brightfield and ii: confocal fluorescence images are shown. Scale bars: 5 μm, time point sequences shown in seconds.

It is also clear that no sub-structure is seen in the droplets until the point that multiple small compartments of dextran are seen. This shows that the flows of separated dextran and TEG are occurring within the whole coacervate matrix which is presumably evenly distributed at this stage.

Figure 4.16 shows 3D reconstructions of droplets containing dextran vacuoles, reconstructed from individual confocal microscopy slices at different heights through the coacervate. These images show the field of coacervates at a mid-point of compartment formation, demonstrating the presence of multiple dextran compartments in some of the larger coacervates where the

dextran has not yet completely coalesced to form a single compartment. They also show a cross section through coacervates, demonstrating the location of the inner compartment.

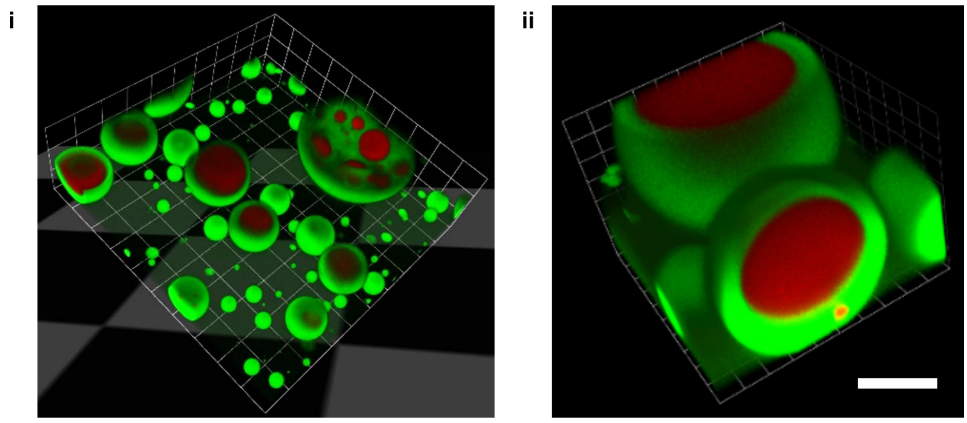

Figure 4.16: The dextran compartment formed as a result of TEG addition is surrounded fully by coacervate matrix. 3D reconstructions from individual slices show that the dextran compartments (red) are surrounded completely by TEG (green), which resides exclusively in the coacervate matrix. Scale bars: i: 1 unit = 3 μm, ii: 5 μm.

Although not explored in the scope of this thesis, there could be some potential in stabilising the dextran compartments before coalescence, in order to generate multiple small sub compartments and more complicated protocellular systems. This could possibly be done by altering the coacervate matrix components to make the matrix more difficult for the dextran to move through, or by adding a gelling component to the droplets after compartment formation. However, the effects of these on either the initial formation of the compartments, or on fully formed compartments have not been examined.

Importantly, these images show that the dextran compartment residues fully enclosed within the coacervate matrix, as opposed to being surrounded by matrix in a doughnut-like structure. This shows that the structure is stabilised by the coacervate droplet and not by an interaction with the glass slide coating. As a result, it is likely that the disappearance of the inner compartments by their sudden release into the supernatant is dependent on re-arrangements within the coacervate matrix, rather than an interaction with any components outside the confines of the droplet.

4.2.3.2 Mechanism

Although the appearance of the system has been fully characterised to this point, it became necessary to determine some more information about the mechanism by which the compartments form, in order to gain a better understanding and more effectively utilise the system for higher order structures. First, the TEG was exchanged for PEG 600, a similar molecule but with more repeating units (Figure 4.17). This increased the molecular weight and chain length, increasing

the number of groups available for inter- and intra- molecular hydrogen bonding. As the PEG 600 was untagged, dextran-FITC with a molecular weight of 150 k was used for this experiment, to be consistent with the majority of other experiments done to date.

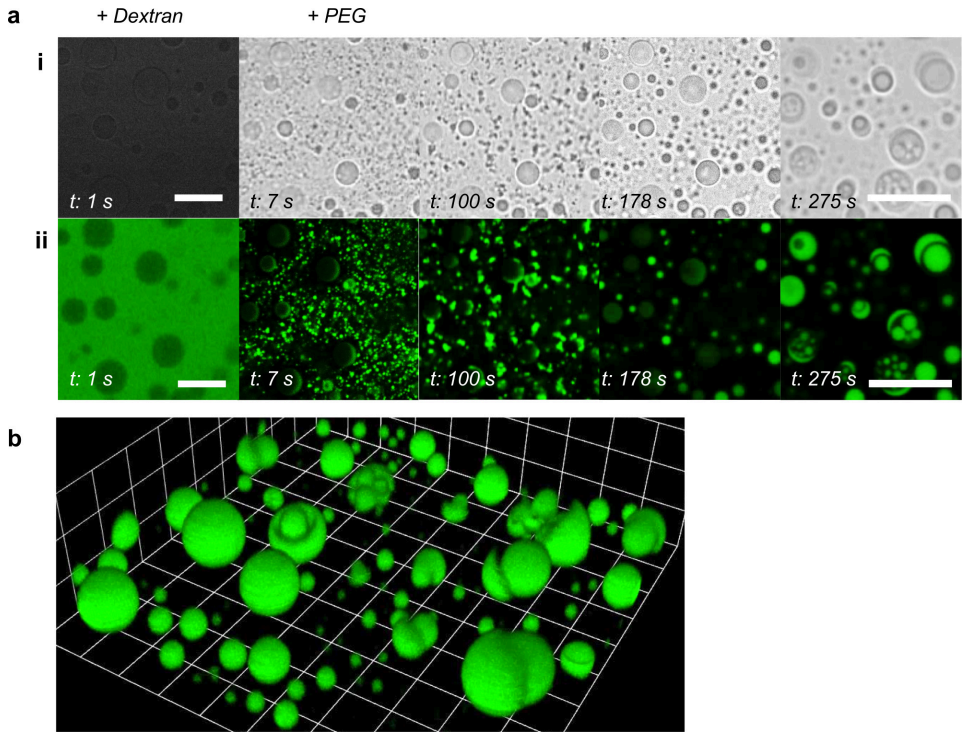

Figure 4.17: Altering the molecular weight of TEG affects compartment formation. a: i: Bright-field and ii: confocal fluorescence timepoint sequences showing the effect of substituting TEG for PEG 600, which has a molecular weight three times larger. The dextran-FITC (green) used has a molecular weight of 150 k, as previously. b: A 3D reconstruction of the system shown in a, at the end of the time point sequences. Scale bars, 10 μm, time point sequence shown in seconds.

The time point sequence shows clearly that this increase has an effect on the system. The dextran resides outside the coacervates, as usual, without PEG. However, upon the addition of PEG, fluorescent aggregates are seen in the supernatant, suggesting that a phase separation is already occurring. These aggregates then temporarily adsorb at the interface, likely due to surface tension interactions, before being sequestered inside the droplet. In contrast to the previous system described, the dextran and PEG enter the coacervate together, rather than the PEG followed by the dextran. This entry again seems to occur from a single point. Once inside, the fluorescence becomes homogeneous which suggests that phase separation may no longer be occurring despite the fact that both molecules are now at a significantly higher concentration. It is possible, therefore, that the coacervate matrix is affecting the phase separation by another mechanism perhaps by interactions of the TEG or dextran with the coacervate components. Specifically it has already been demonstrated that TEG may interact with PDDA in place of ATP so this could cause the TEG to be shielded from the dextran temporarily. Alter-

natively, there could be a local pH change or simply an effect of the additional ATP and PDDA components in the system. However, this could also demonstrate a transient period whereby all the components are re-equilibrating due to the change in environment but then go on to phase separate because the conditions and concentrations are appropriate to do so. Compartments of dextran then form and coalesce to make single compartments, as seen previously.

Interestingly, fluorescence was also seen to extrude and partially coat the outside of the coacervates with PEG 600, and this had no visible effect on the internal compartment, presumably because this was stabilised completely by coacervate matrix and therefore unable to interact. The external localisation of dextran-FITC can also be seen with 3D reconstructions, demonstrating that this is not an effect on an interaction with the coated slide. Although, potentially different in the mechanism of formation, it is intriguing that this produces a similar structure to those seen in Chapter 3, where higher ratios of TEG-FITC doping into untagged were used. The same mechanism seems unlikely but it could be due to increased phase separation causing expulsion of some dextran (and/ or PEG) as some dextran could not make it into internal compartment before being separated or could not make it through the PEG layer as easily. Therefore both mechanisms may be due to an alteration in the repulsive interactions between components.

The same experiment was then done with PEG 3000, which has even more repeating units (Figure 4.18). As anticipated, the dextran can be seen to only reside in the supernatant at the start of the experiment. Upon addition of PEG 3000, some small aggregates are seen in the supernatant and the dextran re-localises to the coacervate matrix. Differently to the addition of PEG 600, the aggregates are seen to form simultaneously to the entry of dextran rather than as a sequential process. This indicates that the PEG 3000 enters the coacervate quicker than PEG 600 or interacts more with dextran-FITC 150 k so that the system reaches an equilibrium with smaller aggregates. However, once the dextran is inside, no compartments are seen to form.

It is possible that if the system was left for a longer period then compartment formation would be observed however, this seems unlikely as no signs of any change in the system were seen over the time course of any repeat of this experiment. It would be expected that PEG 3000 would cause increased compartment formation as it is a larger molecule and therefore would be expected to phase separate to a greater extent from the dextran compared to TEG and PEG 600. However, it has already been pointed out that smaller aggregates were seen with PEG 3000 in the supernatant phase. This could mean that the local concentration upon entry to the coacervate does not drive any form of Marangoni flow as the concentration difference between the smaller but plentiful aggregates and the supernatant surrounding them is not great enough. With the PEG 600 the aggregates are larger so could be a better driving force for Marangoni flow. Another explanation could be that the larger molecule interacts with the coacervate matrix differently, becoming a component whereby its reactive groups are shielded to a greater extent and less phase separation occurs.

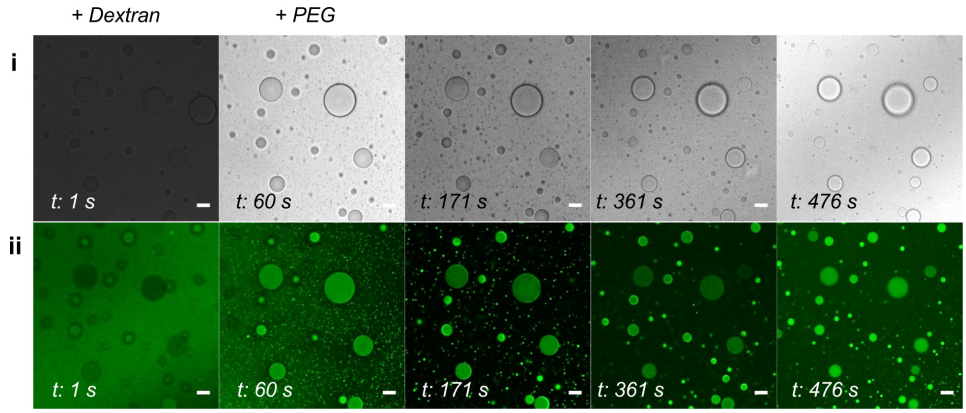

Figure 4.18: Altering the molecular weight of TEG affects compartment formation. a: i: Bright-field and ii: confocal fluorescence timepoint sequences showing the effect of substituting TEG for PEG 3000, which has a molecular weight fifteen times larger. The dextran-FITC (green) used has a molecular weight of 150 k, as previously. Scale bars, 10 μm, time point sequence shown in seconds.

The effect of altering the concentration of TEG was then observed, and this is shown in Figure 4.19. Unfortunately in this experiment, there was an issue with the dextran which meant that some was sequestered in the coacervates as well as residing in the supernatant, before the addition of TEG. It is thought that the dextran had broken down into smaller molecular weight pieces, altering the sequestration slightly so this experiment should be repeated to be conclusive. The final TEG concentration was reduced from 6% to 3%.

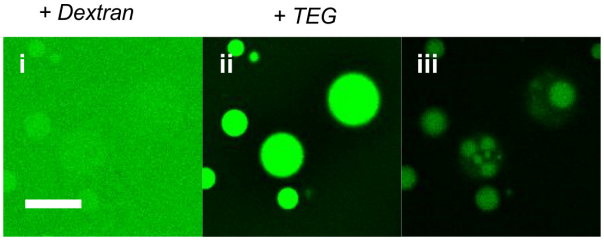

Figure 4.19: Altering the concentration of TEG affects compartment formation. Confocal fluorescent images showing the system when i: dextran is added, ii: TEG is added and iii: after compartment formation has occurred and a quasi-stable phase is reached. TEG concentration is reduced by 50% to a final concentration of 3%. The dextran-FITC (green) has a molecular weight of 150 k and is used at a concentration of 1.3 mg/ mL as previuosly. Scale bars, 10 μm.

The addition of TEG still caused total sequestration of the dextran and elucidated single dextran compartment formation. This was anticipated, as the formation of compartments with this amount of dextran and TEG had previously been shown with untagged components in Figure 4.5. Examining this with fluorescence dextran did not add additional information, as the time point sequences look very similar to that using 6% TEG, indicating once again that it is the same mechanism but the process requires a threshold amount of TEG.

The effect of altering the concentration of dextran was then explored to see if compartment characteristics could be influenced in this way. This is shown in Figure 4.20. Reductions in concentration to $1/20^{th}$ and $1/5^{th}$ of the original concentration were examined. When much lower concentrations of dextran were used, the dextran was seen to coat the coacervates rather than fill the supernatant, suggesting that there is an adsorption of the dextran to the droplets even though dextran is mostly excluded from the interior. It is therefore likely that there is a coating of dextran on all the droplets examined so far, even though this has not been visible due to the high levels of dextran in the supernatant. This should be taken into account when examining the mechanism. When the concentration of dextran is increased, the supernatant becomes fluorescent as well. However, in Figure 4.20 (b), a substantial amount of dextran is seen inside the coacervates, indicating that the dextran sample used here has begun to degrade. Conclusions based on this should be drawn carefully, as it may not be entirely representative of a standard sample.

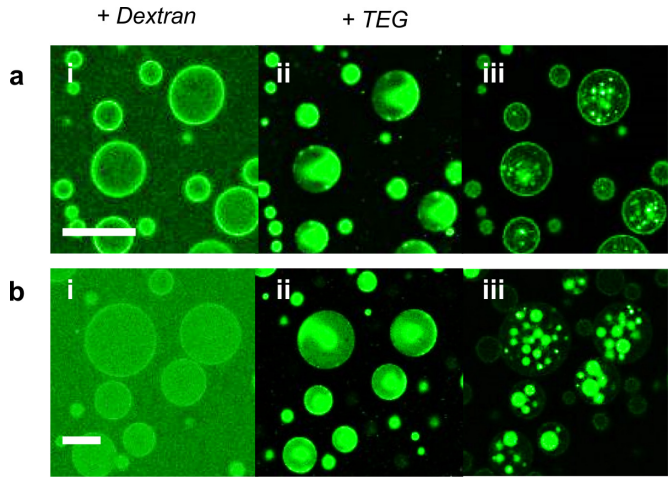

Figure 4.20: Altering the concentration of dextran affects compartment formation. Confocal fluorescent images showing the system when i: dextran is added, ii: TEG is added and iii: after compartment formation has occurred and a quasi-stable phase is reached. Dextran concentration is reduced by i: a factor of 20 and ii: a factor of 5, to final concentrations of 0.06 and 0.3 mg/mL respectively. The dextran-FITC (green) has a molecular weight of 150 k. The TEG is used at a final concentration of 6% as previously. Scale bars, 10 μm.

After the addition of TEG, the two sets of droplets look similar to each other, and to the droplets seen before with the normal concentration of TEG. Internal compartments form in both systems, showing that the threshold of dextran required for phase separation has been reached in both. In both samples, the internal compartments do not coalesce, suggesting that multiple compartment-based systems can be produced by using less dextran. The lower dextran concentrations mean that the evenly dispersed dextran stage that precedes compartment formation contains more space between individual dextran nucleation sites. This space contains TEG which is phase separates from dextran and therefore the dextran nucleation sites are stabilised

against coalescence by the surrounding mantle of TEG.

With the sample containing 20 times less dextran, the coacervates also present an interfacial coating of dextran. This coating does not seem to be present in the intermediate stage, although it is hard to say this definitively. If it is a coating that is formed after, the dextran may be partitioning at the interface of the matrix because it is not able to coalesce with the dextran contained in the internal compartments. It may have therefore been re-localised in an attempt to balance the repulsive forces from the TEG and attractive forces based on a surface tension reduction at the surface.

The effect of adding multiple additions of dextran followed by TEG was then examined. A decision was made to use dextran tagged with two different coloured dyes so that the first and second additions could be visually separated. Dextran-RITC 70 k was available, so dextran-FITC 70 k was used as the other dextran component, to eliminate any chance of the change in molecular weight interfering with the localisation. In the first experiment, dextran-RITC was added, followed by untagged TEG, followed by dextran-FITC, followed by another addition of TEG. In the other experiment, the same sequence was followed but the order of dextran-RITC and dextran-FITC were reversed. The fluorescence confocal time point sequences are shown in Figure 4.21.

This demonstrated again that dextran-RITC and dextran-FITC of the same molecular weight (70 kDa) do not behave exactly the same when added to the coacervates, despite their similar structures (shown previously in Figure 3.36). Although both are excluded from the coacervate interior, dextran-FITC is also observed to form an interfacial layer at the surface of the coacervate, whereas the dextran-RITC shows no preference to be at the interface and is homogeneous throughout the supernatant. This leads to some dextran-FITC creating a boundary layer during the transition into the droplet but this is not seen with RITC. The effect is potentially due to the fact that FITC is neutral at pH8 whereas RITC is slightly positively charged and so could be repelled from the slightly positive coacervates to a greater extent. This is consistent with partitioning studies shown in the previous chapter whereby FITC-dextran partitioned better into the coacervate bulk phase. Alternatively, the dextran-RITC may have a slightly different global structure to the dextran-FITC, even though it has the same molecular weight. Once again it seems that the behaviour of the tagged dextrans with the coacervates is dependent on both the chemical and physical properties of the tag. However, the size of the dextran is likely to dominate the interaction with coacervates. It is therefore possible that one of the dextrans is more branched than the other, and it is this factor that changes the interaction with coacervate droplets. Mass spectrometry of the dextrans would help with clarification of this hypothesis, and was attempted but was not successful .

The effect of adding multiple additions of dextran followed by TEG was then examined, in order to exploit this difference in partitioning. A decision was made to use dextran tagged with two different coloured dyes so that the first and second additions could be visually separated.

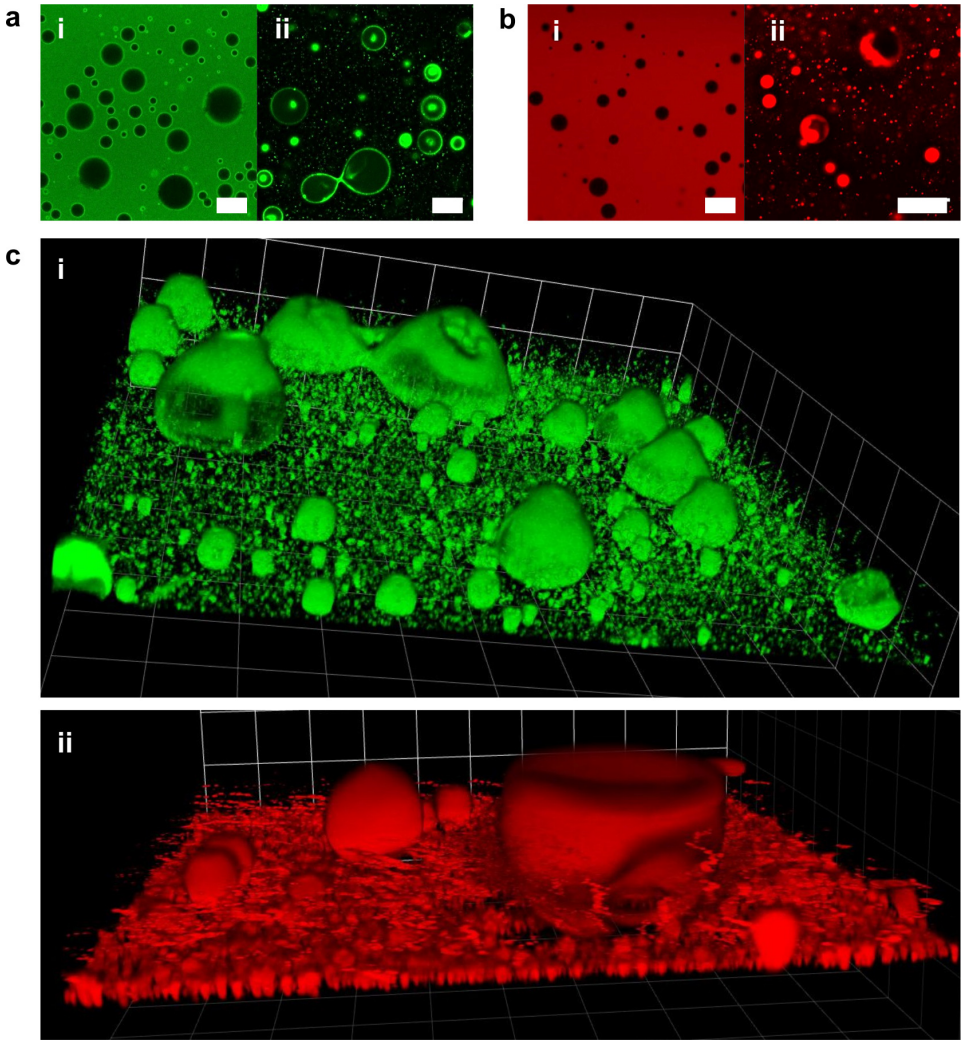

Figure 4.21: Effect of altering the charge on dextran in the TEG dextran phase separated system. Confocal fluorescence microscopy a: dextran-FITC 70k and dextran-RITC 70 kDa i: before and ii: at an intermediate stage of phase separation inside coacervates. c: 3D reconstructed z-stacks of the droplets after TEG addition showing the intermediate transitions with i: dextran-FITC and dextran-RITC. Scale bars: 20 μm

Dextran-RITC 70 k was available, so dextran-FITC 70 k was used as the other dextran component, to eliminate any chance of the change in molecular weight interfering with the localisation. In the first experiment, dextran-RITC was added, followed by untagged TEG, followed by dextran-FITC, followed by another addition of TEG. In the other experiment, the same sequence was followed but the order of dextran-RITC and dextran-FITC were reversed. The fluorescence confocal time point sequences are shown in Figure 4.22.

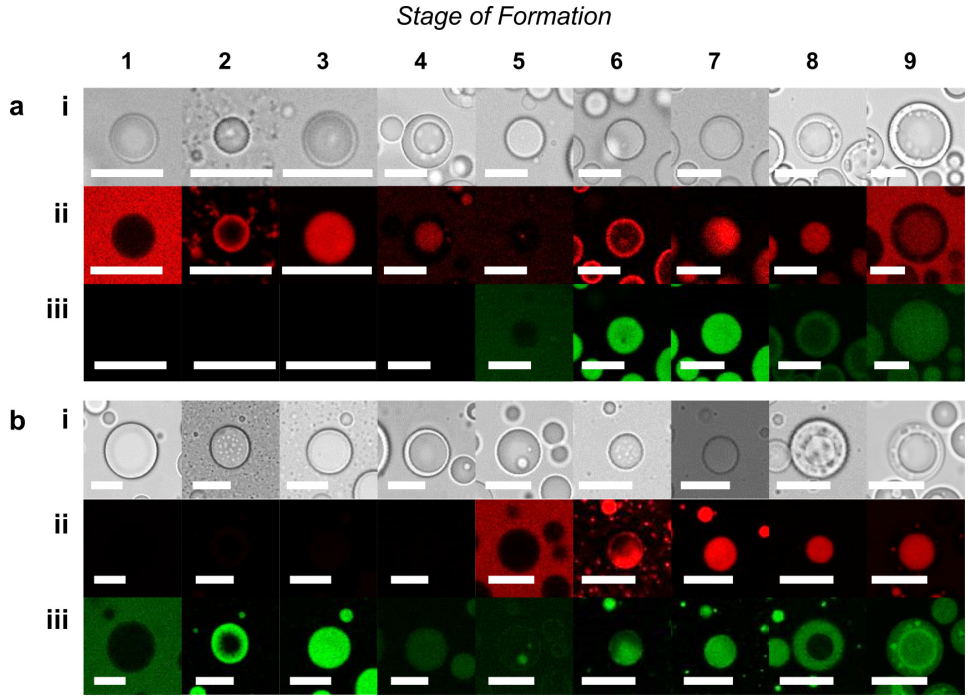

Figure 4.22: Dextran partitioning into the vacuole is influenced by the charge of the dextran. i: Brightfield and ii-iii: confocal fluorescence timepoint sequences showing the effect of adding dextran (to a final concentration of 1.3 mg/ mL) and TEG (to a final concentration of 6%) followed by another addition of dextran (to a final concentration of 1.1 mg/ mL and TEG (to a final concentration of 5%), altering the order of dextran-FITC and dextran-RITC so that a: dextran-RITC is added first or b: dextran-FITC is added first. ii: RITC fluorescence channel (red), iii: FITC fluorescence channel (green). Timeframes: 1: Addition of first dextran, 2: addition of first TEG, 3: dextran totally sequestered by coacervates, 4: dextran is contained in internal compartments, 5: addition of second dextran, 6: addition of second TEG, 7: both dextrans totally sequestered by coacervates, 8: dextran containing internal compartments formed. Note that in a & b, dextran-FITC is localised in the coacervate whilst dextran-RITC is localised in the interior compartment, 9: system reaches quasi-equilibrium state. Note that a representative droplet is shown for each timeframe, rather than the same droplet in all timeframes. Scale bars: 10 μm.

Note that the time point sequences do not show the same droplet in all frames, but rather a representative droplet from an array of droplets. This is due to the difficulties in maintaining the imaging of a single droplet that moves with any flow, which is introduced with the dextran and TEG additions. Further work in this area could benefit hugely from the use of a microfluidic

channel or similar device. The time point sequences have labelled according to the stage of the process, rather than the exact time so that the stages can be compared between the two experiments. However, note that the time for the stages to occur after each addition were similar in both cases. The confocal fluorescence channels for RITC and FITC are displayed separately for each experiment, alongside the brightfield view.

At stage 1, the added dextran surrounds the coacervate droplets, as seen in all other experiments with dextran of this size. No difference is seen between the dextran-RITC and dextran-FITC. At stage 2, TEG is added and the dextran begins to be sequestered into the coacervate matrix. The process looks similar for the two dextrans but there are aggregates in the supernatant surrounding the droplet with dextran-RITC whereas there are not in the droplets with dextran-FITC. This suggests that the dextran-RITC may be phase separating to a greater extent with TEG than dextran-FITC. At stage 3, the dextran-RITC and dextran-FITC droplets again look similar, with both filling the coacervate homogenously. By stage 4 a single internal compartment formation has occurred, and the dextran is contained in this central compartment with no dextran visible in the coacervate matrix.

At stage 5, another addition of dextran is added, with the opposite colour tag. Despite the fact that there is already TEG inside the coacervates, this dextran does not move into the droplet. This demonstrates that the sequestration of large molecular weight dextran into the coacervate is not only driven by the addition of TEG but must occur due to some factors that happen transiently when TEG is added. These factors are unknown, but one suggestion is that there is some temporary destabilisation of the matrix, increasing the mesh size created by the PDDA polymers and allowing entry of larger molecules. The dextran-RITC in the first experiment (Figure 4.22a) is expelled from the internal compartment at this point and the supernatant once again becomes fluorescent. In contrast the dextran-FITC internal compartments in the second experiment (Figure 4.22b) disappear but the dextran-FITC is still sequestered inside the coacervates. This indicates that the dextran-RITC partitions less into the coacervate with TEG than dextran-FITC, and indeed that it is most likely to be excluded from the coacervate matrix entirely. At stage 6, the second addition of TEG occurs and once again the dextran in the supernatant is driven into the coacervate, with dextran-RITC showing some aggregation in the supernatant. In the first experiment, the dextran-FITC which has been added second fills the whole coacervate whereas the dextran-RITC that was also now in the supernatant is seen to exist as a coating under the interface at the same time point. In the second experiment, the two dextrans appear to be occupying the same locations as one another, i.e. the dextran-FITC that already resides homogenously in the coacervate moves to occupy the regions that the dextran-RITC is now occupying as it enters the coacervate. The fluorescence then becomes homogenous throughout with both dextran-FITC and dextran-RITC in both experiments and this is shown in stage 7 (and between stage 7 and 8, which is not shown for simplicity). At stage 8, internal compartments form again but interestingly, in both cases, the internal compartment contains only dextran-

RITC. The dextran-FITC is retained in the coacervate matrix, despite the assumption that TEG resides in this volume.

After a period of time, the dextran-FITC re-localises indicating that the first structure was not the most stable state. At stage 9, the dextran-RITC in the first experiment, that was contained in the interior compartment, is now both in the interior compartment and in the supernatant. This indicates that the compartments are maintained but that some compartments have been released, filling the supernatant with dextran-RITC. However, the dextran-FITC now resides in both the internal compartment and in the coacervate, as though it is as repelled by the dextran-RITC as the TEG. In the second experiment, the dextran-RITC is again maintained in the internal compartment. Dextran-FITC is maintained in the coacervate but is seen in the interior compartment as well. At this point, it can also be seen that the dextran-FITC is coating the interior face of the coacervate that bounds the interior compartment, possibly stabilising this structure further.

It was anticipated that the two dextrans would mix and form one solution based on observations in an Eppendorf tube, whereby mixing the two solutions of dextran resulted in one continuous phase. Additionally, the two dextrans have always behaved similarly to one another experiments when used individually. However, it can be seen from the observations discussed that this is not the case. Regardless of the order of dextran addition, dextran-RITC always ends up in the central compartment at the expense of the sequestration of dextran-FITC to this compartment. When the partitioning of dextran-RITC into the coacervates was compared to that of dextran-FITC in Chapter 3, the partitioning value was slightly lower although similar. Although too similar to dextran-FITC to draw a definitive conclusion, it suggests that dextran-FITC partitions slightly better into the system than dextran-RITC. This could explain the aggregation of dextran-RITC when TEG is added, and the propensity of dextran-RITC to be enclosed in the inner compartment rather than dextran-FITC.

However, there are still some unanswered questions. It is unexpected that the two types of dextran would mix and then de-mix again when they are so similar. Experiments in the previous chapter highlighted that there is little difference between these two types of dextran. It is surprising that this alone would have such a great effect. It may be that the combination of this with a TEG phase separating system enhances the differences between the molecules as it is likely to be the phase separation of TEG and dextran driving this difference, rather than the difference between the two dextrans sequestration properties with respect to the coacervate droplets. In fact, in the final stage, it could be hypothesised that the effects seen are the immediate separation of dextran-RITC from TEG to form an internal compartment in the droplet, followed by the much slower partitioning of dextran into this phase as well. The reduction in rate of the dextran-FITC sequestration could be attributed to its containment in the coacervate, because any movement would now involve interacting with TEG as well as the matrix. Excitingly, the observations from this experiment demonstrate the potential of altering the sequestration of

macromolecules into the inner compartment based on subtle changes in charge, and manipulation of sequestration is explored shortly.

Based on the previous results demonstrating that even small changes to the dextran can cause differences in compartment formation, the effect of altering the size of the dextran was investigated. First the effect of adding dextran-FITC 70 k instead of 150 k was observed more closely with a time point sequence (Figure 4.23). A similar process was seen as with the dextran-FITC 150 k, which was expected because it has previously been shown that 70 k and 250 k dextrans partition very similarly into these coacervates (Chapter 3).

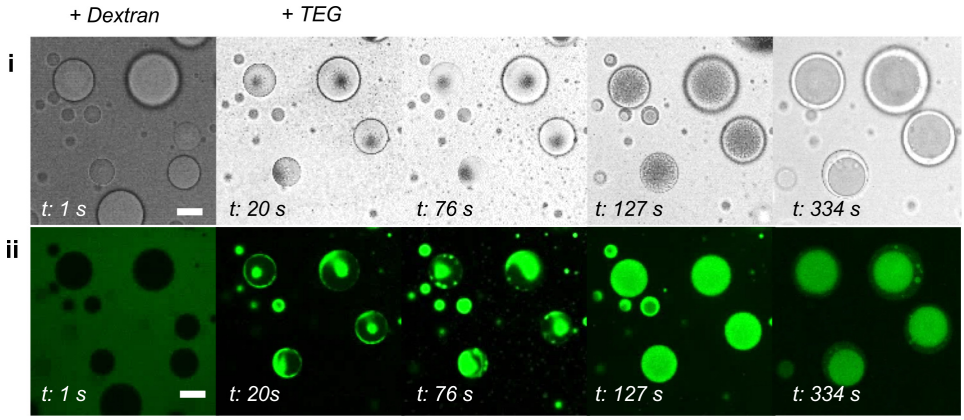

Figure 4.23: Altering the molecular weight of the dextran affects compartment formation. i: brightfield and ii: confocal fluorescent images showing time point sequences. Dextran-FITC (with a molecular weight of 150 k is replaced by dextran-FITC (green) with a molecular weight of 70 k. Scale bars, 10 μm.

The same experiment was then done with dextran with a molecular weight of 4 k, which partition studies showed was not excluded by the coacervate matrix when added without TEG (Figure 4.24). This entered the coacervate immediately upon addition but, even when TEG was added, showed no internal re-structuration. This is interesting as ATPS does occur when dextran-FITC 4 k and TEG are combined in an Eppendorf tube. It may be that the coacervate matrix interferes with the interaction between TEG and dextran inside the droplet, and that the smaller size of 4 k is not large enough to overcome these restrictions and participate in a reaction with TEG. Alternatively, it may be that the influx of dextran is key to initiating the process of compartment formation, and this does not occur if the dextran is already inside the droplet.

Overall, it seems that altering the molecular weight, even by a factor of two, seems to have less effect than slightly altering the charge of a side group on the dextran, so long as the dextran size is above the threshold required for internal compartment formation to occur.

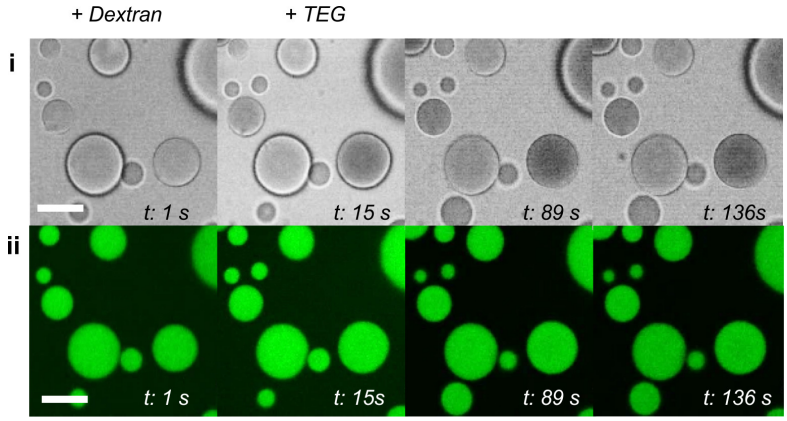

Figure 4.24: Altering the molecular weight of the dextran affects compartment formation. i: brightfield and ii: confocal fluorescent images showing time point sequences. Dextran-FITC (with a molecular weight of 150 k is replaced by dextran-FITC (green) with a molecular weight of 4 k. Scale bars, 10 μm.

4.2.3.3 System Utility

To maximise the capability of the system described, a methodology was devised to test the utility of the storage compartment of dextran in the centre of the droplet. Previous experiments showed that it was still possible to encapsulate enzymes in the coacervate matrix after the creation of the internal compartment. Here, this was attempted with dextranase, which hydrolyses dextran chains at the (1,6)-α-D-glucosidic linkages, creating smaller chains of dextran (and eventually isomaltose). Figure 4.25a demonstrates that dextranase tagged with FITC is indeed localised to the coacervate and does not reside in the central dextran compartment. The next step determined whether dextranase localised in the coacervate was capable of interacting at the interface of the internal compartment/ coacervate boundary. It was hypothesised that if the dextran was being cut into smaller dextran chains, these would re-localise to the coacervate matrix because there would be no reason for exclusion based on the previous few experiments.

Coacervates with dextran compartments were created with and without dextranase in the surrounding coacervate (Figure 4.25b). Confocal microscopy images, and associated line profiles of dextran-FITC intensity at three points were examined; one inside the central compartment, one in the external coacervate, and one in the supernatant, (labelled on the images). The results show that when dextranase is present in the coacervate, the dextran in the central compartment does move into the coacervate region, which therefore becomes significantly more fluorescent. Fluorescence also increases slightly in the supernatant, but this can be attributed to the expulsion of dextran compartments from surrounding droplets releasing dextran. Without dextranase, the dextran remains in the central compartment.

Further enzyme cascades were attempted, developed with the idea that dextran could be further cut to glucose using isomaltase to cut the isomaltose units left by complete dextranase action.

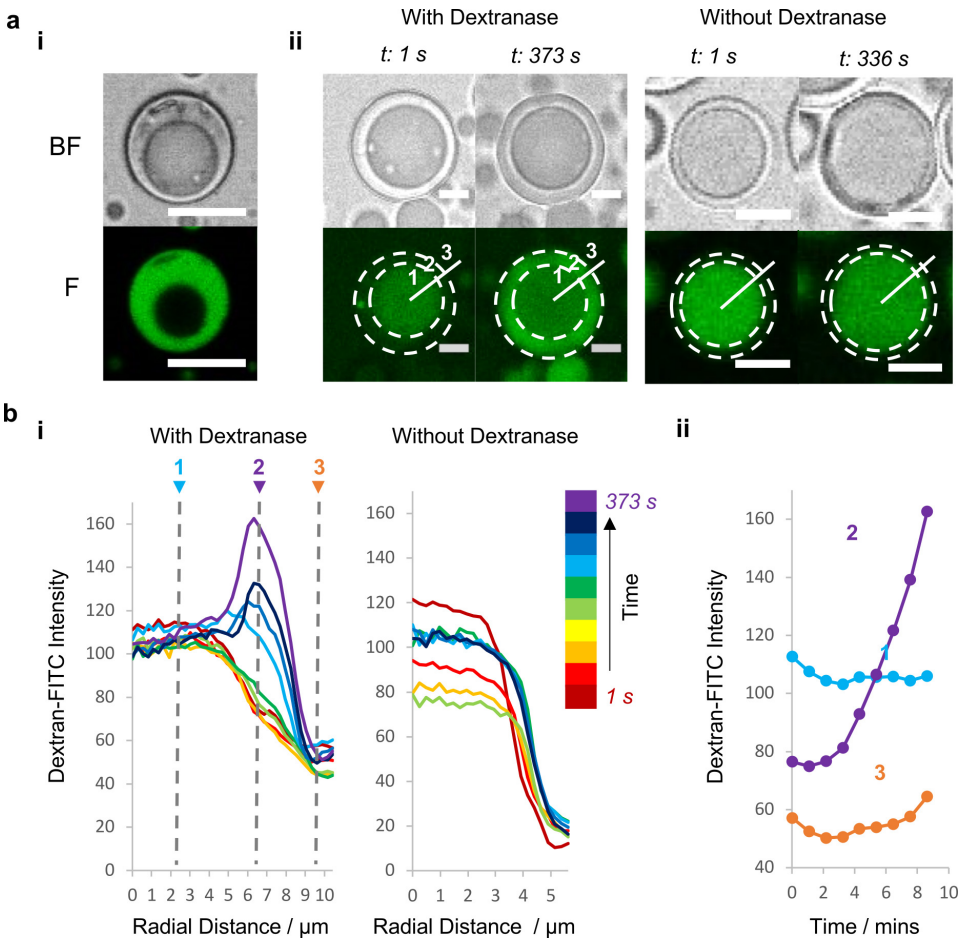

Figure 4.25: A storage compartment can be formed, which is acted on by enzymes in the coacervate. a: brightfield (BF) and confocal fluorescence (F) images showing (i) the location of dextranase tagged with FITC (green) and (ii) the location of dextran-FITC (green) in coacervates over time with and without dextranase present in the coacervate region. Dextran of higher molecular weight are excluded from the coacervate but, after dextranase digestion to lower molecular weight entities, then become sequestered by the outer coacervate region. The boundaries between the coacervate and the dextran compartment, and the coacervate and the supernatant are shown by a dotted circle. Scale bars: 10 μm. b: Radial profile analysis of coacervates with and without dextranase over time, as indicated by the line profile positions in a: (ii). In the droplet with dextranase, an increase in fluorescence intensity is seen in the coacervate region (2), indicating a movement of dextran-FITC (ii) Intensity at radial distances 1, 2 and 3 marked in b: (i), plotted over time.

This could then be used to initiate a proof-of-principle cascade. The well-characterised glucose oxidase, horseradish perioxidase cascade with OPD as the fluorescent output was selected and shown in vitro but the components did not behave similarly in the coacervates, leading to autofluorescence of the cascade in the absence of glucose. Further work could be done in this are to identify the coacervate component causing the issue and to further devop the utility of a dextranase compartment. Additionally, other proteins including BSA and myoglobin were tagged with dextran to see if this could be used to encourage partitioning of these molecules into the dextran compartment. Unfortunately, the overwhelming sequestration characteristics seemed to come from the proteins, and these were still sequestered even when coated with dextran. Further investigations to alter the coacervate components to discourage partitioning of proteins could aid here.

4.3 Conclusions & Further Work

In this chapter, multiple macromolecules were combined in the same coacervate system. Single stranded DNA oligomers were base paired to form double stranded DNA and the effects of this on the coacervate properties were studied.

The further development of the TEG vacuole system was also explored with the addition of other components. A TEG Dextran phase separated system was seen to form, showing that other means, such as ATPS, could also be used to induce vacuole formation in the PDDA: ATP coacervate system. An extensive comparison between the mechanisms of the systems in Chapter 3 and 4 was shown, with the deduction that vacuoles were actually formed by two different mechanisms. However, the underlying theory behind the mechanisms may have some similarity. This system also allowed the internal vacuole to be modified to become a dextran-filled compartment.

Higher order structures were seen with internal compartment boundaries maintained in some cases even after dextran compartment formation. Novel sequestration mechanisms were seen in the coacervates and characterised with tagged TEG and dextran. Interestingly, combinations of dextran-FITC and dextran-RITC allowed selective partitioning of these molecules, altering the properties of the central dextran compartment and the macromolecular sequestration within this. There are few examples of literature utilising ATPS in coacervates but one such example is Long et al. [68]. This research demonstrated that ATPS could be driven within a droplet to segregate proteins and controlled mixing and de-mixing could occur by environmental adjustments. This control from the external environment would be an interesting route to pursue in future work. However, a novel factor in the TEG/ dextran system shown here is that the contents of the internal compartment contain a concentrated molecule and are not simply of the same composition as the external supernatant. This is really interesting and should be explored further with the containment of other molecules as it was discussed in the introduction how important macromolecular crowding is in biological systems.

Finally, the utility of the system was extended, and it was shown that enzymes in the surrounding coacervate matrix could act at the interface of the central compartment the coacervate matrix. This was illustrated with dextranase showing successful cutting and subsequent re-localisation of the dextran-FITC contained in the central compartment. Initial attempts were made to further this system by introducing an enzyme cascade, but this has not been studied extensively. Increased insight here would allow complex systems of coacervates to be built in a controllable manner, perhaps with a view to initiating populations of coacervates able to evolve and communicate through component release or predictable coacervate disassembly. Additionally, more work could be done to extend these compartments to other coacervate systems and alter the partitioning properties of the coacervates such that molecules coated in dextran could be contained in the central compartment and then released with the action of dextranase.

CHAPTER 5

MACROMOLECULAR SURFACE LOCALISATION ON COACERVATES TO CREATE HIGHER ORDER FUNCTIONALISED SYSTEMS

This chapter begins to investigate another topic of protocellular requirements; that of a membrane. Although coacervates do not require a membrane for some simple processes, this addition allows for higher-order functionality. The macromolecular interaction observations previously discussed in the earlier chapters aid the addition of macromolecules to the coacervate bulk/supernatant interface. This is shown to be successful with some block copolymers. The block copolymers are then used to template the addition of purple membrane flakes and some early research is conducted into the light-driven proton pumping behaviour of this new membrane. Finally, the TEG and dextran systems described in Chapters 3 and 4 are introduced to this membrane coated coacervate system, demonstrating the options for further research.

5.1 Introduction

The addition of a membrane to coacervates is explored with the aim of partitioning purple membrane flakes at the interface of coacervates. When layered in a directional manner on the surface of droplets, this can be utilised to induce a pH change in the droplet interior which in turn will be used to activate pH sensitive enzymes within the droplets.

Although applications for this technology have not yet been fully explored, it is hoped that this system will lead to a light generated substrate release mechanism or compartmentalised enzyme activation initiated by light-driven pH effects. Once a protocol has been established for the bacteriorhodopsin templating, it may also be applicable to other membrane proteins and multiple membrane bound cascades could be introduced.

For the reasons explored in the introduction, fatty acids are seen as a beneficial solution for membrane construction. Therefore, Tang et al. established a system where coacervates were coated with a fatty acid bilayer to combine the advantageous of both a fatty acid membrane and a coacervate system [51]. Images from this research are shown in Figure 5.1. As demonstrated by Szostak [62], the fatty acids form a bilayer membrane vesicle when the pH is close to the pKa of the fatty acid which is 7.5 to 8 with the oleic acid used in this case, dependent on whether it is present in a phospholipid bilayer or fatty acid vesicle respectively [198]. However, at a higher pH, of more than 10, micelles are formed and at a lower pH, of less than 8, oil droplets are instead observed [62, 198].

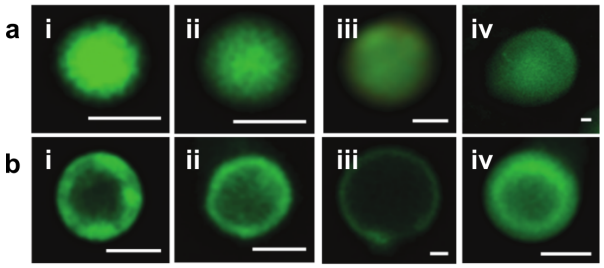

Figure 5.1: A literature illustration of fatty acid assembly on coacervates. Single droplets a: without and b: with a fatty acid coating. Coacervate components are as follows: i: polylysine/ RNA, ii: oligolysine/ RNA, iii: oligolysine/ ATP, iv: PDDA/ ATP. Scale bars: 1 μm. Figure taken from Tang et al. [51]

This phenomenon is due to the interactions formed as a result of the protonation state of the polar carboxylic acid head group. When protonated it becomes less hydrophilic and packing of the molecules therefore changes accordingly. Oleic acid comprises a tail consisting of eighteen carbons and a cis-9 double bond. In monomeric form, head groups are arranged on the surface with tails pointing inwards to an aqueous centre whereas in a vesicle the arrangement shifts so that a bilayer is formed around the aqueous region. Oil structures are spherical aggregates with no aqueous region accommodated and a single layer of monomer head groups at the surface. They may contain pockets of head groups within the structure and small amounts of water [198].

The fatty acid coacervates are membrane enclosed microcompartments with all the advantageous of a coacervate system but with the ability to exhibit semipermeable behaviour and different uptake and exclusion to uncoated droplets [51].

Purple membrane is the name given to patches of bacterial membrane composed of crystalline regions of the light-driven proton pump bacteriorhodopsin, which has a molecular mass of 26 kDa [199]. This protein is comprised of seven transmembrane helices that link the cytoplasmic side of the membrane at the carboxylic acid terminus to the extracellular side at the amino terminus [199]. The structure of bacteriorhodopsin leads it to associate in homotrimers, forming hexagonal two dimensional packing profile. This is shown in Figure 5.1. It has been suggested

that there are approximately ten lipid molecules per bacteriorhodopsin and the ratio of these are thought to be five phospholipids, three glycolipids and two squalenes [200]. Within the purple membrane flake, the bacteriorhodopsin has uniform orientation and is protected so that it can be stable in a range of thermal and chemical environments [200].

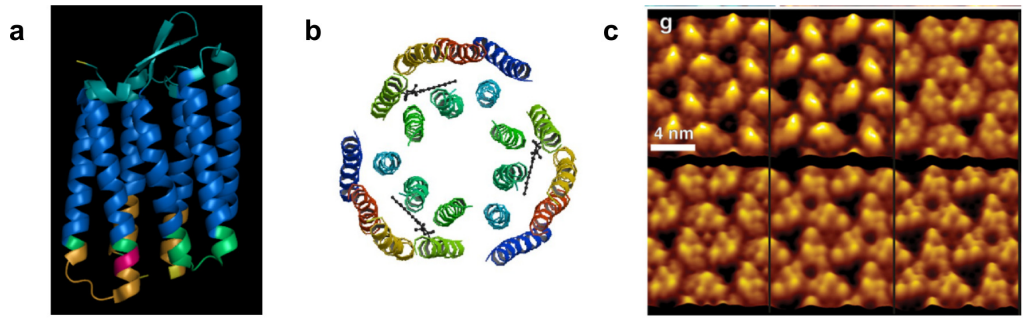

Figure 5.2: The structure of bacteriorhodopsin and it's arrangement in purple membrane flakes. a: Side view of the protein structure of bacteriorhodopsin, the main constituent of purple membrane. b: End view of the association of three bacteriorhodopsin proteins, resulting in a hexagonal flat assembly. Source: Protein Data Bank 1BRD. c: the arrangement of hexagonal regions to form a tightly-packed array of protein within purple membrane. Source: Bippes et al. and Muller et al., Scale bar: 4 nm.

Like many other integral membrane proteins, a single bacteriorhodopsin is able to diffuse laterally within the membrane [201], although close packing with other bacteriorhodopsin molecules limits this behaviour. It exposes hydrophobic amino acid side groups, which are thought to encompass 70 percent of the protein [199], to the interior of the membrane whereas hydrophilic groups interact with the aqueous environment both sides of the membrane [200]. Hydrophobicity of the protein is enhanced by shielding of many of the hydrophilic groups by hydrophobic regions [199].

Upon interaction with light, the protein translocates a proton from one side to the other, setting up a proton gradient which can then be utilised by other mechanisms as an energy source for reactions. This is allowed for by the movement of flexible loop structures in the protein [201]. In natural systems, the proton gradient is used to produce ATP by coupling the processes of bacteriorhodopsin with that of the F0F1 ATP synthase motor protein. Some synthetic research has even mimicked this in polymersomes [202] and showed that the biological function of bacteriorhodopsin can be maintained after incorporation into giant unilamellar vesicles [203].

Bacteriorhodopsin has been researched extensively and is often used as a model membrane protein system. However, due to its preferential membrane environment, it is not without its issues which is why it is often utilised within purple membrane. Function of a protein relies heavily on its structure and the structure of membrane proteins, including bacteriorhodopsin, are influenced hugely by the interactions with the surrounding lipids and the elastic and curvature properties of the membrane bilayer [200]. These interactions are often dynamic to allow

for signal transduction or transportation of molecules [200]. With appropriate detergents, the protein can be unfolded and refolded and stabilised with either urea or SDS. Folding is thought to occur as a result of the formation of a partially structured helical core which then acts as a nucleation site so that the rest of the folding process can occur [204]. It is enhanced with the correct lipid interactions and suitable mechanical properties and thickness of the bilayer [204]. Unlike non-membrane proteins, it is possible that when bacteriorhodopsin is denatured it in fact retains some folding in its hydrophobic core which can cause incomplete binding of SDS leading to smaller than anticipated electrophoretic gel band migration.

When proton pumping assays are required, 8-hydroxypyrene-1, 3, 6-trisulphonic acid (pyranine) is often used as the fluorescence is dependent on the pH of the environment in which it is present. It is therefore used in the interior of vesicles, with any excess removed from the external system, usually by dialysis. In these cases, valinomycin is used to neutralise any existing electrochemical gradient [205].

Another component, block copolymers was also considered. These are covalently joined series of polymers that can self-associate to form vesicles, bilayers and other structures useful for protocellular studies. Properties of the block copolymers depend heavily on their structure however this is very applicable to rational design. Lately, research has been undertaken to use block copolymers to mimic cell bilayers as a method for supporting membrane proteins [206, 207]. The molecules have larger molecular weights than their lipid counterparts and therefore exist in a slightly tangled conformation, increasing the amount of elastic energy in the membrane. They also show increased stability compared to lipids [208]. Side chains can also be added, and in some cases crosslinked, to add other properties or further stabilise the system creating a tough shell-like exterior [209].

Gramicidin A ion channel has been incorporated with a poly(2-methyl-2-oxaline) - poly(dimethylsiloxane) poly(2-methyl-2-oxaline) - (PMOXA-PDMS-PMOXA) block copolymer system [208]. Here, a key factor was to use decane as a solvent instead of chloroform or toluene which would denature membrane proteins. This method has also demonstrated that alamethicin, another ion channel, OmpF, OmpG, TSX, LamB, Complex I, Aquaporin Z, FhuA and alpha-haemolysin can all be directionally inserted. Similarly, PEO-PDMS-PMOXA systems have directionally incorporated aquaporin and shown that a heterotrimeric block copolymer can be constructed to encourage directional insertion [210].

One of the most promising developments with bacteriorhodopsin has been that of the triblock constructed from hydrophilic block poly(2-ethyl-2-oxazoline) (PEtOz) and the hydrophobic block PDMS to form PEtOz-PDMS-PEtOz self-assembled nanoscale bilayer vesicles [202]. This demonstrates long term stability and the bacteriorhodopsin was also shown to have retained its photoactivity within the block copolymer layer [205], even when incorporated by several different methods. It was also shown that the block copolymers formed intercalated loop structures in

aqueous solutions and other conformations when constructed by aperture spreading [211]. A system utilising poly(2-ethyl-2-oxaline) and PDMS (PEtO2-PDMS-PEtO2) has been used to insert purple membrane and bacteriorhodopsin alongside the F0F1 ATP Synthase to set up a proton pumping energy generation system [212]. The similar molecule, proteorhodopsin, has been shown to be included in a poly (4-vinylpyridine) and polybutadiene system (P4VP- PBD-P4VP) [213]. A range of block copolymers produced by BASF have also been utilised for bacteriorhodopsin insertion. These are known commercially as pluronics and poloxamers. Specifically Pluronic F127 [214, 215], P105 63 and P68 (also known as Poloxamer 188) [215] have all been used in this way.

All the systems that have been listed so far are triblock systems but diblock systems can similarly be useful. One such system containing polyethylene oxide (PEO) and poly (ethylethylene) (PEE) has been used to stabilise alamethicin alongside mellitin, polymixin and mastoparan [216]. Two different chain lengths of polystyrene (PS) and poly (4-vinyl-N-methylpyridine iodide) (P4MVP) have been used together to construct membrane analogues [213]. Finally, a poly (butadiene) and poly (ethylene oxide) system has been used to incorporate Claudin-2 [217].

5.2 Results & Discussion

5.2.1 Purple Membrane Tagging

Purple membrane flakes, in lyophilised form, were kindly donated by Dr Hampp at the University of Marburg. As the flakes could not be observed directly on the microscope, due to their low amount of innate emission, a decision was made to tag the flakes with a fluorescent molecule. Fluorescein isothiocyanate (FITC) was selected as this is well characterised and had been shown previously to be successful. Rhodamine b isothiocyanate (RITC) was also chosen, as its similarity to FITC meant that the same tagging procedure could be used. Tagging the purple membrane flakes with multiple coloured fluorescent molecules also allowed for a range of dyes to be used in conjunction with the flakes in further experiments, without overlapping the emission from the flakes.

1.9 μmol of FITC/ RITC (both from sigma Aldrich) were added for each mg of purple membrane in 50 mM TRIS-HCl. The reaction was left to proceed in the dark, at room temperature, for 4 to 6 hours. Any excess FITC/ RITC was removed by centrifugation at 8000 g for 10 minutes. The solutions were then washed twice in 50 mM TRIS-HCl. Finally the solutions were washed in 0.2 M KCl, followed by a wash in distilled water. All washes were done via the centrifugation method described.

It was necessary to check that the FITC and RITC had attached to the purple membrane and were not just free in solution. Therefore, tagged and untagged purple membrane was solubilized and the resulting bacteriorhodopsin ran on a sodium dodecyl sulphate polyacrylamide (SDS-

PAGE) gel to determine the size of the molecule, and whether the tagging had been successful (Figure 5.3). Some samples were run with 7 M urea to aid denaturation of the protein and prevent aggregation of individual bacteriorhodopsin proteins.

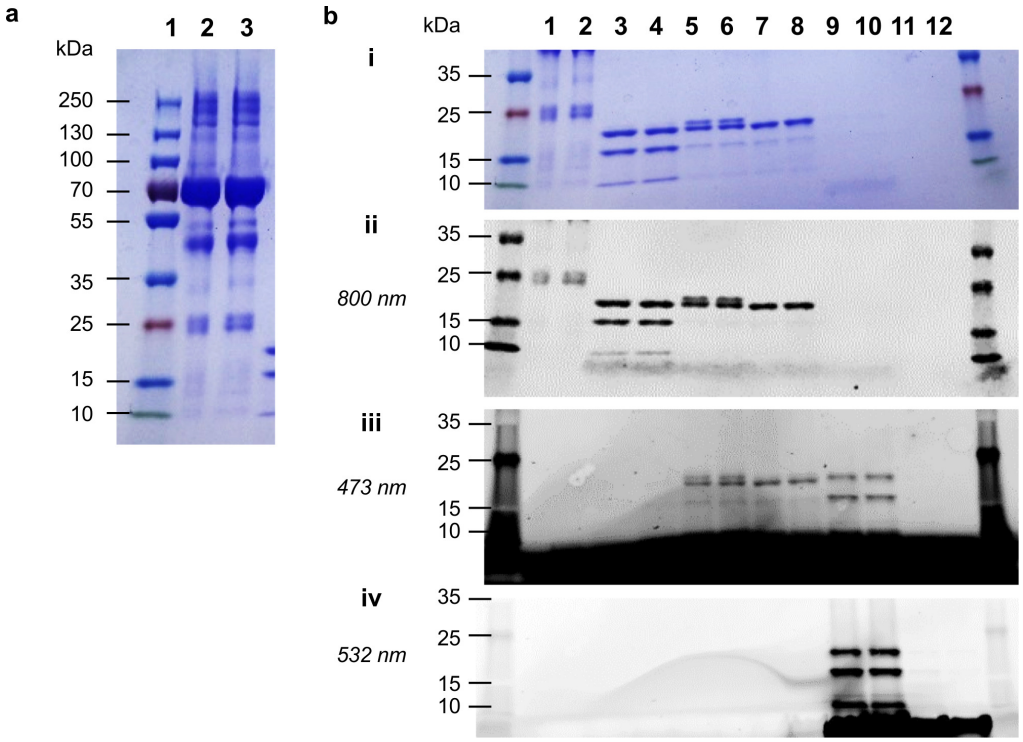

Figure 5.3: SDS-PAGE gel to confirm the presence of fluorescent tags on the purple membrane. Gel showing: a: the ladder compared to a control with lanes (1) PageRuler ladder, (2)-(3) bovine serum albumin (BSA) and b: samples of untagged and tagged bacteriorhodopsin (BR) (solubilised from the purple membrane flakes) on i: a light box, ii: 800 nm excitation to overserve Coomassie stain, iii: 473 nm excitation to observe FITC tagging and iv: 532 nm excitation to observe RITC tagging. Bands shown: (1)-(2) BSA control, (3) untagged BR, (4) untagged BR + urea, (5)-(6) BR-FITC, (7)-(8) BR-FITC + urea, (9)-(10) BR-RITC, (11)-(12) PM-RITC + urea. The expected weight of bacteriorhodopsin is 26.5 kDa.

The bacteriorhodopsin eluted at a size of approximately 20 kDa, compared to a standard PageRuler ladder, rather than the expected 26 kDa. This could be attributed to the fact that bacteriorhodopsin is a membrane protein and difficult to unravel, even with urea. As a result, the protein may not be fully encompassed by SDS, as described in the literature review. It could also be indicating that the bacteriorhodopsin is slightly fragmented. Indeed, the presence of additional smaller bands would also indicate that some of the protein is fragmented or large amounts of internal protein have not unraveled and interacted with SDS. The presence of urea did not appear to make a significant difference to the aggregation of proteins, but very little aggregation was seen in any of the samples anyway.

UV-vis spectroscopy was then run directly on the gel to observe the presence of FITC and RITC

presence (Figure 5.3)b(ii)-(iv)). FITC emission was observed in the samples containing purple membrane with FITC (BR-FITC) and those with RITC (BR-RITC). The RITC emission was only detected in the BR-RITC samples. This is probably due to the filter cubes of the machine detecting the FITC channel in a region where RITC emission was overlapping the FITC emission. As the RITC emission seemed to definitely agree with the samples expected, and not show in the FITC samples, this experiment indicates that the tagging was successful and that FITC and RITC were attached to the protein. Additionally, the emission of the tags in the smaller size bands as well indicates that if fragmentation or incomplete SDS association is occurring, these bands still contain the site of fluorescent molecule attachment. As membrane proteins are often stored in buffer, but the purple membrane cannot be used in buffer with the coacervates, it may be prudent to investigate other forms of storage; either in buffer which is then swapped for water just prior to use or to store it as a dry powder which is likely to be the easier option, in case this is causing an issue with fragmentation.

Controlled proteolytic digestion of the protein and subsequent SDS-gels and mass spectrometry was attempted to identify the sequence containing the fluorescent tag, and to confirm that RITC is attaching at the same site as FITC, as anticipated. However, proteomics on the gel did not yield in depth results, beyond confirming that all the bands contained sequences indicative of bacteriorhodopsin. An attempt to highlight the presence of the FITC or RITC tag by this method did not prove fruitful.

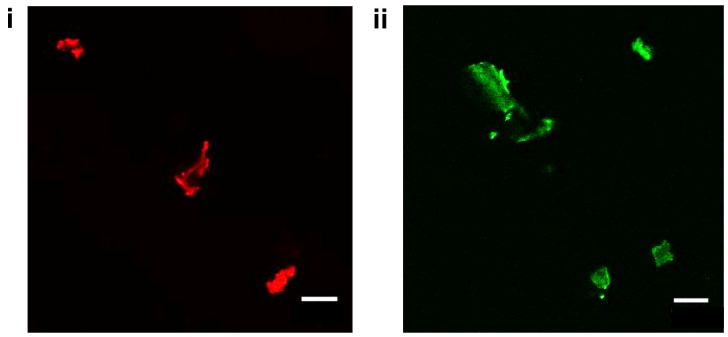

Figure 5.4: Confocal fluorescence microscopy showing that purple membrane samples were successfully tagged. Tagging is shown with i: RITC ii: FITC. Scale bars 10 μm.

Confocal fluorescence microscopy, shown in Figure 5.4, also clearly demonstrates the fluorescence from samples of the tagged purple membrane, both with RITC and FITC. The size of flakes varies between very small fragments and pieces up to 20 μm

Further characterisation was undertaken to compare the fluorescence emission from the FITC tag with that of the innate fluorescence of the sample of purple membrane flakes (Figure 5.5). The emission from FITC is in the same location as that from aggregates of highly concentrated purple membrane, provides a further indication that the tagging has been successful. It is also clear that the location of FITC is easier to visualize by microscopy when the purple membrane

is less concentrated. The emission of FITC was observed with low laser power whereas the location of purple membrane from its innate emission required much higher laser power. This could prove damaging to the samples in further experiments, and the use of a fluorescent tag circumvents this issue.

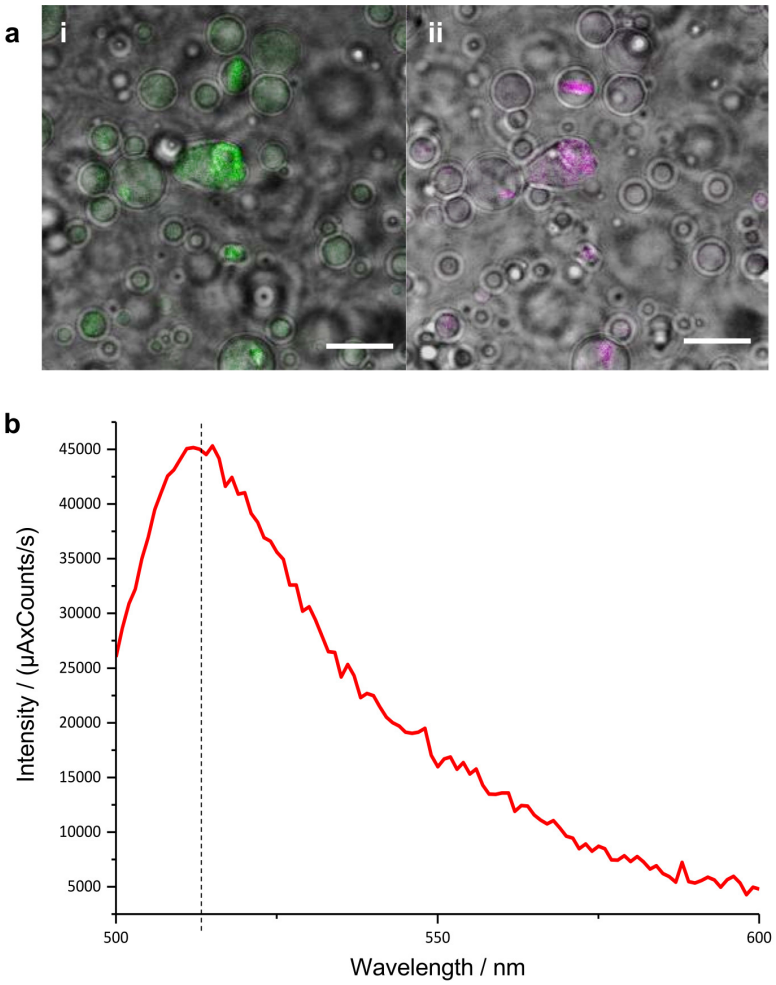

Figure 5.5: Further characterisation of PM-FITC. a: Confocal fluorescence microscopy showing fluorescence emission from i: FITC (green) overlaying ii: the inherent fluorescence from aggregates of purple membrane. b: Emission spectra of purple membrane flakes where bacteriorhodopsin proteins are successfully tagged with fluorescein isothiocyanate (FITC) at an excitation wavelength of 480 nm. A peak can be seen at the 515 nm - the expected emission for tagged FITC.

The fluorescent emission of the sample was also measured with fluorimetry, at an excitation wavelength of 480 nm. This showed that the emission was indicative of FITC, with a peak at 515 nm characteristic of tagged FITC. However, it should be noted that any free FITC in the solution would also contribute to this excitation, although it would be expected that the peak

would be shifted slightly.

Circular dichroism was then carried out to authenticate that the structure of bacteriorhodopsin remained throughout the tagging process (Figure 5.6). Additionally, this allowed observation of whether lyophilisation of the flakes altered their structure, as this was deemed a more appropriate alternative to storing the purple membrane flakes in water without buffer. The data sets were constructed with the assumption that approximately seventy five percent of a flake mass is bacteriorhodopsin, but this could be confirmed with a protein assay such as the Bradford protein assay. It may be possible that the content of bacteriorhodopsin within the same weight of flake is not necessarily the same but this would need to be investigated further.

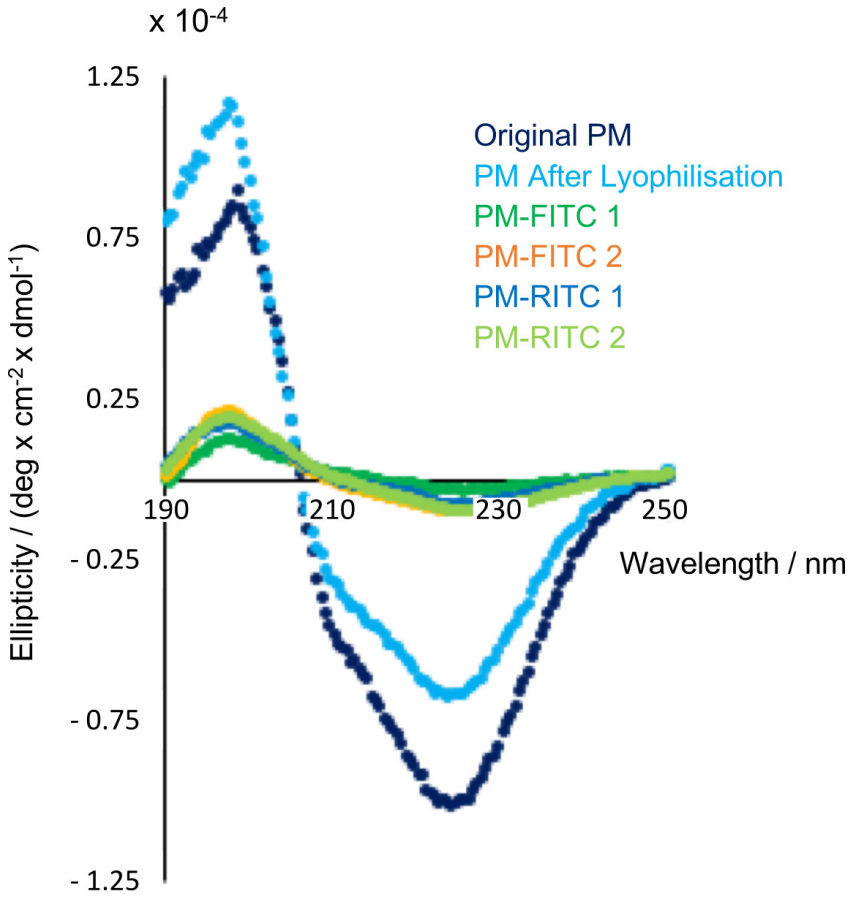

Figure 5.6: Circular dichroism to check the retention of purple membrane structure throughout the tagging process. Comparison between: the original purple membrane flakes (PM) in a solution of Mill-Q water prior to tagging; the same sample after lyophilising and re-solubilising to the same concentration; an aliquot of the same sample tagged with either FITC or RITC.

All the purple membrane flake samples, untagged and tagged, demonstrated double alpha helical peaks consistent with those seen previously in the literature for bacteriorhodopsin within a flake. The amplitude of the peak seems to shift as a result of the lyophilisation, indicating that

this may not be a procedure by which to store the purple membrane flakes if batch repeatability is required. Instead it may be beneficial to flash freeze in liquid nitrogen before storing the samples in a -80° C freezer. A dramatic decrease in peak amplitude is then seen as a result of the tagging procedure, although the peak shape seems to be retained, including the shoulder. As the graphs account for the concentration of the protein, it is likely that the method of tagging causes large losses of flake and therefore the actual concentration does not match the expected concentration of the flake solution. This is corroborated by the fact that the solution observed is much less purple in colour than the starting solution. Some work was conducted to swap the centrifugation process to dialysis or to use spin centrifugation membranes but neither of these were particularly effective. Further work should be done to optimize this methodology and increase the yield of purple membrane flakes after tagging.

5.2.2 Purple Membrane Characterisation

The purple membrane flakes were characterised by a variety of imaging methods including confocal microscopy, atomic force microscopy (AFM) and transmission electron microscopy (TEM), to check the integrity of the flakes. This is shown in Figure 5.7.

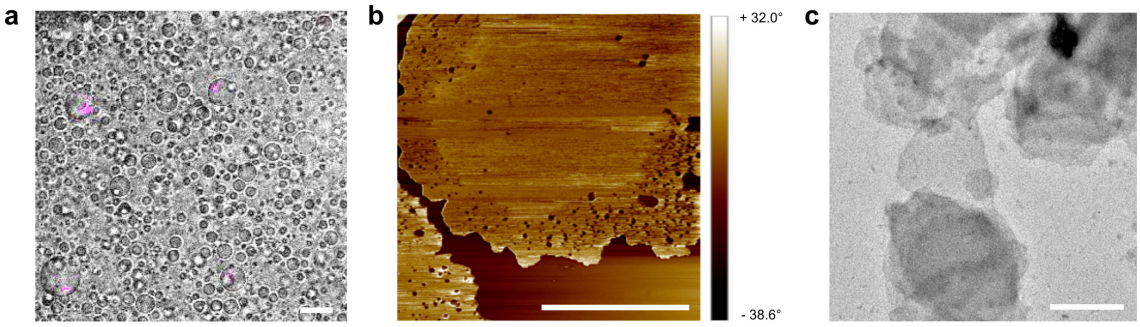

Figure 5.7: Characterisation of purple membrane flakes. a: Confocal microscopy of a field of coacervates containing untagged purple membrane flake (PM) aggregates. The purple colour is the inherent fluorescence of high concentration PM. Scale bar: 10 μm. Dried PM identified by: b: AFM phase image where portions of two flakes are shown as pale structures against the darker hard mica background and c: TEM image of many overlaid flake fragments. A single flake can be seen in the centre of the image. Scale bars: 0.5 μm

The flakes were shown to be approximately 1 μm in diameter by both AFM and TEM. Although purple membrane flakes have an innate fluorescence this could not be detected by fluorimetry (not shown) or confocal fluorescence microscopy unless the sample was at very high concentration, when aggregates of purple membrane were seen (Figure 5.7a).

5.2.3 Attempts to Template Purple Membrane at the Surface of Coacervates

As 1:1 re-suspended ATP: PDDA coacervates have previously been demonstrated to be slightly positively charged, it was postulated that the slightly negatively charged purple membrane flakes may be attracted to the droplets, perhaps creating a membrane-like layer surrounding them. However, Figure 5.8 shows that both the FITC and RITC flakes can still clearly be seen in the supernatant exterior to the coacervates. In addition, homogeneous fluorescence can be seen from within the droplets. Whilst his is not thought to be loose FITC or RITC, this cannot be ruled out completely. It may even be that the bacteriorhodopsin finds the coacervate droplet a more favourable environment than the lipids of the flake. To determine this definitively, a tag should be added to the lipids in the purple membrane flakes. Confirmation that the interior fluorescence is either bacteriorhodopsin or purple membrane could also be obtained from circular dichroism inside the droplets, but a synchrotron source is required for this.

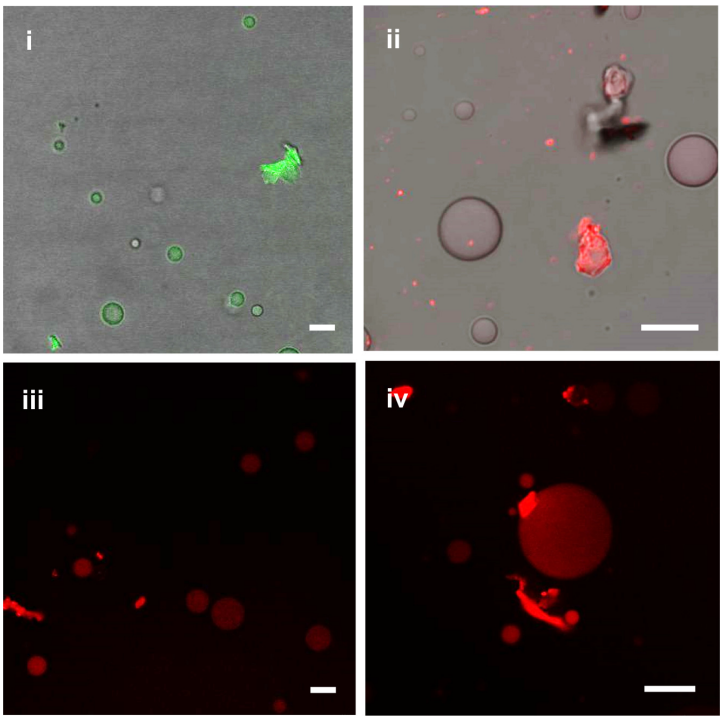

Figure 5.8: Confocal fluorescence images of PDDA: ATP coacervates. Shown with i: PM-FITC and ii-iiv: PM-RITC showing that no templating occurs simply due to the opposing charges of the coacervarte and the purple membrane flakes. i-ii have the brightfield view overlaid. Scale bars: 10 μm.

The components of the coacervate droplet were then altered to encompass a range of positively and negatively charged droplets, and also a range of resuspended and non-resuspended coacervates, to see if this would have any effect on the partitioning of purple membrane flakes at the interface. The confocal fluorescence microscopy images and ζ-potentials are displayed in Figure

5.9.

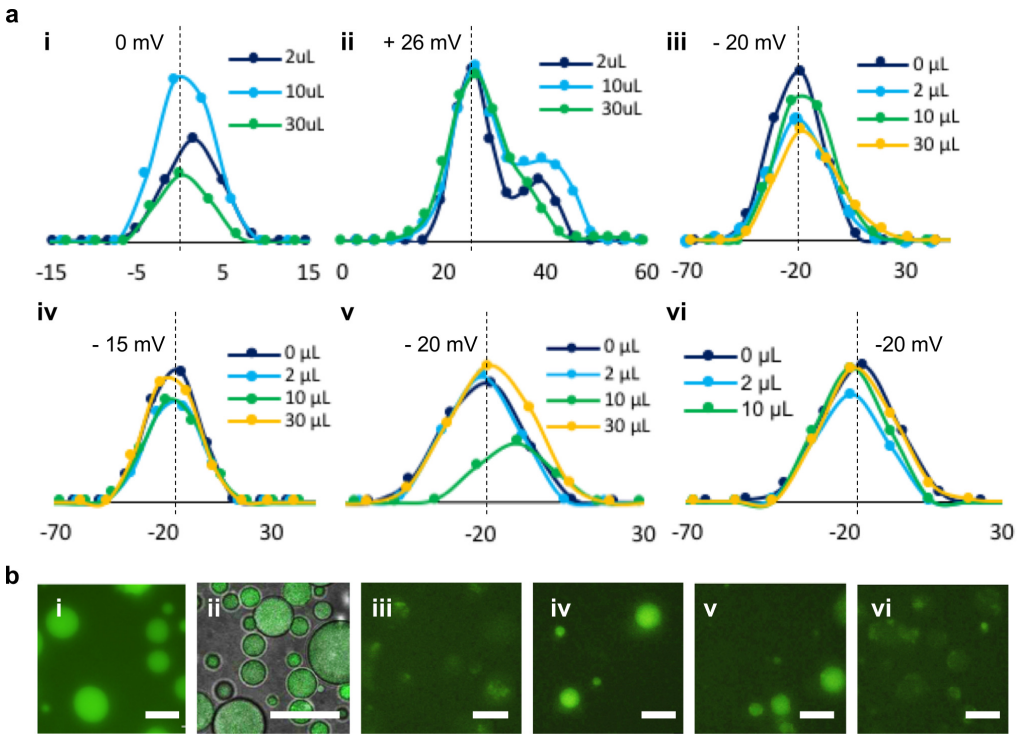

Figure 5.9: Changing the coacervate components does not alter the templating of purple membrane flakes at the coacervate interface. The effect of changing the components is shown in a: Zeta potential diagrams and by b: confocal fluorescence microscopy. The coacervate properties are as follows: i: 1:1 PDDA: ATP re-suspended droplets, 4:1 PDDA: ATP re-suspended droplets, iii: 8:1 CmDextran: PDDA non re-suspended droplets, iv: 8:1 CmDextran: PDDA re-suspended droplets, v: 8:1 CmDextran: polylysine non re-suspended droplets, vi: CmDextran: polylysine non re-suspended droplets. In the zeta potneial diagrmas, the dotted line demonstrates the mean peak potential for each population. In the micrographs, note that ii: also has the brightfield overlaid. Scale bars: 10 μm.

In some of the samples (Figure 5.9 (iii) and (vi)), fluorescent aggregates were also obvious internally. Interestingly, both these samples were non re-suspended droplets, although Figure 5.9 (v) did not show aggregates and was also not re-suspended. This may indicate that there is a difference in the matrices of these coacervates, perhaps a smaller mesh size, encouraging higher localised concentrations of large macromolecules. In all cases. sequential additions of purple membrane flakes appeared to have no effect on the surface charge of the droplets, with the peak values showing similar values in ζ-potential measurements at all concentrations of purple membrane flake tested, and to those without any purple membrane flakes added. The microscopy demonstrated that purple membrane flakes were internalised inside the coacervate matrix, despite the changes to surface charge on the droplet when the components were altered. The positively charged droplets showed no difference in partitioning compared to the negatively

charged droplets. Although the purple membrane flakes are also slightly negatively charged, the data here suggests that the flakes are still being sequestered in negatively charged droplets based on hydrophobic interactions caused by their hydrophobic exterior, which results from their natural environment as bacterial membrane components. It therefore became clear from these experiments that an impermeable barrier would be required to prevent purple membrane flake sequestration into the coacervates, and to maintain them at the interface.

As mentioned earlier, Tang et al. previously showed that fatty acids can be used to form an artificial membrane around the coacervate droplets, through the use of sodium oleate [51]. As these molecules form a hydrophobic bilayer, similar to that in naturally occurring membranes, this was considered as another option for templating the purple membrane flakes at the interface of the coacervate droplets. The location of the sodium oleate was visualised using BODIPY-FL, a hydrophobic fluorescent lipid stain used to observe membranes. Although some membrane formation was seen (Figure 5.10a), these membranes were largely unproducible, resulting in only a few droplets with surface coatings and a large number of samples without any droplets with a surface coating. In many cases, background aggregates of sodium oleate or BODIPY-FL were seen (Figure 5.10b). Alternatively, the sequestration of micelles of sodium oleate rather than the correct partitioning of these at the interface were observed (Figure 5.10c). For this reason, this methodology was abandoned however there is potential for future development in this area, if the procedure for adding oleate membranes to this coacervate system was optimised.

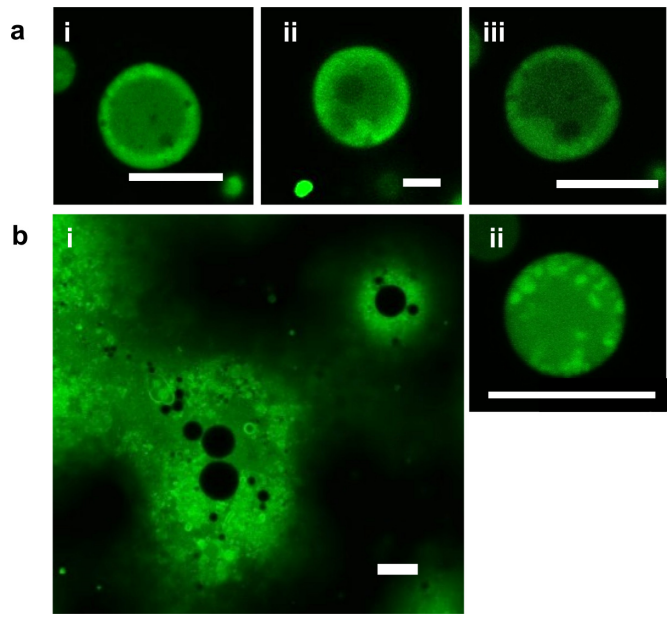

Figure 5.10: Coacervates with oleate fatty acid membranes. PDDA: ATP coacervates with a: successful and b: unsuccessful coatings of sodium oleate.

Although other macromolecules had not been partitioned by dextran coatings on the coacervates (Chapter 3), purple membrane flakes are significantly larger so were attempted. This is shown

in Figure 5.11. Purple membrane tagged with RITC was observed, however the dextran did not inhibit entry of these into the coacervates. It was also noticed that at low concentrations, the structure of the flakes could not be seen in the confocal fluorescence images. Taking into account the size of the droplets, it is therefore possible that it is small fragments of flake that are being sequestered, or the flake fragments are curling up. Care was taken when imaging to avoid the regions where FITC and RITC emission and excitation overlap.

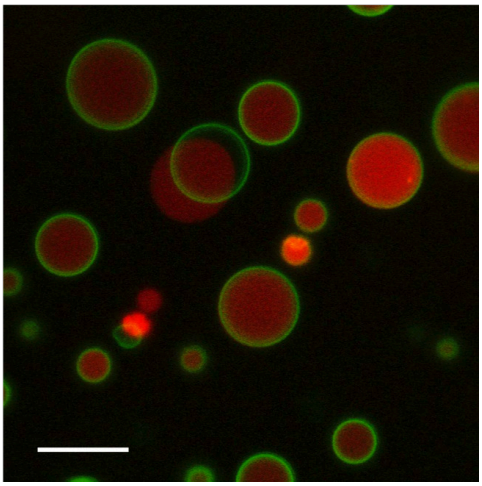

Figure 5.11: Partitioning of purple membrane flakes into coacervates with a dextran coating. Confocal fluorescence microscopy image showing coacervates with a dextran-FITC coating and purple membrane flakes tagged with RITC inside the droplets. Scale bar: 10 μm. Note that this image is constructed from two fluorescent images overlaid which were photographed consecutively. This is the reason why some droplets do not show alignment in both the FITC channel (green) and the RITC channel (red)

5.2.4 Block Copolymer Interactions With Coacervates

Interactions of block copolymers with the coacervates was then explored, to find an appropriate block copolymer for use in the creation of a coacervate membrane. The localisation of all block copolymers was observed with Nile Red, a lipophilic dye that sequesters into the most hydrophobic regions of the system. In these examples, this is the hydrophobic domains of the block copolymers.

After the unsuccessful attempts by other means to template macromolecules at the surface of coacervates, block co-polymer molecules were considered as the next viable option. Hypothetically, if successful, these could be partitioned on the surface as an artificial membrane into which bacteriorhodopsin or purple membrane flake could either be attracted to or positioned within. Two courses of action were deemed to be feasible. The first uses triblock copolymers with a hydrophilic-hydrophobic-hydrophilic motif to simulate a cell membrane or barrier, either by acting as a bilayer or by the construction of a surface on which to attract the purple mem-

brane flakes to interact. The second would use a diblock copolymer with a hydrophobic motif to attract to the coacervate and a hydrophilic positivly charged motif to attract one face of the purple membrane, allowing the flake to sit on top of the block copolymer layer. The latter has not been attempted in this preliminary study but would be a useful course of action for future experiments.

Due to availability, polyethylene glycol-b-polypropylene-b-polyethylene glycol (PEG-b-PPG-b-PEG) (aka Pluronic-L121) was selected as an example triblock copolymer to see if the principle of surface partitioning on the coacervate could be applied. Nile red, a hydrophobic lipid dye, was used to identify its localistion (Figure 5.12). Successful partitioning was seen with clear rings of block copolymer visible around the droplets, although aggregates were seen on the surface which may be block copolymer micelles or agglomerations of Nile Red. Controls where Nile Red was added to coacervates without any block copolymer showed that the nile red does show some interaction with the interface but not to the same extent as when block copolymer was present (data not shown). The nile red forms needle-like crystals which mostly sediment to the glass slide at the bottom of the field of view or show slight preference for interacting with the glass slide coating. Occasional aggregates of nile red are seen co-localised with the coacervate droplet interface but full coatings were not seen.

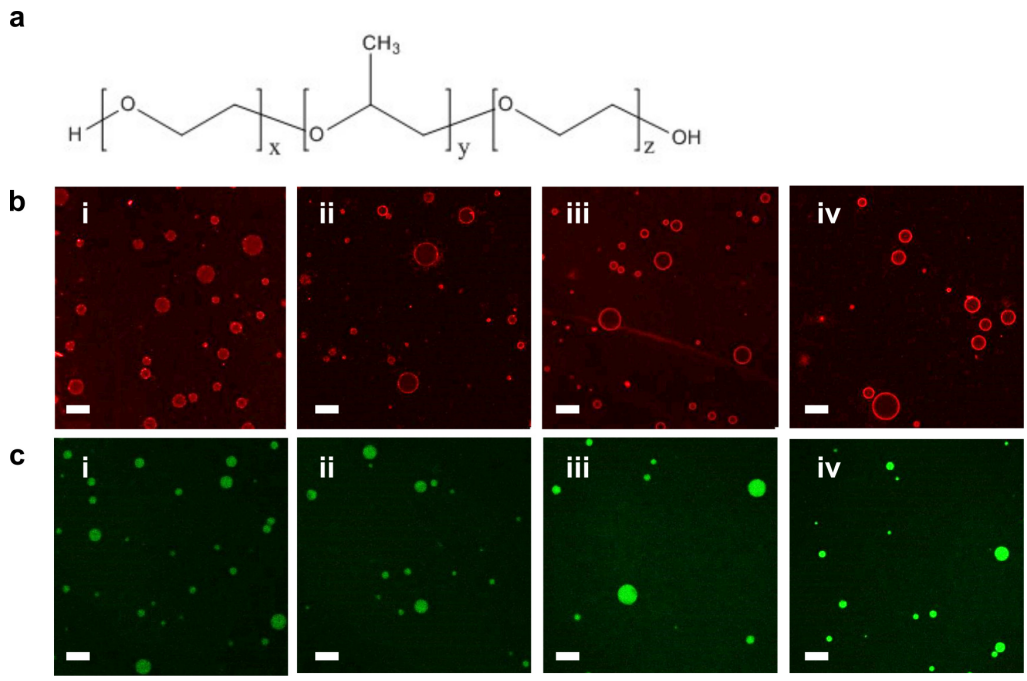

Figure 5.12: Pluronic-L121 block copolymer does not prevent entry of calcein into the coacervate matrix. a: Chemical structure of Pluronic-L121, b: confocal fluorescence microscopy showing coacervates (b) with block copolymer additions of (i) 50 μL, (ii) 100 μ L, (iii) 200 μ L, (iv) 300 μ L and (c) the same block copolymer concentrations with calcein showing entry of calcein in at all concentrations. Scale bars: 10 μm

However, when calcein was added it was still able to diffuse through this block layer into the interior, indicating that it had not formed a complete impenetrable boundary. Increasing the concentration of the block copolymer did make the layer around the droplets brighter, suggesting a thicker or more concentrated layer, but did not have any effect on the inhibition of the entry of calcein. Additionally, when PM-FITC was added it was internalised by the coacervate as seen previously, showing no change in behaviour (data not shown).

Due to the fact that Pluronic L-121 does not prevent sequestration of macromolecules, three other block copolymers were investigated. The structures of these are shown in Figure 5.13, along with their hydrophobic and hydrophilic regions identified. Note that Poloxamer-188 can also be known as Pluronic F-68 and Pluronic 31R1 as poly(propylene glycol)-block-poly(ethylene glycol)-block-poly(propylene glycol) (PPG-PEG-PPG). As these were tri-block structures, it was thought that they may be able to associate with the coacervate in one of two ways. Either they could align to form a hydrophobic-hydrophilic-hydrophobic bilayer (in the case of Pluronic 31R1) or they could kink to form a V-shaped structure, which would align to form a shape similar to a fatty acid coating, with the larger ends wither occupying the interiors (if hydrophobic) or with the larger ends pointing outwards into the supernatant (if hydrophilic such as in Pluronic F-127 or Poloxamer-188). The latter was deemed to be more likely as the interior surface area is smaller than the exterior surface area of a sphere. Unfortunately, due to the information being proprietary, the length of the block regions in each case are unknown. These molecules should therefore not be considered symmetrical as this is not known for certain, although likely in synthesis.

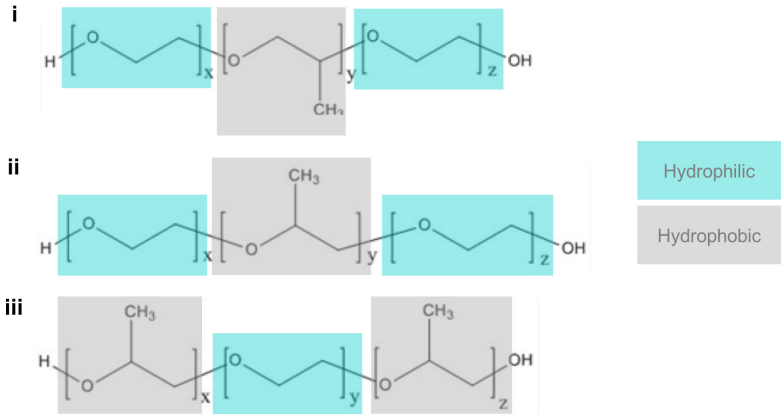

Figure 5.13: The three block copolymers that were selected for further investigations with the coacervates. Structure of the tri-block copolymers i: Pluronic F-127, Poloxamer-188 and Pluronic 31R1 with their hydrophobic (grey) and hydrophilic (blue) regions identified.

Coacervates were then investigated with a range of concentrations of the block copolymer Poloxamer-188 added after droplet formation (Figure 5.14). The Poloxamer was imaged with Nile Red, which co-localises with hydrophobic regions in the block copolymer. In the absence of block

co-polymer, there was some association between aggregates of Nile Red and the coacervate interface. However, it can be seen that with increasing concentrations of block copolymer, this localisation changes. These experiments demonstrated that with increasing concentrations of Poloxamer-188 a membrane interface begins to form. Excitingly, at 5 mM of block copolymer, a clear interface is seen around the droplet. This interface is not completely uniform, but rather appears to be made up of many small spherical objects partitioned together. The possibility that these were block copolymer micelles was considered, but the structures were deemed too small for this to be likely. When the concentration of this block copolymer was increased further, alternative structures were seen to form in both the fluorescent and brightfield channels, suggesting that the block copolymers could have undergone a phase transition to form an alternative structure.

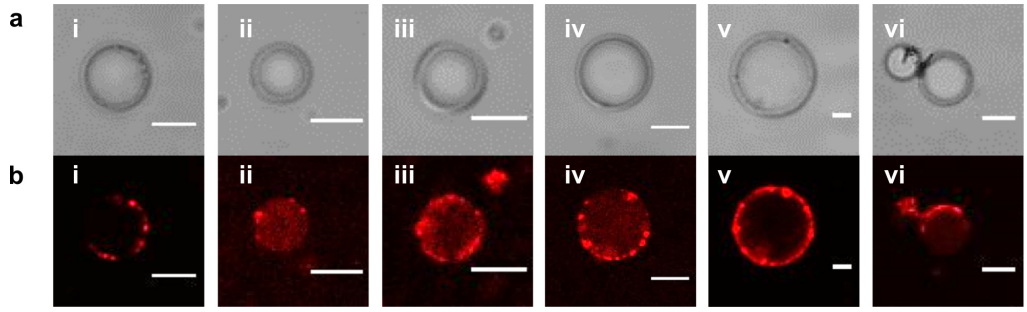

Figure 5.14: Effect of increasing the ratio of Poloxamer-188 block copolymer to coacervate. a: Brightfield and b: corresponding confocal fluorescence images showing increasing concentrations of Poloxamer-188. Final concentrations of block copolymer: i: 0, ii: 1.3, iii: 2.5, iv: 3.8, v: 5.0 and vi: 6.3 mM. Location of block copolymer is shown with Nile Red fluorescent dye. Scale bars: 5 μm.

Further images were taken of a whole field of coacervates with 5 mM concentrations of Poloxamer-188 block copolymer to determine the percentage of droplets that exhibited a membrane surrounding. This is shown in Figure 5.15. It is clear from these images that when the appropriate concentration of block copolymer is reached all droplets develop a membrane coating. This makes the system advantageous in comparison to systems such as the fatty-acid coated droplets, as the sodium oleate membranes were harder to reproduce and also did not occur on every droplet.

Images were also taken at a high magnification in order to identify and sub structures that could be viewed at this scale (Figure 5.16). This demonstrated the multiple spherical objects at the interface ,which form the membrane, and these are also visible in the brightfield views.

Since surface templating seemed to be occurring, the stability of the droplets over time was measured with increasing concentrations of Poloxamer-188, to see if increased additions would create a membrane capable of limiting coaclescence (Figure 5.17). Additions of up to 1.3 mM seemed to have very little effect on the stability to coalescence or the surface stability. This

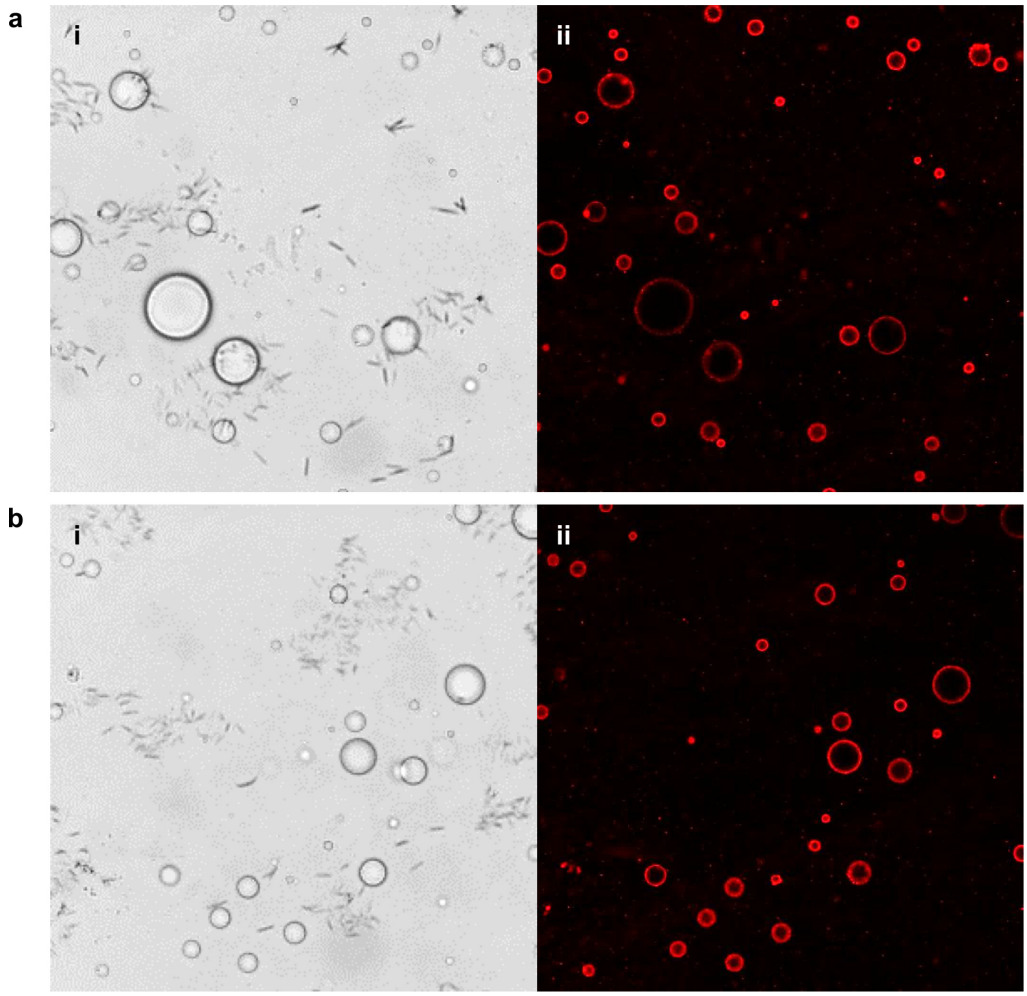

Figure 5.15: Coacervates with Poloxamer 188 at the interface. a and b: Two fields of coacervates coated with Poloxamer-188 block copolymer, visualized with Nile Red fluorescent dye (red). Fields of view shown in the i: brightfield and ii: confocal fluorescent views.

agrees with the confocal fluorescence images showing that no membrane boundary is present at these concentrations. As concentrations of block copolymer increase further both the zeta potential and resistance to coalescence also increase. Misleadingly the most stable seem to be the addition of 6.7 mM of block copolymer, even though no complete surface structure is seen in the confocal fluorescence images at this concentration. It may therefore be that even large aggregates of block copolymer are able to alter the behavior of the coacervate, despite not creating a distinct boundary.

Macromolecular sequestration was then investigated with the Poloxamer-188 block copolymer coated coacervates. The same molecules were attempted as in the Chapter 3 sequestration. This is shown in Figure 5.18. Unfortunately, all the molecules were still sequestered by the coacervate, although it appears that this may be because the block copolymer has not formed the ex-

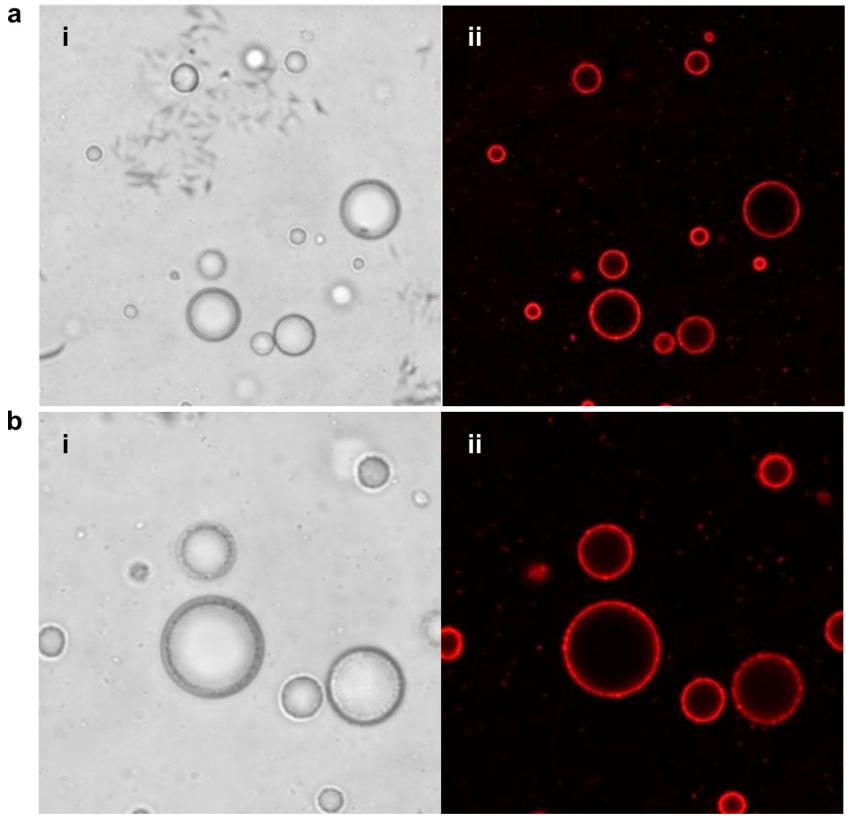

Figure 5.16: Close-up view of coacervates with Poloxamer 188 at the interface. a and b: Two fields of coacervates coated with Poloxamer-188 block copolymer, visualized with Nile Red fluorescent dye (red). Fields of view shown in the i: brightfield and ii: confocal fluorescent views

pected interfacial coating. It is not understood whether this was an anomalous result or whether the macromolecules alter the partitioning of the block copolymer at the surface and this would be interesting to investigate further. However, it should be noted that the block copolymer is not being imaged directly, but rather via the co-localisation of Nile Red. An attempt was made to address this by tagging the Poloxamer-188 with Rhodamine B.

The rhodamine tag was attached to one of the terminal hydroxyl groups on the Poloxamer-188, and was doped into untagged Poloxamer-188 in order to minimise perturbation of the system as a result of the properties of the Rhodamine B. The tagged Poloxamer-188 was characterised by NMR and was shown to be Poloxamer-188 with Rhodamine B. However, when coacervates were imaged with this doped block copolymer, fluorescence was only seen inside the droplets and not at the interface. This disagrees with previous experiments, but it is thought that even at low doping concentrations, the tagged molecule may be affecting the sequestration properties of Poloxamer-188 block copolymer, as Rhodamine B is easily sequestered by these coacervates.

The effect of temperature on the phase of the block copolymer was also investigated (Figure 5.19. Block copolymers were stored at both 25° C and 5° C before addition to coacervate populations.

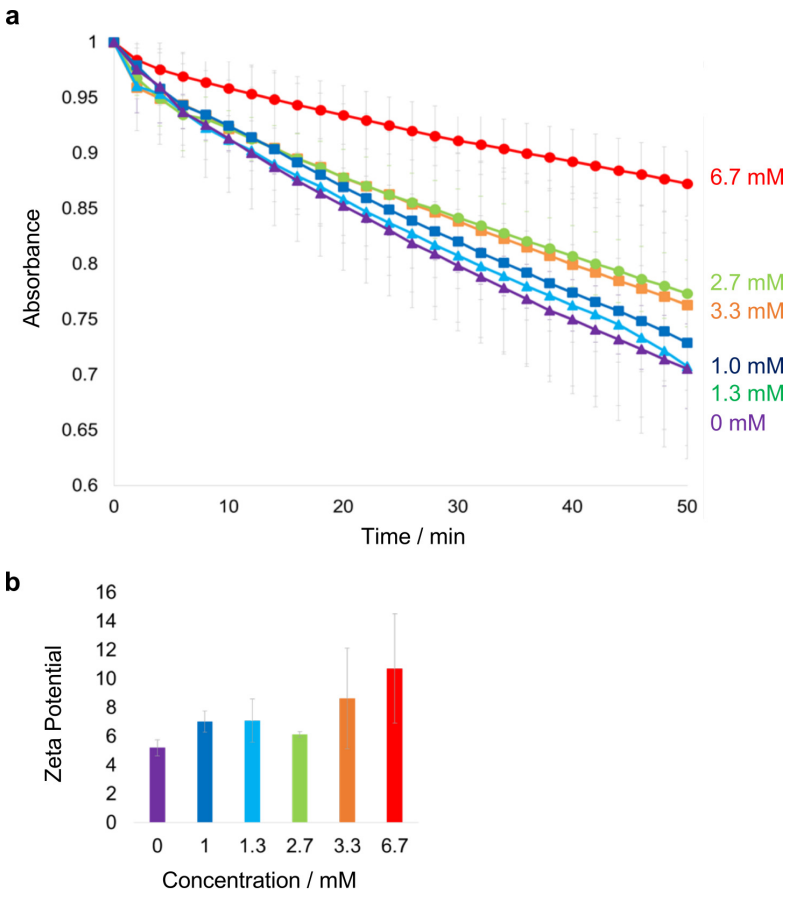

Figure 5.17: Effect of increasing the ratio of Poloxamer-188 to coacervate on droplet stability. a: UV-vis absorbance measurements of turbidity demonstrating coacervate stability over time with b: zeta potentials for increasing Poloxamer-188 concentrations i: 0 mM, 1 mM, 1.3 mM, 2.7 mM, 3.3 mM and 6.7 mM.

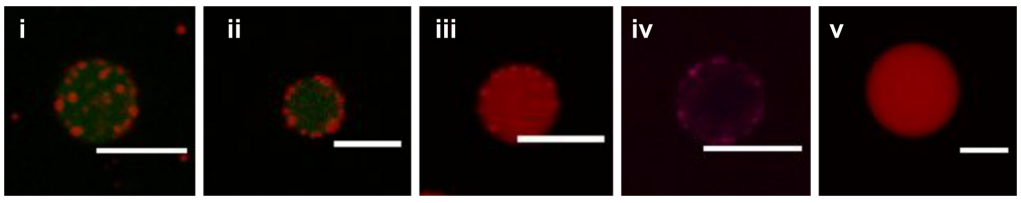

Figure 5.18: The sequestration of fluorescent macromolecules inside coacervates with block copolymer. 5 mM additions of block copolymer were added with Nile Red (red) to image location. a: molecule properties alongside b: confocal fluorescence microscopy showing their sequestration into coacervates. Dyes are as follows: i: acridine orange, ii: eGFP, iii: methylene blue, iv: Kiton red, v: mCherry. Scale bars 5 μm.

The warmer block copolymer was turbid by eye before addition whereas the cooler block copolymer was not. The results show that the warmer block copolymer produces smaller spherical balls which interact with the coacervate interface. In contrast, the cooler block copolymers produce larger spherical objects although these still interact at the interface. This indicates that it is critical to maintain the temperature at a constant level for the membrane formation to occur. However, it also suggests that it could be possible to control the properties of the membrane based on temperature, although this was not investigated further here.

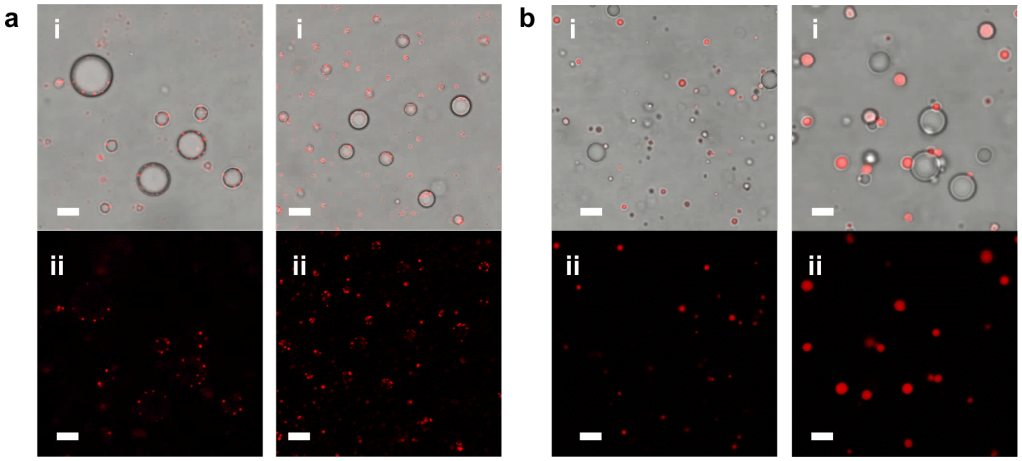

Figure 5.19: Effect of temperature on Poloxamer-188 block copolymer interactions with coacervates. Block copolymer stored at a: 25° C and b: 5° C addition to coacervates. Images are shown in i: the brightfield and ii: confocal fluorescence views. Scale bars: 10 μm

The effect of increasing the concentration of block copolymer was also attempted with Pluronic F-127 and Pluronic 31R1 (Figure 5.20. There was no association seen between Pluronic F-127 and the coacervate interface , and the Pluronic remained in the supernatant regardless of the concentration. When no block copolymer was present, small aggregates were seen at the surface of the coacervate and this was thought to be Nile Red aggregates because there was no strongly hydrophobic region to intercalate into. with Pluronic F-127 (Figure 2 (a)), which remained in the supernatant.

When Pluronic-31R1 was investigated, membranes formation occurred similarly to the Poloxamer-188 and these were seen to be more homogeneous than any seen previously. Rather than having the appearance of multiple spherical structures interacting, these appeared far more continuous than any seen previously. At concentrations of 3.8 mM and above, spherical structures were seen to form. These may be structures composed entirely of block copolymer but further investigation would be beneficial as they could potentially be new coacervate/ block copolymer hybrid structures budding from the existing one.

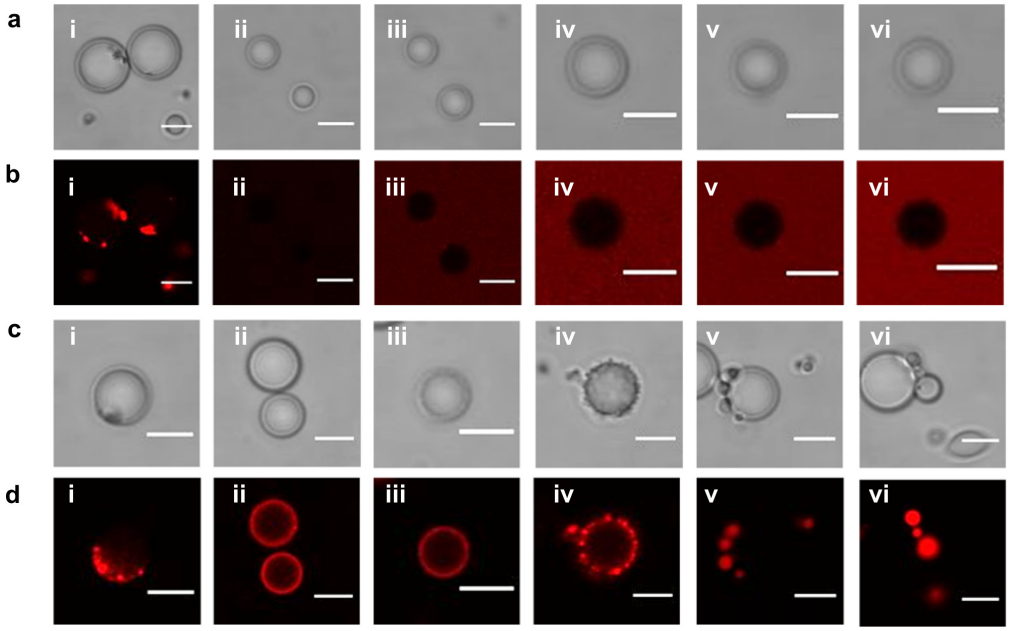

Figure 5.20: Effect of increasing the ratio of Pluronic F-127 and Pluronic 31R1 block copolymers to coacervate. a: Brightfield and b: corresponding confocal fluorescence images showing increasing concentrations of Pluronic F-127. : Brightfield and b: corresponding confocal fluorescence images showing increasing concentrations of Pluronic 31R1. Final concentrations of block copolymer in all cases: i: 0, ii: 1.3, iii: 2.5, iv: 3.8, v: 5.0 and vi: 6.3 mM. Location of block copolymer is shown with Nile Red fluorescent dye. Scale bars: 5 μm.

5.2.5 PEG Dextran Interactions With Block Copolymer Coacervates

The combination of block copolymer coacervates with the TEG dextran system in Chapter 4 was briefly tested (Figure 5.21). The TEG and dextran behaved in the same manner as seen previously but the block copolymer Poloxamer-188 did not remain localised to the coacervate interface. Instead, the smaller block copolymer spheres started to coalesce with one another to form larger spheres without dextran present. The presence of TEG in these systems is unknown but a component of the block copolymer is a longer PEG chain. Itis hypothesised that interactions between these segments and the added TEG lead to shielding of the other segments in the Poloxamer-188 in an effort to localize all poly(ethylene) glycol moieties in the same place.

5.2.6 Functionalisation of Block Copolymer Coating With Purple Membrane

5.2.6.1 System Characterisation

As partitioning at the interface had been seen with the Nile Red imaging, experiments were done to add the purple membrane flakes (PM) to the block copolymer coacervates. After optimization of the conditions, this proved successful (Figure 5.22. The purple membrane flakes were added after the partitioning of the block copolymers at the interface in all cases unless specified. Rings

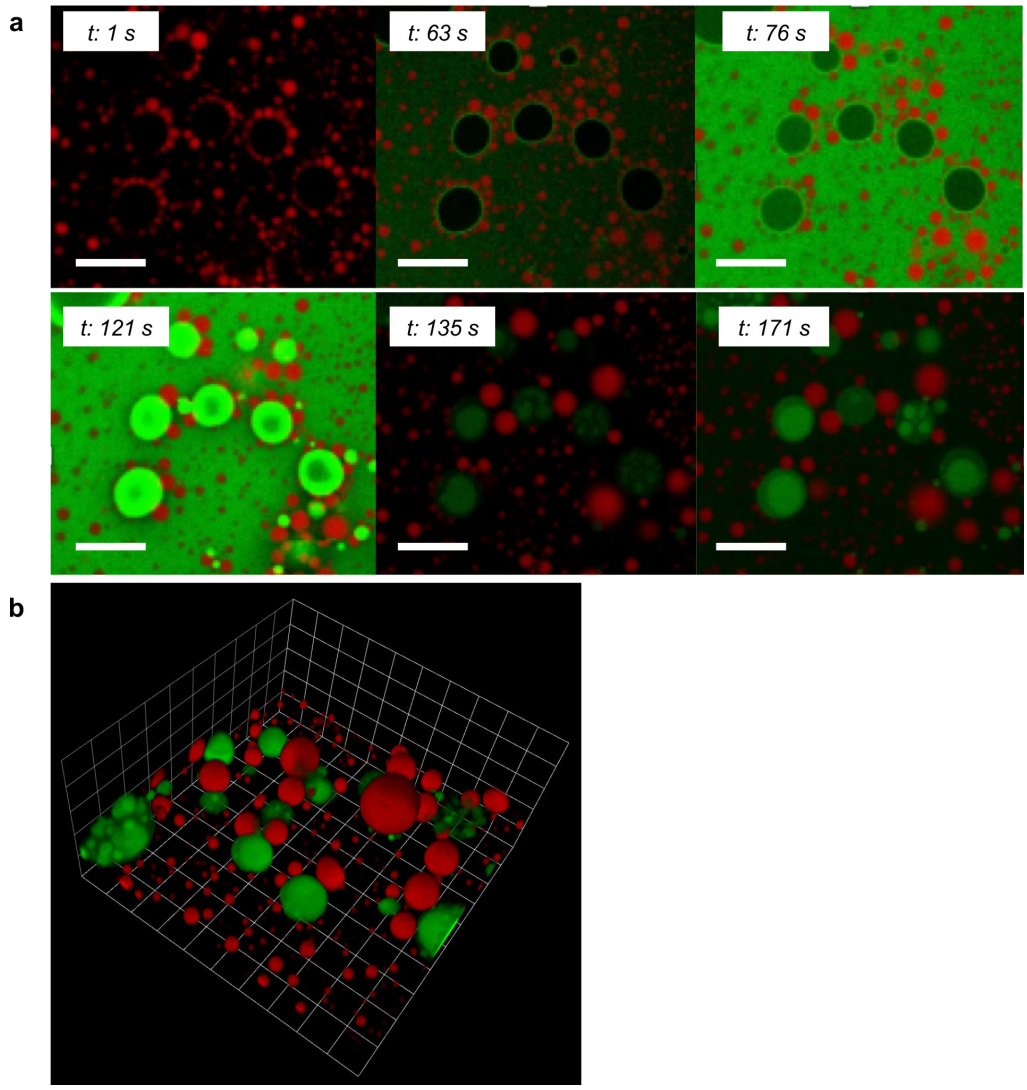

Figure 5.21: Addition of dextran and TEG to block copolymer coacervates. Confocal fluorescence microscopy showing a: time point images of coacervates with block copolymer spherical structures at surface (1 s), the addition of dextran (63 s), more dextran in the field of view (76 s), the addition of TEG causing the dextran to flow into the coacervates (121 s) and the formation of internal dextran compartments (135 s to 171 s). b: Reconstructed z-stack profile showing the final 3D arrangement of coacervates and block copolymers. Poloxamer-188 localisation is shown with Nile Red (red) and dextran-FITC 70 kDa was used (green). TEG is colourless here. Scale bars: 10 /mum.

of PM-FITC can clearly be seen indicating interfacial partitioning. Flakes can still be seen in the background and The rings appear homogenous, which may perhaps indicate that the bacteriorhodopsin is being solubilised from the membrane flakes rather than a whole flake adhering to the droplet. However, this seems unlikely as bacteriorhodopsin strongly favours the native environment within a lipid bilayer.

Increasing the concentration of Poloxamer-188 increases the intensity of these rings although some surface distortion and internal aggregation can still be seen in some droplets. This may be as a result of the block copolymer being at too high a concentration and aggregating or forming micelles before interacting with the coacervates. Decreasing the amount of coacervates whilst maintaining the ratio of block copolymer to purple membrane flakes causes less distinct rings to form, and then eventually no rings, as expected. Controls were also as anticipated, with no interfacial coating seen when PM-FITC is swapped for FITC or the block copolymer is not added. When PM-FITC is switched for PM-RITC at the same concentration, the partitioning seen is no longer uniform. This may be due to differences in concentrations between the two samples (the tagging process involved several rounds of washing which may have removed some components) or may once again demonstrste that the presence of a slight charge on the purple membrane flakes has a large effect on partitioning with this coacervate system. This agrees with previous experiments in Chapters 3 and 4.

The experiments here which have attempted to partition purple membrane flakes at the interface of coacervates are summarized in Figure 5.23. Coacervates with oleic acid coatings were attempted as these had previously been shown to be successful in the literature. However, due to minimal success in this work, this methodology was quickly abandoned. Templating of block copolymer membranes onto the coacervate droplets was then attempted with a range of block copolymers. Successful coatings were then used to template purple membrane flakes onto the surface of the coacervates. The most promising method shown is that involving Poloxamer-188 block copolymer, where purple membrane flake partitioning has been seen. However, experiments with Pluronic 31R1 have also shown some promising results and should be investigated further in future work. Further experiments should also include studies to identify the boundary properties of the layer of purple membrane, to establish whether this is a complete layer or still allows for sequestration of other cargo.
zeta-potential studies could also be conducted to determine whether the surface properties of the coacervte have been altered with the addition of the purple membrane flake coating.

5.2.6.2 System Functionality

Successful partitioning of the purple membrane flake layer allowed for further utility of the system to be explored. As described previously, purple membrane proteins pump hydrogen ions directionally when exposed to light of the correct wavelength, meaning that a pH gradient could be set-up between the interior of the coacervate droplet and the exterior supernatant. A system

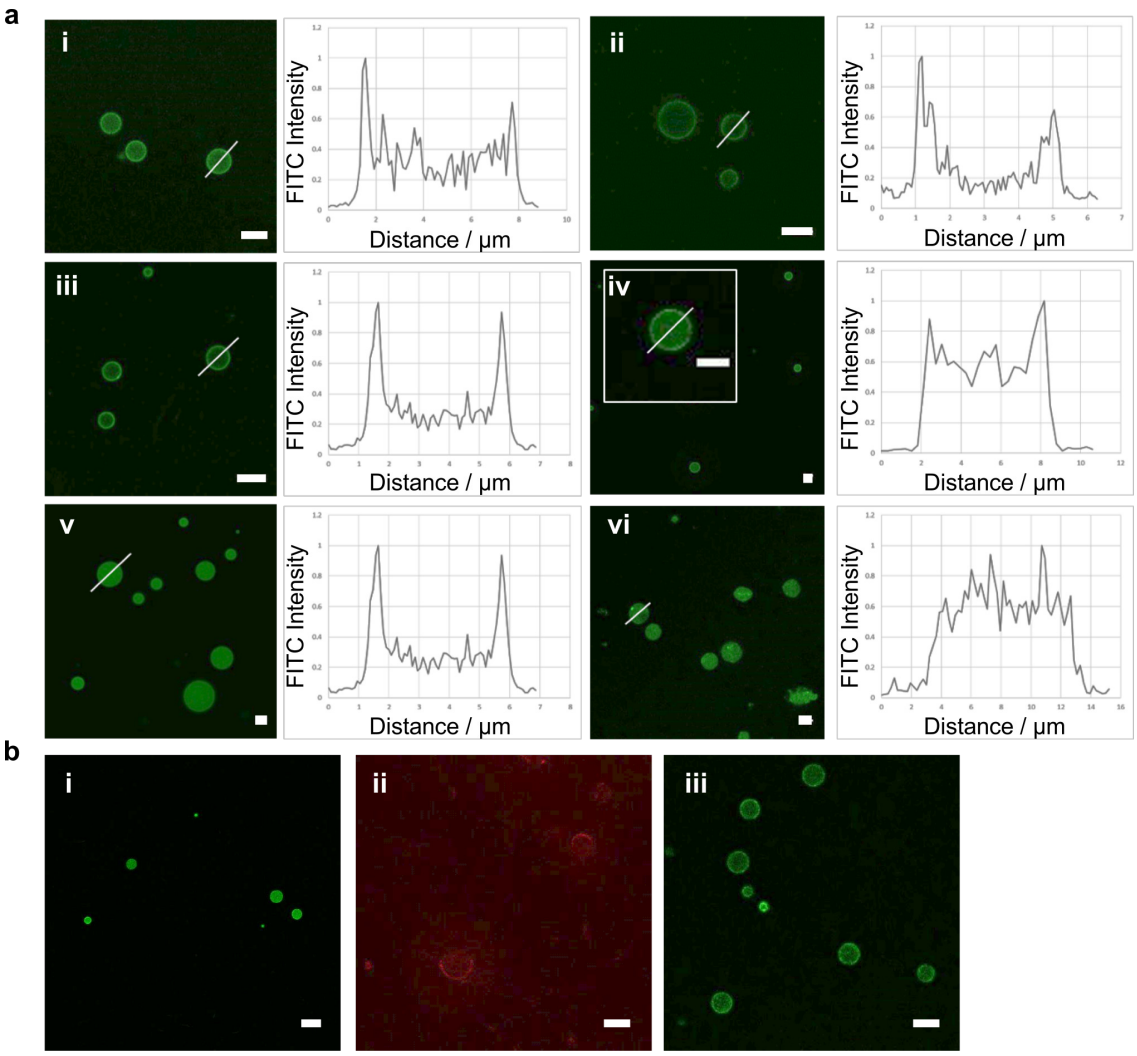

Figure 5.22: Varying the conditions of purple membrane and block copolymer addition to coacervates. a: Confocal fluorescence images of droplets with a line profile of FITC intensity across a representative droplet. Condition alterations investigated include the ratio of block copolymer, purple membrane flakes (PM) and coacervates to one another, swapping the tag molecule on purple membrane from FITC to RITC, and combining the block copolymer and PM-FITC before addition to the coacervates. The images shown are as follows: a: i: The original successful ratio of block copolymer addition (1 : 0.4 : 0.002), ii: increased ratio of PM-FITC (1 : 0.4 : 0.006), iii: Further increase in the ratio of PM-FITC (1 : 0.4 : 0.01), iv: Same ratio of block copolymer to PM with less coacervates (1:0.8:0.004), v: FITC in place of PM-FITC and vi: no block copolymer. These are all also given as the ratio of coacervate (mM): Poloxamer-188 (%) : PM-FITC (mg/mL) for comparison. b: i: Decreasing the amount of block copolymer and increasing the amount of PM-FITC results in no partitioning at the interface (1:0.02:0.004), ii: altering PM-FITC for PM-RITC (1 : 0.4 : 0.01) and iii: combining the block copolymer and PM-FITC before addition to the coacervates rather than addition of the block copolymer followed by addition of the purple membrane flakes. Scale bars: 5 μm.

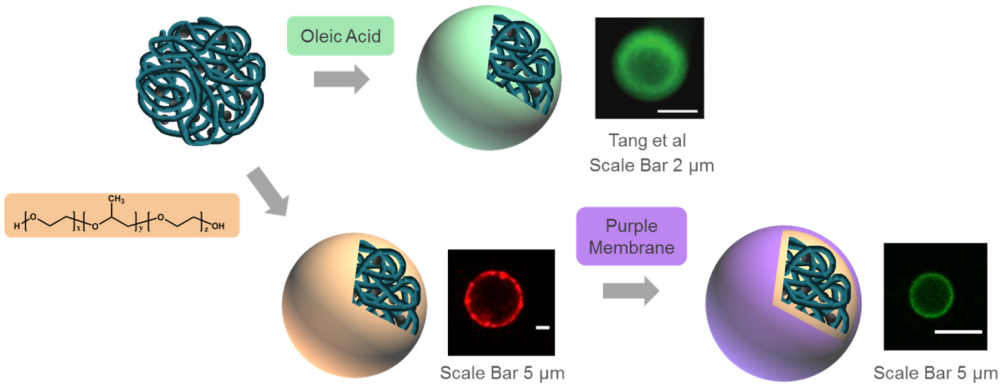

Figure 5.23: Summary of attempts to partition purple membrane flakes on coacervates

such as this would allow for exterior initiation and control of internal reactions coupled to the pH of the internal environment, for example enzyme activation and control. A schematic for this is shown in Figure 5.24. A pyranine assay was first used to establish the internal pH of the droplet. This assay is commonly used to detect internal pH in a droplet system, giving insight into the direction of proton pumping, although ACMA fluorescent probe can be used instead. The hope was that this could be used as a measure of the amount of the purple membrane flake proteins that were aligned in the same direction; as randomly orientated flakes would pump protons out at a similar rate to the movement of protons into the interior. Further experiments could then be conducted to improve the orientation of purple membrane flakes, perhaps by attaching a tag to the proteins that exploits the differences between coacervate interior and exterior, using the pyranine assay to quantitatively measure progress.

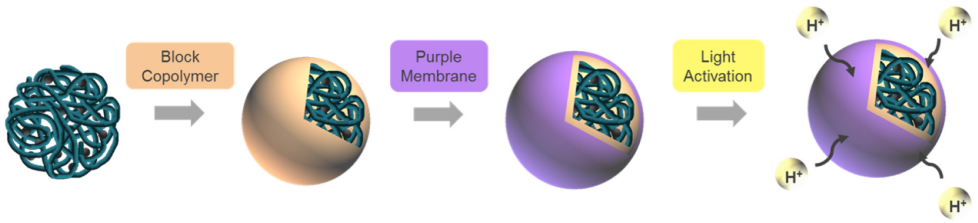

Figure 5.24: Schematic of the successful purple membrane flake partitioning, demonstrating the potential of future investigations

The pyranine assay tracks the emissions at a wavelength of 507 nm, with excitations of 403nm and 460 nm. The ratio between these peaks are representative of the proportion of the pyranine that is in an basic or acidic form respectively. The pyranine also has an isobestic point at excitations of 415 nm, where the emission signal is independent of pH. This can be used to normalize the concentration of pyranine across experiments. Results are determined by dividing the emission at 460 nm by that at 415 nm. The internal pH can be quantitatively back-calculated by the

equation shown in Equation 5.2.6.2.

$$pH = pK_a + log((R - R_a)/(Rb - R_b))$$

where R = Emission F460 / F415, a = the acidic component of pyranine and b = the basic component of pyranine

As the internal environment of the coacervate matrix is very different to that of a water-filled vacuole, where pyranine assays normally take place, it was essential to re-calibrate the pyranine assay for use in this system. The assay would need to recalibrated for use in any other coacervate system apart from the PDDA : ATP system. Preliminary investigations into the use of pyranine in this system are shown (Figure 5.25.

The excitation spectra of pyranine at increasing concentrations is displayed, identifying the peaks of interest for further calculations. Thee pK_a of pyranine was also calculated in water, ATP and PDDA to see if the coacervate components alter the behavior of the pyranine when it is sequestered internally in the droplets. The literature value for pyranine in water is 7.24, the same as calculated from these experiments demonstrating that the titration curves here are appropriate. When in ATP, the pKa is not altered but when PDDA is present, the pK_a of pyranine is decreased. It is likely that free positive charge on the PDDA is increasing the protonation of the the pyranine. This means that the pH calculation equation has to be adjusted for the PDDA component. Increasing the concentration of ATP or PDDA does not affect the position of the pK_a (data not shown).

5.3 Conclusions & Further Work

In the final results chapter, the addition of coacervate membranes was explored with the aim of partitioning purple membrane flakes at the interface of coacervates. These experiments encompassed the unsuccessful partitioning of flakes with fatty acid coatings and dextran interfaces before showing preliminary experiments of successful partitioning with block copolymers. Block copolymers were also shown to increase the stability of the coacervates and some further characterisation of the block copolymer interactions with coacervates were shown without purple membrane. The pyranine assay was characterized in the PDDA: ATP coacervate system, and the modifications that need to be made for this to be useful were determined. Finally, block copolymer coated coacervates were enhanced with the TEG Dextran ATPS development of compartments inside the droplets.

Previous templating at the surface of coacervates has included that by Fothergill et al. by the addition of nanoparticles [218]. It is clear that far more research could be done in this area and that these systems have potential in the construction of higher-order coacervate-based protocell

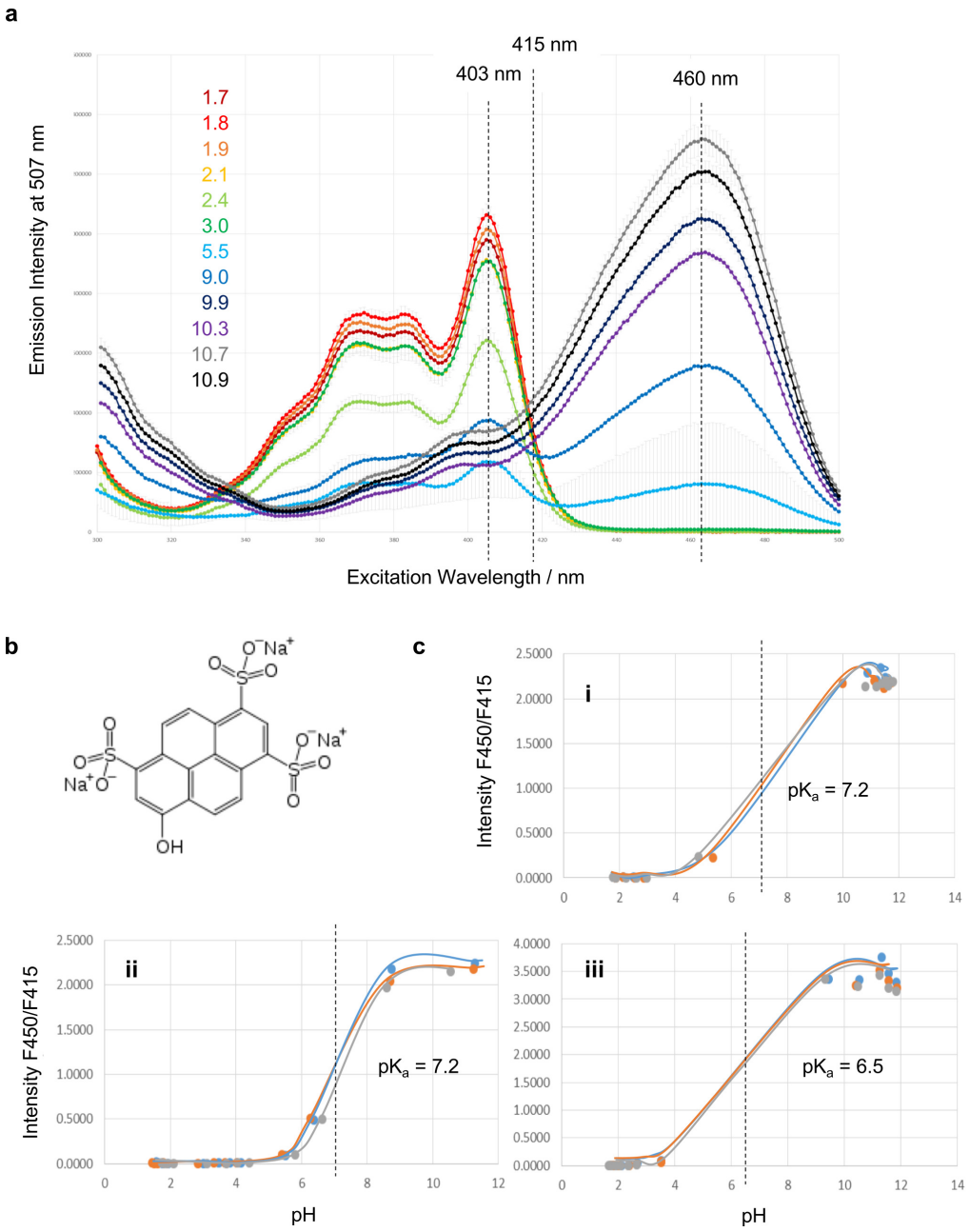

Figure 5.25: Calibration of the pyranine assay for use in ATP: PDDA coacervate droplets to detect pH change in the interior. a: Excitation spectra of pyranine at an emission of 507 nm, with increasing concentrations of pyranine. Concentrations are given in the scale on the figure and are given in μM. Peaks showing the basic form of pyranine (403 nm), the isobestic point (415 nm) and the acidic form (460 nm) are indicated on the figure. B: The chemical structure of pyranine. C: The pKa of pyranine is dependent on its local environment. Plots show calculated pKa values for pyranine in i: water, ii: ATP and iii: PDDA.

systems. Much of the work in this chapter is preliminary but there is a lot of scope to expand the experiments to further develop hybrid protocells. It would be of particular interest to fully characterize the other block copolymers suggested here in the coacervate system, in order to understand the mechanism of membrane assembly at the interface.

CHAPTER 6

GENERAL CONCLUSIONS

6.1 Summary

This thesis aimed to further understand the manipulation of macromolecular uptake for the functional design of protocells, using coacervate droplets as a protocell model. Specifically, this research furthered the area of developing protocellular requirements in cell models through an enhanced understanding of macromolecular interactions with the coacervate. This was demonstrated with an ATP: PDDA coacervate system and several types of enhanced novel hybrid coacervates were constructed.

Chapter 3 aimed to develop an understanding of the macromolecular partitioning and exclusion of molecules in the ATP:PDDA coacervate system. The system was first characterised with regards to its dynamics and stability. The effects of sequestering solutes individually were investigated with both small molecules, such as DNA and tetraethylene glycol (TEG), and larger molecules, including proteins and dextran carbohydrates. Macromolecular sequestration was demonstrated, with the coacervates partitioning a wide range of molecules into the interior at high concentrations. Here, it was shown that even small uncharged molecules are capable of perturbing the system to create internal compartmentation, with compartments free of coacervate components. Manipulation the properties of the TEG added was also used to cause structural changes in the droplets such as finger-like expulsions of coacervate material. It was concluded that the formation of TEG-induced compartments was likely due to the disruption of hydrogen bonding within the coacervates or alterations in the hydrophobicity of the system.

The exchange in a binary population of coacervates was shown, indicating that transfer does not occur between two mixed populations. This further demonstrates that the coacervates are appropriate systems in which to contain components, such as enzyme cascades, with the ability

to act as protocellular compartments. The mechanism of re-suspending coacervate to increase stability was also investigated and it was shown that the re-suspension of coacervates clearly improved stability, except in some cases with the addition of salt, where stability actually decreased. This chapter demonstrated the need to have a fully characterised protocell system in order to develop higher-order functionality, as small additions can have a dramatic, and not always predictable, change on the system as a whole. Finally larger molecule sequestration was then examined with dextrans of varying size and charge used as examples. Stability and partitioning was characterised extensively and the experiments demonstrated that dextran partitioning could be manipulated to induce surface partitioning of dextran on the coacervates.

The observations in Chapter 3 were then used to create functional systems in Chapter 4, where multiple macromolecules were combined in the same coacervate system. Single-stranded DNA oligomers were base paired to form double-stranded DNA and the effects of this on the coacervate properties seen previously investigated. This research also resulted in the construction of an aqueous two-phase systems within the coacervates induced by sequential and synergistic additions of dextran and TEG into the same droplet. A comparison between the mechanisms of the systems in Chapter 3 and 4 was shown, with the deduction that the vacuoles and dextran compartments were actually formed by two different mechanisms, one based on hydrogen bonding disruption and the other on phase separation properties. However, there is some data to suggest similarities between the systems, allowing further systems to be selected, or switched between, with control over the final properties.

This system also allowed the internal vacuole to be modified to become a dextran-filled compartment. Higher order structures were seen with internal compartment boundaries maintained in some cases even after dextran compartment formation. Novel sequestration mechanisms were seen in the coacervates and characterised with tagged TEG and dextran. Interestingly, combinations of dextran-FITC and dextran-RITC allowed selective partitioning of these molecules, altering the properties of the central dextran compartment and the macromolecular sequestration within this. The utility of these to compartments was then shown with the enzymatic degradation of the central dextran compartment with dextranase located in the surrounding coacervate matrix. The dextran could also be re-localised between compartments. Not only did this show that the compartments were able to communicate, it also demonstrated that the coacervates can be enzymatically manipulated to act as a storage-release system.

The final study in chapter 5 explored macromolecular surface localisation on coacervates. The partitioning properties of the coacervates, seen previously in chapter 3 and 4, were used in preliminary studies to explore membrane creation at the interface between the coacervate bulk matrix and the surrounding supernatant. A nanotectonic approach was used to successfully add block copolymers to the surface of the droplets, which were shown to increase the stability of the coacervates. These new interfaces were then further functionalised by the addition of a layer of purple membrane flakes, stabilised by the block copolymer layer. The behaviour of

the TEG-dextran system was also briefly investigated with block copolymer coacervates to show early investigations into a more complex three-component system. The pyranine assay was also characterized in the PDDA: ATP coacervate system, and the modifications that need to be made for this to be useful in this environment were determined.

On the whole, this thesis has shown several novel, exciting concepts and developed these methodologies. Firstly, it has been shown that it is possible to destabilise a coacervate matrix with an uncharged molecule through the introduction of a molecule, TEG, which can interfere with hydrogen bonding or the manipulate the hydrophobicity of the system. This is in contrast to previously published systems which forms vacuoles through rational design of components to produce a layered system or destabilisation of a coacervate matrix with charged molecules or osmotic pressure driven shifts. This system provides a new method of forming compartments inside coacervates. Secondly, this research has also shown the development of an ATPS inside coacervates, which can be constructed in combination with the TEG-only based system. The compartments formed here are unusual because they have been shown to contain much higher concentrations of dextran the the supernatant phase surrounding the coacervates. This suggests that the high sequestration properties of the coacervate can be utilised and manipulated to induce macromolecular crowding, an essential process in biological systems. Finally, the early work on the addition of a functional membrane to coacervates has demonstrated that no only can block copolymers be used as a membrane structure in these cases, but also that they can then be further utilised to template other molecules to the coacervate interface that would not otherwise be able to reside at the surface of the droplet. These molecules could be used to generate pH changes in the droplets or add other functionalities. This last piece of research demonstrates the use of a novel model system with high modularity that, with more research, could be tailored to purpose.

6.2 Further Work

It is suggested that future work should include further development of the systems where only early characterisation has occurred here. This is likely to lead to further protocell systems with more functionality. Specifically, the salt shrinkage of coacervates should be investigated to see if it is possible to regrow coacervates by re-dilution of the salt concentration and, if so, to see if these droplets then contain a mixture of components. This could be used to generate systems whereby reactions could occur and then the products could be randomly mixed allowing evolution. Further studies on the coacervates with high levels of dextran-FITC doped into dextran should also be done as the ability of these droplets to expel their contents is very interesting.

Initial attempts were made to further the TEG/dextran-induced system by introducing an enzyme cascade, but this was not been studied extensively. Increased insight here would allow complex systems of coacervates to be built in a controllable manner, perhaps with a view to initi-

ating populations of coacervates able to evolve and communicate through component release or predictable coacervate disassembly. Additionally, more work could be done to extend these compartments to other coacervate systems and alter the partitioning properties of the coacervates such that molecules coated in dextran could be contained in the central compartment and then released with the action of dextranase.

Much of the work in Chapter 5 was preliminary but there is a lot of scope to expand these experiments to further develop hybrid protocells. It would be of particular interest to fully characterize the other block copolymers suggested here in the coacervate system, in order to understand the mechanism of membrane assembly at the interface and create a toolkit of functional synthetic coacervate systems.

BIBLIOGRAPHY

[1] Stephen Mann.
The origins of life: Old problems, new chemistries.
Angewandte Chemie - International Edition, 52(1):155–162, 2013.

[2] Ricard V. Solé, Steen Rasmussen, and Marc Bedau.
Introduction. Artificial protocells.
Philosophical Transactions of the Royal Society B: Biological Sciences, 362(1486):1725, 2007.

[3] Alicja J Dzieciol and Stephen Mann.
Designs for life: protocell models in the laboratory.
Chemical Society Reviews, 41(1):79, 2012.

[4] Carl R. Woese and George E. Fox.
The concept of cellular evolution.
Journal of Molecular Evolution, 10(1):1–6, mar 1977.

[5] Carl Woese.
The universal ancestor (progenotelateral gene transfergenetic annealingevolutionary temperaturecommunal ancestor).
Proc. Nati. Acad. Sci. USA, 95:6854–6859, 1998.

[6] Steven A Benner, Andrew D Ellingtont, and Andreas Tauer.
Modern metabolism as a palimpsest of the RNA world.
Proc. Nati. Acad. Sci. USA, 86:7054–7058, 1989.

[7] B M Rode.
Peptide and the origin of life.
PEPTIDES, 20(6):773–786, 1999.

[8] Jack T. Trevors and Gerald H. Pollack.
Hypothesis: The origin of life in a hydrogel environment.
Progress in Biophysics and Molecular Biology, 89(1):1–8, 2005.

[9] Kenjii Ikehara.
Possible steps to the emergence of life: The [GADV]-protein world hypothesis.
Chemical Record, 5(2):107–118, 2005.

[10] A. Graham Cairns-Smith.
Chemistry and the missing era of evolution.
Chemistry - A European Journal, 14(13):3830–3839, 2008.

[11] Leslie E. Orgel.
The implausibility of metabolic cycles on the prebiotic earth.
PLoS Biology, 6(1):0005–0013, 2008.

[12] Isabel Baeza, Miguel Ibáñez, Carlos Wong, Pedro Chávez, Patricio Gariglio, and J. Oró.
Possible prebiotic significance of polyamines in the condensation, protection, encapsulation, and biological properties of DNA.
Origins of Life and Evolution of the Biosphere, 21(4):225–242, 1992.

[13] Yuval Elani, Robert V Law, and Oscar Ces.
Vesicle-based artificial cells as chemical microreactors with spatially segregated reaction pathways.
Nature Communications, 5:1–5, 2014.

[14] Roberto J Brea, Michael D Hardy, and Neal K Devaraj.
Towards self-assembled hybrid artificial cells: novel bottom-up approaches to functional synthetic membranes.
Chemistry (Weinheim an der Bergstrasse, Germany), 21(36):12564–12570, 2015.

[15] Andrew Pohorille and David Deamer.
Artificial cells: Prospects for biotechnology.
Trends in Biotechnology, 20(3):123–128, 2002.

[16] Edward N. Trifonov.
Vocabulary of definitions of life suggests a definition.
Journal of Biomolecular Structure and Dynamics, 29(2):259–266, 2011.

[17] Stephen Mann.
Systems of creation: The emergence of life from nonliving matter.
Accounts of Chemical Research, 45(12):2131–2141, 2012.

[18] E. Smith and H. J. Morowitz.
Universality in intermediary metabolism.
Proceedings of the National Academy of Sciences, 101(36):13168–13173, 2004.

[19] Ricard V. Solé, Andreea Munteanu, Carlos Rodriguez-Caso, and Javier Macía.
Synthetic protocell biology: From reproduction to computation.
Philosophical Transactions of the Royal Society B: Biological Sciences, 362(1486):1727–1739, 2007.

[20] James Attwater and Philipp Holliger.
A synthetic approach to abiogenesis.
Nature methods, 11(5):495–498, 2014.

[21] Mei Li, Xin Huang, T-Y Dora Tang, and Stephen Mann.
Synthetic cellularity based on non-lipid micro-compartments and protocell models.
Current Opinion in Chemical Biology, 22:1–11, oct 2014.

[22] Cheemeng Tan, Saumya Saurabh, Marcel P Bruchez, Russell Schwartz, and Philip Leduc.
Molecular crowding shapes gene expression in synthetic cellular nanosystems.
Nature nanotechnology, 8(8):602–608, 2013.

[23] Valdur Saks.
Molecular System Bioenergetics: Energy for Life.
Molecular System Bioenergetics: Energy for Life, pages 1–604, 2007.

[24] Ricard V Solé, Andreea Munteanu, Carlos Rodriguez-Caso, and Javier Macía.
Synthetic protocell biology: from reproduction to computation.
Philosophical transactions of the Royal Society of London. Series B, Biological sciences, 362(1486):1727–1739, 2007.

[25] Renée Roodbeen and Jan C.M. Van Hest.
Synthetic cells and organelles: Compartmentalization strategies, 2009.

[26] C. P. Brangwynne, T. J. Mitchison, and A. A. Hyman.
Active liquid-like behavior of nucleoli determines their size and shape in Xenopus laevis oocytes.
Proceedings of the National Academy of Sciences, 108(11):4334–4339, 2011.

[27] Erkan Tüzel.
Organelle dynamics: A tale of fusing nucleoli.
Current Biology, 21(10), 2011.

[28] Edward Emmott and Julian A. Hiscox.
Nucleolar targeting: The hub of the matter, 2009.

[29] J Strouboulis and a P Wolffe.
Functional compartmentalization of the nucleus.
Journal of cell science, 109 (Pt 8(1996):1991–2000, 1996.

[30] A. P. Minton.
How can biochemical reactions within cells differ from those in test tubes?
Journal of Cell Science, 128(6):1254–1254, 2015.

[31] C. P. Brangwynne, C. R. Eckmann, D. S. Courson, A. Rybarska, C. Hoege, J. Gharakhani, F. Julicher, and A. A. Hyman.
Germline P Granules Are Liquid Droplets That Localize by Controlled Dissolution/Condensation.
Science, 324(5935):1729–1732, jun 2009.

[32] Dustin L. Updike, Stephanie J. Hachey, Jeremy Kreher, and Susan Strome.
P granules extend the nuclear pore complex environment in the C. elegans germ line.
Journal of Cell Biology, 192(6):939–948, 2011.

[33] Harold J. Morowitz, Bettina Heinz, and David W. Deamer.
The chemical logic of a minimum protocell.
Origins of Life and Evolution of the Biosphere, 18(3):281–287, 1988.

[34] J W Szostak, J W Szostak, D P Bartel, D P Bartel, L Luisi, and L Luisi.
Synthesizing life.
Nature, 409:387–390, 2001.

[35] Steen Rasmussen, Liaohai Chen, David Deamer, David C Krakauer, Norman H Packard, Peter F Stadler, and Mark a Bedau.
Evolution. Transitions from nonliving to living matter.
Science (New York, N.Y.), 303(5660):963–965, 2004.

[36] Steen Rasmussen, Liaohai Chen, David Deamer, David C Krakauer, Norman H Packard, Peter F Stadler, and Mark a Bedau.
Evolution. Transitions from nonliving to living matter.
Science (New York, N.Y.), 303(5660):963–965, 2004.

[37] Juli Peretó and Jesús Català.
The Renaissance of Synthetic Biology.
Biological Theory, 2(2):128–130, 2007.

[38] D Bray.
Protein molecules as computational elements in living cells.
Nature, 376(6538):307–312, 1995.

[39] C A Hutchison, S N Peterson, S R Gill, R T Cline, O White, C M Fraser, H O Smith, and J C Venter.
Global transposon mutagenesis and a minimal Mycoplasma genome.

Science (New York, N.Y.), 286(5447):2165–2169, 1999.

[40] A R Mushegian and E V Koonin.
A minimal gene set for cellular life derived by comparison of complete bacterial genomes.
Proceedings of the National Academy of Sciences of the United States of America, 93(19):10268–10273, 1996.

[41] Paul François and Vincent Hakim.
Design of genetic networks with specified functions by evolution in silico.
Proceedings of the National Academy of Sciences of the United States of America, 101(2):580–585, 2004.

[42] Lingchong You, Robert Sidney, Cox Iii, Ron Weiss, and Frances H Arnold.
Programmed population control by cell cell communication and regulated killing.
Nature, 428(April):868–871, 2004.

[43] Daniel G Gibson, John I Glass, Carole Lartigue, Vladimir N Noskov, Ray-Yuan Chuang, Mikkel a Algire, Gwynedd a Benders, Michael G Montague, Li Ma, Monzia M Moodie, Chuck Merryman, Sanjay Vashee, Radha Krishnakumar, Nacyra Assad-Garcia, Cynthia Andrews-Pfannkoch, Evgeniya a Denisova, Lei Young, Zhi-Qing Qi, Thomas H Segall-Shapiro, Christopher H Calvey, Prashanth P Parmar, Clyde a Hutchison, Hamilton O Smith, and J Craig Venter.
Creation of a bacterial cell controlled by a chemically synthesized genome.
Science (New York, N.Y.), 329(5987):52–56, 2010.

[44] C A Hutchison, R.-Y. Chuang, V N Noskov, N Assad-Garcia, T J Deerinck, M H Ellisman, J Gill, K Kannan, B J Karas, L Ma, J F Pelletier, Z.-Q. Qi, R A Richter, E A Strychalski, L Sun, Y Suzuki, B Tsvetanova, K S Wise, H O Smith, J I Glass, C Merryman, D G Gibson, and J C Venter.
Design and synthesis of a minimal bacterial genome.
Science, 351(6280):6253, 2016.

[45] David Miller, Paula J Booth, John M Seddon, Richard H Templer, Robert V Law, Rudiger Woscholski, Oscar Ces, and Laura M C Barter.
Protocell design through modular compartmentalization.
Journal of the Royal Society, Interface / the Royal Society, 10(87):20130496, 2013.

[46] Pier Luigi Luisi, Peter Walde, and Thomas Oberholzer.
Lipid vesicles as possible intermediates in the origin of life, 1999.

[47] David Deamer, Jason P. Dworkin, Scott A. Sandford, Max P. Bernstein, and Louis J. Allamandola.

The First Cell Membranes.
Astrobiology, 2(4):371–381, 2002.

[48] Peter Walde.
Building artificial cells and protocell models: Experimental approaches with lipid vesicles, 2010.

[49] Peter Walde, Katia Cosentino, Helen Engel, and Pasquale Stano.
Giant Vesicles: Preparations and Applications, 2010.

[50] Shogo Koga, David S Williams, Adam W Perriman, and Stephen Mann.
Peptide-nucleotide microdroplets as a step towards a membrane-free protocell model.
Nature chemistry, 3(9):720–724, 2011.

[51] T-Y Dora Tang, C Rohaida Che Hak, Alexander J Thompson, Marina K Kuimova, D S Williams, Adam W Perriman, and Stephen Mann.
Fatty acid membrane assembly on coacervate microdroplets as a step towards a hybrid protocell model.
Nature chemistry, 6(6):527–533, 2014.

[52] Pierre Alain Monnard and David W. Deamer.
Nutrient uptake by protocells: A liposome model system.
Origins of Life and Evolution of the Biosphere, 31(1-2):147–155, 2001.

[53] H. Hotani, T. Inaba, F. Nomura, S. Takeda, K. Takiguchi, T. J. Itoh, T. Umeda, and A. Ishijima.
Mechanical analyses of morphological and topological transformation of liposomes.
BioSystems, 71(1-2):93–100, 2003.

[54] Takeshi Sunami, Kanetomo Sato, Tomoaki Matsuura, Koji Tsukada, Itaru Urabe, and Tetsuya Yomo.
Femtoliter compartment in liposomes for in vitro selection of proteins.
Analytical Biochemistry, 357(1):128–136, 2006.

[55] Pasquale Stano and Pier Luigi Luisi.
Achievements and open questions in the self-reproduction of vesicles and synthetic minimal cells, 2010.

[56] Thomas I. Tikchonenko, Svetlana E. Glushakova, Olga S. Kislina, Natalia A. Grodnitskaya, Anatoly A. Manykin, and Boris S. Naroditsky.
Transfer of condensed viral DNA into eukaryotic cells using proteoliposomes.
Gene, 63(2):321–330, 1988.

[57] J Szelei and E Duda.
Entrapment of high-molecular-mass DNA molecules in liposomes for the genetic transformation of animal cells.
Biochem J, 259(2):549–553, 1989.

[58] Martin M Hanczyc, Shelly M Fujikawa, and Jack W Szostak.
Experimental models of primitive cellular compartments: encapsulation, growth, and division.
Science (New York, N.Y.), 302(5645):618–622, 2003.

[59] Fabio Mavelli and Kepa Ruiz-Mirazo.
Stochastic simulations of minimal self-reproducing cellular systems.
Philosophical transactions of the Royal Society of London. Series B, Biological sciences, 362(1486):1789–1802, 2007.

[60] Andrea Veronese, Nathalie Berclaz, and Pier Luigi Luisi.
Photoinduced Formation of Bilayer Vesicles.
J Phys Chem B., 6(98):7078–7080, 1998.

[61] A Albertsen, S Maurer, K Nielsen, and P Monnard.
Transmission of photo-catalytic function in a self-replicating chemical system: in situ amphiphile production over two protocell generations.
Chemical communications (Cambridge, England), 50(i):8989–8992, 2014.

[62] I Chen and J Szostak.
A Kinetic Study of the Growth of Fatty Acid Vesicles.
Biophysical Journal, 87(2):988–998, aug 2004.

[63] Yang Song, Ulyana Shimanovich, Thomas C.T. Michaels, Qingming Ma, Jingmei Li, Tuomas P.J. Knowles, and Ho Cheung Shum.
Fabrication of fibrillosomes from droplets stabilized by protein nanofibrils at all-aqueous interfaces.
Nature Communications, 7, 2016.

[64] Keitaro Ishikawa, Kanetomo Sato, Yasufumi Shima, Itaru Urabe, and Tetsuya Yomo.
Expression of a cascading genetic network within liposomes.
FEBS Letters, 576(3):387–390, 2004.

[65] T Oberholzer, K H Nierhaus, and P L Luisi.
Protein expression in liposomes.
Biochemical and biophysical research communications, 261(2):238–241, 1999.

[66] Vincent Noireaux and Albert Libchaber.
A vesicle bioreactor as a step toward an artificial cell assembly.
Proceedings of the National Academy of Sciences of the United States of America, 101(51):17669–17674, 2004.

[67] Paul M Gardner, Klaus Winzer, and Benjamin G Davis.
Sugar synthesis in a protocellular model leads to a cell signalling response in bacteria.
Nature chemistry, 1(5):377–383, 2009.

[68] M. S. Long, C. D. Jones, M. R. Helfrich, L. K. Mangeney-Slavin, and C. D. Keating.
Dynamic microcompartmentation in synthetic cells.
Proceedings of the National Academy of Sciences, 102(17):5920–5925, 2005.

[69] Lisa M. Dominak, Erica L. Gundermann, and Christine D. Keating.
Microcompartmentation in artificial cells: PH-induced conformational changes alter protein localization.
Langmuir, 26(8):5697–5705, 2010.

[70] M. Scott Long, Ann Sofie Cans, and Christine D. Keating.
Budding and asymmetric protein microcompartmentation in giant vesicles containing two aqueous phases.
Journal of the American Chemical Society, 130(2):756–762, 2008.

[71] Meghan Andes-Koback and Christine D. Keating.
Complete budding and asymmetric division of primitive model cells to produce daughter vesicles with different interior and membrane compositions.
Journal of the American Chemical Society, 133(24):9545–9555, 2011.

[72] Ravinash Krishna Kumar, Mei Li, Sam N Olof, Avinash J Patil, and Stephen Mann.
Artificial cytoskeletal structures within enzymatically active bio-inorganic protocells.
Small, 9(3):357–362, 2013.

[73] Ravinash Krishna Kumar, Xiaoxiao Yu, Avinash J Patil, Mei Li, and Stephen Mann.
Cytoskeletal-like supramolecular assembly and nanoparticle-based motors in a model protocell.
Angewandte Chemie - International Edition, 50(40):9343–9347, 2011.

[74] Markus Blocher, Peter Walde, and Irving J. Dunn.
Modeling of enzymatic reactions in vesicles: The case of α- chymotrypsin.
Biotechnology and Bioengineering, 62(1):36–43, 1999.

[75] Martin Fischlechner, Yolanda Schaerli, Mark F. Mohamed, Santosh Patil, Chris Abell, and Florian Hollfelder.

Evolution of enzyme catalysts caged in biomimetic gel-shell beads.
Nature Chemistry, 6(9):791–796, 2014.

[76] Jordan M Fletcher, Robert L Harniman, Frederick R H Barnes, Aimee L Boyle, Andrew Collins, Judith Mantell, Thomas H Sharp, Massimo Antognozzi, Paula J Booth, Noah Linden, Mervyn J Miles, Richard B Sessions, Paul Verkade, and Derek N Woolfson.
Self-assembling cages from coiled-coil peptide modules.
Science (New York, N.Y.), 340(6132):595–599, 2013.

[77] Brigitte Städler, Andrew D Price, Rona Chandrawati, Leticia Hosta-Rigau, Alexander N Zelikin, and Frank Caruso.
Polymer hydrogel capsules: en route toward synthetic cellular systems.
Nanoscale, 1(1):68–73, 2009.

[78] E Karzbrun, a. M Tayar, V Noireaux, and R H Bar-Ziv.
Programmable on-chip DNA compartments as artificial cells.
Science, 345(6198):829–832, 2014.

[79] Maximilian Weitz, Jongmin Kim, Korbinian Kapsner, Erik Winfree, Elisa Franco, and Friedrich C Simmel.
Diversity in the Dynamical Behaviour of a Compartmentalized Programmable Biochemical Oscillator.
Nature Chemistry, 6(4):295–302, 2014.

[80] Helen Song, Delai L. Chen, and Rustem F. Ismagilov.
Reactions in droplets in microfluidic channels.
Angewandte Chemie - International Edition, 45(44):7336–7356, 2006.

[81] Christine D Keating.
Gated access to microreactors.
Nature Publishing Group, 5(6):449–451, 2013.

[82] Mei Li, David C. Green, J. L. Ross Anderson, Bernard P. Binks, and Stephen Mann.
In vitro gene expression and enzyme catalysis in bio-inorganic protocells.
Chemical Science, 2(9):1739, aug 2011.

[83] Bernard P. Binks and Ryo Murakami.
Phase inversion of particle-stabilized materials from foams to dry water.
Nature Materials, 5(11):865–869, nov 2006.

[84] Anand Bala Subramaniam, Jiandi Wan, Arvind Gopinath, and Howard A. Stone.
Semi-permeable vesicles composed of natural clay.
Soft Matter, 7(6):2600, mar 2011.

[85] Chaoyang Wang, Hongxia Liu, Quanxing Gao, Xinxing Liu, and Zhen Tong.
Facile Fabrication of Hybrid Colloidosomes with Alginate Gel Cores and Shells of Porous CaCO3 Microparticles.
ChemPhysChem, 8(8):1157–1160, jun 2007.

[86] Jie Zhang, Yu-Fei Song, Leroy Cronin, and Tianbo Liu.
Reverse-Vesicle Formation of Organic-Inorganic Polyoxometalate-Containing Hybrid Surfactants with Tunable Sizes.
Chemistry - A European Journal, 16(37):11320–11324, aug 2010.

[87] Yongqiang He, Fei Wu, Xiying Sun, Ruqiang Li, Yongqin Guo, Chuanbao Li, Lu Zhang, Fubao Xing, Wei Wang, and Jianping Gao.
Factors that Affect Pickering Emulsions Stabilized by Graphene Oxide.
ACS Applied Materials & Interfaces, 5(11):4843–4855, jun 2013.

[88] Angelika Bachinger and Guido Kickelbick.
Pickering emulsions stabilized by anatase nanoparticles.
Monatshefte für Chemie - Chemical Monthly, 141(6):685–690, jun 2010.

[89] Jun Zhou, Lijun Wang, Xiuying Qiao, Bernard P. Binks, and Kang Sun.
Pickering emulsions stabilized by surface-modified Fe3O4 nanoparticles.
Journal of Colloid and Interface Science, 367(1):213–224, feb 2012.

[90] Nancy Zgheib, Jean-Luc Putaux, Antoine Thill, Franck D'Agosto, Muriel Lansalot, and Elodie Bourgeat-Lami.
Stabilization of Miniemulsion Droplets by Cerium Oxide Nanoparticles: A Step toward the Elaboration of Armored Composite Latexes.
Langmuir, 28(14):6163–6174, apr 2012.

[91] Jie He, Yijing Liu, Taarika Babu, Zengjiang Wei, and Zhihong Nie.
Self-Assembly of Inorganic Nanoparticle Vesicles and Tubules Driven by Tethered Linear Block Copolymers.
Journal of the American Chemical Society, 134(28):11342–11345, jul 2012.

[92] Tobias Bollhorst, Tim Grieb, Andreas Rosenauer, Gerald Fuller, Michael Maas, and Kurosch Rezwan.
Synthesis Route for the Self-Assembly of Submicrometer-Sized Colloidosomes with Tailorable Nanopores.
Chemistry of Materials, 25(17):3464–3471, sep 2013.

[93] Rachel T. Rosenberg and Nily Dan.
Designing Nanoparticle Colloidal Shells for Selective Transport.
Soft Materials, 11(2):143–148, apr 2013.

[94] Olivier J. Cayre, James Hitchcock, Mohamed S. Manga, Sam Fincham, Amandine Simoes, Richard A. Williams, and Simon Biggs.
pH-responsive colloidosomes and their use for controlling release.
Soft Matter, 8(17):4717, apr 2012.

[95] Rhutesh K. Shah, Jin-Woong Kim, and David A. Weitz.
Monodisperse Stimuli-Responsive Colloidosomes by Self-Assembly of Microgels in Droplets.
Langmuir, 26(3):1561–1565, feb 2010.

[96] Huai Nyin Yow and Alexander F. Routh.
Release Profiles of Encapsulated Actives from Colloidosomes Sintered for Various Durations.
Langmuir, 25(1):159–166, jan 2009.

[97] Mei Li, Xin Huang, and Stephen Mann.
Spontaneous Growth and Division in Self-Reproducing Inorganic Colloidosomes.
Small, 10(16):3291–3298, aug 2014.

[98] Xin Huang, Mei Li, David C. Green, David S. Williams, Avinash J. Patil, and Stephen Mann.
Interfacial assembly of proteinpolymer nano-conjugates into stimulus-responsive biomimetic protocells.
Nature Communications, 4:2239, jul 2013.

[99] Xin Huang, Avinash J. Patil, Mei Li, and Stephen Mann.
Design and Construction of Higher-Order Structure and Function in Proteinosome-Based Protocells.
Journal of the American Chemical Society, 136(25):9225–9234, jun 2014.

[100] Dennis E Discher and Adi Eisenberg.
Polymer vesicles.
Science (New York, N.Y.), 297(5583):967–73, aug 2002.

[101] Daniel A. Hammer and Neha P. Kamat.
Towards an artificial cell.
FEBS Letters, 586(18):2882–2890, aug 2012.

[102] Ruud J. R. W. Peters, Iria Louzao, and Jan C. M. van Hest.
From polymeric nanoreactors to artificial organelles.
Chem. Sci., 3(2):335–342, jan 2012.

[103] Pavel Broz, Sergey Driamov, Joerg Ziegler, Nadav Ben-Haim, Stephan Marsch, Wolfgang Meier, and Hunziker Patrick.
Toward Intelligent Nanosize Bioreactors: A pH-Switchable, Channel-Equipped, Functional Polymer Nanocontainer.
Nano Letters, 6(10):2349–2353, 2006.

[104] M. Kumar, M. Grzelakowski, J. Zilles, M. Clark, and W. Meier.
Highly permeable polymeric membranes based on the incorporation of the functional water channel protein Aquaporin Z.
Proceedings of the National Academy of Sciences, 104(52):20719–20724, dec 2007.

[105] Kyoung Taek Kim, Jeroen J. L. M. Cornelissen, Roeland J. M. Nolte, and Jan C. M. van Hest.
A Polymersome Nanoreactor with Controllable Permeability Induced by Stimuli-Responsive Block Copolymers.
Advanced Materials, 21(27):2787–2791, jul 2009.

[106] Xin Huang, Dietmar Appelhans, Petr Formanek, Frank Simon, and Brigitte Voit.
Tailored Synthesis of Intelligent Polymer Nanocapsules: An Investigation of Controlled Permeability and pH-Dependent Degradability.
ACS Nano, 6(11):9718–9726, nov 2012.

[107] Jens Gaitzsch, Dietmar Appelhans, Linge Wang, Giuseppe Battaglia, and Brigitte Voit.
Synthetic Bio-nanoreactor: Mechanical and Chemical Control of Polymersome Membrane Permeability.
Angewandte Chemie, 51(18):4448–4451, apr 2012.

[108] Daniela A. Wilson, Roeland J. M. Nolte, and Jan C. M. van Hest.
Autonomous movement of platinum-loaded stomatocytes.
Nature Chemistry, 4(4):268–274, apr 2012.

[109] Silvie A. Meeuwissen, Kyoung Taek Kim, Yingchao Chen, Darrin J. Pochan, and Jan C. M. van Hest.
Controlled Shape Transformation of Polymersome Stomatocytes.
Angewandte Chemie, 50(31):7070–7073, jul 2011.

[110] Matthijs C. M. van Oers, Floris P. J. T. Rutjes, and Jan C. M. van Hest.
Tubular Polymersomes: A Cross-Linker-Induced Shape Transformation.
Journal of the American Chemical Society, 135(44):16308–16311, nov 2013.

[111] Ruud J. R. W. Peters, Maïté Marguet, Sébastien Marais, Marco W. Fraaije, Jan C. M. van Hest, and Sébastien Lecommandoux.

Cascade Reactions in Multicompartmentalized Polymersomes.
Angewandte Chemie, 53(1):146–150, jan 2014.

[112] Clifford P. Brangwynne.
Soft active aggregates: mechanics, dynamics and self-assembly of liquid-like intracellular protein bodies.
Soft Matter, 7(7):3052, mar 2011.

[113] Priya R Banerjee, Anthony N Milin, Mahdi Muhammad Moosa, Paulo L Onuchic, and Ashok A Deniz.
Reentrant Phase Transition Drives Dynamic Substructure Formation in Ribonucleoprotein Droplets.
Angewandte Chemie, pages 1–6, 2017.

[114] Hermann Broder Schmidt and Rajat Rohatgi.
In-Vivo Formation of Vacuolated Multi-phase Compartments Lacking Membranes.
Cell Reports, 16(5):1228–1236, 2016.

[115] Fenghua Meng, Zhiyuan Zhong, and Jan Feijen.
Stimuli-Responsive Polymersomes for Programmed Drug Delivery.
Biomacromolecules, 10(2):197–209, feb 2009.

[116] T.-Y. Dora Tang, Massimo Antognozzi, James a. Vicary, Adam W Perriman, and Stephen Mann.
Small-molecule uptake in membrane-free peptide/nucleotide protocells.
Soft Matter, 9(31):7647, 2013.

[117] F W Tiebackx.
Gleichzeitige Ausflockung zweier Kolloide.
Zeitschrift fur Chemie und Industrie der Kolloide, 8(4):198–201, 1911.

[118] H B Bungenberg de Jong and H R Kruyt.
Coacervation (Partial Miscibility in Colloid Systems).
Proc. Sect. Sci, Koninkijke Nederlandse Akademie van Wetenschappen, 32(1927):849–856, 1929.

[119] Suojiang Zhang, Xingmei Lu, Qing Zhou, Xiaohua Li, Xiangping Zhang, and Shucai Li.
Ionic Liquids.
Ionic Liquids, 2009.

[120] J Israelachvili and H Wennerström.
Role of hydration and water structure in biological and colloidal interactions., 1996.

[121] Emily E Meyer, Kenneth J Rosenberg, and Jacob Israelachvili.
Recent progress in understanding hydrophobic interactions.
Proceedings of the National Academy of Sciences of the United States of America, 103(43):15739–46, 2006.

[122] P. L. Madan.
Microencapsulation I. Phase separation or coacervation.
Drug Development and Industrial Pharmacy, 4(1):95–116, 1978.

[123] Amarnath Gupta, Reena, and H. B. Bohidar.
Free-energy landscape of alcohol driven coacervation transition in aqueous gelatin solutions.
Journal of Chemical Physics, 125(5), 2006.

[124] Asami Ohsugi, Hidemitsu Furukawa, Akira Kakugo, Yoshihito Osada, and Jian Ping Gong.
Catch and release of DNA in coacervate-dispersed gels.
Macromolecular Rapid Communications, 27(15):1242–1246, 2006.

[125] a I Oparin and K L Gladilin.
Evolution of self-assembly of probionts.
Bio Systems, 12(3-4):133–145, 1980.

[126] Jian Qin, Dimitrios Priftis, Robert Farina, Sarah L. Perry, Lorraine Leon, Jonathan Whitmer, Kyle Hoffmann, Matthew Tirrell, and Juan J. De Pablo.
Interfacial tension of polyelectrolyte complex coacervate phases.
ACS Macro Letters, 3(6):565–568, 2014.

[127] Arthur Veis.
A review of the early development of the thermodynamics of the complex coacervation phase separation.
Advances in Colloid and Interface Science, 167(1-2):2–11, sep 2011.

[128] Dimitrios Priftis, Nicolas Laugel, and Matthew Tirrell.
Thermodynamic Characterization of Polypeptide Complex Coacervation.
Langmuir, 28(45):15947–15957, nov 2012.

[129] David S. Williams, Shogo Koga, C. Rohaida C. Hak, Animesh Majrekar, Avinash J. Patil, Adam W. Perriman, and Stephen Mann.
Polymer/nucleotide droplets as bio-inspired functional micro-compartments.
Soft Matter, 8(22):6004, jun 2012.

[130] Paul J. Flory.
Principles of polymer chemistry.
Cornell University Press, 1953.

[131] Rungsima Chollakup, Wirasak Smitthipong, Claus D Eisenbach, and Matthew Tirrell.
Phase behavior and coacervation of aqueous poly(acrylic acid)-poly(allylamine) solutions.
Macromolecules, 43(5):2518–2528, 2010.

[132] Mathai Mammen, Seok-Ki Choi, and George M. Whitesides.
Polyvalent Interactions in Biological Systems: Implications for Design and Use of Multivalent Ligands and Inhibitors.
Angewandte Chemie International Edition, 37(20):2754–2794, 1998.

[133] Boris Rybtchinski.
Adaptive supramolecular nanomaterials based on strong noncovalent interactions, 2011.

[134] I. Michaeli, J. TH. G. Overbeek, and M. J. Voorn.
Phase Separation of Polyelectrolyte Solutions.
J. Polym. Sci., 23:443–450, 1957.

[135] A. Basak Kayitmazer, Sabina P. Strand, Christophe Tribet, Werner Jaeger, and Paul L. Dubin.
Effect of polyelectrolyte structure on protein - Polyelectrolyte coacervates: Coacervates of bovine serum albumin with poly(diallyldimethylammonium chloride) versus chitosan.
Biomacromolecules, 8(11):3568–3577, 2007.

[136] K. Kaibara, T. Okazaki, H. B. Bohidar, and P. L. Dubin.
pH-induced coacervation in complexes of bovine serum albumin and cationic polyelectrolytes.
Biomacromolecules, 1(1):100–107, 2000.

[137] Fanny Weinbreck, Harry S. Rollema, R. Hans Tromp, and Cornelis G. De Kruif.
Diffusivity of whey protein and gum arabic in their coacervates.
Langmuir, 20(15):6389–6395, 2004.

[138] T. N. Evreinova, W. N. Karnaukhov, T. W. Mamontova, and G. R. Ivanizki.
The interaction of biological macromolecules in coacervate systems.
Journal of Colloid And Interface Science, 36(1):18–23, 1971.

[139] Hugo Espinosa-Andrews, Ofelia Sandoval-Castilla, Humberto Vázquez-Torres, Eduardo Jaime Vernon-Carter, and Consuelo Lobato-Calleros.

Determination of the gum Arabic-chitosan interactions by Fourier Transform Infrared Spectroscopy and characterization of the microstructure and rheological features of their coacervates.
Carbohydrate Polymers, 79(3):541–546, 2010.

[140] Cornelus G. De Kruif, Fanny Weinbreck, and Renko De Vries.
Complex coacervation of proteins and anionic polysaccharides, 2004.

[141] S. Santinath Singh, A. K. Siddhanta, Ramavatar Meena, Kamalesh Prasad, S. Bandyopadhyay, and H. B. Bohidar.
Intermolecular complexation and phase separation in aqueous solutions of oppositely charged biopolymers.
International Journal of Biological Macromolecules, 41(2):185–192, 2007.

[142] J. Xia, K. Mattison, V. Romano, P. L. Dubin, and B. B. Muhoberac.
Complexation of trypsin and alcohol dehydrogenase with poly(diallyldimethylammonium chloride).
Biopolymers, 41(4):359–365, 1997.

[143] Ling Qi, Jean Paul Chapel, Jean Christophe Castaing, Jérôme Fresnais, and Jean François Berret.
Organic versus hybrid coacervate complexes: Co-assembly and adsorption properties.
Soft Matter, 4(3):577–585, 2008.

[144] Nathalie Lefèvre, Charles André Fustin, and Jean François Gohy.
Polymeric micelles induced by interpolymer complexation.
Macromolecular Rapid Communications, 30(22):1871–1888, 2009.

[145] C Wandrey, J Hernández-Barajas, and D Hunkeler.
Diallyldimethylammonium Chloride and its Polymers.
Radical Polymerisation Polyelectrolytes, 145:123–183, 1999.

[146] Kevin W. Mattison, Isabelle J. Brittain, and Paul L. Dubin.
ProteinPolyelectrolyte Phase Boundaries.
Biotechnology Progress, 11(6):632–637, 1995.

[147] Emek Seyrek, Paul L. Dubin, Christophe Tribet, and Elizabeth A. Gamble.
Ionic strength dependence of protein-polyelectrolyte interactions.
Biomacromolecules, 4(2):273–282, 2003.

[148] S. Chodankar, V. K. Aswal, J. Kohlbrecher, R. Vavrin, and A. G. Wagh.
Structural study of coacervation in protein-polyelectrolyte complexes.
Physical Review E - Statistical, Nonlinear, and Soft Matter Physics, 78(3), 2008.

[149] Margarita Antonov, Malek Mazzawi, and Paul L. Dubin.
Entering and exiting the protein-polyelectrolyte coacervate phase via nonmonotonic salt dependence of critical conditions.
Biomacromolecules, 11(1):51–59, 2010.

[150] Ebru Kizilay, A. Basak Kayitmazer, and Paul L. Dubin.
Complexation and coacervation of polyelectrolytes with oppositely charged colloids.
Advances in Colloid and Interface Science, 167(1-2):24–37, 2011.

[151] Christine D. Keating.
Aqueous Phase Separation as a Possible Route to Compartmentalization of Biological Molecules.
Accounts of Chemical Research, 45(12):2114–2124, dec 2012.

[152] Bach T. Nguyen, Taco Nicolai, and Lazhar Benyahia.
Stabilization of Water-in-Water Emulsions by Addition of Protein Particles.
Langmuir, 29(34):10658–10664, aug 2013.

[153] Daniel C. Dewey, Christopher A. Strulson, David N. Cacace, Philip C. Bevilacqua, and Christine D. Keating.
Bioreactor droplets from liposome-stabilized all-aqueous emulsions.
Nature Communications, 5:4670, aug 2014.

[154] T.-Y. Dora Tang, Massimo Antognozzi, James A. Vicary, Adam W. Perriman, and Stephen Mann.
Small-molecule uptake in membrane-free peptide/nucleotide protocells.
Soft Matter, 9(31):7647, aug 2013.

[155] David S. Williams, Avinash J. Patil, and Stephen Mann.
Spontaneous Structuration in Coacervate-Based Protocells by Polyoxometalate-Mediated Membrane Assembly.
Small, 10(9):1830–1840, may 2014.

[156] T.-Y. Dora Tang, C. Rohaida Che Hak, Alexander J. Thompson, Marina K. Kuimova, D. S. Williams, Adam W. Perriman, and Stephen Mann.
Fatty acid membrane assembly on coacervate microdroplets as a step towards a hybrid protocell model.
Nature Chemistry, 6(6):527–533, jun 2014.

[157] Yudan Yin, Lin Niu, Xiaocui Zhu, Meiping Zhao, Zexin Zhang, Stephen Mann, and Dehai Liang.
Non-equilibrium behaviour in coacervate-based protocells under electric-field-induced excitation.

Nat Commun, 7:1–7, 2016.

[158] George M. Whitesides, John P. Mathias, and Christopher T. Seto.
Molecular self-assembly and nanochemistry: A chemical strategy for the synthesis of nanostructures.
Science, 254(5036):1312–1319, 1991.

[159] Gerald S. Manning.
The molecular theory of polyelectrolyte solutions with applications to the electrostatic properties of polynucleotides.
Quarterly Reviews of Biophysics, 11(2):179–246, 1978.

[160] Charl F.J. Faul and Markus Antonietti.
Ionic self-assembly: Facile synthesis of supramolecular materials.
Advanced Materials, 15(9):673–683, 2003.

[161] Marguerite Rinaudo.
Non-covalent interactions in polysaccharide systems.
Macromolecular Bioscience, 6(8):590–610, 2006.

[162] G D Rose and R Wolfenden.
Hydrogen Bonding, Hydrophobicity, Packing, and Protein Folding.
Annual Review of Biophysics and Biomolecular Structure, 22(1):381–415, 1993.

[163] Ken A. Dill, Thomas M. Truskett, Vojko Vlachy, and Barbara Hribar-Lee.
Modeling Water, the Hydrophobic Effect, and Ion Solvation.
Annual Review of Biophysics and Biomolecular Structure, 34(1):173–199, 2005.

[164] Leica.
Step by Step guide To Fluorescence Microscopy.

[165] Leica.
Light Sheet Microscopy.

[166] JIC.
Microscopy.

[167] Malvern Instruments Limited.
Measuring Surface Zeta Potential using the Surface Zeta Potential Cell.
2014.

[168] Malvern Instruments Limited.
Zeta potential: An Introduction in 30 minutes.
2011.

[169] Malvern Instruments Limited.
Technical Note: Zeta Potential - An Introduction in 30 minutes.
2015.

[170] Malvern Instruments Limited.
Zeta Potential Measurments of Non-Aqueous Particulate Suspensions.
2014.

[171] J Rheims, J Köser, and T Wriedt.
Refractive-index measurements in the near-IR using an Abbe refractometer.
Measurement Science and Technology, 8(6):601–605, 1999.

[172] Elizabeth a Jares-Erijman and Thomas M Jovin.
FRET imaging.
Nature biotechnology, 21(11):1387–1395, 2003.

[173] Aaron R Clapp, Igor L Medintz, and Hedi Mattoussi.
Forster resonance energy transfer investigations using quantum-dot fluorophores.
ChemPhysChem, 7(1):47–57, 2006.

[174] David Beljonne, Carles Curutchet, Gregory D Scholes, and Robert J Silbey.
Beyond Forster Resonance Energy Transfer in Biological and Nanoscale Systems Forster Resonance Energy Transfer in Biological and Nanoscale Systems.
J Phys Chem B., 113(19), 2009.

[175] G Binnig and C F Quate.
Atomic Force Microscope.
Physical Review Letters, 56(9):930–933, 1986.

[176] Stefan B Kaemmar.
Introduction to Bruker's ScanAsyst and PeakForce Tapping AFM Technology.
Application note, 133(Rev. A0):12, 2011.

[177] Toshio Ando, Takayuki Uchihashi, and Takeshi Fukuma.
High-speed atomic force microscopy for nano-visualization of dynamic biomolecular processes.
Progress in Surface Science, 83(7-9):337–437, 2008.

[178] Marina I Giannotti and G Julius Vancso.
Interrogation of single synthetic polymer chains and polysaccharides by AFM-based force spectroscopy.
ChemPhysChem, 8(16):2290–2307, 2007.

[179] a. D L Humphris, M J Miles, and J K Hobbs.
A mechanical microscope: High-speed atomic force microscopy.
Applied Physics Letters, 86(3):34106, 2005.

[180] Bruker.
Discover How the Legendary MultiMode AFM Keeps Getting Better.

[181] Norma J Greenfield.
Using circular dichroism collected as a funcion of temperature to determine the thermodynamics of protein unfolding and binding interactions.
Nature protocols, 1(6):2527–2535, 2009.

[182] Hermann Schägger.
TricineSDS-PAGE.
Nature Protocols, 1(1):16–22, 2006.

[183] Arianna Rath, Mira Glibowicka, Vincent G Nadeau, Gong Chen, and Charles M Deber.
Detergent binding explains anomalous SDS-PAGE migration of membrane proteins.
Proceedings of the National Academy of Sciences of the United States of America, 106(6):1760–1765, 2009.

[184] Per Åke Albertsson, Shigeru Sasakawa, and Harry Walter.
Cross partition and isoelectric points of proteins.
Nature, 228(5278):1329–1330, 1970.

[185] Göte Johansson.
Partition of salts and their effects on partition of proteins in a dextran-poly(ethylene glycol)-water two-phase system.
Biochimica et Biophysica Acta - Protein Structure, 221(2):387–390, 1970.

[186] Vithaldas P Shanbhag and Claes-Göran Axelsson.
Hydrophobic interaction determined by partition in aqueous two-phase systems.
Eur. J. Biochem., 60:17–22, 1975.

[187] Boris Yu Zaslavsky, Larisa M. Miheeva, Natalia M. Mestechkina, Valerii M. Pogorelov, and Sergei V. Rogozhin.
General rule of partition behaviour of cells and soluble substances in aqueous two-phase polymeric systems.
FEBS Letters, 94(1):77–80, 1978.

[188] H. Hustedt, K. H. Kroner, W. Stach, and M.-R Kula.
Procedure for the simultaneous large scale isolation of pullulanase and 1,4-alpha-glucan phosphorylase from Klebsiella pneumoniae involving liquid-liquid separations.

Biotechnology and Bioengineering, 20(12):1989–2005, 1978.

[189] Joseph R. Simon, Nick J. Carroll, Michael Rubinstein, Ashutosh Chilkoti, and Gabriel P. López.
Programming molecular self-assembly of intrinsically disordered proteins containing sequences of low complexity.
Nature Chemistry, 9(6):509–515, 2017.

[190] Alan D. Diamond and James T. Hsu.
Protein partitioning in PEG/dextran aqueous two-phase systems.
AIChE Journal, 36(7):1017–1024, jul 1990.

[191] Christine D Keating.
Aqueous phase separation as a possible route to compartmentalization of biological molecules.
Accounts of Chemical Research, 45(12):2114–2124, 2012.

[192] P.-Å. Albertsson.
History of Aqueous Polymer Two-Phase Partition.
In *Partitioning in Aqueous Two-Phase System*, pages 1–10. Elsevier, 1985.

[193] Per Åke. Albertsson.
Partition of cell particles and macromolecules.
Wiley, 1986.

[194] John Crosby, Tom Treadwell, Michelle Hammerton, Konstantinos Vasilakis, Matthew P. Crump, David S. Williams, and Stephen Mann.
Stabilization and enhanced reactivity of actinorhodin polyketide synthase minimal complex in polymernucleotide coacervate droplets.
Chemical Communications, 48(97):11832, 2012.

[195] Daniel C Dewey, Christopher a Strulson, David N Cacace, Philip C Bevilacqua, and Christine D Keating.
Bioreactor droplets from liposome-stabilized all-aqueous emulsions.
Nat. Commun., 5(May):4670, 2014.

[196] L. E. Scriven and C. V. Sternling.
The Marangoni Effects.
Nature, 187(4733):186–188, 1960.

[197] M. Schmitt and H. Stark.
Marangoni flow at droplet interfaces: Three-dimensional solution and applications.
Physics of Fluids, 28(1), 2016.

[198] J Joel Janke, W F Drew Bennett, and D Peter Tieleman.
Oleic Acid Phase Behavior from Molecular Dynamics Simulations.
Langmuir, 30(35):10661–10667, 2014.

[199] H G Khorana, G E Gerber, W C Herlihy, C P Gray, R J Anderegg, K Nihei, and K Biemann.
Amino acid sequence of bacteriorhodopsin.
Proceedings of the National Academy of Sciences, 76(10):5046–5050, 1979.

[200] Paula J Booth and Paul Curnow.
Folding scene investigation: membrane proteins.
Current Opinion in Structural Biology, 19(1):8–13, 2009.

[201] Christian a Bippes and Daniel J Muller.
High-resolution atomic force microscopy and spectroscopy of native membrane proteins.
Reports on Progress in Physics, 74(8):86601, 2011.

[202] Hyo Jick Choi and Carlo D Montemagno.
Artificial organelle: ATP synthesis from cellular mimetic polymersomes.
Nano Letters, 5(12):2538–2542, 2005.

[203] Philippe Girard, Jacques Pécréaux, Guillaume Lenoir, Pierre Falson, Jean-Louis Rigaud, and Patricia Bassereau.
A new method for the reconstitution of membrane proteins into giant unilamellar vesicles.
Biophysical journal, 87(1):419–429, 2004.

[204] Paula J Booth and Paul Curnow.
Membrane proteins shape up: understanding in vitro folding.
Current Opinion in Structural Biology, 16(4):480–488, 2006.

[205] Hyo-Jick Choi, Hyeseung Lee, and Carlo D Montemagno.
Toward hybrid proteo-polymeric vesicles generating a photoinduced proton gradient for biofuel cells.
Nanotechnology, 16(9):1589–1597, 2005.

[206] Katarzyna Kita-Tokarczyk, Julie Grumelard, Thomas Haefele, and Wolfgang Meier.
Block copolymer vesicles - Using concepts from polymer chemistry to mimic biomembranes.
Polymer, 46(11):3540–3563, 2005.

[207] Xiaoyan Zhang, Pascal Tanner, Alexandra Graff, Cornelia G Palivan, and Wolfgang Meier.
Mimicking the cell membrane with block copolymer membranes.
Journal of Polymer Science, Part A: Polymer Chemistry, 50(12):2293–2318, 2012.

[208] Alfredo González-Pérez, Karin B Stibius, Thomas Vissing, Claus H Nielsen, and Ole G Mouritsen.
Biomimetic triblock copolymer membrane arrays: A stable template for functional membrane proteins.
Langmuir, 25(18):10447–10450, 2009.

[209] Daniel a. Hammer and Neha P Kamat.
Towards an artificial cell.
FEBS Letters, 586(18):2882–2890, 2012.

[210] Roxana Stoenescu, Alexandra Graff, and Wolfgang Meier.
Asymmetric ABC-triblock copolymer membranes induce a directed insertion of membrane proteins.
Macromolecular Bioscience, 4(10):930–935, 2004.

[211] Hyo-Jick Choi, Evan Brooks, and Carlo D Montemagno.
Synthesis and characterization of nanoscale biomimetic polymer vesicles and polymer membranes for bioelectronic applications.
Nanotechnology, 16(5):S143—-S149, 2005.

[212] Hyeseung Lee, Dean Ho, Karen Kuo, and Carlo D Montemagno.
Vectorial insertion of bacteriorhodopsin for directed orientation assays in various polymeric biomembranes.
Polymer, 47(9):2935–2941, 2006.

[213] Liangju Kuang, Donald A Fernandes, Matthew O'Halloran, Wan Zheng, Yunjiang Jiang, Vladimir Ladizhansky, Leonid S Brown, and Hongjun Liang.
"Frozen" Block Copolymer Nanomembranes With Light-Driven Proton Pumping Performance.
ACS Nano, 8(1):537–545, 2014.

[214] Ying Zhang, Wen Zhu, Biaobing Wang, and Jiandong Ding.
A novel microgel and associated post-fabrication encapsulation technique of proteins.
Journal of Controlled Release, 105(3):260–268, 2005.

[215] Dewang Ma, Yingchun Zhao, Jia Wu, Ting Cui, and Jiandong Ding.
A block-copolymer hydrogel encapsulates bacteriorhodopsin and produces the longest photochromic response of the membrane protein under high water content conditions.
Soft Matter, 5:4635–4637, 2009.

[216] Kandaswamy Vijayan.
Interactions of membrane-active peptides with thick, neutral, non- zwitterionic bilayers.
J Phys Chem B., 4(109):14356–14364, 2005.

[217] Madhavan Nallani, Mirjam Andreasson-Ochsner, Cherng-Wen Darren Tan, Eva-Kathrin Sinner, Yudi Wisantoso, Susana Geifman-Shochat, and Walter Hunziker.
Proteopolymersomes: in vitro production of a membrane protein in polymersome membranes.
Biointerphases, 6(4):153–157, 2011.

[218] James Fothergill, Mei Li, Sean A. Davis, John A. Cunningham, and Stephen Mann.
Nanoparticle-based membrane assembly and silicification in coacervate microdroplets as a route to complex colloidosomes.
Langmuir, 30(48):14591–14596, 2014.

Attached Experimental Videos

The attached CD-ROM includes experimental microscopy timepoint videos for data discussed in the thesis. These videos are in standard .mp4 format and should play with most media player software. A list of the contents of the CD-ROM is shown below.

1. Chapter 3 - Dextran-FITC 70 kDa coated coacervates over time. Size on disk: 1.3 Mb

2. Chapter 4 - Dextran-FITC 150 kDa compartment formation with addition of TEG Part 1. Size on disk: 2.7 Mb

3. Chapter 4 - Dextran-FITC 150 kDa compartment formation with addition of TEG Part 2 Zoomed Droplets. Size on disk: 3.8 Mb

4. Chapter 4 - Dextran-FITC compartment formation with PEG 600 Part 1. Size on disk: 10.3 Mb

5. Chapter 4 - Dextran-FITC compartment formation with PEG 600 Part 2. 2.2 Mb

6. Chapter 4 - Phase Separation with Dextran-RITC and TEG-FITC in Coacervates. Size on disk: 709 Mb

7. Chapter 5 - Association of Poloxamer-188 at 5 degrees with Coacervates . Size on disk: 2.2 Mb

8. Chapter 5 - Association of Poloxamer-188 at 25 degrees with Coacervates . Size on disk: 5 Mb

9. Chapter 5 - Coacervates with Poloxamer-188 combined with the TEG Dextran System. Size on disk: 15.4 Mb